Palmitoylation and regulation of divalent cation transport by TRPM7 and TRPM6

Xing Gao

BSc (Hons), MSc

Thesis submitted in fulfilment of the requirements for the degree of Doctor of Philosophy (PhD)

University of Glasgow

Institute of Cardiovascular and Medical Sciences
College of Medical, Veterinary and Life Sciences
University of Glasgow

July 2022

Abstract

Magnesium regulates numerous cellular functions and enzymatic reactions, and abnormal magnesium homeostasis contributes to vascular dysfunction and the development of hypertension. The transient receptor potential melastatin 7 (TRPM7) is ubiquitously expressed and regulates embryonic development and pathogenesis of several common diseases. It is also a key player in cardiovascular magnesium homeostasis, cardiac fibrosis, and angiotensin II-induced hypertension. The TRPM7 integral membrane ion channel domain regulates transmembrane movement of divalent cations, primarily Ca, Mg and Zn, and its kinase domain controls gene expression via histone phosphorylation. Mechanisms regulating TRPM7 are elusive. TRPM7 not only localizes on the cell surface where it controls divalent cation fluxes but also exists in intracellular vesicles where it controls zinc uptake and release. Palmitoylation is a dynamic reversible posttranslational modification, which regulates ion channel activity, stability, and subcellular localization. We found TRPM7 is palmitoylated at a cluster of cysteines (Cys1143, Cys1144 and Cys1146) at the C terminal end of its TRP domain in multiple cell types. Palmitoylation controls the exit of TRPM7 from the endoplasmic reticulum and the distribution of TRPM7 between cell surface and intracellular pools. Using the Retention Using Selective Hooks (RUSH) system, we arrested TRPM7 in the Golgi and manipulated its palmitoylation with 2-boromopalmitate (2-BP). Pharmacological reduction of TRPM7 palmitoylation reduced its delivery to the cell surface membrane when it was released from the Golgi. we discovered that palmitoylated TRPM7 traffics from the Golgi to the surface membrane whereas non-palmitoylated TRPM7 is sequestered in intracellular vesicles. In addition, we engineered chimeric forms of TRPM7 in which the palmitoylation sites were replaced with the analogous region of TRPM2 or TRPM5, which do not contain cysteines. It also concludes that inhibiting palmitoylation of TRPM7 results in reduced TRPM7 abundance on cell surface. We identified the Golgi-resident enzyme zDHHC17 as responsible for palmitoylating TRPM7 and find that TRPM7 is de-palmitoylated by some acyl-thioesterases post-Golgi and re-palmitoylated by plasma-membrane-resident zDHHC5. The close homologue TRPM6 is also palmitoylated on the C-terminal side of its TRP domain. To investigate the impact of palmitoylation on TRPM7 ion transport activity, we attempted to measure Mg influx at cell surface and Zn

influx in intracellular vesicles, but these two assays were unsuccessful. Using fluo4 to measure intracellular Ca we determined that TRPM7 mediated transmembrane calcium uptake is significantly reduced when TRPM7 is not palmitoylated. In addition, we also measured the relationship between phosphorylation/cleavage of TRPM7 and Its palmitoylation. Phosphorylation and palmitoylation are two independent post-translational modifications of TRPM7. Phosphorylated TRPM7 was palmitoylated to the same extent as total TRPM7. Non-palmitoylated TRPM7 chimeras were less phosphorylated, probably as a result of their reduced abundance at the cell surface. Quantitative proteomic analysis of the protein partners of wild type and non-palmitoylated TRPM7 identified vesicular proteins as more enriched with non-palmitoylated TRPM7, and nuclear proteins more enriched with palmitoylated TRPM7, suggesting cleavage and nuclear translocation of the TRPM7 kinase domain may be influenced by palmitoylation. Our findings illustrate palmitoylation controls ion channel activity of TRPM7 and that TRPM7 trafficking is dependent on its palmitoylation. Palmitoylation of TRPM7 might implicated in control of gene transcription by altering nuclear localization of its cleaved kinase domain. In conclusion, we defined palmitoylation as a new mechanism for post translational modification and regulation of TRPM7 other TRPs.

Table of Contents

List of Tables

List of Figures

List of publications

1. Gao, X., Kuo, C. W., Main, A., Brown, E., Rios, F. J., Camargo, L. L., Mary, S., Wypijewski, K., Gök, C., Touyz, R. M., & Fuller, W. (2022). Palmitoylation regulates cellular distribution of and transmembrane Ca flux through TRPM7. Cell calcium, 106, 102639. https://doi.org/10.1016/j.ceca.2022.102639

2. ZouZ., LuQ., WangY., GaoX., ZhuX., LuX., & PuJ. (2022). Magnesium in aging and aging-related disease. *STEMedicine*, *3*(2), e119. https://doi.org/10.37175/stemedicine.v3i2.119

3. Gök, C., Main, A., Gao, X., Kerekes, Z., Plain, F., Kuo, C. W., Robertson, A. D., Fraser, N. J., & Fuller, W. (2021). Insights into the molecular basis of the palmitoylation and depalmitoylation of NCX1. *Cell calcium*, *97*, 102408. https://doi.org/10.1016/j.ceca.2021.102408

4.Zou, Z. G., Rios, F. J., Neves, K. B., Alves-Lopes, R., Ling, J., Baillie, G. S., Gao, X., Fuller, W., Camargo, L. L., Gudermann, T., Chubanov, V., Montezano, A. C., & Touyz, R. M. (2020). Epidermal growth factor signaling through transient receptor potential melastatin 7 cation channel regulates vascular smooth muscle cell function. *Clinical science (London, England : 1979)*, *134*(15), 2019–2035. https://doi.org/10.1042/CS20200827

Acknowledgement

First and foremost, I would like to thank my supervisors Prof. Will Fuller and Prof. Rhian Touyz for giving me the opportunity to complete this project with them. Especially to Will, thanks for accepting my application when I totally had no lab experience at beginning (I suggest you never done that again!). I am hugely appreciating all the support you have given me throughout my 4-year PhD life. To be honest, being your student is the luckiest thing happened to me in these years. You are literally the best supervisor who is so patient and never complaining, guiding me step by step through the scientific field. Also, lots of thanks to Rhian, she is the most effective and busy superwomen I have ever known. I had seen she dealt thousands of emails on half day, directly had groups meeting after long flight without jet lag, but she always put students in high priority. In addition, special thanks to the graduate school of College of Medical, Veterinary & Life Sciences (MVLS) for waiving my tuition fee, which is a great financial support to me.

To the Fuller Lab, the warmest lab family, it is my great honour to work with all of you. Sharon, thanks for your patience (not usually seen now) and old school teaching way to show me lots of scientific techniques when I was a rookie. Jacquie, I have to admit that I stole many your reagents and I assume you allowed that! Olivia, my lovely desk mate, thank you for providing many hilarious (and ridiculous) stories in these years. Elaine, I can always rely on you if I struggle with mutagenesis. Alan, the one who knows the most extensive (might not that useful) knowledge I have ever known, thanks for making all the orders for me. Krzys and Caglar, I am very appreciating all the challenging techniques you taught me. Emily, I would miss your random singing and dancing in the lab. Special massive thanks to my dearest friends Alice and Samitha, you are always such supportive to me no matter in science or personal life. I am grateful to have your company during my PhD which makes it much easier.

Also, I would thank to all the support from Rhian Lab. Fran, lots of thanks for all your help and I wish you have great career future in Canada. Steve, you are such a working machine, but you always kindly give me suggestion when we both suffering from TRPM7. Guto and Livia, thanks for all the samples and cells you provided. In addition, special thanks to Sheon, you helped me with many times

proteomics experiments, and you are so patient to explain every details. Dr. Vladimir, thanks for the very useful advice you gave us when we measured ion channel activity.

Furthermore, thanks to all my friends, Yilin, Zhaoyang and Mengyi, we have known each other for years and you are like the “Glasgow family” to me. Joyce, I would miss all the meals and all sweating gym session we had together. Yu and Jiteng, thanks for your lovely couple bring me to travel (not infecting covid part!) and hiking many times. Alex, 5-star free uber driver, thanks for giving me lift many times and I would miss pleasure time with you and Alice. Trupti, I would miss the feast you and Samitha provided.

In the end, the biggest thanks to my domestic family. Mum, thanks for you always being such supportive of my decisions. You love me so much even over yourself and I am deeply grateful everything you did for me. Fei, you are a great sister and have taken so much responsibility in these years. You are already being a doctor and I hope you got your Philosophy Doctor soon!

It has been the best 4-year time to me. Massive thanks to all you guys for making my PhD life an enjoyable journey.

Author's Declaration

I declare that the following thesis is based on the results of experiments carried out by myself, and that this thesis is of my own composition. Apart from myself, Work based on other contributions is clearly indicated in the text by reference to the relevant researchers or their publications. This dissertation has not been accepted or previously submitted in whole, or in part, for a higher degree.

Definitions/Abbreviations

2BP	2-bromopalmitate
ABHD17	α/ß hydrolase domain-containing 17 family
ACh	Acetylcholine
acyl-CoA	acyl coenzyme A
Acyl-RAC	acyl resin assisted capture
AD	Alzheimer's disease
ADPKD	Autosomal dominant polycystic kidney disease
ADPR	ADP-ribose
AF	Atrial fibrillation
AMD7	Amphiphile-mediated de-palmitoylation 7
APT	Acyl protein thioesterase
AQP4	Aquaporin-4
AR	Ankyrin repeat
ARD	Ankyrin repeat domain
ARL15	G-protein ADP-ribosylation factor-like protein 15
BBB	Blood-brain barrier
CAD	Coronary heart disease
CaM	Calmodulin
cAMP	Cyclic AMP
CB	Carotid body
CBPs	Calcium-binding proteins
CF	Cardiac fibroblasts
CALWY	CFP-Atox1-linker-WD4-YFP
CI-MPR	Cationic-independent mannose 6-phosphate receptor
CNNM	Cyclin M
CNS	Central nervous system
COSHH	Control of Substances Hazardous to Health
CRAC	Calcium release-activated calcium channels
Cryo-EM	cryo-electron microscopy
CSF	cerebrospinal fluid
CRD	cysteine-rich domain
CTD	C-terminal domain
DAG	diacylglycerol
DAPI	4',6-diamidino-2-phenylindole
DCT	distal convoluted tubules
dH2O	distilled water
DHHC-PAT	DHHCs palmitoyl acyl transferase
DIC	Differential Interference Contrast
DMEM	Dulbecco's modified eagle medium
DMSO	dimethyl sulfoxide
DPG	Asp-Pro-Gly
DRG	dorsal root ganglia
DTT	dithiothreitol
EADs	early after depolarisations
ECM	extracellular matrix
EDTA	ethylenediaminetetraacetic acid
eEF2	Eukaryotic elongation factor 2
EGF	Epidermal growth factor
EGFR	Epidermal growth factor receptor
ER	Endoplasmic reticulum

ERK	Extracellular signal-regulated kinases
FBS	Foetal bovine serum
FGF	Fibroblast growth factor
Flot2	Flotillin 2
FRET	fluorescence resonance energy transfer
GO	Gene ontology
GOCC	Gene ontology of cell components
HEK	human embryonic kidney
HF	Heart failure
HIF	hypoxia-inducing factor
HMG-CoA	3-hydroxy-3-methylglutaryl coenzyme A
HOMG1	primary hypomagnesemia type 1, intestinal
HSH	hypomagnesemia with secondary hypocalcaemia
HTT	Huntingtin
HUVEC	umbilical vein
hVSMCs	human vascular smooth muscle cells
IGF-1	insulin-like growth factor-1
IL	interleukins
INCL	infantile neuronal ceroid lipofuscinosis
JNK	Jun N-terminal kinase
KChip	K channel-interacting protein
KD	kinase domain
Ki-RasA	Kirsten Ras
LC-MS	liquid chromatography mass spectrometry
Leprb	leptin receptor
LPR6	Lipoprotein receptor-related protein 6
M7CK	TRPM7 cleaved kinase
MagT1	Magnesium transporter 1
MAP6	microtubule-associated protein 6
MD	molecular dynamic
MEND	massive endocytosis
MHR	melastatin Homologous Regions
MLIV	mucolipidosis type IV
MMgTs	membrane Mg transporters
MMR	mismatch repair
MMTS	methyl methanethiosulfonate
MPTP	Mitochondrial permeability transition pore
MR	mineralocorticoid receptor
MRGs	magnesium responsive genes
Mrs2	mitochondrial RNA splicing 2
NCL	native chemical ligation
NCT	nicastrin
NCX1	Na/Ca exchanger
NER	nucleotide excision repair
NH2OH	hydroxylamine
NMDARs	N-methyl-D-aspartate glutamate receptors
NPHP	nephronophthisis-like phenotype
NS	neural stem
OD	organ donor
OGD	oxygen-glucose deprivation
OS	oxidative stress
P/S	Penicillin/Streptomycin
PaCCT	palmitoyltransferase conserved C-terminus

PalmB	palmostatin B
palmitoyl-CoA	palmitoyl-coenzyme A
PATs	protein acyltrasnferases
PC-1	Polycystin-1
PD	Parkinson disease
PDB	Protein Data Bank
PDZ	PSD95-DlgA-zo-1
PEN2	presenilin enhance 2
PFA	paraformaldehyde
PIP2	phosphatidylinositol 4,5-bisphosphate
PKA	protein kinase A
PKD	polycystic kinase disease
PLC	phospholipase C
PM	plasma membrane
PMTs	photomultiplier tubes
PNGase	Peptide-N (4) -(N-acetyl-beta-glucosaminyl) asparagine amidase
PNS	post-nuclear supernatant
PPTs	palmitoyl-protein thioesterases
PRDX5	peroxiredoxin-5
PSD-95	postsynaptic density protein 95
PSSM	position-specific scoring matrix
PTH	parathyroid hormone
PTM	post-translational modification
PVDF	polyvinylidene difluoride
RDA	recommend daily allowance
RDF	rat cardiac myofibroblasts
ROS	reactive oxygen species
RTKs	Receptor Tyrosine Kinases
RUSH	retention using selective hooks
S100A1	S100 calcium-binding protein A1
SBP	streptavidin binding protein
SDS-PAGE	Sodium dodecyl sulphate-polyacrylamide gel electrophoresis
Ser/Thr	Serine/Threonine
SHR	spontaneously hypertensive rat
SHRSP	Spontaneously Hypertensive Stroke Prone Rat
SLC41	Solute carrier family 41
SLC41A1	Solute carrier family 41, member 1
SM	staring material
SOCE	store operated Ca entry
SPP	S-palmitoylated protein
SR	sarcoplasmic reticulum
ssABE	site-specific-Acyl-Biotin-Exchange
SSAC	stretch- and swelling- activated cation
T2DM	Type 2 diabetes mellitus
TAL	thick ascending limb
TdP	Torsades de Pointes
Tet	Tetracycline
TGF	transforming growth factor
TMD	transmembrane domain
TNF-α	tumor necrosis factor-alpha
TRP	Transient Receptor Potential
TRPM	Transient Receptor Potential Melastatin

TTxE	Thr-Thr-x-Glu
TUSC3	Tumor Suppressor Candidate 3
UB	unbound
UF	unfractionated
VCAM-1	vascular cell adhesion molecule 1
VEGF	vascular endothelial growth factor
VR1	Vanilloid Receptor 1
VSMCs	Vascular smooth muscle cells
VSVGts045	vesicular stomatitis virus glycoprotein ts045
WKY	Wistar Kyoto
YFP	yellow fluroscent protein
yMrs2p	Yeast Mrs2 protein
zDABM	zDHHC ankyrin repeat-binding motif

Chapter 1 Introduction

1.1 Magnesium homeostasis

1.1.1 Intracellular and extracellular magnesium homeostasis

Magnesium is the fourth most abundant mineral in the human body and the second most abundant intracellular cation after potassium in mammalian cells. It is essential to regulate numerous cellular functions and enzymes, modulating ion channels as well as participating in various signalling pathways and metabolism cycles. On average, an adult body (~70kg body weight) contains approximately 25 grams (about 1 mole) of Mg (Bancerz et al., 2012) in reserve with most (approximately 53%-67%) in bones, ~27% in muscle, ~19% in soft tissues and less than 1% in serum (Saris et al., 2000, Vormann, 2003). Detection of cellular Mg content by different techniques consistently indicates that total Mg concentration ranges between 17-20mM in most mammalian cell types (Romani and Scarpa, 1992). The major proportion of ~90%-95% of magnesium is bound to ATP in cytosol or sequestered within different cellular organelles (Chakraborti et al., 2002). ATP is the largest metabolic pool which is capable of binding Mg with highly affinity within both the cytoplasm and in the matrix of cellular organelles (more than 5mM) (Lüthi et al., 1999). Through various detection technique, the intracellular free cytosolic magnesium concentration ([Mg]i) is estimated to be 0.5-1mM and the rest bound to ATP, phosphor-nucleotides and phosphometabolites, as well as proteins (Vormann, 2003, Romani, 2011). For example, on the one hand, the concentration ranging from 15mM to 18mM magnesium was detected in cellular organelles such as mitochondria, nucleus and endo-(sarco)-plasmic reticulum which is closely equivalent to levels in whole cells (Romani, 2011). On the other hand, the free magnesium concentration only accounts for a small proportion varying from 15% to 22% in the lumen of those compartments (Romani, 2011). For instance, free [Mg] in cardiac mitochondria matrix is only 0.8mM and it is 1.2mM in matrix of liver mitochondria (Jung et al., 1990, Rutter et al., 1990). However, free [Mg] cannot be reliably determined in the nucleus and the endo-(sacro)-plasmic reticulum, because Mg indicator is based on APTPA (O-aminophenol-N,N,O-triacetic acid), which is also sensitive to Ca (London, 1991, Raju et al., 1989), and these organelles contain elevated concentrations of Ca. Overall, genetic and electrophysiological approaches have identified a limited Mg gradient changes across cell surface membrane or

cellular organelles membrane, which is important for normal physiology of cells and organelles (Wolf and Trapani, 2008).

Furthermore, extracellular magnesium only accounts for approximately 1% of total body magnesium, ranging from 1.2-1.4mM (Romani, 2011). In plasma, nearly one third of this magnesium is bound to extracellular proteins such as albumin/globulins and 10% forms complexes with other biochemical moieties like phosphate and citrate (Swaminathan, 2003). The other 60% of magnesium exists in the ionized free form, which exert important influences on plasma physiological functions. In normal adults, total plasma magnesium ranges from 0.70-1.10mmol/L and serum ionised magnesium within an even narrower range about 0.54-0.67 mmol/L (Swaminathan, 2003, Jahnen-Dechent and Ketteler, 2012). Serum magnesium concentration is considered as magnesium depleted when it falls below 0.75 mmol/L (1.8 mg/dL). It is generally recognized that serum magnesium concentration cannot directly reflect total body magnesium nor intracellular magnesium content.

Both intracellular and extracellular magnesium homeostasis play essential roles in development of cardiovascular disease. Experimental research has identified the association between decreased intracellular Mg concentration in vascular smooth muscle cells and primary hypertension (Kisters et al., 2000). Moreover, randomised controlled trails has proved magnesium supplementation improves endothelial function (Cunha et al., 2017), insulin resistance (Simental-Mendia et al., 2016), arterial stiffness (Joris et al., 2016) and reduces blood pressure (Zhang et al., 2016). Environmental factors such as lifestyles and dietary habits are determinants in developments of several cardiovascular diseases including atherosclerosis and coronary heart disease (CAD) (Maier, 2012). However, A Mendelian randomisation (MR) study about serum magnesium levels and risks of CAD reveals genetic variants predisposing to higher serum magnesium levels may render decreased risks of CAD. Specifically, every 0.1mmol/L increase in serum magnesium levels reduces the risk of developing CAD by 12% (Larsson et al., 2018). MR utilises genetic variants as instrumental variables of an exposure to strengthen causal inference regarding an exposure-outcome relationship (Larsson et al., 2018). It could diminish interference by confounding variables, such as lifestyle and behaviours, because genetic variants are randomly allocated at meiosis.

1.1.2 Magnesium metabolism

1.1.2.1 Magnesium consumption

As about 60% of human body magnesium is present in bone, of which 30% is exchangeable (Swaminathan, 2003), so serum magnesium concentration is primarily maintained by the dynamic balance between intestinal and renal transport and interplay with bone exchange (Reddy et al., 2018). The recommend daily allowance (RDA) for magnesium in adults is 4.5mg/Kg/day (Saris et al., 2000). The institute of Medicine recommends 310-360g for adult women and 400-420mg for adult man in daily magnesium consumption (Jahnen-Dechent and Ketteler, 2012), which varies in accordance with individual age, sex and physiological status. For example, daily requirement is in higher range (~355mg) in pregnant and lactating women(Elin, 1988, Jahnen-Dechent and Ketteler, 2012). Food enriched in magnesium includes green leafy vegetables, almonds, cereal, black beans, broccoli, grain, nuts, sweet corn, tofu and legumes (Razzaque, 2018). In contrast, diet high in protein, fat, calcium, phosphorus, phytates, or alcohol decrease available magnesium and absorption (Reddy et al., 2018). Moreover, drinking water, especially ‘hard water’ which contains up to 30 mg/L of magnesium, is another important source (Sengupta, 2013). In general, the intake of magnesium is closely related to overall energy intake, but the complicated refining or processing of food would lead to significant loss of magnesium.

1.1.2.2 Magnesium intestinal absorption

There is around 12mmol/day intake of magnesium in a healthy adult and about 6mmol of this is absorbed by intestine and stored in bone and soft tissue (Swaminathan, 2003). In addition to this, approximately 2 mmol/day of magnesium is secreted into the intestinal tract in bile and pancreatic and intestinal juices resulting in a (~30%) net absorption with 4mmol/day (Seo and Park, 2008).Notably, functional intestinal absorption of magnesium is inversely related to magnesium intake, specifically 80% at low dietary magnesium and 11% at the high one (Philipp Schuchardt and Hahn, 2017). The predominantly intestinal absorption occurs in the small intestine via paracellular passive pathway and a small amount also occurs in colon mainly through transcellular active pathway (De Baaij et al., 2015, Graham et al., 1960). The majority,

nearly ~90% magnesium is absorbed via a paracellular mechanism driven by the electrochemical gradient and transepithelial concentration gradient (Quamme, 2008, Philipp Schuchardt and Hahn, 2017). The transepithelial electrical voltage is normally about $^{+}$5mV in small intestine with lumen positive (Quamme, 2008). Meanwhile, the driving force for passive magnesium transport in the distal jejunum and ileum relies on lumen-positive transepithelial voltage of ~15 mV (Philipp Schuchardt and Hahn, 2017). In general, magnesium is absorbed in the ionised form, so the bound magnesium has no impact on transepithelial gradient. Therefore, transepithelial concentration gradient is established due to the serum Mg^{2} concentration which is normally only ~0.7mM. The transcellular active absorption occurring in the caecum and colon of the large intestine is mediated by transient receptor potential channel melastatin member (TRPM) 6 and 7, which contribute to the saturable active transcellular Mg movement from the intestinal lumen into the cells (Philipp Schuchardt and Hahn, 2017, Quamme, 2008), as well as facilitating intestinal calcium absorption at the same time(Touyz, 2004). TRPM7 is ubiquitously expressed in tissues and TRPM6 is mainly localized to the apical membrane of the intestine and renal distal convoluted tubule, where it is essential for epithelial magnesium transport (Quamme, 2008). Hereditary hypomagnesemia called hypomagnesemia with secondary hypocalcaemia (HSH) is an autosomal-recessive disorder cause by loss-functional mutation of TRPM6 (Schlingmann et al., 2007).

1.1.2.3 Renal magnesium elimination

The kidney plays an important role in magnesium homeostasis as plasma magnesium concentration is maintained by its excretion in urine (Elin, 1988). Under physiological conditions, for a health adult, approximately 2400mg of Mg in plasma is filtered by the glomeruli daily, of which ~90%-95% is reabsorbed along the nephron resulting in 3%-5% (~100mg) excreted in the urine (De Baaij et al., 2012). Therefore, urinary magnesium excretion normally matches with the net intestinal absorption as ~4mmol/day (100mg/day) (Seo and Park, 2008). Meanwhile, the serum magnesium concentration is primarily maintained by control of renal magnesium reabsorption. Interestingly, in contrast to other electrolytes such as Na, K and Cl, only around 10-25% of Mg is retrieved by proximal tubule (PT) (De Baaij et al., 2012, Le Grimellec et al., 1975). The majority (~50%-70%) of filtered Mg is reabsorbed along thick ascending limb

(TAL) of the loop of Henle and in fact Mg is the only bulk transported ion in the loop of Henle (Blaine et al., 2015, De Baaij et al., 2012). The driving force for the passive paracellular magnesium transport in TAL is transepithelial voltage which is positive in tubular lumen relative to the blood (De Baaij et al., 2012). In addition, claudins-16 and -19 interact to assessable a cation-selective tight junction structure to contribute to magnesium transport in the TAL (Hou et al., 2009). Apart from those, the fine-tuning of Mg reabsorption, which represents 10% of the total reabsorption, occurs in the distal convoluted tubule (DCT), where Mg reabsorption via TRPM6 is an active transcellular process (De Baaij et al., 2012).

In conclusion, magnesium metabolism depends on the integrated effect of magnesium absorption in the intestine, excretion and reabsorption via kidneys and exchange through storage in bone. Many regulatory factors were discovered in magnesium absorption but remain incompletely characterised. For instance, in distal convoluted tubules (DCT), epidermal growth factor (EGF) regulates TRPM6 activity and plasma membrane availability (Ikari et al., 2008). And parathyroid hormone (PTH) could stimulate magnesium reabsorption without altering TRPM6 expression (Groenestege et al., 2006, Curry and Alan, 2018).

1.1.3 Biological function of Magnesium

Magnesium is an essential divalent cation in the human body. It acts as a co-factor in over 300 enzymatic reactions and is especially important for those enzymes that use nucleotides as cofactors or substrates and adenosine triphosphate (ATP) metabolism (Grubbs and Maguire, 1987, Saris et al., 2000, Swaminathan, 2003). Magnesium is indispensable for major cellular processes, especially involving in energy metabolism, apoptosis, and proliferation. For example, magnesium is crucial to the phosphotransferase and hydrolase ATPases to exert functions in cellular biochemistry particularly in energy metabolism (Saris et al., 2000). Interfering with magnesium metabolism also influences universal ATP-dependent processes such as glucose utilization, synthesis of proteins, fat, nucleic acids and coenzymes, muscle contraction and methylation (Jahnen-Dechent and Ketteler, 2012). Magnesium regulates cell proliferation via the cell cycle inhibitors p27 and p53 and other negative modulators of cell proliferation (Wolf and Trapani, 2008). The role of magnesium in cell apoptosis

remains unconclusive. In many experimental investigations, magnesium deprivation results in cell death and dietary deficiency of magnesium accelerates apoptosis (Martin et al., 2003). Magnesium stabilizes DNA conformation in a concentration dependent manner and contributes to the secondary and tertiary structure of DNA via electrostatic force and hydrogen bonds (SantaLucia Jr and Hicks, 2004).Consequently, magnesium homeostasis is important for DNA stabilization meanwhile it is required for many enzymes that control nucleic acid metabolism, such as nucleotide excision repair (NER), base excision repair (BER) and mismatch repair (MMR), in DNA repair pathways (Calsou and Salles, 1994). Therefore, physiological levels of magnesium maintain genomic stability (Hartwig, 2001).

Moreover, cytosolic free magnesium plays a key role in the transport of calcium and potassium across the cell membrane which is fundamental to regulate muscle contraction, nerve impulse conduction and vasomotor tone (Gröber et al., 2015). One neurological function of Mg is to serve as a natural calcium antagonist to blunt methyl-d-aspartate (NMDA) receptor influence on membrane potential. When Mg is reduced, the increased excitatory postsynaptic potential exacerbates oxidative stress and neuronal cell death (De Baaij et al., 2015, Fiorentini et al., 2021). In addition during muscle contraction, magnesium stimulates calcium re-uptake by calcium activated ATPases of the sarcoplasmic reticulum (Jahnen-Dechent and Ketteler, 2012). Magnesium competitively binds to the calcium binding sites such as troponin, parvalbumin, myosin and calmodulin to regulate muscle contraction and maintain the low resting intracellular free calcium ion concentration (Potter et al., 1981). Furthermore, magnesium is generally recognized to have important effects on cardiovascular system. Epidemiological, clinical, and experimental evidence has suggested that Mg levels (serum and tissue) and blood pressure have an inverse association (Kesteloot and Joossens, 1988, Whelton and Klag, 1989). Magnesium regulates vascular tone and reactivity to control its contraction/relaxation by competing with Ca to bind key myocardial contractile protein such as myosin and actin (Chakraborti et al., 2002). Mg acts as a calcium channel antagonist and by stimulating generation of nitric oxide and prostacyclin magnesium modifies vasoactive agonists (Sontia and Touyz, 2007). To sum up, magnesium disorder

might be associated with the development of many diseases due to its importance in biological processes.

1.1.4 Mg disorders and related diseases

1.1.4.1 Magnesium and cancer

As previously mentioned, magnesium is involved in multiple biological reactions which are important to cell proliferation, differentiation, apoptosis and angiogenesis (Wolf and Trapani, 2008). Hypomagnesemia has been discovered in patients consuming diuretics and some anticancer drugs which both promote Mg wasting (Maier et al., 2007). A recent large epidemiological prospective study on Swedish women revealed an inverse association between magnesium dietary intake and colorectal cancer (Larsson et al., 2005). However, the relationship between magnesium and cancer is still a puzzle to disentangle. Compared to normal cells, tumor cells show less growth-dependence on magnesium availability because they have higher capability to sequester and reserve Mg (Sgambato et al., 1999). The growth of tumor cells only decreased when extracellular Mg was lower than 0.03mM (Sgambato et al., 1999). Meanwhile, the Na-dependent magnesium extrusion mechanism has been identified to be different in tumor and normal cells resulting in retaining higher intracellular Mg concentration in tumor cells (Wolf et al., 1998, Wolf et al., 1996). In addition, overexpression of TRPM7 in breast tumours and in neoplastic cultured cells might also be an underlying reason for the enhanced ability of cancer cells to acquire extracellular Mg (Guilbert et al., 2009).

Intracellular magnesium impacts on the process of carcinogenesis are mainly through affecting oxidative stress reactions and DNA repair mechanisms (Wolf et al., 2007). It has been demonstrated that magnesium deficiency can directly inhibit development of primary tumours via downregulating cyclin B and D3 and upregulating p21, p27 and Jumonji thereby inhibiting tumour cell proliferation (Nasulewicz et al., 2004). However, magnesium deficiency facilitates DNA oxidative damage and impairs angiogenesis (Maier et al., 2007). Mg deficiency suppresses hypoxia-inducing factor (HIF)-1α activity in paraganglion cells, which is triggered by upregulation of IPAS cause by the activation of NFκB, the collaborating transcription factor of inflammation in tumor cells (Torii et al.,

2009, Karin et al., 2002). Therefore, inflammation in Mg deficient mice might contribute to cancer metastases. Tumour Necrosis Factor (TNF)α, the target of NFκB and prototypical pro-inflammatory cytokines, interleukins (IL) 1 and 6 are all increased in Mg deprivation to promote the capacity of cancer cells to metastasize (Royuela et al., 2008). Currently, radiotherapy and drugs such as cetuximab, a monoclonal antibody against the epidermal growth factor (EGF) receptor, both induce hypomagnesemia (Cohen and Kitzes, 1985, Vincenzi et al., 2008). But the importance of magnesium supplementation to cancer patients remains controversial.

1.1.4.2 Magnesium and cardiovascular disease

Observational data demonstrated an association between mild to moderate magnesium deficiency and increased risk of atherosclerosis, ischemic heart disease, coronary artery disease and congestive heart failure (HF), while severe magnesium deprivation leads to sudden cardiac death (Tangvoraphonkchai and Davenport, 2018). In the vasculature, magnesium controls vascular tone and contractility of cardiomyocytes by affecting calcium concentrations. Epidemiological and experimental data show that serum magnesium concentration has an inverse association with blood pressure and magnesium supplementation may decrease peripheral vascular resistance and blood pressure (Romani, 2018). A meta-analysis of 20 randomized clinical trials involving 1220 participants found that magnesium supplementation significantly reduced blood pressure in dose-dependent manner (Jee et al., 2002). In addition, the mechanism whereby magnesium reduces blood pressure might be via its antioxidant and anti-inflammatory function (Weglicki et al., 1992). The presence of physiological concentrations of magnesium would inhibit reactive oxygen species (ROS) reaction subsequently antagonizing the vasoconstriction effect (Taniyama and Griendling, 2003). To be specific, the decrease of extra- and intracellular mg concentration stimulate inflammation consequently inducing oxidative stress (OS) (Mazur et al., 2007). It has been indicated magnesium deficiency indirectly promote oxidative damage of biomolecules by inducing stress responses (Zheltova et al., 2016). Decrease ratio of Mg/Ca stimulate release of catecholamine, which would increase the production of ROS. In addition, magnesium deficiency leads to the activation of rennin-angiotensin system which also accumulates OS (Zheltova et al., 2016). Furthermore,

magnesium was also found to impact the development of atherosclerosis by regulating the production of prostacyclin and NO and altering vascular responses to many vasoactive substances including endothelin-1, angiotensin-II, and catecholamines) (Weglicki et al., 1992, Kostov and Halacheva, 2018). Mg deficiency promotes expression of vascular cell adhesion molecule 1 (VCAM-1), an important factor in the progress of atherosclerosis, as well as erythrocyte, tissue, and lipoprotein peroxidation which are all implicated in early stages and progression of atherosclerotic lesions (Sobhani et al., 2020, Mazur et al., 2007). Meanwhile, Mg deficiency also induces insulin resistance, hyperglycaemia and dyslipidaemia which all contributes to atherosclerosis. In contrast, magnesium supplementation attenuates development of atherosclerotic lesions (Bo and Pisu, 2008).

Ventricular tachycardia and Torsades de Pointes (TdP) have been observed in several cases of magnesium deficiency (Bibawy et al., 2013). Hypomagnesemia could impair intracellular potassium handling resulting in prolongation of the QT interval via change of cellular repolarization (Bibawy et al., 2013). Dysfunction in the L-type Ca channel, which makes a fundamental contribution to development of early after depolarisations (EADs), is also mediated by magnesium deficiency. Consequently, administration of magnesium sulphate is recommended as a treatment for TdP.

1.1.4.3 Magnesium and neurological disease

The major function of magnesium in the nervous system is to block the calcium channel in the NMDA receptor, a glutamate receptor and ion channel important for neurotransmission and synaptic plasticity (Fiorentini et al., 2021). Lower magnesium levels potentiate glutamatergic neurotransmission causing excitotoxicity and leading to oxidative stress and neuronal cell death (Castilho et al., 1999). Also magnesium is much abundant in cerebrospinal fluid (CSF) than it is in the blood due to the active transporting across the blood-brain barrier (BBB), which is positively correlated with cognitive function (Xiong et al., 2016, Morris, 1992). Decrease of magnesium concentration in CSF is correlated with the development of seizure (Morris, 1992). Protracted deficiency of magnesium in humans and animals has been implicated in a variety of neurological and

psychiatric disease, ranging from migraine, epilepsy, Alzheimer's, Parkinson's and stroke (Kirkland et al., 2018).

However, the of quality data associating magnesium with neurological disorders is relatively poor. Strong data supports the concept that magnesium administration could serve as therapy for migraine (Kirkland et al., 2018) via blocking the NMDA receptor, an active contributor to pain transmission (Hoffmann and Charles, 2018). A recent study found a negative correlation between magnesium intake and depression, particularly the lower CSF and serum magnesium levels in the individuals diagnosed with depression (Li et al., 2017, Rechenberg, 2016). Meanwhile, a meta-analysis of 11 studies demonstrates that 320mg/day of magnesium substantially reduces the risk of depression (Li et al., 2017). Alzheimer's disease (AD) is a neurodegenerative disorder with synaptic loss and cognitive impairments which is characterized with beta-amyloid and tau tangles, along with neuroinflammation, excitotoxicity and mitochondrial dysfunctions (Zádori et al., 2018). Compared to the healthy controls, AD patients have significantly reduced magnesium levels in many compartments ranging from to CSF, hair, plasma to red blood cells (Veronese et al., 2016). Magnesium depletion has also been found in the hippocampus in patients with AD (Andrasi et al., 2000),and magnesium deficiency correlates with tumor necrosis factor-alpha (TNF-α) elevation in the serum and brains in AD patients (Yu et al., 2018). Magnesium-L-threonate (MgT) supplementation recovers magnesium levels to suppress the TNF-α expression in glial cells in mice. Additionally, Magnesium elevation inhibits the expression of presenilin enhance 2 (PEN2) and nicastrin (NCT), whose function assists synthesis of amyloid ß-protein (Aß) in a PI3K/AKT and NFkB-dependent manner (Yu et al., 2018). However, there is still a distinct lack of research of magnesium administration as a treatment for AD in human. Finally, magnesium-deficient mice have a tendency to develop Parkinson's disease (PD) (Oyanagi et al., 2006). PD is associated with a decrease in TRPM7 and SLC41A1 (Solute carrier family 41, member 1) mRNA expression which suggests magnesium transporters play a role in PD (Lin et al., 2018, Vink et al., 2009). Although an increasing number of studies implicate magnesium disorders in PD in animals, evidence in patients remains poor.

1.1.4.4 Magnesium and metabolic syndrome

Metabolic syndrome is a pathological condition which is associated with obesity, diabetes, hyperlipoproteinemia, hyperuricemia, and hepatic steatosis (Haller, 1977). Its incidence in human population involves more than 500 million people worldwide, with a common symptom of hypomagnesemia. Magnesium has been found to modulate the activity of a series of enzymes involved in lipid metabolism, such as 3-hydroxy-3-methylglutaryl coenzyme A (HMG-CoA) reductase, lipoprotein lipase, and lecithin-cholesterol acyltransferase (Dos Santos et al., 2021). Meanwhile, magnesium is also essential for genes that participate in adipogenesis, lipolysis, and inflammation. Reduced serum magnesium concentration has been discovered in type 2 diabetic patients (Volpe, 2008), and magnesium is speculated to influence development of diabetes through increasing insulin resistance (Volpe, 2008). Oral administration of magnesium has been found to improve fasting and postprandial glucose levels and insulin sensitivity in Type 2 diabetes mellitus (T2DM) patients with hypomagnesemia (Barbagallo and Dominguez, 2015).

1.1.4.5 Hypermagnesemia

In conclusion, magnesium disorders might result from a variety of factors including abnormal gastrointestinal and renal functions. magnesium deficiency has been implicated a variety of clinical diseases ranging from hypocalcaemia, hypokalaemia, cardiac and neurological manifestations, to multiple chronic disease (hypertension, diabetes, osteoporosis etc.). In contrast, hypermagnesemia ($\geqslant$1.1mmol/L or 2.5mg/dL), triggered by increased intake or decreased excretion (Qazi et al., 2021), is less frequent than hypomagnesaemia. Symptoms of hypermagnesemia usually emerge when serum magnesium concentrations exceed 2mmol/L however the serum concentration at which the different symptoms appear differ sharply. The most common complications of hypermagnesemia are neuromuscular and cardiovascular toxicity. Mild symptoms including nausea, light-headedness and confusion exacerbate into worsening drowsiness, loss of deep deep tendon reflexes, hypotension and bradycardia when its concentration exceeds 7mg/dL (Qazi et al., 2021). In addition, serious hypermagnesemia higher than 12mg/dL is life-threatening inducing paralysis, respiratory depression, and cardiac arrhythmias (Qazi et al., 2021). Heart block

and cardiac arrest would also appear in extreme case when magnesium exceeds 15mmol/L (Morisaki et al., 2000). Clearly as well as playing a crucial role in numerous physiological processes, defects in magnesium homeostasis contribute to many clinical diseases. An understanding of magnesium transporters is therefore important to understand disease mechanisms.

1.2 Mg transporters

The magnesium transport mechanisms operating at the level of the cell membrane or cellular organelles membranes, mainly mitochondria and Golgi, are regulated by ion channels and exchangers. Generally, the channels are predominantly involved in Mg accumulation while exchangers mainly mediate Mg extrusion (Romani, 2011). Energy-coupled mechanisms are required for Mg efflux because this occurs against the electrochemical gradient. Specifically, a large body of experimental evidence indicates that Mg efflux occurs via Na-dependent and Na-independent routes (Romani, 2007a). The 41st family of solute carriers' member 1 (SLC41A1), has been characterized as a Na/Mg exchanger responsible for Mg efflux (Fleig et al., 2013). In contrast, Mg influx normally by diffusion from the higher free concentration in extracellular lumen and facilitated by the negative potential on cytosolic side (Romani, 2011). The transporters responsible for Mg influx mechanisms include claudins, transient receptor potential melastatin 7 (TRPM7), TRPM6, solute carrier family 41 (SLC41), ancient conserved domain protein/cyclin M (CNNM), magnesium transporter 1 (MagT1), membrane Mg transporters (MMgTs)-1 and-2 in Golgi, and mitochondrial RNA splicing 2 (Mrs2) etc. (Romani, 2011).

1.2.1 Magnesium transporter (MagT1)

MagT1 was firstly discovered in 2005 by Goytain et al. as a gene upregulated in low magnesium conditions (Goytain and Quamme, 2005b). It is highly expressed in liver, heart, kidney and colon, which is also detectable in intestine, spleen, brain and lung in mice (Goytain and Quamme, 2005b). MagT1 contains 5 transmembrane domains but the mature MagT1 protein only has 4 transmembrane domains owing to the cleavage of the first transmembrane segment near the N-terminus (Romani, 2011). Unlike other ion channels, MagT1 is highly selective for magnesium (Km=0.23mM) rather than permeable to other

divalent cations (Ravell et al., 2014), and does not share homology with other prokaryotic Mg transporters (Goytain and Quamme, 2005b). MagT1 is ubiquity expressed in the plasma membrane, is particularly abundant in epithelial cells, and is also involved in the immune functions of T and B cells (Wolf and Trapani, 2011). Magnesium and MagT1 are key regulators of T-cell-mediated immune reactions, whose deficiency results in the delayed phosphorylation of phospholipase Cγ1 (PLCγ1) as well as reduced downstream calcium flux (Ravell et al., 2014). Meanwhile, the loss of function mutation in the gene encoding MagT1 (located in human chromosome Xq 13.1-13.2) generates XMEN disease (X-linked immunodeficiency with magnesium defect, EBV infection, and neoplasia), which is characterized by chronically high-level of EBV (Epstein-Barr virus) and increased infected B-cells subsequently leading to lymphomas (Ravell et al., 2014). Tumor Suppressor Candidate 3 (TUSC3) is a homologue of MagT1 and the two proteins function co-operatively to control magnesium uptake (Zhou and Clapham, 2009). Knockdown of either transporter impairs magnesium uptake or inhibits vertebrate embryonic development. However, exposure to low magnesium concentration environment, significantly up regulates the mRNA levels of MagT1 but not those of TUSC3 (Zhou and Clapham, 2009). Therefore, MagT1, with high selectivity for Mg, is strongly suggested to be the crucial regulator of magnesium homeostasis in mammalian cells.

1.2.2 Mitochondrial RNA splicing 2 (Mrs2)

Mitochondrial RNA splicing 2 (Mrs2) was firstly discovered in yeast and shares short regions of homology to the bacterial magnesium transporter CorA (Bui et al., 1999). Yeast Mrs2 protein (yMrs2p) shares a similar membrane topology of 2 transmembrane domains with CorA. The human Mrs2 gene, localized on chromosome 6 (6p22.1-p22.3), encodes hsaMrs2p protein, which is functionally homologous to yMrs2p (Zsurka et al., 2001). The involvement of Mrs2 in mitochondrial magnesium homeostasis in yeast has been well documented. Mrs2 forms a high conductance Mg-selective channel in the inner mitochondrial membrane, and its deficiency in yeast causes reduced magnesium in the mitochondrial matrix (Kolisek et al., 2003). Meanwhile, its function is affected by mitochondrial dysfunction and inhibitors of the F0-F1-ATPase, the power source of ATP synthesis (Zheng and Ramirez, 2000). Knockdown of Mrs2 in HEK293 cells has been reported to impair complex I expression in mitochondria

(Piskacek et al., 2009), additionally cells shows increased incidence of apoptosis. Whether magnesium deficiency is simply caused by the absence of Mrs2 or collaboratively with absence of complex I requires further investigation. To conclude, Mg is dynamically regulated by Mrs2 within mitochondria in which it plays a significant role in modulating mitochondrial dehydrogenases and oxygen consumption (Romani, 2011).

1.2.3 Claudin-16 and Claudin-19

Claudin-16 and Claudin-19 play important roles in magnesium reabsorption in the thick ascending limb (TAL) of the loop of Henle (Hou and Goodenough, 2010). The claudin family contains 4 transmembrane spans coordinated by 2 extracellular loops and both N- and C- termini on the cytoplasmic side (Lal-Nag and Morin, 2009). Positional cloning strategy has identified missense mutation in claudin-16 and claudin-19 within FHHNC (Familial hypomagnesaemia with Hypercalciuria and Nephrocalcinosis) patients (Simon et al., 1999). FHHNC is a rare autosomal recessive tubular disease characterized by rapid loss of renal Mg and Ca and leads irreversibly to renal failure (Simon et al., 1999). The TAL is responsible for reabsorption of 50-60% of the magnesium that is filtered. The actual route taken by the magnesium is paracellular, and the driving force comes from the transepithelial potential. Paracellular reabsorption of Mg and Ca is driven by the positive transepithelial potential (V_{te}), which is composed of a diffusion potential (V_{di}) and an active transport potential (V_{sp}) (Hou and Goodenough, 2010). It has been reported that V_{di} but not V_{sp} is dramatically reduced in claudin-16 knockout mice compared to the wild-type mice (Hou and Goodenough, 2010), which is the underlying reason for the lack driving force of Mg and Ca reabsorption. Specifically, V_{sp} is generated by net luminal K secretion and basolateral Cl absorption polarizing the TAL epithelium in its early segment. Lumen-positive V_{di} crossing the epithelium is produced by back diffusion of Na through the cation-selective tight junction (Hou and Goodenough, 2010). Therefore, the claudin-16 known-down mice with V_{di} distinctly reduced usually accounts for a concomitant loss of Na absorption through the paracellular pathway. In fact, the increased Na excretion in claudin-16 knockdown nice consequently causes hypotension and secondary hyperaldosteronism (Hou et al., 2007). Claudins on adjacent cells interact ‘head-to-head’ and control tight junction ion permeability. Interaction of Claudin-19 with Claudin-16 forms a

cation-selective tight junction that mediates Mg and Ca reabsorption (Hou et al., 2008). Although the functions of claudin-16 are not dependent on recruitment of claudin-19, the heteromeric association with claudin-19 would switch the co-polymer channel from anion selectivity to cation selectivity (Hou et al., 2008). In conclusion, claudin-16 and -19 play an indispensable role in the development of FHHNC, interestingly, of which symptoms cannot ameliorated via magnesium supplementation (Simon et al., 1999).

1.2.4 SLC41A1 (MgtE)

Solute carrier family 41, member 1 (SLC41A1) is involved in magnesium homeostasis and transport in cells of eukaryotes (Kolisek et al., 2008), which is a distant homolog of prokaryotic MgtE Mg transporters (Wabakken et al., 2003). SLC41A1 gene is widely distributed but its abundance varies among tissues, with the highest expression in heart and testis and the lowest expression in hematopoietic tissues and cells (Wabakken et al., 2003). SLC41A1 can serve as a Mg transporter to facilitate cellular Mg uptake as well as acting as Mg extrusion mechanisms dependent on the concentration gradient (Arjona et al., 2019). SLC41A1 is mainly expressed in the tubules adjacent to macula densa, distal convoluted tubules (DCTs) as well as thick ascending limb (TAL) in human kidney (Hurd et al., 2013), whose expression in kidney could be regulated by dietary Mg content (Goytain and Quamme, 2005a). Notably, co-localization of SLC41A1 and claudin-16 has been found in rat kidney sections (Hurd et al., 2013). An exon-skipping mutation in SLC41A1 (c.698G>T) has been identified associated with a nephronophthisis-like phenotype (NPHP) (Hurd et al., 2013).

Normally SLC41A1 is characterized as being a Na/Mg exchanger serving as Mg efflux mechanism (Kolisek et al., 2012). Overexpression of SLC41A1 in human embryonic kidney (HEK)-293 cells has been found a five- to ninefold increase of Mg efflux and the amplitude of Mg loss depends on the amount of SLC41A1 and induction time (Kolisek et al., 2012). However, the molecular mechanism of SLC41A1-mediated Mg transport remains elusive. Kolisek et.al suggests that SLC41A1 functions in Na-dependent manner, which could be inhibited by imipramine and quinidine, non-specific Na/Mg exchanger inhibitors (Kolisek et al., 2012). But according to the investigation by Arjona et.al, SLC41A1-mediated extrusion is not altered by ouabain, an inhibitor of Na/K-ATPase, suggesting it

functions via an electroneutral transport mode and Na-independent mechanism (Arjona et al., 2019). As well as NPHP, SLC41A1 has also implicated in other human pathophysiology. SLC41A1 gene is located within the PARK 16 (Parkinson's disease 16) locus, making it a candidate to Parkinson disease (Sturgeon and Perry Wu, 2016). Expression profiling of magnesium responsive genes (MRGs) has demonstrated that approximately 55% of preeclamptic placentas samples significantly overexpressed SLC41A1 by six-fold (Kolisek et al., 2013). Additionally, SLC41A2, another isoform of SLC41 family, which shares over 70% homology with SLC41A1 also mediates voltage-dependent Mg current but without influence by low Mg diet (Romani, 2011).

1.2.5 Na-dependent and Na-independent Exchanger

A large body of experimental evidence indicates that cellular Mg efflux involves Na-dependent and Na-independent systems. Na-dependent Mg extrusion mechanism was first identified by Günther et al., (Günther and Vormann, 1985), occurring by stimulation of cAMP production in the presence of a physiological concentration of extracellular Na (Cefaratti and Ruse, 2007). It is generally accepted that the transcellular Mg transport consists of Mg influx, such as TRPM6 and TRPM7 (Chubanov et al., 2016, Schmitz et al., 2003), at the apical membrane and Mg efflux at the basolateral membrane, playing important role in transepithelial Mg absorption. It has been reported that Na/Mg exchangers are responsible for basolateral Mg efflux (Funato et al., 2018, Quamme, 1997). Although Na-dependent magnesium transport activity has been identified in a variety of mammalian cell types, the protein responsible for this has not been identified yet (Standley and Standley, 2002). For example, Cyclin M (CNNM) belongs to one type of Na/Mg exchanger, and is necessary for in Mg efflux at the basolateral membrane to maintain magnesium homeostasis (Yamazaki et al., 2016, Funato et al., 2018). In HEK293 cells transfected with CNNM4, fluorescent Mg-sensitive probes detect Mg efflux activity which is abolished by removing extracellular Na (Yamazaki et al., 2016) . CNNM is a type of evolutionarily conserved protein from bacteria. Recessive mutations in CNNM4 are related to Jalili syndrome (Daneshmandpour et al., 2019), and dominant CNNM2 mutation associated with hypomagnesemia (Stuiver et al., 2011). CNNM2 is crucial in the development for brain and its mutation also leads to seizures (de Baaij, 2015).

Meanwhile, CNNM3 and CNNM4 could selectively bind to the TRPM7 to mediate the uptake of divalent cation (Bai et al., 2021).

An alternative Na-independent Mg extrusion mechanisms has been detected in the absence of extracellular Na, mainly in erythrocytes and hepatic cells (Keenan et al., 1996). This mechanism utilises different cations (Ca or Mn) and anions (HCO3, Cl or choline) to achieve Mg efflux (Ebel et al., 2004). However, this transporter is far from being well characterized. Besides, Mg efflux observed in experimental models also includes Mg/Mg antiporter, Mn/Mg antiporter and Ca/Mg exchanger (Romani, 2007a). The mechanisms of Na-dependent Mg extrusion rely on the presence of physiological concentrations of cellular ATP but the Na-independent mechanisms do not demonstrate strong ATP-dependence (Ebel et al., 2004, Günther and Vormann, 1990). However, the underlying mechanisms and specificity of these exchangers require further investigation.

1.2.6 TRPM6 and TRPM7

TRPM6 and TRPM7 both belong to the transient receptor potential melastatin (TRPM) family, composed of divalent cation permeable ion channel and α-kinase domain. TRPM6 was first confirmed as an important Mg regulator owning to its association with hypomagnesemia with secondary hypocalcaemia (HSH) (Lainez et al., 2014). Loss of function mutations in TRPM6 gene (also known as CHAK2) were identified within HSH patients by genetic analysis. TRPM6 is predominantly expressed in the colon and the distal convolute tubule (DCT) of the nephron (Schlingmann et al., 2002), and its tissue distribution emphasises its role in controlling whole body Mg homeostasis via intestinal absorption and renal reabsorption. Furthermore, Nadler et al first identified TRPM7, sharing ~50% sequence homology with TRPM6, plays a key role in transporting Mg into cells and modulating cell growth (Nadler et al., 2001). Deletion of TRPM7 in B-lymphocytes induces proliferative arrest and cellular quiescence and it is lethal in early embryonic mice (<day7.5) (Nadler et al., 2001, Jin et al., 2008). Supplementing with high concentrations of Mg or co-expression of phosphotransferase-deficient TRPM7-mutant, plasma membrane Mg transporters MagT1 and SLC41A2 could ameliorate Mg uptake and assist growth of TRPM7-deficient cells (Schmitz et al., 2003, Deason-Towne et al., 2011, Sahni et al., 2007). TRPM7 protein is ubiquitously expressed in a varying extent in all

mammalian cells and forms a tetramer (Nadler et al., 2001). TRPM6 also forms heterologous tetramer with TRPM7 to function at the plasma membrane. TRPM7 kinase-deficient mice demonstrate hypomagnesaemia and defects in intestinal Mg absorption (Ryazanova et al., 2010). Localized TRPM7 deficiency affects organogenesis in a tissue-specific manner. Targeted deletion of TRPM7 in kidney leads to a reduction in glomeruli number, dysfunction of the basement membrane and renal tubular dilation (Jin et al., 2012). Notably, TRPM7 is unique with its kinase domain which could phosphorylate itself and a series of substrates, which allows it to play a broader role in cellular biology beyond maintaining magnesium homeostasis. For example in neurons, inhibition of TRPM7 reduces anoxia-induced Ca uptake, reactive oxygen species production and cell death (Aarts et al., 2003). Owing to the important biological and pathological roles of TRPM7 and TRPM6 in magnesium homeostasis and cell growth, those mechanisms would be discussed in detail subsequently.

1.3 TRP family

1.3.1 Superfamily of TRP channel

Transient receptor potential (TRP) multigene superfamily encodes a large and diverse family of integral membrane proteins that form channels that are cation permeable, which is an ancient protein highly conserved in animals, yeast, algae and other unicellular organisms (Montell, 2005). The TRP ion channel consists of non-selective monovalent and divalent cation channels with variable Ca/Na permeability, specifically some without permeability to Ca whereas some with high Ca selectivity, such as TRPV5 and TRPV6 (PCa:PNa>100) (Montell, 2005). As the most diverse ion channel superfamily, TRP channel has been divided into seven subfamilies in accordance with sequence homology, including TRPC (canonical), TRPV (vanilloid), TRPM (melastatin), TRPA (Ankyrin), TRPML (mucolipin), TRPP (polycystin) and TRPN (NOMPC-like) (Nilius and Owsianik, 2011) (Figure 1.1). Among those, the first four subfamilies are closer to Drosophila TRP homology with TRPC being the closest one. TRPML and TRPP were found when characterizing the human phenotypes triggered by mutant genes, mucolipidosis type IV (MCOLN, Mucolipin) and polycystic kinase disease (PKD) separately (Pan et al., 2011). TRPN, which is a mechano-sensitive channel, only exists in invertebrates and fish (Nilius and Owsianik, 2011). A few known

characteristics are shared among their structures, including six putative transmembrane domains, the ion pore formed between segments 5 and 6, the highly conserved TRP domain (23-25 amino acids) (Montell, 2005).

TRP channels normally assemble as homo- or hetero- tetramers to form channels, with multiple gating mechanisms ranging from ligand binding, voltage change to covalent modification to nucleophilic residues (Nilius and Owsianik, 2011). Many TRP channels could be activated by multiple stimulations which are governed by specific cellular context such as lipidation, phosphorylation, and protein interactions. The established activation modes for TRP channels are generally divided into 3 categories: 1) receptor activation such as G protein coupled receptors and receptor tyrosine kinase activating phospholipase C (PLCs); 2) ligand activation like exogenous small organic molecules (capsaicin, icilin), endogenous lipids or metabolites (diacylglycerols, phosphoinositide), purine nucleotides and their metabolites or inorganic ions (Mg, Ca); 3) direct activation such as changes in ambient temperature (Ramsey et al., 2006).

It is generally acknowledged that TRP ion channels are involved in diverse biological functions due to universal expression in numerous cell types. For instance, they sense diverse stimuli including vision and hearing in invertebrate and temperature and pain sensation in mammalian, additionally they also sense osmotic stress and maintain ionic homeostasis such as magnesium and calcium (Clapham, 2003).

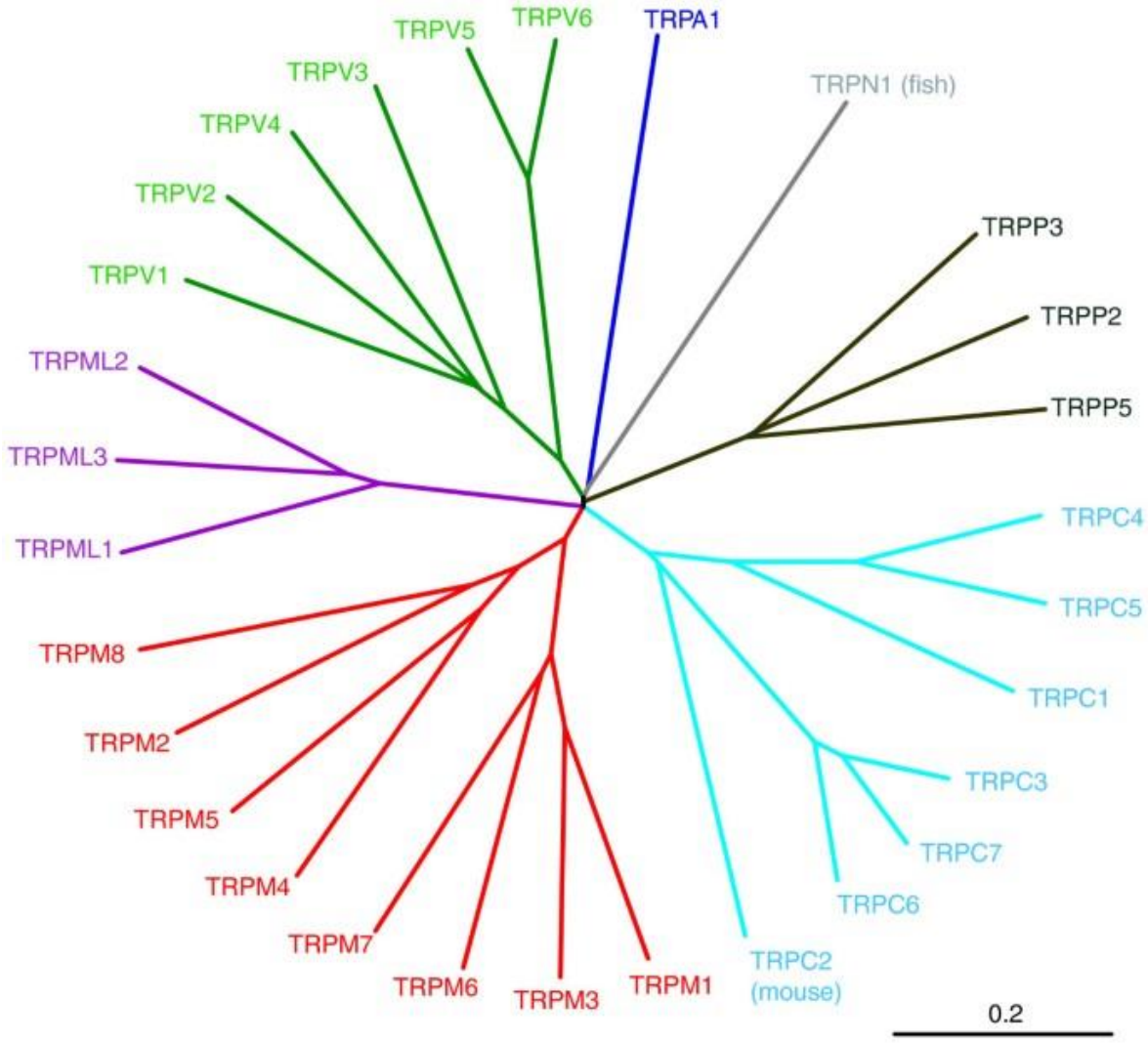

Figure 1.1 The phylogenetic tree of human TRP channels (Nilius and Owsianik, 2011)
There are 7 subfamilies of TRP channels. However, TRPC2 is the pseudogene in human and TRPNs are not present in mammals. Every TRP subfamily is represented by distinct colours. The scale bar represents 0.2 substitutions.

1.3.1.1 TRPCs channels

The first TRP subfamily identified are referred as the “classical “or “canonical” TRPCs channels, containing three to four ankyrin repeats, which share considerable homology with Drosophila TRP (Montell, 2005). Drosophila TRP is a necessary phototransduction gene, which responds to the inositol phospholipid signalling cascades (Wes et al., 1995). In many cells, after activating phospholipase C(PLC), Inositol 1,4,5-trisphosphate (IP3) production is normally accompanied by accumulation of cytosolic Ca (Wes et al., 1995). The initial burst of calcium is due to the direct action of IP3 on IP3-dependent internal stores mobilizing the release of Ca. This is followed by protracted Ca entry through the plasma membrane, which is referred to as store-operated Ca entry (SOCE) (Wes et al., 1995, Montell, 2005). In accordance with the light-induced

phosphoinositide hydrolysis in drosophila, two types of ion channels were activated: one is Ca-selective and the other is cation-nonselective (Hardie and Minke, 1993). TRP is the candidate channel for the SOCE mechanism. Therefore, Mammalian TRPC proteins, sharing at least 30% homology with Drosophila TRP, have the common feature of activation via different isoforms of phospholipase C (PLC) (Venkatachalam et al., 2002).

Mammalian TRPC subfamily is composed of seven members (TRPC1-7) and only six of them are expressed in human, excluding TRPC2 as pseudogene whose complete gene has been lost in human evolution (Yildirim and Birnbaumer, 2007, Gees et al., 2010). All mammalian TRPC proteins contains 3-4 ankyrin repeats domains (ARD) and coiled-coli domain in N-termini, six putative transmembrane domains, a hydrophobic loop assisting the outer vestibule and upper gate of the pore, and conserved TRP domain and proline-rich motif in cytoplasmic C-termini (Asghar and Törnquist, 2020, Formoso et al., 2020). Based on the functional and sequence similarities, TRPCs can be divided into 4 subgroups: TRPC1, TRPC4/5, TRPM3/6/7 and TRPC2 (Gees et al., 2010). TRPC1 is a voltage insensitive ion channel which is ubiquitously expressed in human tissues including brain, testis, ovaries and in the cardiovascular system (Zhu et al., 1995). It has been identified interacting with IP3R (inositol 1,4,5-trisphosphate receptor) to mediate SOCE (ROSADO and SAGE, 2000). This association could be block by xestospongin (an IP3R antagonist blocker) and subsequent studies revealed this interaction is reversible, specifically the TRPC1-IP3R complex dissociates upon refilling of the stores (ROSADO and SAGE, 2000, Rosado et al., 2002). Besides, TRPC1 also interacts with caveolin-1 which contributes to its localization in plasma membrane, regulating SOCE in endothelial cells (Sundivakkam et al., 2009). With those features, TRPC1 has been implicated in many biological progresses. For example, TRPC1 channel localizing in sarcoplasmic reticulum (SR) of cardiomyocytes regulates [Ca]i is proposed to regulate cardiac hypertrophy (Hu et al., 2020), and its expression in skeletal muscles could maintain cellular Ca homeostasis, regulate myoblast migration and differentiation (Yeung et al., 2017).

Similarly, functional coupling and a physical interaction between TRPC3 and IP3R has also been demonstrated (Zhu and Tang, 2004). The structurally related TRPC3 family members TRPC6 and TRPC7 (which share 75% identity) are also

activated in a PLC-dependent manner, involving diacylglycerol (DAG) but without dependence on G protein or IP3 (Zhu and Tang, 2004). In addition, TRPC3 is abundant in in brain, cardiac and smooth muscle cells (Riccio et al., 2002), and TRPC6 is highly expressed in lung and brain whereas TRPC7 is enriched in the kidney and pituitary gland (Gees et al., 2010). TRPC3 activation via IP3 leads to constriction of cerebral arteries and induces synaptogenesis and growth cone guidance (Gees et al., 2010). TRPC6, as the vascular α1-adrenoceptor-activated Ca-permeable cation channel in smooth muscle, plays an important role in regulating vascular smooth muscle contractility and blood pressure (Dietrich et al., 2005). TRPC3, TRPC6 and TRPC7 normally assembled either homo-tetrameric or hetero-tetrameric channels by complexing among themselves (Trebak et al., 2003).

TRPC5 is mainly expressed in brain tissues, where functions include neurite extension and growth cone morphology as well as neurotransmission and learning (Greka et al., 2003). Alongside TRPC4, TRPC5 also maintains blood pressure at aortic baroreceptors and plays a crucial role in endothelium-dependent contraction in carotid arteries (Wang et al., 2020). TRPC1 can form a hetero-tetrameric complex with TRPC4 or TRPC5, where it serves as negative modulator of TRPC4 and TRPC5, and might be the new targets in neurological disorders such as Parkinson’s disease (Kim et al., 2019).Overall, most TRPCs can be activated via a store-operated mechanism involving PLC, and IP3 results in transmembrane calcium influx. Besides, the comprehensive expression of TRPCs in multiple cell types and tissues contributes its functions in a broad spectrum of cellular functions and physiological roles.

1.3.1.2 TRPVs channels

Apart from TRPC channels, the rest of TRP subfamilies are named after the original designation of the first discovered member of each subfamily (Montell, 2005). TRPV subfamily is named based on Vanilloid Receptor 1 (VR1), now known as TRPV1, which is activated by vanilloid compounds such as capsaicin found in spicy food (Montell et al., 2002, Clapham, 2003). There are six members in TRPV subfamily (TRPV1-6), which can be further divided into two subgroups, TRPV1-4 and TRPV5/6, sharing approximately 40-50% and 75% sequence identity separately (Zheng, 2013, Pumroy et al., 2020). Structures of TRPV channels have

common features of all TRPs, consisting of six transmembrane domains and ion pore formed between segment 5-6. Similarly, TRPV subunits also form both homo-tetrameric and hetero-tetrameric channels (Baylie and Brayden, 2011). TRPV1-4 have been recognized as the thermosensitive channels, which could convert the thermal energy into electrical activity in host cells (Yang et al., 2010). TRPV1-4 homomeric channels are weakly Ca-selective, however, TRPV5 and TRPV6 are highly Ca-selective in both homomeric and heteromeric channels but without heat-activation (Zheng, 2013). The temperature activation sites of TRPV1-4 might reside around the pore forming regions which are also crucial to temperature sensitivity (Kim et al., 2013). For instance, mutations of specific sites in the putative sixth transmembrane helix and the adjacent extracellular loop in the pore region of TRPV3 abolish its heat activation without interfering with its chemical activation (Grandl et al., 2008). In addition, the N-terminus of TRPV channels contains six ARDs (Baylie and Brayden, 2011). The ARD1-3 display long and flexible fingers with numerous exposed aromatic residues, whereas the ARD5-6 contain unusual long outer helices (Jin et al., 2006). These ARDs are required for trafficking to membrane, subunits tetramerization and protein interactions (Erler et al., 2004, Jin et al., 2006). The cytoplasmic C terminus also participates in membrane trafficking (Becker et al., 2008), subunit assembly and temperature sensitivity (Baylie and Brayden, 2011). The highly conserved hydrophobic domain on the C terminal side of transmembrane domains, the TRP box, allows TPRVs to be modulated by PIP2 like the other TRPs (Rohacs, 2009).

Clusters of sensory neurons, dorsal root ganglia (DRG), localizing in the vertebral column lateral to the spinal cord, and cranial nerve ganglia such as the trigeminal ganglion allow mammals to sense temperature stimulation (Patapoutian et al., 2003). TRPV channels as the principal heat temperature sensors in the sensory nerve ending of mammals subsequently allow generation of appropriate reflexive and cognitive response to peripheral stimulation (Voets et al., 2004). TRPV1-4 are all classified as thermosensitive channels whose temperature thresholds are graded (Cheng et al., 2007). TRPV1 is activated by hot temperature in noxious range >43 °C with an upper threshold of approximately ~52 °C (Caterina et al., 1999). Heat-induced activation of TRPV1 is the result of a drastic leftward shift of the voltage dependence of activation (Voets et al., 2004). TRPV2, sharing ~44% with TRPV1, is activated at higher

temperature of >52 °C but without sensitivity to capsaicin (Caterina et al., 1999). In addition, the activation temperature threshold of TRPV3 is between 31°C and 39°C (Kim et al., 2013) whereas TRPV4 is activated by innocuous warm temperature >27°C (Cheng et al., 2007). TRPV1 has been proved important in the thermal hyperalgesia during inflammation or after tissue injury (Caterina et al., 2000). TRPV3 is not only distributed in the neuron system such as dorsal root ganglia and trigeminal ganglion but also expressed in epithelial cells of skin, tongue and gastrointestinal tract, which allow it to act in warm-sensitive neurons as well as maintaining skin health (Clapham, 2003). In contrast, TRPV5 and TRPV6, only sharing around 30% sequence identity with TRPV1, are a distinct subfamily of homomeric and heteromeric channels distributed in transporting epithelia of the kidney and intestine (Clapham, 2003). They are the most Ca-permeable TRP channels (PCa:PNa >100)with strong inwardly rectifying currents (Zheng, 2013).

1.3.1.3 TRPA channel

Mammalian TRPA subfamily is only composed of 1 family member, founding TRPA1, which is distinguished by a large number (~14) of ankyrin repeats in its N-terminal domain (Clapham, 2003). TRPA1 channel is activated by noxious cold temperature < 17°C (Story et al., 2003), however it is distinct from TRPM8, another cold-/menthol-activated channel. Meanwhile, TRPA1 is also activated by bradykinin via the PLC-coupled signaling pathway (Montell, 2005), as well as by chemical stimulation from plants or spices such as cumin aldehyde, an unsaturated aldehydes (Legrand et al., 2020). TRPA1, as the Ca-permeable cation channel, is expressed in sensory neurons and epithelial cells in many organs, and is implicated in acute and chronic pain and inflammation progress (Talavera et al., 2020). In addition, TRPA1 is proposed to form a mechanically gated channel which is necessary for hearing mechano-transduction (Corey et al., 2004).

1.3.1.4 TRPML channels

The TRPML subfamily is named after human protein encoded genes, mucolipidin (MOCLN), constituting 3 family members (Montell, 2005), respectively TRPML1 (MCOLN1), TRPML2 (MOCLN2) and TRPML3 (MOCLN3). They are all non-selective

Ca-permeable tetrameric cation ion channels with six putative transmembrane domains(S1-S6) and a large extracellular loop between S1-S2 (Chen et al., 2017, Montell, 2005). TRPML is predominately localized in lysosomes where it controls lysosomal Ca release, transport and pH homeostasis (Morgan et al., 2011). Mutation of MCOLN1 is associated with phenotype of mucolipidosis type IV (MLIV), a lysosomal storage disorder triggering severe neurodegenerative deficits (Clapham, 2003).Apart from neurons, TRPML1 is expressed in many tissues such as adrenal gland, lung, bladder, spleen, and placenta (Santoni et al., 2020). However, TRPML2 has limited expression in lymphoid and myeloid tissues, and might be a potential player in immune cell development and inflammatory reactions (Cuajungco et al., 2016). Additionally, TRPML3 is mainly found in the cochlear and vestibular sensory hair cells and melanocytes (Santoni et al., 2020), whose deficiency leads to early-onset deafness and pigmentation defects in varitint-waddler mice (Di Palma et al., 2002).

1.3.1.5 TRPP channels

The archetypal TRPP channel member, TRPP2 (also known as polycystin 2), was identified as a gene mutated in many cases of autosomal dominant polycystic kidney disease (ADPKD). ADPKD is a potentially lethal monogenic disorder in humans with incidence of ~1/400 to 1/10000 which is caused by either one or two genes mutation, PKD1 or/and PKD2, encoding Polycystin-1(PC-1) and TRPP2 respectively (Hofherr and Köttgen, 2011). Mammalian TRPP subfamily also includes two more proteins which are predicted to contain six transmembrane domain and form non-selective cation permeable channels, TRPP3 and TRPP5 (Hofherr and Köttgen, 2011). TRPP3 is a cation channel activated by calcium and proton involved in sour tasting and intestinal development, whose function would be regulated by palmitoylation and phosphorylation of N-terminus (Zheng et al., 2016). TRPP5 is developmentally expressed in testis where it is proposed to control intracellular free calcium homeostasis (Xiao et al., 2010). However, TRPP5 channel activity still needs further investigation. TRRP orthologues in mammals are highly conserved, ranging from ~80% (TRPP5) to ~90% (TRPP3) identities compared to TRPP2 (Qian and Noben-Trauth, 2005). The larger protein TRPP1 contains 11 transmembrane (TM) domains which includes a C-terminal 6-TM TRP-like channel domain (Clapham, 2003). Complex of co-expression of TRPP1 and TRPP2 assists TRPP2 translocation to the plasma membrane and

increases its channel activity (Hanaoka et al., 2000). The localization of TRPPs to both motile and primary cilia in different organs allows them to respond to fluid flow (Montell, 2005). For instance, TRPP2 and PKD1 localise targeted to primary cilia of renal cells, where their deficiency induces alterations in polarization and function of cyst-lining epithelial cells resulting in ADPKD (Hofherr and Köttgen, 2011).

1.3.2 TRPM family

The TRPM (transient receptor potential melastatin) is the largest and the most diverse subfamily of the TRP superfamily, with eight family members in mammals (TRPM1-8) (Huang et al., 2020). All the TRPM channels have several large domains of 732-1611 amino acids for each subunit, sharing several common characters such as N-terminal TRPM homology region (MHR) domain, six transmembrane domain (TMD), a hydrophobic TRP helix, a C-terminal coiled-coil domain and C-terminal domain (CTD) (Huang et al., 2020). TRPM2, TRPM6 and TRPM7 are unique proteins of TRPM subfamily with encoded enzymatically active protein fused to ion channel structures (Ramsey et al., 2006). In accordance with the sequence identity, TRPM family could be divided into 4 subgroups, respectively TRPM1/3, TRPM2/8, TRPM6/7 and TRPM4/5 (Ramsey et al., 2006). All those members are widely expressed and most of them are non-selective Ca-permeable cation channels, except TRPM4 and TRPM5. TRPM4 and TRPM5 are both activated by intracellular Ca but they are only permeable to monovalent cations (Launay et al., 2002, Hofmann et al., 2003). Openings of TRPM4 channels are long-term(several hundred milliseconds) whereas those of TRPM5 channels are transient (Liman, 2006).

TRPM1 is highly expressed in skin melanocytes and its expression level is reduced in highly metastatic cell lines, suggesting it may act as a prognostic marker for metastasis of localized melanoma (Duncan et al., 1998). Its close homologue TRPM3, is mainly expressed in human kidney and brain (Fleig and Penner, 2004). Human TRPM3 is predominantly found in the collecting tubular epithelium in kidney where it controls Ca entry to maintain renal Ca homeostasis (Grimm et al., 2003). TRPM2 is an enzymatic ion channel with nucleotide pyrophosphatase activity in the Nudix domain at its C-terminus (Perraud et al., 2001), which is crucial for channel gating by ADP-ribose (ADPR). TRPM2 is highly expressed in

the brain, particularly cerebral cortex, where it is primarily localized in the microglial cells, the host macrophages in central nervous system (CNS) responding to brain injury and neurological disease (Kraft et al., 2004, Gees et al., 2010). Transcription analysis also illustrates that TRPM2 is widely expressed in the immune system, gastrointestinal tissues, and pancreatic islet-derived cells (Perraud et al., 2003). TRPM2 channels could be activated by ADP-ribose and reactive oxygen species (ROS), allowing it to participate in oxidant responses of mammalian immune cells and self-induced removal of cells irreversibly damaged by exposure to oxidants (Perraud et al., 2003). Circulating uromodulin blocks TRPM2 mediated calcium influx and prevents oxidant-induced damage to the kidney and systemically (LaFavers et al., 2019). TRPM8 was initially identified from the prostate cancer cells, and subsequently found in cold-responsive dorsal root ganglia (DRG) neurons and trigeminal ganglia (Peier et al., 2002). TRPM8 is activated by cold temperature (8-28°C) and chemicals which produce a cold sensation such as menthol (Peier et al., 2002). Although little is known about a role for TRPM8 in prostate cancer, its role as cold thermosensor in sensory neurons is delete clear. Meanwhile, some other TRPM family members are also sensitive to temperature, for instance, TRPM4/5 are warm-temperature activated (15°C-35°C) (Talavera et al., 2005) and TRPM3 ion channels localized in neurons are activated by temperatures around 40°C (Vriens et al., 2011). As previously mentioned, TRPM4 and TRPM5 generate nonselective monovalent cation currents such as Na and K. Although TRPM4 is non-permeable for Ca, it can mediate Ca entry/efflux via membrane potential depolarization depending on cell types (Fleig and Penner, 2004). TRPM4 is relatively highly expressed in heart, pancreas and placenta, and TRPM5 is mainly expressed in taste buds of the tongue, where it exerts large effects on the perception of sweet, Unami and bitter tastes (Talavera et al., 2005).

The molecular structure and electrophysiological functions of TRPM7 and TRPM6 are quite close. They both could activated by free Mg and Mg-ATP complex, as well as forming hetero-tetrameric ion channel to conduct Ca and Mg with same current-voltage relationship and sensitivity to blockers (Fleig and Penner, 2004). As the accumulating evidence revealed importance of TRPM6 and TRPM7 in maintaining magnesium homeostasis and mediating signalling cascade in

different cells, we are interested to investigate the regulatory mechanism of TRPM7 and TRPM6.

1.4 TRPM7/TRPM6

1.4.1 TRPM7 and TRPM6 characterization & function

Alongside TRPM2, TRPM7 and its close homologue TRPM6 (~50% identity) are other two extraordinary bifunctional proteins in TRPM subfamily. They have two distinct functional moieties, respectively an ion channel and α-type serine/threonine kinase domain (Fleig and Chubanov, 2014). Although they were most commonly studied as modulators of magnesium homeostasis, both ion channel are characterized by highly unusual permeation properties with a range of essential and toxic divalent metal ions including Ca and Zn (Gees et al., 2010). Their enzymatic domain has been classified as atypical alpha protein kinase (Yamaguchi et al., 2001). The initial identification of kinase activity is due to a strong sequence similarity between ~300 residues of C-terminal region and atypical protein kinases known as α-kinases, which is phospholipase C-interacting kinase (Yamaguchi et al., 2001). Subsequently, the kinase domain activity and ion channel activity of TRPM7 were identified.

From phylogenetic analysis, orthologs of mammalian TRPM7 and TRPM6 have been identified in genomes of birds (Gallus gallus) and fish (Fugu rubripes), suggesting those genes were generated approximately 450 million years ago before divergence of fish and land vertebrates (Chubanov et al., 2005). As highly evolutionarily conserved ion channel, TRPM7 and TRPM6 play important roles in embryonic development and cell growth. Compared to all other TRP facility members, RT-PCR finds TRPM7 to be the most abundantly expressed TRP channel in most adult mouse organs (such as brain and kidney) (Kunert-Keil et al., 2006). Specifically, TRPM7 is abundantly expressed in dorsal root ganglia along the vertebral column in mouse, and shows two peaks in expression, one at embryonic day 18 and the other one after postnatal day 4 (Staaf et al., 2010, Fonfria et al., 2006). Tamoxifen-induced disruption of TRPM7 using multiple Cre recombinase lines in mice reveals its importance globally and in specific organ developments during embryonic development. In general, Global disruption of TRPM7 induces mice lethality before embryonic day 7 (E7) but its deficiency in

adults or after late embryonic stage(>E14.5) does not result in distinct phenotypic difference (Jin et al., 2012). Meanwhile, TRPM7 specific-deficiency in the immune system results in developmental block of thymocytes (Jin et al., 2008), and it is essential for kidney development in metanephric mesenchyme but not in ureteric bud (UB) after day E10.5-11.5 (Jin et al., 2012). Early-stage disruption of TRPM7 in neural crest leads to loss of dorsal root ganglion neurons and pigmentation whereas its late-stage disruption has no influence on normal brain development after day 10.5 (E10.5) (Jin et al., 2012). In addition, its disruption in neural stem (NS) cells does not interfere with self-renewal and differentiation into neurons and astrocytes, but does prevent differentiation of pluripotent stem cells to NS cells by blocking formation of NS cell monolayers (Jin et al., 2012). Furthermore, compared to the global TRPM7 inactivation, specific kinase functional deficiency of TRPM7 does not impede embryonic development but the adult kinase-deficient mice are resistant to dietary magnesium deprivation but have a reduced magnesium content in bone (Ryazanova et al., 2014).

In contrast to TRPM7, TRPM6 expression is predominantly limited to intestines and brain (Fonfria et al., 2006). TRPM6 activity in the placenta and yolk sac is also required for survival of embryonic development (Chubanov et al., 2016). Knockout of TRPM6 is lethal for the majority of mice at day 12.5 (E12.5), and those that survive to term have neural tube defects including exencephaly and spina bifida occulta (Walder et al., 2009). Adult TRPM6-deficent mice have shortened lifespan and impaired metabolism but can be protected by administration of high-dose magnesium. In humans loss of function mutations of TRPM6 lead to autosomal recessive hypomagnesemia, also known as primary hypomagnesemia type 1, intestinal (HOMG1) or hypomagnesemia with secondary hypocalcaemia (HSH) (Schlingmann et al., 2002). In detail, TRPM6 mutations induce impaired intestinal magnesium absorption accompanied by renal magnesium excretion, resulting in severe hypomagnesemia and hypocalcaemia associated with seizures, tetany and muscle spasms (Zhao et al., 2013).

TRPM6 cannot efficiently form a homomeric channel in the plasma membrane unless it is in combination with TRPM7, while the TRPM6 kinase is able to cross-phosphorylate TRPM7 (Schmitz et al., 2005). Heteromeric TRPM6/7 has higher constitutive activity than their individual homomers. In the presence of TRPM7

the ability of Mg to inhibit TRPM6 homomers is reduced, while TRPM6 relieves TRPM7 from inhibition by Mg-ATP (Ferioli et al., 2017). TRPM7 and TRPM6 are involved in many physiological and biological functions via maintaining ionic homeostasis and participating in signalling pathways, whose functional defects give rise to many diseases.

1.4.2 TRPM7 ion channel and kinase domain structure

TRPM7 encodes a very large integral membrane protein (1863 residues in human TRPM7), containing a characteristic N-terminal melastatin homology region (MHR) domain, six transmembrane helixes (S1-S6) similar to other TRP channels, a highly conserved TRP helix, a C-terminal coiled-coil (CC) domain and an autophosphorylation domain enriched with serine and threonine (Ser/Thr) linked to an α-type kinase domain (KD) (Figure 1.2) (Zou et al., 2019). Like other TRP channels, the linker between transmembrane segments 5 and 6 folds into a pore helix (PH) which subsequently forms the channel pore by assembling into a tetrameric complex. It is predicted that pore loops (PL) of four channel subunits contribute to an ion selectivity filter (Chubanov et al., 2018). Most TRPM channels share a similar three-layered structure, respectively transmembrane domain (TMD), melastatin homologous regions 3-4 (MHR3/4) and MHR1/2 from top to bottom, but TRPM7 and TRPM6 has a fourth layer specifically, the C-terminal kinase domain (Figure 1.3A). The pore helix (PH) is surrounded by the S1-S4 domain, which includes binding sites for agonist Ca and other ligands, considered to be key players in the gating of TRP channels (Huang et al., 2020). The MHR1/2 domain in TRPM7 forms a large hollow penetrated vertically by a part of the coiled-coil domain of the C terminus, and horizontally by a second part of coiled-coil domain (helical rib) (Figure 1.3) (Huang et al., 2020), forming a umbrella-like shape functioning in subunit assembly (Winkler et al., 2017). The helix rib is connected to the TRP helix, which is the typical feature of TRP channel, and it is adjacent to transmembrane segment 6. Importantly, TRPM6 and TRPM7 are both regulated by calcium and calcium-binding proteins (CBPs), such as Calmodulin (CaM) and S100 calcium-binding protein A1 (S100A1). Those two representative CBPs have been identified to share same binding regions in the N-terminal of TRPM6 (Zouharova et al., 2019) and in the MHR4 of N-terminal of TRPM7 (Bousova et al., 2021). This suggests that the tetrameric structure of TRPM6 and TRPM7 might allow signal from MHR of N-terminal transferring to S6

gating helix via the vertically penetrating C-terminal coiled-coil, to facilitate modulation of TRPM channel.

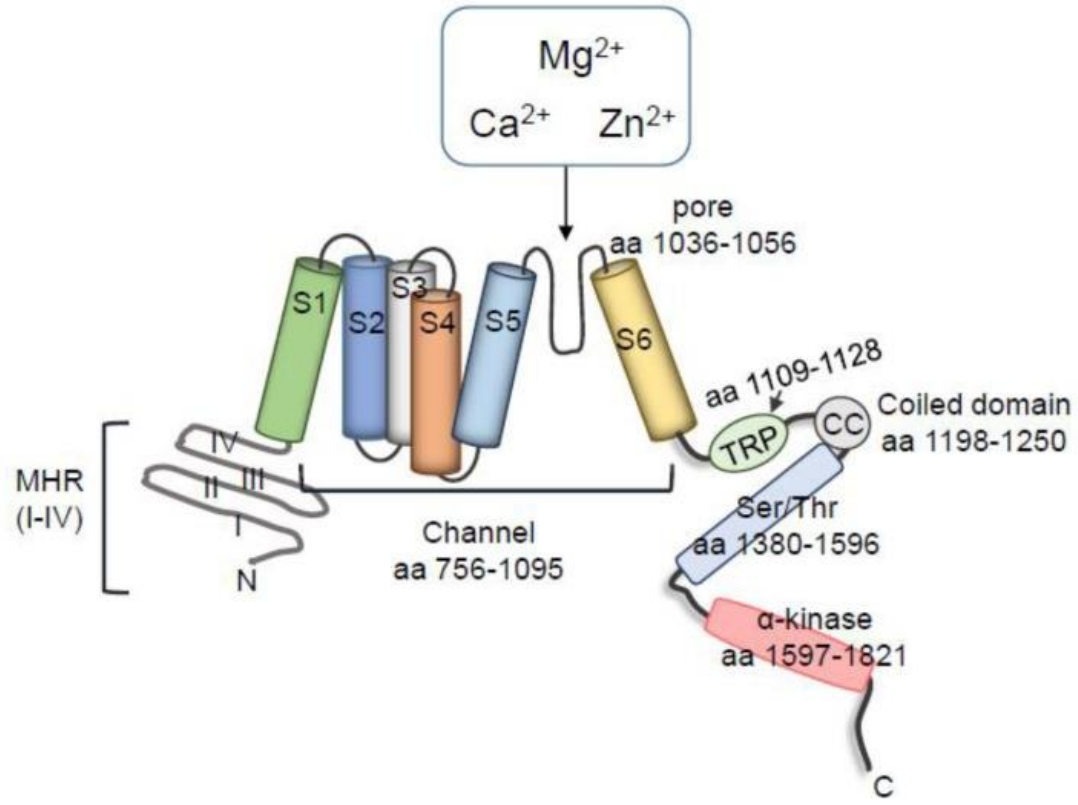

Figure 1.2 Schematic structure of TRPM7 subunit (Zou et al., 2019).
The general subunit structure of TRPM7 has four melastatin homologous regions (MHR) in N-termini and six transmembrane segments with ion pore formed between s5-s6.

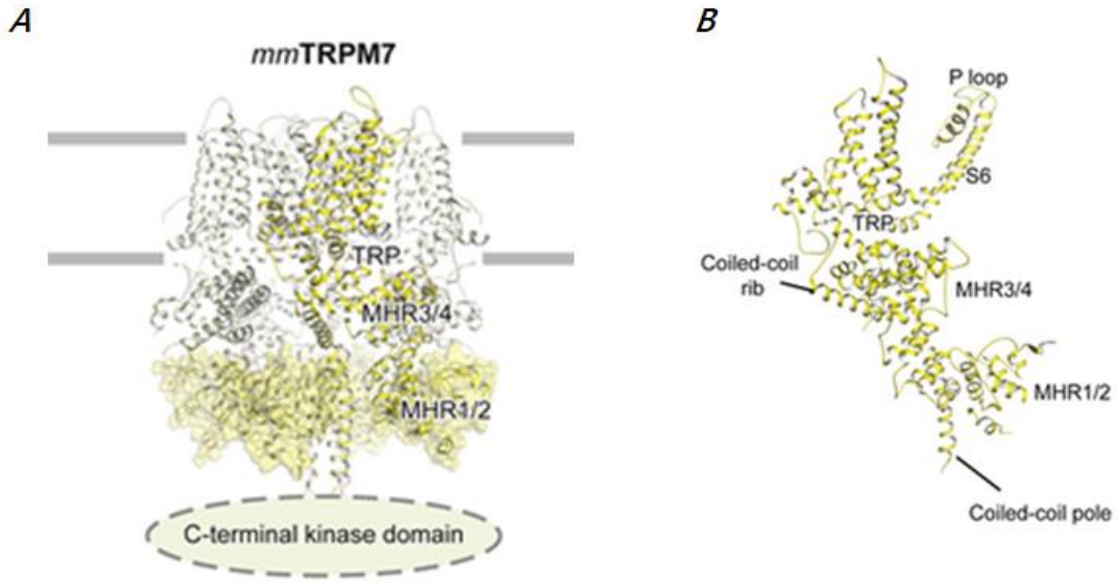

Figure 1.3 Tetrameric architecture and single subunit of mmTRPM7 (Mus musculus) (Huang et al., 2020).
Highlighting area is the interactions between the N terminal MHRs and the C terminal coiled coil.

The high-resolution crystal structure of the C-terminal coiled-coil (CC) domain and kinase domain (KD) of TRPM7 was first reported using X-ray crystallography. Unlike assembly domain of voltage-gated channels like Kv7, TRPM7 CC domain is antiparallel with D2 (dimeric kinase domains)-symmetry (Fujiwara and Minor Jr, 2008). Meanwhile, the crystallized N terminus of the TRPM7 KD is similar in its topology to the corresponding lobe of classical protein kinase such as PKA, but its C-terminal lobe resembles ATP-grasp fold enzymes (Yamaguchi et al., 2001) (Figure 1.4A). The kinase domain of TRPM7 forms a dimer which is distinct from classic protein kinase in containing a zinc ion in its hydrophobic core, which is characterized by tetrahedral geometry coordination of His 1751, His-1808, Cys-1810 and Cys-1814 (Yamaguchi et al., 2001) (Figure 1.4B). The correct coordination of this Zn binding motif is crucial to the kinase domain, where replacing two cysteines with alanine leads to complete loss of kinase activity (Diggle et al., 1999, Yamaguchi et al., 2001). Furthermore, the C-terminal of kinase domain does not have the “catalytic loop”, the characteristic features of protein kinase-fold to distinguish it from the ATP-grasp fold (Yamaguchi et al., 2001). In its C-terminus, Asp-1765 and Gln-1767 which are important for catalysis are separated by only one residue on a continuous ß strand. This would mean the lysine is the residue that separates the α-phosphate group and the adenine ring of ATP (Yamaguchi et al., 2001) (Figure 1.4A). TRPM6 has the similar structure in its kinase domain, and it can form heteromeric structure with TRPM7. It has been discovered that the dimerization motif of TRPM6 plays an important role in regulating kinase activity and ion channel activity. Site-mutagenesis of the dimerization motif or dimerization pocket (formed by linkage of extended alpha-helix of dimerization motif between two kinase monomers) would abolish dimerization and inhibit kinase activity (van der Wijst et al., 2014). In addition, disrupting the interaction between the dimerization motif and dimerization pocket substantially diminishes the ion channel activity in the kinase activity-independent manner (van der Wijst et al., 2014).

As bifunctional proteins, the functions of TRPM6 and TRPM7 are associated with kinase domain, which is proteolytically cleaved and then translocated into the nucleus to phosphorylate histones and regulate gene expression (Duan et al., 2018).However, the specific association between kinase and ion channel activities still need further investigation. TRPM7 ion channel function is

regulated by the Mg-nucleotide binding to the kinase domain (Demeuse et al., 2006) and is enhanced after cleavage of kinase domain (Desai et al., 2012). Additionally, the endogenous kinase is required for cAMP and PKA regulation (Takezawa et al., 2004). In conclusion, the unique assembly structure of TRPM7 allow it to function as an integral chanzyme connecting the tetrameric ion channel and dimer kinase domain.

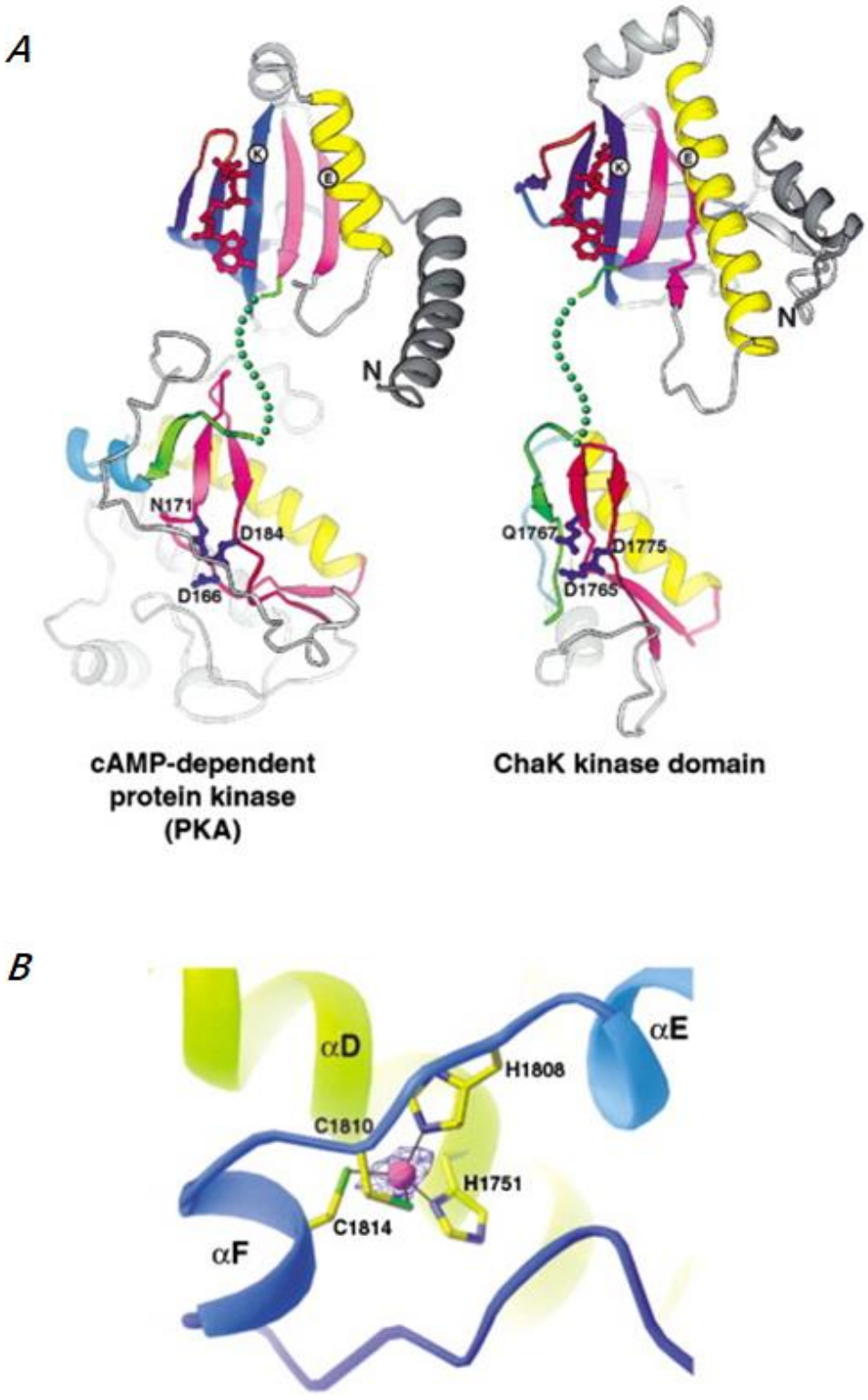

Figure 1.4 Ribbon diagrams of cAMP-dependent protein kinase (PKA) and TRPM7 (ChaK) kinase domain (Yamaguchi et al., 2001).
A) The "open book" diagram of N-terminal lobes and C-terminal lobes. The three conserved residues for catalysis are coloured in blue. B) The zinc binding motif in the ChaK kinase domain, which is coordinated by His1751, His-1808, Cys-1810 and Cys-1814.

1.4.3 Divalent cation conduction by TRPM7

As well as being a Mg channel, TRPM7 also conducts Ca and Zn. Zn conduction of TRPM7 has only been investigated in intracellular vesicles, where it releases Zn under oxidative activation (Abiria et al., 2017a). Intracellular calcium has been implicated in many cellular processes, including contractile function in muscle (Fearnley et al., 2011), gene transcription, cell proliferation and apoptosis (Zhivotovsky and Orrenius, 2011). Abnormal cytosolic [Ca]i cause by dysfunction of Ca channel, Ca transporters and Ca-binding proteins is involved in multiple pathologies. For example, mutation of voltage-operated calcium channel in plasma membrane in nervous system results in paralysis, ataxia, or migraine (Mekahli et al., 2011) and dysfunction of calcium-release channel in sarcoplasmic reticulum (SR) leads to tachycardias and tachyarrhythmias in the heart (Gyorke, 2009).

TRPM7 regulates store-opened calcium entry (SOCE) through its kinase domain which mediates Ca influx to maintain endoplasmic reticulum (ER) calcium concentration (Faouzi et al., 2017a). In addition, TRPM7 is abundantly expressed in neuronal cells where discrepancy of function and expression leads to anoxic neuron death and neurodegenerative disease (Sun et al., 2015a). During oxidative stress, reactive oxygen species (ROS) activate TRPM7 channel inducing calcium overload and increasing currents which results in cell death (Aarts et al., 2003). Besides, TRPM7 also regulates axonal outgrowth and maturation both by regulating Ca influx and by forming a scaffold to colocalize F-actin and α-actinin-1 protein complex (Turlova et al., 2016b). In heart, TRPM7 as the only calcium channel expressed in the cell membrane of cardiac fibroblasts is critical for the formation of cardiac fibrosis (Zhang et al., 2012b). Because TRPM7 ion channel is blocked by Mg, ion channel activity is often assessed by measuring the Ca uptake in experimental settings (Chubanov et al., 2012).

1.4.4 Signalling pathways of TRPM7

TRPM6 and TRPM7 have been associated with many signaling pathways and most evidence indicates they function in growth factor signaling pathways through receptor tyrosine kinases (RTK). The kinase domain of TRPM7 phosphorylates a series of substrates involved in RTK signal transduction, including annexin-A1,

myosin IIA, calpain II, Src,SMAD2 and phospholipase Cγ2 (PLCγ2) (Zou et al., 2019). Apart from those, TRPM7 with active kinase phosphorylates its relative, eukaryotic elongation factor 2 cognate kinase (eEF2-K), under hypo-magnesic condition. This regulates the eEF2 activity, which is an important modulator of ribosomal translocation during protein translation (Perraud et al., 2011). In addition, activation of TRPM7 predominantly leads to autophosphorylation within its ser/thr rich domain (Figure 1.2), which subsequently accelerates the phosphorylation of substrates (Clark et al., 2008b). It has been illustrated that the autophosphorylation of Ser/Thr enriched domain does not directly promote its enzymatic activity but does improve access of the catalytic domain to the substrates (Clark et al., 2008b). For instance, TRPM7 kinase domain accelerates phosphorylation of annexin-1 and the heavy chain of myosin IIA, suggesting a role for TRPM7 in vesicle fusion and cell adhesion (Clark et al., 2006). Importantly, TRPM7 is cleaved by caspases at Asp1510 in the Ser/Thr rich domain, and the kinase domain then translocates to the nucleus (Krapivinsky et al., 2014).

As TRPM7 has been recognized to conduct numerous divalent cation conduction, including Ca, Mg, and trace metal ions such as Fe, Zn, Cu, Mn and Co, which act as vital cofactors to the catalytic function of diverse types of enzymes in most cellular process (Monteilh-Zoller et al., 2003) . The RTKs, which induce phosphorylation of downstream kinases, crosstalk with TRPM7 ion channel and kinase domain signal transduction (Figure 1.5) (Zou et al., 2019). For example, in low intracellular [Mg] i-, TRPM7 current is inhibited by PLC-activation whereas PLC activation is associated with increase of TRPM7 currents under physiological [Mg]I- condition (Langeslag et al., 2007). Meanwhile, emerging evidence has demonstrated that EGF could activate EGFR signaling to enhance the TRPM6-current and its abundance in the plasma membrane in a Src-kinase and Rac1 dependent manner (Thebault et al., 2009). Subsequently, TRPM7 has been found to co-localized with EGFR which directly interacts with TRPM7 via c-Src dependent processes (Zou et al., 2020). These discoveries map the new crosstalk of EGF/EGFR and TRPM6/7 signaling cascade. Moreover, TRPM7 has been discovered to activate JAK2/STAT3 and/or Notch signaling pathways consequently promoting cell proliferation, migration and invasion of glioma cells (Liu et al., 2014). And in prostate cancer, knockdown of TRPM7 inhibits

cholesterol-induced Akt or ERK phosphorylation suggesting PI3K/Akt and MAPK are both downstream signaling mechanisms of TRPM7 (Luo et al., 2016).

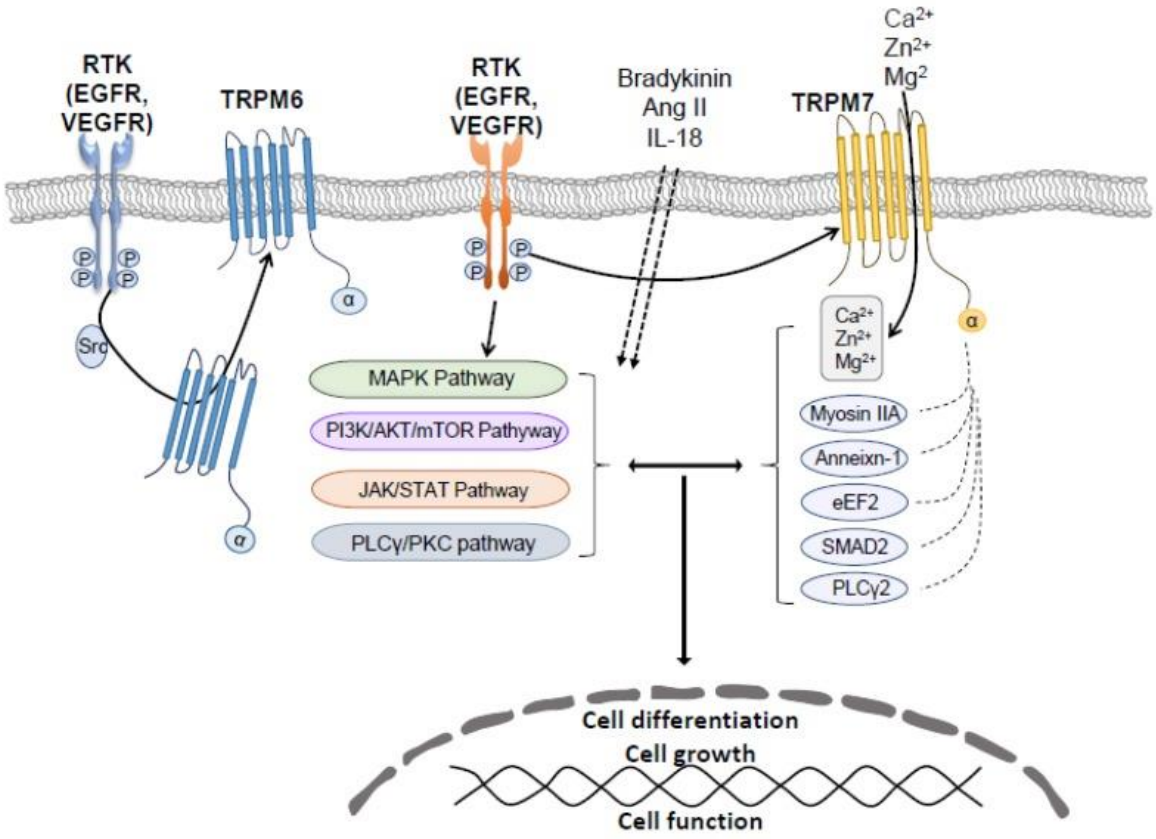

Figure 1.5 Crosstalk between Receptor Tyrosine Kinases (RTKs) downstream signaling mechanisms and TRPM7 (Zou et al., 2019).
TRPM7 is a non-selective divalent cation channel that conducts Ca, Mg and Zn and phosphorylates a series of substrates annexin-1, myosin IIA heavy chain, eEF2, SMAD2, and PLCγ2. The ionic alterations through ion channel and downstream signalling interacts with many RTK signalling pathways.

Hence the two properties of TRPM7, regulation of ionic homeostasis (Mg metabolism, Ca signaling) and phosphorylation activities produce up-/down-regulation of the effector molecules in the epidermal growth factor or other cytokines signaling mechanisms. Consequently TRPM7 regulates cellular proliferation, survival, differentiation, growth, adhesion, motility, and migration (Yee et al., 2014).

1.4.5 Regulatory mechanisms of TRPM7

Given the vital roles of TRPM7 and TRPM6 in physiological responses and embryonic development, the regulatory mechanisms of these proteins are important to investigate.

1.4.5.1 Mechanical Stress

Like other TRP channels, Homo- or hetero-tetramers TRPM7 are activated by a broad range of mechanical stimuli. Mechano- or osmomechano-sensitive channels can be activated by many mechanisms, including 1) lipid bilayer-dependent manner with deformation or bending the membrane leading to conformational change of the channel and possible activation; 2) lipid bilayer-independent manner in which forces exerted on the accessory molecules such as cytoskeletal protein further activating those associated channels; and 3) indirect manner where the channel activated by the secondary signaling components (lipases, kinases, G-proteins) generated by the mechanical force (Jin et al., 2011).

In the human epithelial Hela cells, TRPM7 serves as an intrinsic stretch- and swelling- activated cation (SSAC) channels to mediate Ca influx in a swelling-induced manner playing a vital role in cell volume regulation (Numata et al., 2007b). Meanwhile, emerging evidence illustrated that TRPM7 could be directly activated by shear stress via incorporation into plasma membrane in an exocytosis-independent manner which is not affected by a blocker of vesicular protein traffic, brefeldin A (Numata et al., 2007a). Therefore, TRPM7 could directly be activated by some mechanical or osmomechanical stimuli.

1.4.5.2 Intracellular and extracellular [Mg] i and Mg·ATP

Electrophysiological recordings have found the cytosolic concentrations of free Mg and Mg·ATP have been identified as key feedback regulators of TRPM7 (Nadler et al., 2001). The TRPM7 current inhibited by [Mg]i is named MIC (magnesium inhibited current) and the current regulated via Mg·ATP is termed as MagNuM (magnesium-nucleotide-regulated metal ion current), which both have been detected in a large number of tissues. Under physiological conditions, Mg·ATP concentrations can inhibit TRPM7 channels and strongly enhance the channel blocking efficacy of free Mg. In addition, nearly all Mg-nucleotides (TTP, CTP and GTP) can inhibit TRPM7 activation to diverse degrees (Demeuse et al., 2006). The nucleotide binding sites residing in the kinase domain are the key modulators of nucleotide-dependent regulation of TRPM7 (Demeuse et al., 2006). As a consequence, although the TRPM7 kinase domain is independent from the ion channel activation it could influence sensitivity to Mg.

In addition, TRPM7 current is also regulated by extracellular Mg levels. Higher concentration of extracellular Mg increases inward currents and supresses outward currents of TRPM7 in cells exposed to isotonic $MgCl_2$ solution (in absence of external Ca) (Nadler et al., 2001). Furthermore, inward fluxes of monovalent cations via TRPM7 is obstructed by its high affinity for Mg and Ca, so monovalent cation flux through TRPM7 is amplified when extracellular divalent cations are removed (Nadler et al., 2001). Meanwhile, another investigation also demonstrated that extracellular Mg might block the ion channel pore, and exerts strong negative feedback from the intracellular side of the pore (Monteilh-Zoller et al., 2003). Compared to the divalent cations, TRPM7 is barely selective for monovalent cations at physiological membrane potentials (-40 to -80mV) but the monovalent and divalent ions do not permeate independently (Nadler et al., 2001). In contrast, monovalent permeation becomes dominant at very positive potentials (Nadler et al., 2001). As we mentioned before, TRPM7/6 heteromeric complex has higher constitutive activity to Mg and Mg·ATP at physiological condition compared to their homomeric complex (Ferioli et al., 2017).

1.4.5.3 pH value

As a unique bifunctional protein, TRPM7 could be regulated by alterations of intracellular and extracellular pH values. Endogenous TRPM7-like current, respectively MIC and MagNuM, is dramatically increased by the acidic extracellular pH value and the small inward current of TRPM7 at voltage (-40mV to -100mV) was ~10-fold increased at pH 4.0 (Jiang et al., 2005). It is proposed that as extracellular H increases the affinity of TRPM7 for Ca and Mg decreased consequently promoting conduction of monovalent cations (Jiang et al., 2005). In contrast, during the perforated-patch recording, endogenous MIC or recombinant TRPM7 currents are activated by cytosolic alkalinization and inhibited by acidification as pH value changes (Chokshi et al., 2012a). Meanwhile, kinase domain of TRPM7 is also regulated by intracellular pH alterations but with different features, specifically its phosphotransferase function is diminished at both acidic and basic pH conditions (Kozak et al., 2005). This further confirms that kinase domain and ion channel activity are independent to some degrees.

1.4.5.4 Phosphatidylinositol 4,5-bisphosphate (PIP2)

It has long been known that Muscarinic type 1 (M1) receptor could activate phospholipase C-ß (PLC-ß) through Gαq-containing heterotrimeric G proteins, which is a negative modulating system of TRPM7 current (Takezawa et al., 2004). The underlying mechanism was is further investigated by Clapham and his colleagues (Runnels et al., 2002), revealing that phosphatidylinositol 4,5-bisphosphate (PIP2) is the key regulator of TRPM7. In the native cardiac cells and heterologous expression systems, receptor-mediated (Gαq-linked receptors or tyrosine kinase receptors) activation of PLC induces the hydrolysis of PIP2, directly resulting in inactivation of TRPM7 channel (Runnels et al., 2002). Furthermore, TRPM7 could bind to the C2 domain of ß and γ PLC family members but the PIP2 metabolites IP3 and DAG do not directly affect TRM7 ion channel activity.

Although the ion channel activation is not required for enzymatic activity of kinase domain, the intrinsic kinase is also a regulatory domain affecting TRPM7 ion conduction. For example, TRPM7 current is inhibited by G-protein-coupled receptors which reduce cellular cyclic adenosine monophosphate (cAMP) (Takezawa et al., 2004). Elevated cytosolic cAMP level would promote TRPM7 activity and prevent receptor-mediated inhibition on TRPM7 activity by muscarinic and adrenergic agonists (Takezawa et al., 2004). These effects are mediated by the cAMP-dependent kinase PKA, but also depend on the activity of the TRPM7 kinase domain.

To date, there are several regulators of TRPM7 ion channel have been illustrated but we have still not fully mapped the activation mechanisms of TRPM7. To sum up, in resting cells, the channel activity of TRPM7 is suppressed by intracellular [Mg]i and Mg·ATP at physiological levels. Its constitutive ion channel activity is maintained by adjacent PIP2 in the plasma membrane while the channel could be activated by cytosolic cAMP and intracellular alkalinization (Yee et al., 2014). Additionally, hydrolysis of PIP2, high intracellular free Mg and Mg·ATP, cytosolic acidity (lower PH value) all deactivate TRPM7 channel activity. Besides, the extracellular mechanical stress, PH alteration (acidity), oxidative stress, and ionic changes such as extracellular Mg, all co-ordinately regulate TRPM7 current.

Meanwhile, as we mentioned previously (section 1.4.3), RTKs induce phosphorylation of downstream kinases also influence TRPM7 activity.

1.4.6 TRPM7 in human pathologies

Applying two different properties, cation conduction and enzymatic activity of kinase domain, TRPM7 and TRPM6 are implicated in a large number of clinical diseases.

1.4.6.1 Cancer

Many studies have already illustrated that TRPM7 exerts important effects on cellular proliferation, survival, cell cycle progression, migration, and invasion in numerous cancer cell lines. Aberrant expression of TRPM7 has been discovered in different cancer phenotypes, especially pancreatic adenocarcinoma, and breast cancer. In the tissue of human pancreatic adenocarcinoma, the expression of TRPM7 is positively correlated with primary tumor size and stage and the hairpin RNA-mediated suppression of TRPM7 impairs cell invasion (Yee et al., 2015). Overexpression of TRPM7 is also discovered in breast cancer (Meng et al., 2013, Cordier et al., 2021) and glioblastoma (Chen et al., 2015). Carvacrol, the TRPM7 inhibitor, blocks the constitutive TRPM7-current and endogenous TRPM7 current in human U87 glioblastoma cell line via inhibiting Ras/MEK/MAPK and PI3K/Akt signaling pathways, and also suppresses proliferation, migration and invasion in these cells (Chen et al., 2015). Meanwhile, TRPM7 has been regarded as a novel target for diagnosis and treatment of breast cancer where it is a key modulator facilitating migration and invasion of cancer cells via MAPK pathway (Meng et al., 2013). In addition, somatic mutations or polymorphisms of TRPM7 have been discovered in breast carcinoma, gastric carcinoma, colon carcinoma, and ovarian carcinoma (Greenman et al., 2007, Yee, 2017). The increasing number of cancer types in which TRPM7 is involved suggest it might be a new treatment target.

1.4.6.2 Cardiovascular diseases

TRPM7 as a magnesium regulator is critically implicated in hypertension. In the TRPM7-deficient mouse model, angiotensin II (Ang II)-induced blood pressure elevation was exaggerated, and the deleterious effects of Ang II on cardiac remodeling and left ventricular dysfunction were also amplified (Antunes et al.,

2016). Besides, elevation of aldosterone in hypertension may be associated with TRPM7-mdediated signalling pathways (Yogi et al., 2013). Aldosterone signal transduction is regulated by TRPM7 ion channel and TRPM7 α-kinase differentially. Respectively aldosterone rapidly stimulates Mg influx via mineralocorticoid receptor(MR)-dependent process, whereas aldosterone regulation of pro-inflammatory signalling requires an active TRPM7 kinase domain (Yogi et al., 2013). Recently, obesity induced resistant hypertension induced by high plasma levels of leptin was associated with TRPM7 (Shin et al., 2019). TRPM7 channel is abundantly expressed in carotid body (CB) glomus cells where it co-localises with the leptin receptor (Leprb). Leptin-induced hypertension requires TRPM7 ion channel activity in CB (Shin et al., 2019).

TRPM7 also has been implicated in the pathogenesis of fibrosis-related cardiac diseases, such as heart failure, cardiomyopathies, arrhythmia and hyperaldosteronism (Hu et al., 2021). The atrial fibroblasts from atrial fibrillation (AF) patients exhibit striking upregulation of TRPM7-like current and Ca influx (Du et al., 2010). Transforming growth factor (TGF)- ß1 influence on fibroblast proliferation and differentiation is dependent on TRPM7-mediated Ca signaling pathway (Du et al., 2010). TRPM7 exerts protective anti-inflammatory and anti-fibrotic effects in a Mg-dependent manner (Rios et al., 2020). TRPM7-kinase deficient mice show pro-inflammatory and pro-fibrotic cardiovascular and renal phenotype with increase in pro-inflammatory mediators (SMAD3, TGFß) and cytokines (Interleukin-6, IL-10 and TNF-α) (Rios et al., 2020).

1.4.6.3 Neurodegenerative diseases

TRPM7 and MagT1 regulate magnesium transport in the blood-brain barrier (BBB) in vivo. TRPM7 is highly expressed in the tips of the growth cone, where alterations of cytoskeleton contribute to neuronal growth. In addition, TRPM7 has been found to influence astrocyte proliferation and migration by regulating extracellular regulated protein kinase (ERK) and c-Jun N-terminal kinase (JNK) activities (Zeng et al., 2015). TRPM7 also inhibits axonal outgrowth and maturation by regulating F-actin and α-actinin-1 protein complex in a Ca-dependent manner (Turlova et al., 2016a). Therefore, TRPM7 serves as a unique mechanosensitive regulator of neuronal cytoskeleton. Besides, TRPM7 localized in the membranes of acetylcholine (ACh)-secreting synaptic vesicles of

sympathetic neurons, plays a major role in vesicular trafficking, membrane reorganization, and neurotransmitter release (Sun et al., 2015b).

TRPM7 has been reported to be associated with neurodegenerative disorders including Alzheimer's disease (AD) and Parkinson disease (PD). On one hand, overproduction of reactive oxygen species (ROS) is a crucial mechanism of pathogenesis of neurodegenerative diseases (Nunomura et al., 2007). Oxidative stress would lead to cellular defects and accelerated Ca cascades, induing cytoskeleton alterations and cell death (Ureshino et al., 2014, Sun et al., 2015b). Inhibition of TRPM7 rescues anoxic neurons which were previously destined to die from prolonged anoxia (Aarts et al., 2003). On the other hand, neurons expressing Alzheimer's disease-associated mutant presenilins have suppressed TRPM7-like current due to reduced PIP2 levels (Landman et al., 2006). This indicates TRPM7 channel is fundamental for Ca entry deficits in presenilin FAD mutant cells and PIP2 also corelates with accumulation of 42-residue amyloid ß-peptide (Aß42) (Sun et al., 2015b).

1.5 Cellular Control and Functional Effects of Protein S-Palmitoylation

1.5.1 S-palmitoylation

Protein lipidation increases the hydrophobicity of protein, facilitating their insertion into intracellular and plasma membrane consequently regulating protein-membrane and/or protein-protein interactions, protein stability and enzymatic activities (Jiang et al., 2018). Palmitoylation (C:16) (Sobocińska et al., 2018), prenylation (farnesyl C:15 or geranylgeranyl C:20) (Zhang and Casey, 1996) and myristoylation (C:14) (Wright et al., 2010) are the three most common lipid modifications that occur in cells. Palmitoylation can refer to two different modifications, respectively thioester bond covalently linking C16 carbon saturated fatty acid to cytoplasmic cysteine residues (S-palmitoylation) or amide bond linking C16 carbon fatty acyl chain to glycine/cysteine residues in the cytoplasm or endomembrane system (N-palmitoylation) (Charollais and Van Der Goot, 2009). Only S-palmitoylation (Figure 1.6) is the unique reversible post-translational modification in which the fatty acid palmitate is covalently attached to cysteine resiude(s) on protein via palmitoyl acyltransferases (PAT)

and is removed by lysosomal palmitoyl-protein thioesterase (PPT) or cytosolic acyl-protein thioesterase (APT) (Figure 1.6) (Brown et al., 2017). S-palmitoylation turnover speed varies from proteins to proteins. In order to globally profile dynamic palmitoylation, Martin et.al. used the palmitate analogue 17-ODYA (17-octadecynoic acid) in combination with stable isotope labeling of cells (SILAC)11 successfully to identify over 400 dynamically palmitoylated proteins in mouse T-cell hybridoma cells (Martin et al., 2012). For some proteins, such as PSD-95, GNAS and HRAS, palmitoylation turns over dynamically whereas for some others it serves as a “static modification” with a long turnover process (Martin et al., 2012). Meanwhile, S-palmitoylation could occur at any time point in protein lifespan, either happening at beginning of protein synthesis or dynamically during their life cycle.

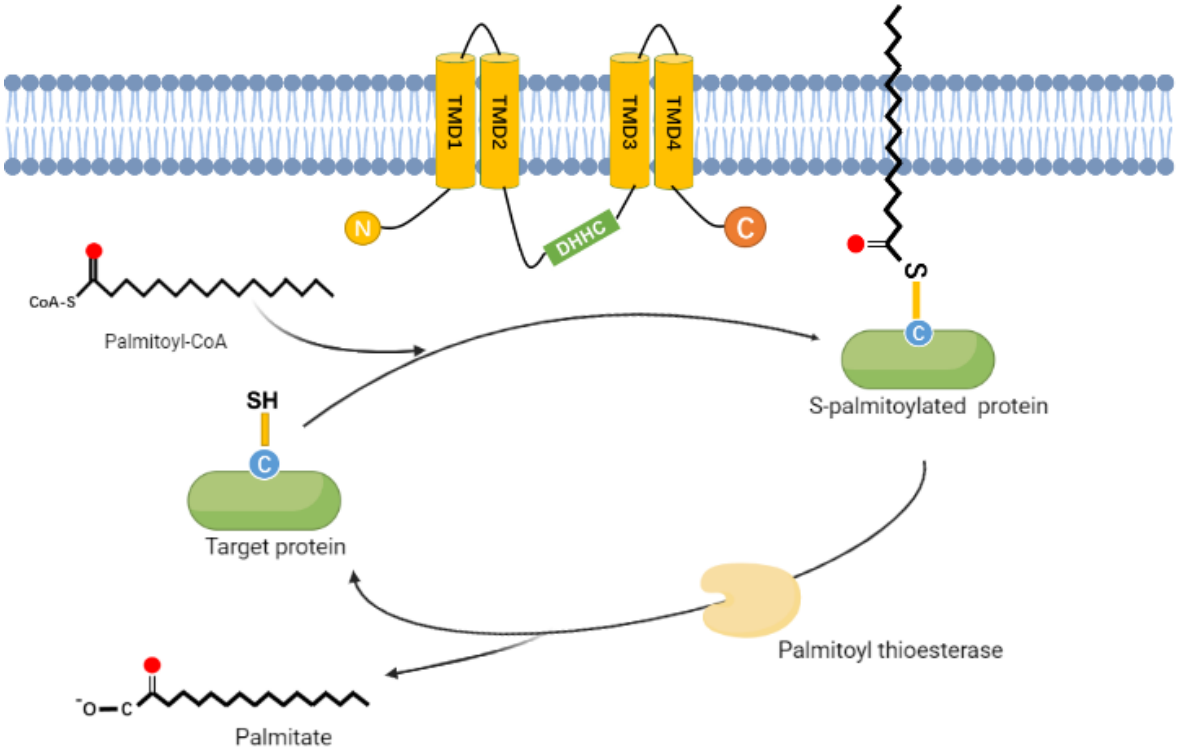

Figure 1.6 Dynamic protein S-palmitoylation.
The long-chain saturated Palmitic acid (C16:0) is attached to protein cysteine residues via a thioester covalent linkage via integral membrane zDHHC-family palmitoyl acyltransferases. S-palmitoylated protein are de-palmitoylated by acyl-thioesterases such as APT1/2.

1.5.2 Palmitoylation function

Palmitoylation is an important post-translational modification which assists correct protein folding, anchoring on membrane and trafficking between cytosolic compartments through palmitoylation and de-palmitoylation cycles.

The most universal role of S-palmitoylation is helping proper membrane association (Charollais and Van Der Goot, 2009), in which proteins can be singly modified or dually lipidated in combination with other modifications such as N-palmitoylation, prenylation or myristoylation (Guan and Fierke, 2011). For example, mammalian H-Ras, a small GTPase, firstly is prenylated to weakly attach to membrane then subsequently palmitoylated to generate enough hydrophobicity to enhance membrane affinity (Baker et al., 2003). For some transmembrane proteins, S-palmitoylation is required for targeting to the plasma membrane. For example, absence of palmitoylation in Lipoprotein receptor-related protein 6 (LPR6) results in its retention in the endoplasmic reticulum (ER) (Charollais and Van Der Goot, 2009). In addition, palmitoylation also controls protein trafficking between cellular compartments and acts as a determinant of their endocytic route. For example, it has been demonstrated to control lysosomal receptor sorting and trafficking (McCormick et al., 2008). Cationic-dependent and -independent mannose 6-phosphate receptors and sortilin are required to bind cargo in the Golgi apparatus forming clathrin-coated trafficking vesicles and trafficking lysosomal proteins to the endosomes (McCormick et al., 2008). The retrograde trafficking of MPR by the mammalian retromer complex requires its palmitoylation and palmitoylation-deficient cationic-independent mannose 6-phosphate receptor (CI-MPR) becomes trapped in endosomes and unable to cycle between compartments (McCormick et al., 2008).

In addition, palmitoylation can negatively or positively influence protein-protein interactions through steric hindrance, altering conformation and membrane localization (Charollais and Van Der Goot, 2009). For instance, as previously mentioned, MPR functioning in cargo trafficking must collaborate with the retromer complex (McCormick et al., 2008), where palmitoylation promotes their interaction. AMPA receptor (α-amino-3-hydroxy-5-methyl-4-isoxazole propionate), a receptor of excitatory neurotransmitter Glutamate, is palmitoylated at 2 sites on transmembrane domain (TMD)2 and C-terminal domains (CT) (Hayashi et al., 2005). Palmitoylation of the former (TMD2) leads to accumulation in Golgi apparatus whereas palmitoylation of the later region (CT) inhibits its interaction with 4.1N protein (Hayashi et al., 2005). Finally, palmitoylation might be required for regulation of transmembrane protein

activity especially through its influence on protein localization which can influence downstream signaling pathways. For example in heterotrimeric G-protein signaling, palmitoylation initially mediates localization of heterotrimeric G protein alpha subunits at the plasma membrane (Smotrys and Linder, 2004b). Disruption of palmitoylation in Gα subunit exerts negative consequences on signal transduction.

In the past few decades, many aspects of our understanding of the mechanisms of palmitoylation have been furthered, such as recognizing several palmitoyl-transferases (PATs) and de-palmitoylating enzymes, exploiting many approaches to measure palmitoylation activity both in vitro and in vivo etc. Palmitoylation is characterized in numerous proteins leading to an increased understanding of the role of palmitoylation in many physiological processes.

1.5.3 Palmitoylating enzymes

The majority of palmitoylation and de-palmitoylation events are enzymatic reactions. A small number of proteins could bind to palmitoyl-coenzyme A (palmitoyl-CoA) directly and undergo a PAT-independent auto-palmitoylation. It has been reported that G protein Giα1, the downstream effector of many receptors, is auto-palmitoylated at cysteine 3 (C3) in presence of palmitoyl-CoA (Duncan and Gilman, 1996). In addition, the yeast transporter protein Bet3 is auto-palmitoylated in the presence of physiological concentrations of palmitoyl-CoA (1-10μM) (Kümmel et al., 2006). This suggests that palmitoylation might be a spontaneous modification dependent on local fatty acid concentration. However, palmitoylation regulatory mechanisms of most proteins was revealed when the zDHHC-palmitoyl acyltransferase (zDHHC-PAT) was discovered in yeast (Lobo et al., 2002).

1.5.3.1 DHHCs

Initially, Erf2 and Erf4 were recognized as the first genes encoding the palmitoyl-transferase for Ras GTPase in yeast, which are enriched with a conserved DHHC cysteine-rich domain (DHHC-CRD) (Lobo et al., 2002), now known as the zDHHC-palmitoyl acyltransferase (zDHHC-PAT). There are 7 catalytic ((Asp-His-His-Cys) containing enzymes responsible for S-palmitoylation

in yeast and 23 members in human (Mitchell et al., 2006). DHHC enzymes are integral membrane proteins with 4-6 transmembrane domains (TMD) and 2 cytoplasmic ends, N- and C-termini, the latter of which is often long, poorly conserved, and disordered, as well as a highly conserved ~51 amino acid cysteine-rich domain with Asp-His-His-Cys motif between TMD2 and TMD3 (Main and Fuller, 2022). Apart from the DHHC-CRD, there are 3 other conserved motifs, respectively Asp-Pro-Gly (DPG), Thr-Thr-x-Glu (TTxE) and PaCCT (palmitoyl transferase conserved C-terminus) facing the cytosol (Rana et al., 2019). Most DHHC enzymes have four transmembrane domains but DHHC-13,-17 and -23 putatively have six TMD (Tabaczar et al., 2017). DHHC13 and DHHC17 are two specialised mammalian PATs with unique ankyrin repeat (ANK) domains located at their N-terminus (Tabaczar et al., 2017) which are responsible for substrate recognition and protein interactions. For example, Golgi-resident DHHC13 and DHHC17 which are highly abundant in the brain, recognize conserved and closely related sequences of a [VIAP][VIT]XXQP consensus in SNAP25, SNAP23, cysteine string protein, Huntingtin etc via its ankyrin repeats (Lemonidis et al., 2015).

The human genome mostly encodes DHHCs localized at the endomembrane compartments such as Golgi, endoplasmic reticulum, endosomes and only a few of them discovered in plasma membrane (DHHC-5,-20,-21)(Table 1.1) (Ohno et al., 2006, Korycka et al., 2012). In addition, DHHC enzymes can cycle between different compartments especially in the closely positioned cellular compartments, but it is still unclear the mechanisms underlying DHHC specific localization. Dilysine sequences with in pentapeptide in the C-terminal end might play a vital role in sorting signals (Gorleku et al., 2011). To be specific, the consensus sequence KKEK in DHHC4 and KKXX in DHHC6 determines targeting to the ER, and their removal results in sorting to different compartments (Gorleku et al., 2011).

Table 1.1. Intracellular localization of Human DHHC enzymes.

Protein	Localization
zDHHC1	ER

zDHHC2	ER/Golgi
zDHHC3	Golgi
zDHHC4	Golgi
zDHHC5	Plasma membrane
zDHHC6	ER
zDHHC7	Golgi
zDHHC8	Golgi
zDHHC9	ER/Golgi
zDHHC11	ER
zDHHC12	ER/Golgi
zDHHC13	ER/Golgi
zDHHC14	ER
zDHHC15	Golgi
zDHHC16	ER
zDHHC17	Golgi
zDHHC18	Golgi
zDHHC19	ER
zDHHC20	Plasma membrane
zDHHC21	Plasma membrane

zDHHC22	Golgi/ER
zDHHC23	ER
zDHHC24	ER

1.5.3.2 De-palmitoylating enzymes

Protein de-palmitoylation is the process of removal of thioester-linked palmitate fatty acids from cysteines residues in proteins. Some proteins must be depalmitoylated before being degraded in lysosomes. To date, several groups of de-palmitoylation enzymes have been demonstrated, respectively palmitoyl protein thioesterase (PPT1/PPT2), acyl protein thioesterases (APT1/ATP2) and α/ß hydrolase domain-containing 17 family (ABHD17s) (Sobocińska et al., 2018). PPT1 is the first characterized de-palmitoylating enzyme which localises in lysosomes (Verkruyse and Hofmann, 1996), whose function is crucial to morphological development of neurons. Some proteins need de-palmitoylated before lysosomal degradation. APT1/ATP2 are extensively studied broad spectrum de-palmitoylating enzymes (Won et al., 2018). Both of them de-palmitoylate a large number of proteins but there is not complete redundancy between them. APT1 and APT2 share nearly 70% homology sequence and binds substrates in a similar way (Won et al., 2018). The mechanistic differences of APT1 and APT2 are not fully understood although their high-resolution structures bound to respective inhibitors (ML348 and ML349) were presented (Won et al., 2016). APT1 and APT2 are expressed and active in nearly all tissues but their absence in most large-scale profiling efforts suggests they may not be stoichiometrically S-palmitoylated (Bachovchin et al., 2010, Won et al., 2018). This low-level S-palmitoylation might be related to dynamic auto-depalmitoylation. APT1 not only depalmitoylates itself own but also facilitate dynamic palmitoylation cycle of APT2 (both of them palmitoylated at Cys-2) (Kong et al., 2013).It is still unclear if APT1 and APT2 are functionally redundant or hydrolyse distinct substrates. But it has been suggested that ATP1 and APT2 have an interdependent S-palmitoylation cycle since knockdown of APT1 promotes plasma membrane association of APT2 (Kong et al., 2013). In addition, APT2 de-palmitoylates GAP43 rather than APT1 and APT2 is responsible for

DHHC6 de-palmitoylation instead of APT1, suggesting they might access different pools of substrates (Tomatis et al., 2010).

Although APT1/APT2 are capable of depalmitoylating many proteins in different tissues, their knockdown has no effect on R7 RGS-binding protein (R7BP) depalmitoylation suggesting there may be other candidate de-palmitoylating enzymes (Jia et al., 2014). Through activity profiling of hydrolase targets of Palmostatin B (APT1/2 inhibitor), a novel de-palmitoylating enzyme, ABHD17, has been identified to depalmitoylate PSD95 and N-Ras (Lin and Conibear, 2015). ABHD17 hydrolases are extensively expressed in all vertebrates and possess multiple conserved cysteines in their N-termini which must be palmitoylated for plasma membrane association and proximity to potential palmitoylated substrates (Won et al., 2018). However, absence of this cysteine enriched domain does not diminish its enzymatic activity (Won et al., 2018). Recently, ABHD17 was identified as accelerating N-Ras deplamitoylation as its over-expression trans-locating N-Ras from the plasma membrane to internal membranes, and it was also discovered as a novel player in neuronal and synaptic proteins regulation (Lin and Conibear, 2015). In addition, ABHD10 is a novel S-depalmitoylase of APT family and affects redox homeostasis via peroxiredoxin-5 (PRDX5) (Cao et al., 2019).

1.5.4 Palmitoylation impacts on ion channel activity

Emerging evidence suggests S-palmitoylation is a fundamental, dynamic and widespread post-translational modification to control the properties and functions of ligand and voltage-gated ion channels. As well as acting as determinant of channel modulation by other signaling pathways (Shipston, 2011).

Firstly, palmitoylation can exert an influence on different stages of protein trafficking to control its surface expression and abundance. For example, palmitoylation controls internalisation of Kv1.5 channel, and non-palmitoylated channels show increased cell surface abundance as a result of a reduced internalisation rate (Shipston, 2011). In addition, palmitoylation also controls the spatial organization of channels localised to plasma membrane. Assembly of orthogonal arrays of particles in glial cell water channel aquaporin-4 (AQP4) is controlled by palmitoylation of C terminal cysteines (Crane and Verkman, 2009).

Meanwhile, regulatory subunits and adaptor proteins of ion channels are also affected by palmitoylation. For example, Palmitoylation of K channel-interacting protein (KChip), the auxiliary subunits for voltage-gated potassium channel (Kv4 family), is required for plasma membrane localization and increasing Kv4.3 current (Takimoto et al., 2002).

Aside from surface association, palmitoylation controls channel activity either indirectly or in co-operation with other post-translational modifications (PTMs). For example, ß2a, one of the four genes encoding ß subunits of voltage gated Ca channels, is palmitoylated and consequently controls voltage-dependent inactivation (Qin et al., 1998). Additionally, crosstalk between palmitolyation and phosphorylation can positively or negatively regulate protein phosphorylation. For example the PKC-mediated phosphorylation of GluR1 subunit of the AMPA receptor is inhibited by palmitoylation whereas the Fyn-dependent tyrosine phosphorylation of the NR2A subunit of NMDA receptors is abolished when it cannot be palmitoylated (Shipston, 2011). That crosstalk might partly rely on steric hindrance as the palmitoylated cystine is adjacent to the phosphorylation sites.

To conclude, palmitoylation regulates a large number of ion channels' activity in multiple pathways, such as trafficking, membrane localization, internalization, crosstalk with other signaling pathways, which is important in many physiological processes. Furthermore, many investigations have highlighted that dynamic palmitoylation process acting as new targets for disease treatment, including caner, neuroscience and cardiovascular disease (Fraser et al., 2020).

1.6 Project Aims

Magnesium is the one of the abundant cations in human body, which exerts considerable influence on energy transfer, storage, and utilization. Magnesium homeostasis is crucial for stable biological processes and its disruption is correlated with many clinical diseases, such as cardiovascular disease, neurological disease, cancer and metabolism disorders. TRPM7 and TRPM6 are two of few acknowledged Mg regulators, especially TRPM7 which is ubiquitously expressed in whole body.

TRPM7 is a bifunctional protein with ion channel conduction and kinase domain enzymatic activity. Palmitoylation is a reversible dynamic post-translational modification which regulates the activity and subcellular localisation of numerous ion transporters in the cardiovascular system. The hypothesis of our project is palmitoylation regulates the channel activity and/or kinase activity of TRPM7. The long-term aims of this project are to study the role of palmitoylation in controlling the behaviour of TRPM7 and further investigate its function and regulation. Specific aims of the present project are:

1) Mapping the palmitoylation site(s) of TRPM7 and TRPM6

2) Determine the influences of palmitoylation on TRPM7 ion channel activity, as Mg, Zn and Ca conduction

3) Investigate the influence of palmitoylation on crosstalk with phosphorylation of TRPM7's kinase domain and related signaling cascades.

4) Identify the regulatory mechanisms of TRPM7 palmitoylation, such as enzymes responsible for palmitoylation of TRPM7.

5) Investigation of changes in TRPM7 palmitoylation in disease models.

Chapter 2 Materials and Methods

2.1 General Laboratory Practice

All experiments were carried out in Laboratories based in Sir James Black building and British Heart Foundation Glasgow Cardiovascular Research Centre of Institute of Cardiovascular and Medical Sciences (ICAMS). All experimental reagents were processed and disposed in accordance with Control of Substances Hazardous to Health (COSHH) guidelines. COSHH Risk Assessment Forms were read carefully and signed before conducting any experiment. Personal protective equipment was worn accordingly during all procedures. Daily activities in Laboratory followed guidelines formulated by Prof Fuller and ICAMS.

2.2 Chemicals and reagents

Unless otherwise specified, all chemicals and reagents were supplied by Sigma Aldrich (Dorset, UK) and Themo Fisher Scientific (Loughborough, UK). The primary antibodies suppliers described in the following section 2.10.4). All of them were detected with secondary antibodies α-Mouse or α-Rabbit (section 2.10.4) from Jackson ImmunoResearch (Cambridgeshire, UK).

2.3 Statistical analysis

All data are presented as mean ± standard error (SEM) using GraphPad Prism software. Comparisons between multiple groups was made using One-way ANOVA followed by Dunnett's multiple comparison test. Comparisons between two groups were made using an unpaired t-test with Welch's correction. Statistical significance levels were denoted by the range of P-value, specifically * $P<0.05$, ** $P<0.01$, *** $P<0.001$ and **** $P<0.0001$.

2.4 Ethics statement

All experimental procedures using animal cells and tissue were approved by the University of Glasgow Animal Welfare and Ethical Review Board and were conducted under the authority of a project licence granted by the UK Home Office.

2.5 Plasmid preparation

2.5.1 TRPM7, TRPM6 plasmids and their Mutants

TRPM6 and TRPM7 cDNAs with yellow fluorescent proteins (YFP) fused at the C terminus were kindly provided by Dr.Vladimir Chubanov, Munich, Germany. TRPM7 N-terminus and C-terminus fragments were amplified using CloneAmp HiFi PCR premix (Clontech). PCR fragments were then purified and ligated to EYFP-C1 vector using In-fusion cloning enzyme (Clontech). The cloning of the N-terminus and C-terminus of TRPM7 as YFP fusion protein was made by Dr. Chien-Wen Kuo, Postdoc in Fuller Lab. All other mutant Plasmids derived from the TRPM7-YFP and TRPM6-YFP vector were generated in accordance with relevant cloning kits protocol, Q5® Site-Directed Mutagenesis Kit (BioLabs), Quik-change Lighting Site-Directed Mutagenesis kit (Agilent) and In-Fusion HD Cloning kit (Takara) separately.

Table 2.1. Mutant plasmids for deletion of N-terminus or C-terminus of TRPM7-YFP cDNA made using Q5® Site-Directed Mutagenesis.
Primers were designed with NEbasechanger primer design software.

Mutagenesis reaction	Plasmids	Targeted mutations	Primer sequence
1	TRPM7-N-del-YFP	Delta16-738	ACACAGATGTTGTTATCTGATATG (24) **-Forward** CTCCCTCTTGGTCAAAGTG (19) **-Reverse**
2	TRPM7-C-del-YFP	Delta 1143-1814	CGAAAGCTTAAACTTCCAG (19) **-Forward** AAACAGTGAAACTATATGGC (20) **-Reverse**

Table 2.2. Mutant plasmids were generated using Quik-change Lighting Site-Directed mutagenesis Kit
The details of primers sequences used for mutagenesis designed using Takara online primer design tool.

Mutagenesis reaction	Plasmids	Targeted mutations	Primer sequence (5'-3')
1	1143-4-6_AAA	Cys1143 Cys1144 Cys1146 Cys-Ala	CATCGGAAGTCTTATCTTTCTTTCTTCTTTT GGCTACAGCGGCAAACAGTGAAACTATA TGGCTGAGGATGATAA (75)
2	1143/4_AA	Cys1143 Cys1144 Cys-Ala	TCCTCTTATCATCCTCAGCCATATAGTTTCACT GTTTGCCGCTGTATGCAAAAGAAGAAAG (61)
3	1146_A	Cys1146 Cys-Ala	CATATAGTTTCACTGTTTTGCTGTGTAGCCAAAAGA AGAAAGAAAGATAAGACTTC (56)

Table 2.3. Mutant plasmids were generated using In-fusion HD cloning Kit.
The details of forward and reverse primer sequences of Oligo mutagenesis of TRPM7-YFP and TRPM6-YFP designed using Takara online primer design tool.

Mutagenesis reaction	Plasmids	Targeted mutations	Primer sequence
1	TRPM7-M2	1143-1146 CCVC-KRIV	TTAAGAGGATCGTGAAAAGAAGAAAGAAAGAT AAGAC (37) **-Forward** TCACGATCCTCTTAAACAGTGAAACTATATGG CTGAGG (38) **-Reverse**
2	TRPM7-M5	1143-1146 CCVC-KQVF	TTAAGCAGGTGTTCAAAAGAAGAAAGAAAGAT AAGAC (37) **-Forward** TGAACACCTGCTTAAACAGTGAAACTATATGG CTGAGG (38) **-Reverse**
3	TRPM6-M5	1125-1126 CC-FR	GTCTGTTCAGGCGCCCAGCCCCACAGGAC (29) **-Forward** GGCGCCTGAACAGACCTCGGAGGAGGAGAC AC (32) **-Reverse**
4	TRPM6-AA	1125-1126 CC-AA	GTCTGGCCGCCCGCCCAGCCCCACAGGAC (29) **-Forward** GGCGCAGCACCAGACCTCGGAGGAGGAGAC AC (32) **-Reverse**
5	TRPM6-M2	1125-126 CC-VL	GTCTGGTGCTGCGCCCAGCCCCACAGGAC (29) **-Forward** GGCGCAGCACCAGACCTCGGAGGAGGAGACAC (32) **-Reverse**

TRPM7-YFP and TRPM6-YFP acted as parental DNA template for mutant strand synthesis. Master Mix for DNA amplification were prepared in accordance with recommended volume from relevant manufacturers. The master mix was prepared at room temperature, but individual reaction components were kept

on ice when adding primers and template to the reaction. Constituents of individual reactions are shown in Table 2.4. Mutations were achieved through programming several thermal cycling according to recommended PCR parameters (Table 2.5)

Table 2.4. Components of individual PCR amplification according to different manufacturer.

Individual DNA Amplification reaction components								
Q5® site-directed mutagenesis			QuikChange Lighting site-directed (Agilent)			In-Fusion® HD Cloning (Takara)		
Reagents	Vol.	Final conc.	Reagents	Vol.	Final Conc.	Reagents	Vol.	Final conc.
Q5 Hot start High-Fidelity			10x reaction buffer	5µl	1x	CloneAmp HiFi PCR	12.5µl	1x
2x Master Mix	12.5µl	1x	Primer1	1.25µl	0.5µM	Premix		
Forward Primer	1.25µl	0.5µM	Primer2	1.25µl	0.5µM	Primer1	5-7.5pmol	0.2-0.3µM
Reverse Primer	1.25µl	0.5µM	Template DNA	-----	10-100ng	Primer2	5-7.5pmol	0.2-0.3µM
Template DNA	1µl	1-25ng	dNTP mix	1µl		Template DNA	<100ng	
Nuclease-free water	9µl		QuikSolution reagents	1.5µl		Nuclease-free water	up to 25µl	
			QuikChange Lightning Enzyme	1µl				
Total vol.	25µl		Total vol.	50µl		Total vol.	25µl	

Table 2.5. PCR cycling parameters
Annealing temperature might be changed according to the *Tm* of different primers.

Steps	Process	Temperature	Time
1	Initial Denaturation	95 ^{O}C	2mins
2 （x30）	Denaturation	95 ^{O}C	20s
	Annealing	55 ^{O}C	30s
	Extension	72 ^{O}C	30s/kb
3	Final extension	72^{O}C	5mins
4	Infinity hold	4^{O}C	∞

PCR fragments were analysed using agarose gel electrophoresis and then treated with treated with DpnI restriction enzyme, mixed thoroughly, and incubated on 37ºC for overnight to ensure cleavage of methylated parental DNA. The resulting PCR product was transformed into XL-10 Gold ultracompetent cells (Agilent) and plated onto on Amp Agar Plates. Single colonies picked from plates were grown in Lysogeny Broth (LB) with conical flask for 12-16h in 37ºC. In general, plasmid DNA was first prepared from 1-2ml of culture (insert name of miniprep kit) and the sequence checked (see below). A single clone with the correctly targeted sequence was selected for midi prep using QIAGEN Plasmid Plus Midi Kit (QIAGEN). 50ml bacterial culture was pelleted at high-speed centrifuge and followed by resuspension, lysis, and neutralization using buffers supplied by the kit manufacturer. After clearing the lysate using a centrifuge or syringe filter, the supernatant containing plasmids DNA was applied to a resin column, which was washed to remove endotoxin and contaminants before the plasmids were eluted with Tris-CL based elution buffer or nuclease-free water. The details of procedures were conformed to QIAGEN Plasmid Plus Midi Kit (QIAGEN).

DNA sequencing was performed using Eurofins Genomics company. Except CMV Forward and CMV Reverse Primers which were already provided on Eurofins Website, we also specifically designed several sequencing primers for TRPM7 which targeting its different fragments (Table 2.6). Sequencing results were analyzed by 4peaks software (Nucleobites.com) and Basic Local Alignment

Search Tool (BLAST, NCBI) to estimate if it contains correct mutagenesis with good quality.

Table 2.6. TRPM7 sequencing primers.
Designed different primers to sequencing interested fragments of TRPM7.

Primer Name	Sequence	Anneals (cDNA)	Region of interest (protein)
TRPM7_200	TTTAACTGGAGGAGTCAATACAGG	512-536	~200
TRPM7_400	TTCACATTGGATCAGAGGATCATC	1142-1166	~400
TRPM7_600	AAACAGCCCAACCCTACAGAC	1745-1765	~600
TRPM7_800	TTCCACCTGCCATATTAATGC	2300-2320	~800
TRPM7_1000	GGTATGTGCGTTTGCTAGACTTTC	2915-2938	~1000
TRPM7_1200	ATTCAATTCTGGGAGTGAAGAGAG	3564-3587	~1200
TRPM7_1430	AAAGTCACTTGGAATCCACAAC	4232-4254	~1430
TRPM7_1640	TAAGTAAAGAGGAAATGGGAGGTG	4836-4854	~1640

2.5.2 Endoplasmic Reticulum and Golgi Retention Hook system

To investigate TRPM7 trafficking between intracellular compartments, we developed the Golgi and Endoplasmic reticulum (ER) retention using selective hooks (RUSH) system (Boncompain et al., 2012). It is a two-state assay based on the reversible interaction of core streptavidin and streptavidin-binding peptide (SBP). The assay relies on a hook protein of choice fused to core streptavidin anchored in donor compartments binding to TRPM7 fused to SBP with high affinity. This interaction would be outcompeted by biotin, a nontoxic vitamin, which releases TRPM7 from the donor compartment to follow its normal route through the secretory pathway. We purchased plasmids Str-Golgin84_VSVG-SBP-EGFP (#65305) for Golgi-Hook and Str-li_neomycin (#65312) for ER-Hook via Addgene. Meanwhile, we inserted SBP at N-terminus of TRPM7-YFP. The details of DNA synthesis would be described in the specific section 4.3.1.

2.6 Cell culture

2.6.1 Culture condition and sub-culture of cells

Cell culture reagents were supplied by Gibco™ (Life Technologies, Paisley, UK) including Dulbecco's modified eagle medium (DMEM), foetal bovine serum (FBS) and penicillin with streptomycin. 10% (v/v) foetal bovine serum (FBS) and 1%

Penicillin/Streptomycin (P/S) was added to culture media for maintenance of cell growth. Cells were grown in vented cap flasks in the presence of 5% CO_2 and 95% humidity while maintained at 37°C in a Heracell™ *VIOS CO2* incubator (ThermoFisher Scientific). All tissue culture practices were carried out in a sterile class II biological safety cabinet. All reagents used were sterile and pre-warmed to 37°C. Different cell types were maintained in appropriate culture medium (Table 2.7).

Table 2.7. Culture medium for different cell types.
The details of origins, growth condition and suppliers of cell types used for the project.

Cell Type	Origin	Growth Media	Supplier	Cat. Number
HEK 293	Human Embryonic Kidney	DMEM 10% FBS 1% Pen/Strep	Gibco Invitrogen	2401247 2378409 15140122
rVSMCs	Wistar Kyoto Rats/ stroke-prone spontaneously hypertensive rats	DMEM+Glutamax 10% FBS 1% Pen/Strep	Gibco Invitrogen	2348943 2378409 15140122
FT293 Parental cells	Human Embryonic Kidney	DMEM 10% FBS 1% Pen/Strep 15µg/ml Blasticidin 100µg/ml zeocin	Gibco Invitrogen InvivoGen	2348943 2378409 15140122 ant-zn-1 Ant-bl-1
DHHC5 KO	Human Embryonic Kidney	DMEM 10% FBS 1% Pen/Strep	Gibco Invitrogen	2401247 2378409 15140122
FT293-ER-Hook FT293-Golgi-Hook	Human Embryonic Kidney	DMEM 10% FBS 1% Pen/Strep 100µg/ml Hygromycin B	Gibco Invitrogen	2401247 2378409 15140122 10687010
FRT/TO-ER-Hook FRT/TO-Golgi-Hook FRT/TO-WT-TRPM7-YFP FRT/TO-TRPM7-M2-YFP FRT/TO-TRPM7-M5-YFP	Human Embryonic Kidney	DMEM 10% FBS 1% Pen/Strep 15µg/ml Blasticidin 100µg/ml Hygromycin B	Gibco Invitrogen InvivoGen	2401247 2378409 15140122 10687010 Ant-bl-1

All cell lines were adherent and cultured in T75cm^2 vented cap flasks. Cells were typically passaged at 1:6 ratio every 3-4 days once reaching 90%-100% confluence. Except VSMCs which were usually passaged at 1:4 after reaching 90%-100% confluency with 7-10 days and medium was regularly changed every 2-3 days. Cells were gently washed with warmed PBS then detached in 2ml 0.05% trypsin-EDTA (Gibco, UK) in the 37°C incubator for 2 minutes. 10ml of culture medium was added to flasks and the cells were mixing evenly by pipetting. Specific proportion of the cell suspension was transferred to a fresh T75 cm^2 flask subsequently adding 10ml fresh medium. The rest of the cell suspension was discarded.

2.6.2 Culture of rat Vascular smooth muscle cells (rVSMCs)

Primary rat Vascular Smooth Muscle Cells (rVSMCs) were isolated from mesenteric arteries dissected from Wistar Kyoto (WKY) rats and stroke-prone spontaneously hypertensive rats (SHRSP). Primary mouse vascular smooth muscle cells (mVSMCs) were isolated from mesenteric arteries dissected from wild type (WT) mice and heterozygous TRPM7+/Δkinase mice (Rios et al., 2020). VSMCs were kindly provided by Drs Francisco Rios and Augusto Montezano. In this study, VSMCs at passage 2-13 were used in *in vitro* experiments.

2.6.3 human Vascular smooth muscle cells (hVSMCs) samples

Lysis samples of human Vascular Smooth Muscle Cells (hVSMCs), including samples from normotensive and hypertensive individuals, were kindly provided by Dr Livia de Lucca Camargo and Prof Rhian Touyz. Ethics approval was obtained from the West of Scotland Research Ethics Service (WS/12/0294) and the research ethics board of the Ottawa Hospital Research Institute (OHRI), Canada (#997392132). Written informed consent was obtained for all study participants in accordance with the Declaration of Helsinki.

2.6.4 Cardiac myocytes from human ventricular biopsies from heart failure patients

Heart Failure cardiac myocytes samples were kindly supplied by Alice Main, Fuller Lab. Human heart tissue from organ donors and heart failure patients for

Acyl-RAC analysis was kindly provided by Kenneth Campbell, the Gill Cardiovascular Biorepository at the University of Kentucky. The study conformed with the principles in the Declaration of Helsinki and all procedures were approved by the local IRB, with collection previously described (Blair et al., 2016). All samples were labelled with patient ID's (detailed in Table 2.8) and were not unblinded until after analysis was completed.

Table 2.8. Human organ donor and heart failure information.

Record ID	Case type	Sex	Primary diagnosis
24713	Organ Donor	Female	N/A
2B487	Organ Donor	Male	N/A
31331	Organ Donor	Female	N/A
4B3FA	Organ Donor	Female	N/A
4D931	Organ Donor	Male	N/A
5155D	Organ Donor	Male	N/A
632FD	Organ Donor	Male	N/A
8CB30	Organ Donor	Female	N/A
B23E3	Organ Donor	Male	N/A
BC90C	Organ Donor	Female	N/A
DOF54	Organ Donor	Male	N/A
D61ZE	Organ Donor	Male	N/A
FC3CB	Organ Donor	Female	N/A
046E	Heart Failure	Male	Ischaemic cardiomyopathy
05FF7	Heart Failure	Female	Ischaemic HFrEF
14C39	Heart Failure	Male	Ischaemic cardiomyopathy
3F6DC	Heart Failure	Male	Ischaemic cardiomyopathy
58545F	Heart Failure	Male	Ischaemic cardiomyopathy s/p MI
6DB85	Heart Failure	Male	HFrEF from Ischemic cardiomyopathy
7CE52	Heart Failure	Female	Ischaemic heart failure
8296A	Heart Failure	Male	Ischaemic cardiomyopathy
8E8D8	Heart Failure	Male	Ischaemic cardiomyopathy
97CDC	Heart Failure	Male	Ischaemic cardiomyopathy
9D7E9	Heart Failure	Male	Ischaemic cardiomyopathy
AF1FF	Heart Failure	Male	Chronic systolic HF
B8BE2	Heart Failure	Male	Ischaemic heart failure
BO644	Heart Failure	Female	Ischaemic cardiomyopathy
C3B57	Heart Failure	Male	Ischaemic cardiomyopathy
CB8A5	Heart Failure	Male	Ischaemic cardiomyopathy
DA820	Heart Failure	Male	Ischaemic cardiomyopathy
EF5CB	Heart Failure	Male	Ischaemic heart failure
FE8E2	Heart Failure	Male	Chronic systolic HF

2.6.5 Freezing and revival of cells

Freshly produced stable cell lines and low passage cell lines were frozen in -80°C freezer for a short term or liquid nitrogen for a long term for storage. A fully confluent T75cm^2 flask of cells was washed with 37°C PBS then cells were detached by treating with 2ml 0.05% trypsin-EDTA at 37°C. 10ml of culture media was added to the cell suspension then it was transferred to a sterile 15ml falcon tube. Cells were pelleted by centrifuge at 500-700rpm for 5minutes at room temperature. The supernatant was discarded, and pellet was re-suspended with 2ml of freezing medium (20% FBS, 7.5% dimethyl sulfoxide (DMSO),72.5%

DMEM). Freezing medium for VSMCs was composed of 30% FBS,10% DMSO and the rest of DMEM. 1ml of cell suspension was stocked in a 1.5ml cryo-vial (Alpha laboratories, UK) which was placed in -80°C freezer covering with several layers of cotton wool. The vials were transferred to liquid nitrogen the next day.

For retrieving frozen cell stocks, frozen vials were stood for few seconds at room temperature, then was defrosted in 37°C water bath. The thawed suspension was mixed with 10ml pre-warmed culture medium gently. Then, cells were pelleted in centrifuge at 500rpm for 3minutes at room temperature. The supernatant was removed, and cells were re-suspended with 5ml fresh culture media. Entire cell suspension was mixed well to disperse equally in T25cm^2 flask and placed in the culture incubator. The culture medium was changed if need in the next day and cells were transferred to a T75cm^2 flask until reaching 90% confluency. Antibiotics as hygromycin B and blasticidin for stable cells were added at the point when they transferring to a T75cm^2 flask. Cells were sub-cultured as usual as described previously (section 2.6.1).

2.7 Cell based Assay

2.7.1 Transient Transfection of cell lines

Cells were normally seeded to 70%-80% confluency to 6-well plate or 12-well plates. Poly-L-lysine coated coverslips in 12-well plates were used in the case of cells for confocal microscopy. Meanwhile, poly-L-lysine coated 6-well plate was used when cells were prepared for cell surface biotinylation assay (section 2.8.2). Poly-L-lysine sterile solution was beneficial to cells adhesion and attachment. In generally, 0.1%(w/v) poly-L-lysine was diluted at 1:10 with PBS and added to each well in sufficient quantity to cover the culture surface. The solution was discarded after 15 minutes incubation at room temperature, then wells were washed 3 times with PBS and allowed to dry at room temperature for 30 minutes. All cells were left at 37°C incubator for overnight before transfection.

Lipofectamine 2000 (Invitrogen) was applied as transfection reagent, so the following procedures were according to manufacturer's guidelines. The amount of DNA and lipofectamine 2000 was in the ratio of 1:3 for 6-well plate and 1:4

for 12-well plate. For a 12-well plate, 1µg DNA and 100µl Opti-MEM reduced serum medium (Thermo Fisher Scientific) was added to a 1.5ml sterile tube. In addition, 4µl lipofectamine 2000 and 100µl Opti-MEM was mixed in a sperate tube followed by 5 minutes incubation at room temperature. For the 6-well plate, the amount of components are described in Table 2.9. After incubation, the components of two different tubes were mixed well and subsequently incubated for 15-20 minutes at room temperature. Approximately 250µl master mix of DNA/Lipofectamine 2000 was added to each well and cells were incubated for 48 hours at 37°C incubator. TRPM7 expression was poor 24 hours after transfection, but usually detectable 48 hours after transfection. The large (11kb) TRPM7 plasmid required careful handling. It is better to defrost plasmids on ice rather than room temperature, and aliquot in different tubes to avoid thaw more times.

Table 2.9. Transfection reagent mixture compositions.
Amount of component required for transient transfection of cells in accordance with Lipofectamine 200 manufacturer's protocol.

Component	**6-well plate** (per reaction)	**12-well plate** (per reaction)
Opti-MEM	150µl	100µl
DNA	2µg	1µg
Lipofectamine	6µl	4µl

2.7.2 Generation of stable cell lines

Flp-In™ 293 T-Rex cell line was designed to rapidly generate stable cell lines that ensure expression of protein of interest. These cells contain a single stably integrated FRT site at a transcriptionally active genomic locus which allows targeted integration with Flp-In™ vector (e.g., pcDNA™5/FRT, pcDNA™5/FRT/TO and pcDNA5/FRT/V5-His-TOPO®) to ensure high-level expression of gene of interest. In this project, co-transfection of pcDNA™5/FRT/TO inducible expression vector or pcDNA™5/FRT vector containing gene of interest and Flp recombinase vector, pOG44, results in targeted integration of the expression vector to the same locus in every cell, ensuring homogeneous levels of gene expression. We routinely used GeneJuice transfection reagent (Sigma Aldrich) and 3 different ratios of pcDNA5 vectors of gene of interest with pOG44 were used to allow optimum results (Table 2.10)

Table 2.10. Three ratios of pcDNA5 vectors of gene of interest and poG44 for stable cell lines generation.
Compositions of reagent mixtures required to improve success rate.

Component Ratio	PcDNA5 vectors (gene of interest)	pOG44	Gene juice
Low ratio	1µg	5µg	12µl
Medium ratio	1µg	9µg	20µl
High ratio	1µg	12µg	26µl

Flp-In 293 cells were plated into a 6-well plate and incubated at 37°C for overnight to allow 50%-60% confluency. Antibiotics were removed at this time to reduce toxicity as they will severely interfere with transfection efficiency. On the second day, cells were added with mixture of poG44&pcDNA5 in Opti-MEM (100µl) and GeneJuice in Opti-MEM (100µl) as previously described (section 2.7.1), then they were incubated at 37°C for 48 hours. For selecting the cells successfully transfected, cells were detached with 200µl trypsin and transferred into a T25cm^2 flask and maintained in 5ml DMEM supplemented with 100µg/ml hygromycin. Hygromycin required up to one week to fully exert effect resulting in massive cell death of any cell which has not incorporated with gene of interest. Cells were checked every day and fresh media was changed to remove dead cells debris, then leaving the flask in the incubator for several days to adaption of selection. Once cells had grown to approximately 30%-40% confluency, 15µg/ml blasticidin was reintroduced to the flask. Cells were cultured in growth media containing both antibiotics until small colonies clusters of resistant cells appeared. Small clusters were broken up to encourage cells to grow in an even monolayer. The insertions of gene of interest were tested with 10µg/ml tetracycline to investigate whether the gene had stably incorporated into the cells. Afterwards, successful created stable cells were cultured regularly with appropriate ratio as described previously (section 2.6.1).

2.7.3 Confocal microscopic analysis of transiently transfected cells

Cells for confocal microscopy were seeded on poly-L-lysine coated glass coverslips (Ø20mm) and incubated at 37°C for 48 hours after transfection. The following procedures for cells fixation were required to avoid direct light. Cells

were briefly washed with PBS for 2-3 times and followed by fixation with 4% paraformaldehyde (PFA) in PBS for 20 minutes at room temperature. Afterwards, 10mM Glycine/PBS was applied twice (5min each time) to quench any unreacted aldehyde and to offset the increase in background fluorescence caused by fixation. Then cells were washed with PBS for 5 minutes once before briefly rinsed in distilled water (dH_2O) to get rid of salt and air-dried on filter paper. Eventually, coverslips were mounted with Duolink® mounting medium (Fisherbrand™), where 4',6-diamidino-2-phenylindole (DAPI) was added for fluorescent DNA staining, to microscopic slides. Slides were covered with aluminium foil to avoid direct light and dried overnight. Coverslips were sealed with clear nail polish to ensure the oil used for confocal oil objectives would not contaminate the cells. The confocal images were taking by Zeiss LSM 520 microscope or Zeiss LSM 880 microscope with a 63x oil immersion objective (Carl Zeiss, Cambridge, UK). Qualitative analyses were assessed with LSM image browser (version4.2.0.121) and ZEN Blue (version 3.3.89.0000) software.

Several fluorescent plasmids were co-transfected with YFP fused constructs to stain targeted organelles. Grasp65, a Golgi-reassembly-stacking protein, fused with mCherry was applied to stain for Golgi apparatus. DsRED2-ER, which encoding the ER targeting sequence of calreticulin fused to the 5' end of DsRed2 and the ER retention sequence KDEL fused to its 3' end, was used to stain the endoplasmic reticulum. The detection wavelength and excitation laser applied were all shown in following Table 2.11.

Table 2.11. Wavelengths and excited filters for fluorescent signals.
Details of wavelengths and filters setting for Zeiss LSM confocal microscope.

Name	Wavelength range	Excited filter
DAPI	410nm-513nm	405nm
YFP	519nm-580nm	514nm
DsRED2-ER	575nm-644nm	543nm
Grasp65-mCherry	580nm-700nm	543nm
Anti-rat Alexa Fluor 546	540nm-638nm	543nm
Anti-rat Alexa Fluor 633	654nm-738nm	633nm

2.7.4 Confocal microscopic analysis with immunofluorescence on stable cells

In addition to transfection with fluorescent fused plasmids, the cells were also stained with immunofluorescence (in short, IF) technique which relies on application of antibodies chemically labelled with fluorescent dye to visualization under microscope. When ligating Golgi-hook from Str-Golgin84_VSVG-SBP-EGFP (Addgene 65305) into PcDNA5-FRT/TO plasmid vector, a HA tag sequence was also amplified during PCR reaction. Hence, IF was used to detect the HA tag in cells stably expressing the Golgi Hook. Cells were seeded and fixed as described previously (section 2.7.3) on poly-L-lysine coated coverslips. 4% paraformaldehyde was quenched with 100mM glycine/PBS for 5 minutes and additionally quenched in 10mM glycine/PBS for 5 minutes. Cells were washed with PBS 3 times, then incubated with 0.1% Triton X-100/PBS at room temperature for 10 minutes to permeabilise membrane. Subsequently, 3% BSA in PBS was added to block non-specific binding site at room temperature for 1 hour. Afterwards, cells were washed with 3 times PBS and 5 minutes each time before incubation with HA primary antibody (1:200) in 0.1% BSA/PBS overnight at 4°C. On the second day, cells were washed with PBS for 3 times then incubated with fluorescent secondary antibody (1:400 anti-rat) in 0.1% BSA for 1 hour at room temperature. Finally, coverslips were washed 3 times with PBS and rinsed with dH_2O, followed by air-dry with filter-paper and mounting in slides. DAPI was added to mounting media if needed (1µl per ml). During the steps of antibodies incubation, a piece of parafilm was placed on top of a damp piece of blotting pad inside a cassette. 100µl antibodies were dropped in parafilm and coverslips flipped over for incubation. Two different fluorescent secondary

antibodies of anti-Rat were used, separately Alexa Fluor 546 And Alexa Fluor 633 (Thermo Fisher Scientific). Other wavelengths and exited filters were used as described as section 2.7.3 (Table 2.11).

2.8 Protein analysis

2.8.1 Purification of palmitoylated proteins by Resin Assisted Capture (Acyl-rac)

To purify palmitoylated protein from cell lysates or tissues, Resin Assisted Capture of acylated proteins (Acyl-RAC) was applied, based on the approach developed by Forrester et al. (2010) with minor modifications. All the procedures were conducted in room temperature except if specified otherwise. Following the indicated treatments or transfections, cells were pre-washed using PBS, then lysed and solubilized in 500µl (6-well plate) of blocking buffer (100 mM HEPES, 1 mM EDTA, 2.5% (w/v) SDS, pH 7.5), freshly supplemented with 1% methyl methanethiosulfonate (MMTS)(sigma), a sulfhydryl reactive compound that blocks free cysteines. Lysates were transferred to 2ml microcentrifuge tubes and incubated on a heat block shaker at 1200rpm for 4h at 40˚C. Then protein was precipitated by adding 3 volumes of pre-chilled 100% acetone followed by incubating at -20˚C for a minimum 20min. Precipitated protein were pelleted by centrifuging at 17,000g followed by thoroughly washing with 70% acetone for 5 times to remove MMTS, one-time quick wash and four times extensive wash with rotator for 2-3mins. Protein pellets were air-dried before re-dissolving in 300µl binding buffer (100 mM HEPES, 1 mM EDTA, 1% SDS, pH 7.5) by shaking at 1200rpm and 40˚C. When protein had dissolved, they were centrifuged at 17,000g for 10 minutes to remove any particles or insoluble material. Meanwhile, thiopropyl sepharose beads (GE Healthcare) were equilibrated with Binding buffer in a 15ml falcon tube for 15 minutes on rotator. For each sample, 30µl supernatant was retained and mixed with 1:1 SDS-PAGE buffer as unfractionated (UF) sample. 120µl of remaining lysate was added to a 1.5 ml microcentrifuge tubes containing 50µl thiopropyl sepharose beads slurry and 25µl fresh 2M hydroxylamine (NH_2OH), PH=7.5, which mediated thioester bond cleavage and exposed previously palmitoylated cysteines. In some experiments, 2M NaCl was used instead of HA as a negative control. Palmitoylated proteins were captured on a rotator at room temperature for

2.5h. The beads containing samples were washed five times with binding buffer, 5 minutes for each time, then bound protein was eluted from beads with 1:1 2x SDS PAGE buffer containing 100 mM dithiothreitol (DTT). Prior to electrophoresis, samples were incubated at 60°C for 10 minutes and chilled to room temperature, following with centrifuged at maximum speed for 3mins to pellet the beads. 2M NaCl reaction as negative control never captured proteins, so it was occasionally applied to check Acyl-RAC efficacy. When the negative control was excluded, 220µl resolubilised lysate and 40µl 2M Hydroxylamine were added to 50µl thiopropyl sepharose beads slurry as HA sample.

2.8.2 Purification of biotin labelled cell surface proteins via streptavidin affinity capture

To identify protein present at the cell surface, cells were lablelled with the cell-impermeable amine reactive biotinylation reagent sulfo-NHS-SS-biotin (APE_XBIO), then purified with streptavidin affinity capture. Cells were seeded at poly-L-lysine coated 6-well plate (details in section 2.7.1) then treated or transfected. Cells were gently washed with warm PBS for 3 times then 1ml of 1mg/ml sulfo-SS-NHS-biotin/PBS was added to each well, and cells were incubated at 37°C for 30 minutes. Biotinylating solution of sulfo-SS-NHS-biotin was made freshly each time. Cells were lysed with 500µl of cold cell lysis buffer (Table 2.12) at 4°C after being washed with PBS for 3 times. Cell lysates were transferred to 1.5ml microcentrifuge tubes and incubated on a rotator for 30 minutes at 4°C. Meanwhile, streptavidin Sepharose beads (GE Healthcare) were equilibrated in cold cell lysis buffer for 1 hour at 4°C. For each individual sample, 50µl supernatant of lysate was kept as unfractionated staring material (SM) after centrifugation at 4°C with 17,000g. The remaining supernatant was transferred into a new 1.5ml tube then added into 30µl streptavidin Sepharose beads followed incubation at 4°C for 1-4 hours (overnight was acceptable). Subsequently, samples were centrifuged at 17,000g for 5 minutes at 4°C and 100µl supernatant was retained as unbound sample (UB). The remaining supernatant was discarded, and beads were washed with 1ml cold cell lysis buffer for 3 times at 4°C, 5 minutes each time. Following the final wash, 50µl SDS-PAGE buffer containing 5% β-ME and 100mM DTT was added into the beads which were incubated for 15mins at 60°C to elute captured proteins. Since the biotin tag could be cleaved with reducing agents, before analysis the

unfractionated start material and unbound samples were split and 5% β-ME plus 100mM DTT were added to half. The other half was left unreduced to estimate labelling efficiency and capture of biotinylated proteins.

Table 2.12. Composition of cell lysis buffer.
All procedures after sulfo-SS-NHS-biotin incubation were conducted at 4°C.

Buffer	Composition
Cell lysis buffer	1% Triton X-100 0.1% SDS Protease inhibitor cocktail (Merck Millipore) Rest of PBS

2.9 Protein interaction

2.9.1 Immunoprecipitation TRPM7 with GFP-Trap Agarose Resin

To identify protein interactions of TRPM7 and how these are modified depending on palmitoylation status, TRPM7 was immunoprecipitated using GFP-Trap Agarose resin (Chromotek). Stable cell lines expressing WT-TRPM7-YFP and TRPM7-M5-YFP were seeded on T75cm2 flasks, for which 5 flasks of each cell line were used for the experiment. Cells were briefly washed 3 times with PBS and lysed with 1.5ml chilled cell lysis buffer (1% v/v Triton X-100+PBS+Protease inhibitor cocktails) per flask. Cell lysate was transferred to 5x 1.5ml microcentrifuge tube and incubated at 4˚C for 30 minutes on a rotor. After incubation, 30µl cell lysate was collected (6µl of each tube) then mixed with 1:1 2x SDS-PAGE buffer as 'whole lysate' sample. After centrifugation at 17,000g for 5 minutes at 4˚C, 30µl supernatant was collected and mixed with 1:1 2x SDS-PAGE buffer as 'soluble lysate' sample. The rest of the supernatant was added into another 1.5ml microcentrifuge tube containing 5µl GFP-Trap beads (25µl in total) following incubation at 4˚C for 1 hour on rotor. GFP-Trap beads were pelleted at 2,500g and 4˚C for 5 minutes then 30µl of supernatant was retained as unbound samples (UB). The rest of the supernatant was discarded and beads were washed 3 times with lysis buffer, for which wash was 5 minutes each. The beads were combined into the same tube before the last wash following elution with 50µl SDS-PAGE buffer. Samples were heated at 60˚C for 10 minutes before analysis using gel electrophoresis western blotting. Co-purified proteins with

TRPM7 were identified using Coomassie dye on a gel. Meanwhile, they were used for a quantitative proteomic comparison.

2.9.2 Proteomics with Mass spectrometry

After immunoprecipitation of TRPM7 with GFP-Trap agarose beads (details in section 2.9.1), samples were analysed using 10% polyacrylamide gels (details in 2.10.1) then digested with Trypsin Gold (Promega). Liquid Chromatography - Mass spectrometry (LC-MS) were conducted by Dr.Sheon Samji. Samples were analysed using 3 hours of Liquid Chromatography (LC) gradient with LTQ Velos Orbitrap (Thermo Scientific). Data analysis on MaxQuant v1.6.5.0 Database: uniprot-proteome_UP000005640_human_22042020.

2.10 Gel Electrophoresis and western blotting

2.10.1 Gel preparation

Gradient Sodium dodecyl sulphate-polyacrylamide gel electrophoresis (SDS-PAGE) gels were cast with 12 pairs of 0.75mm spacer plates and short pates assembled into a Mini-PROTEAN 3 multi-casting chamber (BIO-RAD, Cat.1654110). The components for 6%-20% gradient gels were mixed through a bottom port with the Model 485 gradient former (BIO-RAD, Cat. 1654120) via peristaltic pump. Gels were left to polymerise for 1 hour topped with 150µl distilled water saturated butan-1-ol to produce a smooth, completely level surface. Butan-1-ol was removed and washed thoroughly with distilled water, then sloping the chamber or using filter-paper to get rid of leftover water. Stacking gels were adding to the top of resolving gels and 15 well comb was immediately inserted to individual gel. Stacking gels were polymerised within 15-20 minutes. The components for 6%-20% gradient gels are described in Table 2.13. Meanwhile, single percentage gels were simply formed with spacer plates and short plates assembled into Mini-PROTEAN® Tetra Cell Casting Module (BIO-RAD, Cat. 1658011). Components for different single gels were showed in Table 2.14.

Table 2.13. Components of 6%-20% gradient gels.
Respective volumes of buffer stocks required to prepare 12 gels (LD= light density, HD= heavy density).

	For 30ml	For 25ml	For 30ml
Component	**6% LD gel**	**20% HD gel**	**Stack gel**
dH_2O	16ml	1.6ml	20.4ml
1.5M Tris.Cl (PH=8.8)	7.6ml	6.3ml	
1.0M Tris.Cl (PH=6.8)			4ml
10% SDS	300µl	250µl	300µl
30% Acrylamide	6ml	16.7ml	5ml
TEMED	12.5µl	12.5µl	30µl
			Split into 3x 15ml tubes, 10ml each
10% APS	125µl	80µl	100µl per 10ml

Table 2.14. Components of single percentage gels.
Respective constituents of resolving and stacking for single percentage gel.

Component	Resolving Gel (For 10ml)				Stacking gel (For 5ml)
	8%	10%	12%	15%	5%
dH_2O	4.6ml	4.0ml	3.3ml	2.3ml	3.4ml
1.5M Tris.Cl (PH=8.8)	2.5ml	2.5ml	2.5ml	2.5ml	
1.5M Tris.Cl (PH=6.8)					630µl
10% SDS	100µl	100µl	100µl	100µl	50µl
30% Acrylamide	2.7ml	3.3ml	4.0ml	5.0ml	830µl
10% APS	100µl	100µl	100µl	100µl	50µl
TEMED	6µl	4µl	4µl	4µl	5µl

2.10.2 Sample preparation for electrophoresis

Samples to be analysed with electrophoresis were mixed thoroughly with 1:1 2x SDS-PAGE buffer (Table 2.15) supplemented with 100mM DTT as reducing agent. Prior to gel electrophoresis, samples were heated at 60°C for 10-15 minutes and allowed cool down to room temperature. Afterwards, samples were centrifuged at 17,000g for 3 minutes in case of those containing beads were interfering gel loading.

2.10.3 Gel electrophoresis conditions

After accommodating 0.75mm thickness gels to Mini-PROTEAN Tetra Cell chamber (BIO-RAD, cat.1658000FC), samples containing 2X SDS-PAGE buffer were loaded into the gels with 10µl loading volume per well. 5µl of Precision Plus Protein™ dual colour standards (BIO-RAD, Cat.1610374) was loaded as the protein ladder. 1x Tris-Glycine based running buffer (Table 2.15) was used for electrophoresis under the appropriate voltage, particularly 100V for 30minutes then increasing to 200V until the dye reached at the bottom of gels.

2.10.4 Western blotting

Following gel electrophoresis, separated proteins were transferred to the 0.45µm pore size polyvinylidene difluoride (PVDF) membranes (Merck) via semi-dry Bio-RAD Trans-Blot Turbo Transfer system (BIO-RAD, cat.1704155). 8.5cm x 6cm PVDF membranes were prewetted using methanol for 2 minutes and equilibrated in transfer buffer (Table 2.15) for minimum 5 minutes. The stacking gel were removed and discarded, then the PVDF membrane was placed onto the resolving gel besides getting rid of additional air bubbles with roller. The gel and membrane were assembled between two sheets of extra thick filter paper (Themo Fisher, Cat.88620). This sandwich was assembled into a semi-dry transfer cassette and transferred at 25V, 1.0A for 45 minutes within appropriate amount of transferring buffer. After transfer, PVDF membranes were incubated in 5% skimmed milk/PBS-T (Table 2.15) for 1 hour to block nonspecific protein binding sites. Membranes were incubated in primary antibody (Table 2.16) for overnight at 4°C.

The following day, primary antibodies were re-collected, and membranes were washed with 1x PBS-T briefly for 3-4 times for 10 minutes in total. Relevant secondary antibodies were applied to membranes with 1 hour incubation at room temperature. Finally, membranes were washed with 1X PBS-T for 2.5 hours with at least 5 times change after removing secondary antibodies. Proteins were visualised by chemiluminescence in Bio-Rad ChemiDoc XRS imaging system after incubation for 5 minutes of Immobilon HRP substrate (Merck-Millipore, Cat.no.11556345). Solution A and B of Immobilon HRP substrate were mixed with 1:1 ratio and 2ml as final volume for per blot. Membranes covered with cling film were stored in -20°C freezer for several days or air-dried in room temperature for storage.

Table 2.15. Components of buffer for Gel electrophoresis and Western blotting.
All buffers were storage at room temperature.

Buffer	Constituents
2x SDS-PAGE buffer	100mM Tris 4% (w/v) SDS 20% (w/v) Glycerol 0.02% (w/v) Bromophenol Blue 5% β -mercaptoethanol
Running buffer	1x Tris-Glycine (25Mm Tris, 192mM Glycine) 0.01% (w/v) SDS
Transfer buffer	1x Tris-Glycine (25mM Tris, 192mM Glycine) 0.01% (w/v) SDS 20%(v/v) methanol
1X PBS-T	137 mM NaCl 2.7 mM KCl 10 mM Na_2HPO_4 1.8 mM KH_2PO_4 0.1% (w/v) Tween-20
1x TBS	20mM Tris 150mM NaCl (PH=7.4 with HCl)

Table 2.16. Antibodies used for western-blotting analysis
The details of primary antibodies and secondary antibodies, manufacturers and dilution of each antibody used at experiments.

Antibody	Species	Manufacturer	Dilution
Anti-TRPM7 (ab109438)	Rabbit	Abcam	1:1000
Anti-TRPM7 (#ACC-047)	Rabbit	Alomone Labs	1:200
Foltillin2	Mouse	BD Biosciences	1:2000
Na/K ATPase α1	Mouse	DSHB	1:50
GFP	Rabbit	Abcam	1:2000
GAPDH	Mouse	Abcam	1:10,000
HA	Rat	Roche	1:5000
DHHC5	Rabbit	Sigma	1:2000
FLAG	Mouse	Abcam	1:2000
α-Rat	__	Invitrogen	1:400
α-Rabbit	__	Jackson	1:2000
α-Mouse	__	Jackson	1:2000

2.10.5 Analysis

Western blot images were analysed with the Quantity One Analysis software which supported by Bio-Rad imaging system.

2.10.6 Detection of total protein using SimplyBlue™ SafeStain Gel Stain

In some experiments, polyacrylamide gels were stained with SimplyBlue™ to visualise all separated proteins. After electrophoresis, gels were rinsed with 100ml deionized water 3 time with 5 minutes each, to remove SDS and buffer salts. Following adding a sufficient volume of SimplyBlue™ SafeStain (~20ml), gels were incubated 1 hour at room temperature with gentle shaking. Note: 20ml of SimplyBlue™ SafeStain added to gels could be boiled by microwave at high power for 45 seconds to 1 minute, which would improve sensitivity. Gels were washed with 100 mL of water for 1–3 hours. Meanwhile, to obtain the clearest background for photography, performing a second 1-hour wash with 100 mL of water to the gels. 20 mL of 20% NaCl (w/v) were added if gels need store in

water for few days. Gels were imaged using transillumination on a Bio-Rad imaging system.

2.11 Ion uptake measurement

2.11.1 Measurement of intracellular free Mg with magnesium green by flow cytometry

Intracellular free Mg levels in stably transfected cells were assessed using fluorescent Mg indicator Magnesium Green (Thermo Fisher Scientific) via flow cytometry. Flow cytometry is the technique used to detect and measure physical and chemical characteristics of a population of cells or particles (Figure 2.1). The cells or particles suspended in salt-based buffer were injected into the flow cytometer instrument. Cells flow individually through a laser beam, where the light scattered was characteristic to the cells and their components. Cells were labelled with fluorescent markers, magnesium green indictor (Ex_{max}=490nm, Em_{max}=520nm), then light was absorbed and emitted following channelling by a set of filters and mirrors, consequently detected by different photomultiplier tubes (PMTs). Tens of thousands of cells were examined rapidly, and data generated by computer software.

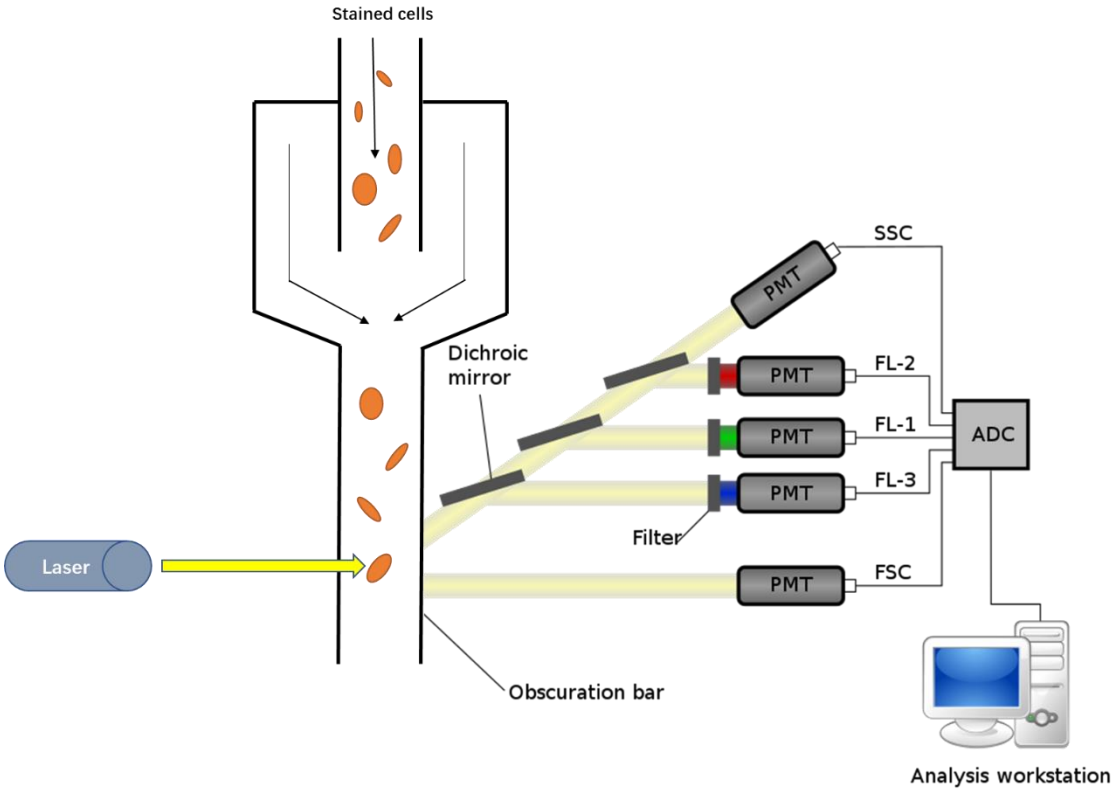

Figure 2.1 Overview working system of flow cytometer.
In the flow cytometer, cells pass individually through a laser light beam. Forward and side scattered light is detected to distinguish cell populations based on differences in cell size and granularity. Fluorescence from stained cells or particles are channelled by a set of filters and mirrors, consequently detected by different photomultiplier tubes (PMTs) (McKinnon, 2018).

To identify the influence of palmitoylation of TRPM7 on intracellular free Mg levels, Magnesium Green™ AM indictor (Zou et al., 2020) were applied to FRT/TO-WT-TRPM7 stable cells and non-palmitoylated TRPM7 stable cells (FRT/TO-TRPM7-M5 and FRT/TO-TRPM7-M2). Cells were seeded on 6-well plates and incubated for 48 hours at 37°C with DMEM (-/+ Tetracycline). Culture medium was removed and replaced with 800µl of Mg free HEPES buffer (Table 2.17) for each well when cells reached ~90% confluency. Cells were incubated for 10 minutes at 37°C to allow stabilization and equilibration of ion gradients. During this time, Magnesium Green working solution was prepared by diluting 5µl of the stock Mg indicator in 2.5ml of Mg free HEPES buffer resulting final concentration as 5µM. This solution was covered with aluminium foil to avoid the direct light. HEPES buffer was discarded and 400µl of the Mg Green working solution was added to per well followed by incubation for 1 hour at 37°C. Stained cells were washed twice with 1.5ml PBS before detachment using 400µl trypsin for 3 minutes. Cell suspensions were transferred into FACS tubes and centrifuged at 500g for 5 minutes. The supernatant was discarded and cell

pellets were resuspended in 250µl Mg free HEPES buffer following incubation for 30 minutes at 37°C in darkness to allow complete de-esterification of intracellular AM ester before measurement. To measure the intracellular free Mg, cells were gently vortexed and measured with fluorescein isothiocyanate (FITC, Ex/Em 492/517) channel via flow cytometry. Otherwise, to assessment of Mg influx, 25µl of 50mM MgCl2 (final concentration 5mM $MgCl_2$) was added to the resuspended cells and incubated for 10 minutes at room temperature during darkness. Same FITC channel was applied to measure Mg influx levels of cells under those extracellular Mg condition as 5mM.

Table 2.17. Magnesium free HEPES buffer.
Compounds were dissolved into dH_2O and adjusted pH to 7.2.

Buffer	Compounds
HEPES buffer (PH=7.2)	130mM NaCl 5mM KCl 1mM $CaCl_2$ 20mM HEPES 10mM D-Glucose Made up with dH_2O

2.11.2 Measurement of intravesical free Zn level via FRET Zn sensor

To identify if alterations of palmitoylation on TRPM7 have influence on intravesicular free Zn level, genetically encoded Forster Resonance Energy Transfer (FRET)-based sensors, eCALWY4ic, was used to monitor fluctuations in intracellular free zinc levels. FLAG-TRPM7-eCALWY4ic Zn sensor was kindly provided by Sanchez Martinez in Dr. David Clapham Lab (Howard Hughes Medical Institute). e-CALWY4ic Sensor encoded into S1-S2 loop of M7, which could measure intravesical Zn level (Abiria et al., 2017b). CALWY (CFP-Atox1-linker-WD4-YFP) consists of two metal binding domains (Atox1 and domain 4 of ATP7B) linked via a long flexible linker, with each domain providing two cysteines to co-ordinate zinc (Figure 2.2). Zn binding changes the separation of the fluorophores YFP and CFP causing a change in energy transfer (FRET). FLAG-TRPM7-M5-eCALWY4ic Zn sensor was derived from the template FLAG-TRPM7-eCALWY4ic Zn

sensor with TRPM7-M5 primer through mutagenesis via In-Fusion HD Cloning kit (Takara), with details described previously (section 2.5.1).

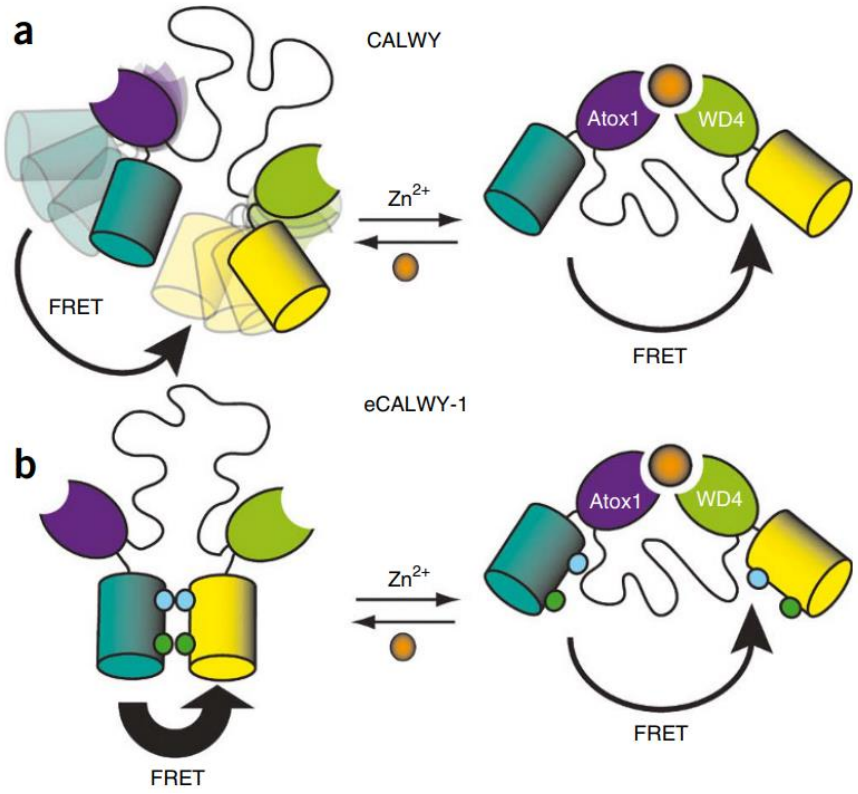

Figure 2.2 Overview structure of CALWY Zn sensor (Abiria et al.)**.**
Atox1 and the fourth domain of ATP7B (WD4) were used as metal-binding domains. The CALWY sensor yielded a small FRET change owing to the presence of a distribution of conformations in the Zn-free state.

HEK293 cells was seeded on poly-L-lysine coated glass coverslips (Ø34mm) in 6-well plate with DMEM cell growth medium until cells reached semi-confluence. FRET experiments were performed on them 48 hours after transfection with 2µg FLAG-TRPM7-eCALWY4ic or FLAG-TRPM7-M5-eCALWY4ic Zn sensor. Cells were maintained in HBT-A buffer (Table 2.18) at room temperature before coverslips were assembled to Differential Interference Contrast (DIC) optical. FRET signals in basal Zn levels were measured by maintaining cells in 200-300µl HBT-A buffer. To study Zn influx, FRET signals were recorded immediately after addition of 100–500 µM extracellular $ZnCL_2$ (Sigma Aldrich) and saturation with 50µM Zn/20µM pyrithione (Sigma Aldrich, Cat.13463-41-7). Each experiment concluded with addition of 50µM TPEN (Sigma Aldrich, Cat.16858-02-9) to chelate extracellular Zn.

FRET activity was imaged using an inverted camera equipped in Olympus IX71 microscope via PlanApon, 60X, NA 1.42 oil immersion objective, 0.17/FN 26.5 (Olympus, UK). The microscope was equipped with a beam splitter optical device (Dual-channel simultaneous imaging system, DV2 mag biosystem (ET-04-EM) and a cooled CCD camera (SNAP HQ Monochrome, Photometrics) to detect emitted photons. MetaFluor 7.1 (Meta imaging system) was used for image acquisition and analysis. FRET ratio was measured as the changes in the background subtracted 480/545nm fluorescent emission intensity on excitation at 430nm.

Table 2.18. Compounds of HBT-A buffer.
Cells were imaged and stimuli at HBT-A buffer as basement.

Buffer	Constitutes
HBT-A	20 mM HEPES 120 mM NaCl 0.8 mM $MgCl_2$ 1.8 mM $CaCl_2$ 10 mM glucose (PH=7.5, adjusted with HCl)

2.11.3 Measurement of Calcium influx with Fluo-4 Direct™ Calcium Assay

To investigate influence of palmitoylation level of TRPM7 on Ca influx, Fluo-4 Direct™ Calcium reagent (Themo Fisher, Cat. no. F10471) was used. Stable cells of FRT/TO-WT-TRPM7 and FRT/TO-TRPM7-M5 with distinct difference on palmitoylation were seeded on a 96-well poly-L-lysine coated microplates then incubated at 37˚C for 48 hours within DMEM (-/+ tetracycline) medium. Cells were maintained until a monolayer formed. A 2x concentrated stock of Fluo-4 Direct™ was prepared by adding Ca free assay buffer 1 (10ml) to Fluo-4 and 250mM (200µl) probenecid. This solution was diluted 1:1 with Ca free assay buffer 1 before use.

Cells were briefly washed once in Ca free buffer then 100µl of 1x Fluo-4 Direct™ Calcium reagent was added to each well and cells incubated at 37˚C for 1hr in the dark. Basal fluorescence intensity of cells was assessed immediately at 37˚C after incubation via POLARstar OPTIMA Multidetection Microplate Reader (BMG

LABTECH). The Ca fluorescence intensity measurement was performed at appropriate wavelength (Ex=494nm and Em=516nm) with 1450 gain value from bottom optic of microplate. Subsequently, Buffer1 was completely removed and 100µl of 1mM Ca Buffer2 was added into the plate followed by immediately measuring its fluorescent intensity. After that, buffer 2 was discarded and 100µl of 5mM Ca Buffer3 was added before same measurement procedure was repeated immediately. The data was collected and exported with MARS Data Analysis Software (OPTIMA, program version 2.10 R3) (Chubanov et al., 2012).

Table 2.19. Basal and stimulating buffers for Fluo-4 Direct™ Calcium reagent.
1mM Ca and 5mM Ca HEPES buffer were used for measuring Ca influx.

Buffer	Compounds
0mM Ca Buffer1 (PH=7.4)	140mM NaCl 6mM KCl 10 mM HEPES 5mM Glucose
1mM Ca Buffer2 (PH=7.4)	140mM NaCl 6mM KCl 10 mM HEPES 5mM Glucose 1mM $CaCl_2$
5mM Ca Buffer3 (PH=7.4)	140mM NaCl 6mM KCl 10 mM HEPES 5mM Glucose 5mM $CaCl_2$

Chapter 3 Palmitoylation site mapping in TRPM6 and TRPM7

3.1 Introduction

3.1.1 TRPM7 and TRPM6

Transient receptor potential melastatin cation channel 6 (TRPM6) and 7 (TRPM7) are extraordinary proteins consisting of non-selective divalent cation permeable ion channels and an α-type serine/threonine kinase domain. Both the kinase domain and the ion channel have been implicated in ion homeostasis and many cellular physiological processes. The kinase domain is proteolytically cleaved from the ion channel in a cell-type-specific manner and then translocates to the nucleus and binds transcription factors to regulate gene expression (Krapivinsky et al., 2014). TRPM7 ion channel and its kinase activities are interdependent in the regulation of cellular and systemic Mg homeostasis. Specifically, TRPM7 ion channel acts as the main Mg conduction pathway, whereas the Mg concentration in the proximity of the channel pore regulates activity of the kinase domain (Nadolni and Zierler, 2018). In addition, TRPM7 has been reported to exacerbate Zn mediated neuronal injury (Inoue et al., 2010) and TRPM7-mediated Ca influx causes cellular Ca overload and cell death during anoxia in neurons (Aarts et al., 2003). In contrast, TRPM6 is unable to form a tetrameric channel, and requires TRPM7 co-expression to target it to the cell surface and function in Mg absorption (Chubanov et al., 2004).

As a reversible post-translational modification, palmitoylation not only occurs shortly after protein synthesis but also throughout the lifetime of a protein in the secretory pathway. It regulates protein trafficking, protein stability, membrane micro localization, and protein-protein interactions (Greaves et al., 2009, Linder and Deschenes, 2007, Resh, 2006). In the present investigation, to investigate our hypothesis that palmitoylation regulates TRPM7 activity, we need to map the palmitoylated cysteines of TRPM7 to generate the un-palmitoylated mutants to compare with wild type.

3.1.2 DHHCs palmitoyl acyl transferase (DHHC-PAT) structure and localization

Palmitoylation has diverse effects on proteins and cell function, likely dominated by properties of saturated palmitate fatty acid, particularly its hydrophobicity/membrane affinity and preference for ordered cholesterol-rich

membrane domains or rafts (Melkonian et al., 1999). Most protein S-palmitoylation is catalysed by a family of polytopic eukaryotic integral membrane enzymes known as DHHC-palmitoyl transferases, which are defined by conserved zinc finger and aspartate–histidine–histidine–cysteine (zDHHC) domains in an intracellular loop (Rana et al., 2018). The predicted DHHC integral membrane proteins structure usually has 4 transmembrane (TM) domains (rarely have six), with the conserved aspartate–histidine–histidine–cysteine catalytic domain located in a cytosolic loop with N- and C- termini also in cytosol (Figure 3.1) (Tabaczar et al., 2017). Overall, most of the DHHC enzymes localize at endoplasmic reticulum (ER) and Golgi apparatus, however overexpressing DHHC-5, and -20 have been observed in the plasma membrane of HEK 293T cells and yeasts DHHCs (Ohno et al., 2006). DHHC proteins could cycle among different compartments. For example, zDHHC5 palmitoylates its substrates in an activity-dependent manner relying on changes in its subcellular localization, specifically it internalised to find its substrate δ-catenin in dendritic shafts (Brigidi et al., 2015).But the underlying mechanism of DHHC protein specific localization is unclear.

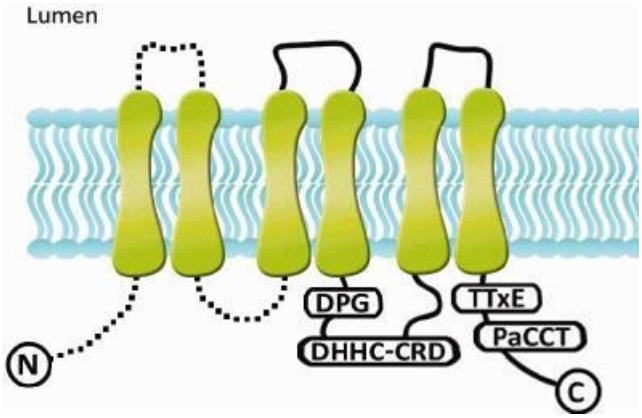

Figure 3.1 Predicted structure of DHHC acyltransferases (Tabaczar et al., 2017).
DHHC proteins usually have four transmembrane domains, rarely have six (shown with dotted lines). The conserved Asp-His-His-Cys domain is in a cytosolic loop, for which is indicative of cysteine-rich domain (CRD). Besides the DHHC proteins contain a highly conserved cytosol-facing DPG motif. In addition, most DHHC enzymes have a threonine-threonine-x-glutamate (TTxE; x stands for any amino acid residue) and palmitoyltransferase conserved C-terminus (PaCCT) motifs at its C-terminus.

Human DHHC20 is the only zDHHC acyl-transferase for which the crystal structure has been solved (Rana et al., 2018). The four transmembrane domains of hDHHC20 comes close together on the lumen side and spreads apart on cytoplasmic side, which is thought to be convenient for substrate attachment and catalysis (Figure 3.2A). The mechanism of palmitoylation proceeds in two

stages. Firstly, DHHC enzyme pointing inward into the lipid bilayer forms a hydrophobic cavity, allowing the fatty acyl coenzyme A (acyl-CoA) to be inserted and the active site cysteine to be auto-acylated. Secondly, the palmitoyl group covalently linked to DHHC is immediately transferred to its substrate proteins (Figure 3.2B) (Rana et al., 2018). In the second step, previously protonated His154 has been regard as the key of acyl-enzyme thioester activation by providing a proton to the carbonyl oxygen, subsequently allowing the palmitoyl transfer to the substrates (Rana et al., 2018). Furthermore, the structure surrounding active sites means one side of the acyl-enzyme thioester is shielded by hydrophobic residues, consequently only exposing the front side of the acylated DHHC to the approach of substrate cysteines. The palmitoylated cysteines in different substrates resides in different sequence context with different chemical and structural environment.

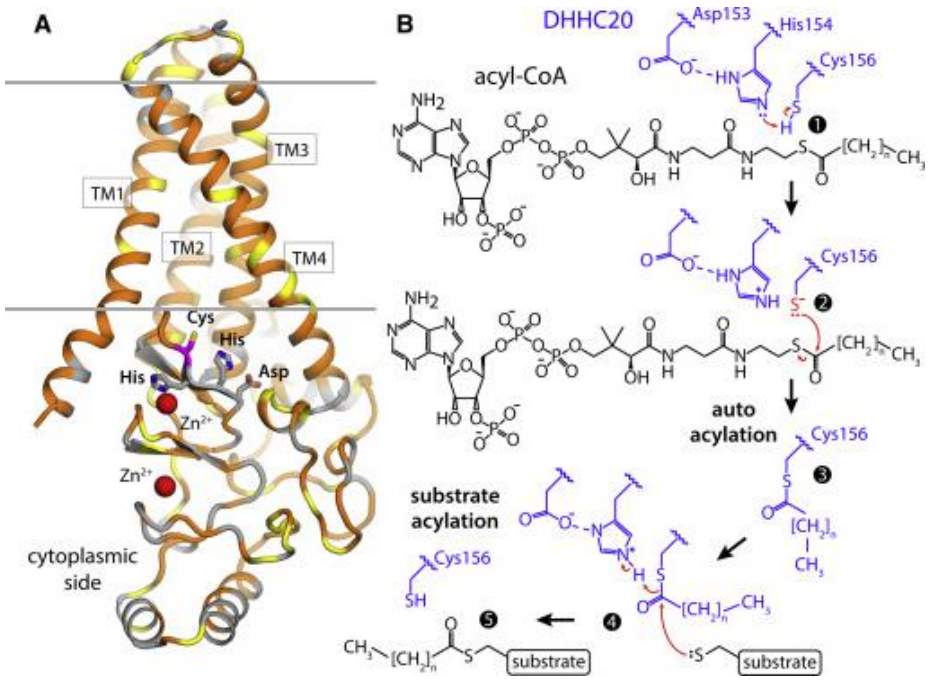

Figure 3.2 Crystal structure of human DHHC20 and mechanism of palmitoylation (Stix et al., 2020).
A) Crystal structure of hDHHC20. In the transmembrane (TM) domain (TM1-TM4), hydrophobic and aromatic residues are coloured in orange, serine and threonine residues in yellow and the others in grey. Two red spheres represent the Zn ions. B) the procedures of DHHC20 enzyme palmitoylation mechanism. Steps1-3 are DHHCs auto-acylation stage and steps 4-5 are the stage of acyl-chain transferring to a substrate.

3.1.3 Common features of potential palmitoylation cysteine(s)

With previously described structure of DHHC20 and its palmitoylation mechanism, the zDHHC enzymes active site is established to localize at

membrane/cytosol interface. Therefore, we assume the potential palmitoylated cysteines of substrates may be commonly required to be in close membrane proximity, or near hydrophobic amino acids to accept palmitoyl motif transfer by DHHCs. For instance, the validated palmitoylation site (Cys739) of Na/Ca exchanger (NCX1) in Rat is localized in large intracellular loop (between transmembrane domain 5 and 6) (Reilly et al., 2015). The secondary structure prediction algorithm Jpred4 predicts residues 740-757 close to the palmitoylated cysteine forms an alpha helix with a large hydrophobic face and a small hydrophilic face (Drozdetskiy et al., 2015). Disruption this α-helical geometry either by introducing of negatively changed amino acids to hydrophobic face or applying alanine mutagenesis to hydrophilic face all diminish or abolish NCX1 palmitoylation (Plain et al., 2017). Additionally, insertion of the amphipathic α-helix induces palmitoylation of cysteines not originally palmitoylated (Plain et al., 2017). Therefore, NCX1 palmitoylation depends on the secondary structure α-helix, to which changes in hydrophobicity or hydrophilicity alter NCX1 palmitoylation. As well as this, potential palmitoylated cysteines may be required to reside close to transmembrane domain, or near hydrophobic amino acids or near positively charged amino acids all of which can bind to the membrane.

Proteomics research has revealed many putative palmitoylated proteins (Roth et al., 2006), but comprehensive palmitoylation site characterization is absent. Collins et al developed a quantitative site-specific-Acyl-Biotin-Exchange (ssABE) method allowing the global identification of 906 putative palmitoylation sites on 641 proteins in mouse forebrain (Collins et al., 2017). The common feature of those 906 palmitoylation sites is that there are single or double cysteines motifs with hydrophobic residues at specific position. Separate analysis of transmembrane and soluble proteins found di-cysteine motifs like CC* and C*C (* presents as palmitoylation sites) are enriched at Transmembrane proteins whereas single cysteine and hydrophobic amino acids (Leucine, Isoleucine, Tryptophan and Phenylalanine) are commonly found in soluble proteins (Collins et al., 2017). Moreover, a website tool named SwissPalm based on more than 5000 S-palmitoylated protein from 7 species which contain 500 specific palmitoylation sites (Blanc et al., 2015). It provides valuable information about

s-palmitoylation sites prediction and validation. TRPM7 has been identified in SwissPalm but no palmitoylated cysteines have been identified.

3.1.4 Evolution of TRP superfamily and TRPM subfamily

Transient Receptor Potential (TRP) channels are a large and diverse family of cation permeable ion channel proteins that are expressed in animals, yeast, algae, and other unicellular organisms (Huffer et al., 2020). Based on sequence homology the mammalian TRP channel superfamily has been classified into seven main subfamilies, TRPC (Canonical), TRPV (Vanilloid), TRPM (Melastatin), TRPA (Ankyrin), TRPML (Mucolipin), and TRPP (Polycystic) (Nilius and Owsianik, 2011, Samanta et al., 2018). TRP multigene superfamily encodes integral membrane proteins, which are involved in diverse biological functions such as sensation of different stimuli, nociception, ion homeostasis and many fundamental cellular physiological function (Clapham et al., 2001, Ramsey et al., 2006). Specifically, many TRPA and TRPV channels are stimulated by alterations of temperature and various ligands to function (Nilius et al., 2012). TRPC channels take part in neuronal signal transduction and TRPM channel are involved in numerous types of signal transduction, responding to chemical stimuli and thermosensation of cold temperatures (Peng et al., 2015). The TRPN family (which form mechanosensitive channels (Yan et al., 2013)) was lost from most vertebrates during evolution and is only present in invertebrates and fish (Nilius and Owsianik, 2011). In contrast, the number of TRPs involved in ionic homeostasis, thermosensation and chemoreception or calcium signalling (TRPCs, TRPVs, TRPMs) are doubled in mammalian compared to whose amount in Choanoflagellates, the common ancestor of animals (Nilius and Owsianik, 2011).

TRPM is the largest subfamily in TRP superfamily. Typically this family forms six transmembrane domain ion channels with highly conserved cytoplasmic N- and C-terminal structure and a TRP domain just on the C terminal side of the transmembrane domains (Fleig and Penner, 2004). The TRPM family is an ancient channel. In some species there is a single TRPM protein with multiple function (e.g. Drosophila) but in others, they can be compartmentalized in a set of diverse paralogs each of which may be multifunctional (e.g., Human TRPM1-8) (Himmel et al., 2020).We know little about the TRPM evolutionary history. Since the mammalian TRPM family contains a number of specific amino acids residues

related to menthol sensitivity, phylogenetic and sequence analysis were performed to access conservation of these residues across taxa to evaluate TRPM evolution (Himmel et al., 2019). Phylogenetic trees illustrated that TRPM channel group into two main monophyletic clades (αTRPM and ßTRPM) which may have existed prior to the protostome–deuterostome split, additionally have a unsorted basal clade always including Xenacoelomorpha (Himmel et al., 2019). Later, genomic research based on over 1,300 predicted TRPM-like sequences from 14 diverse eumetazoan phyla revealed TRPM might have an ancient, previously unrecognized sister family, TRP soromelastatin (TRPS),that wholly explained the basal clade (Himmel et al., 2020). It suggested that two duplication events, TRPS–TRPM split and α–ß TRPM split, happened before Cnidaria–Bilateria split. Moreover, vertebrate TRPM1-8 expansion occurred after vertebrate–tunicate split (Himmel et al., 2019). TRPM8 first emerged until lobe-finned fish emerged which indicated TRPM8 forms a sister clade to TRPM2, the later containing both lobe-finned and non-lobe-finned sequences. This finding also partly confirms the most commonly acceptable four subgroups classification of vertebrate TRPM1-8 in accordance with sequence similarities: TRPM2/8, TRPM1/3, , TRPM4/5, and TRPM6/7 (Huang et al., 2020). They are all Ca permeable cation channel except TRPM4 and 5.

3.2 Aims

The aim of this study is to map palmitoylation sites of TRPM7 and TRPM6, therefore we can make comparison through the non-palmitoylated mutants generated to further understand the influence of palmitoylation on TRPM7 and TRPM6 function. The main focus of our research relates to TRPM7, which is more widespread than TRPM6. TRPM6, as its closest homologue, is partly included in our investigation.

3.3 Methods

3.3.1 General protein analysis and statistical analysis

All protein analysis assays involved into this chapter have been described in Chapter2. Statistical analysis of duplicate experiments was presented with bar chart of Mean± standard error of the mean (SEM) via GraphPad Prism software.

Comparisons between multiple groups was made using One-way ANOVA followed by Dunnett's multiple comparison test. Comparisons between two groups were made using an unpaired t-test with Welch's correction.

3.3.2 Cryo-EM structure and TRP family sequences

Published Cryo-EM structures of TRP channels were obtained from Uniprot and Protein Data Bank (PDB) website. The diagrams of TRPM7 and TRPV6 subunit were made with PyMOL software. In addition, the TRPM family members from all species of different phylum were obtained from supplement database of research from Himmel, N.J., et al.(Himmel et al., 2020). Alignments a phylogenetic trees of TRP channels were produced using Clustal Omega.

3.4 Results

3.4.1 TRPM7 is palmitoylated in many cell types.

To investigate whether TRPM7 is post-translationally modified by protein S-palmitoylation, Acyl-RAC was performed to capture palmitoylated cysteines from many different cell types (Figure 3.3). After alkylation of non-palmitoylated cysteines under strongly denaturing conditions, Thiol reactive Sepharose resin was used to capture the previously palmitoylated cysteines which were revealed by cleaving thioester bonds using neutral hydroxylamine (NH_2OH). We found endogenous TRPM7 is palmitoylated in monocytes and a human monocyte-like cell line, THP-1 (Chanput et al., 2014) (Figure 3.3 A), cardiac fibroblasts from mouse (Figure 3.3C), cardiac ventricular tissue from rats and rabbit (Figure 3.3D), vascular smooth muscle cells (Figure 3.3E) and human embryonic kidney cells (Figure 3.3B). Murine TRPM7 with YFP fused at its C terminus was also palmitoylated when expressed in HEK cells (Figure 3.3 B), which was detected by GFP antibody. These experiments used two different TRPM7 antibodies. One from Abcam recognised only human TRPM7 (Figure 3.3 B) and the other, from Alomone, raised to 1146-1165 of human TRPM7 reacted with all species investigated.

Flotllin-2 (Flot2) is a constitutively palmitoylated protein routinely used to confirm the success of the Acyl-RAC assay. Meanwhile, sodium chloride was used instead of hydroxylamine as a negative control for capture palmitoylated

proteins. These experiments demonstrate that TRPM7, as a ubiquitously expressed ion channel for mediating Mg and Ca influx (Zou et al., 2020), is palmitoylated in many cell types. However, Magnesium transporter protein 1 (MagT1), as a widely known regulator in magnesium homeostasis (De Baaij et al., 2015), is not regulated by post-translational palmitoylation (Figure 3.3A). These results inspired us to investigate the importance of palmitoylation to TRPM7 ion channel activities.

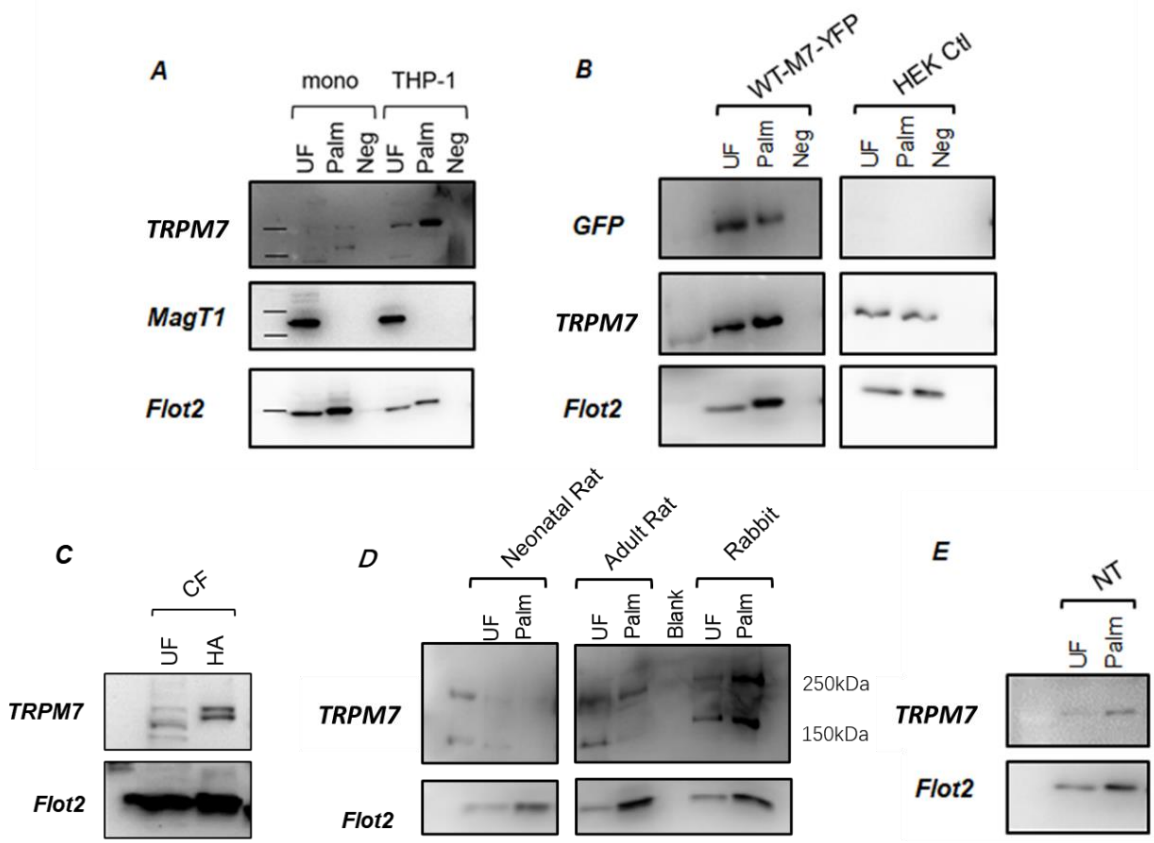

Figure 3.3 TRPM7 is palmitoylated in many different cell types.
A) Western-blot of Palmitoylation of TRPM7 in monocytes, THP-1. Molecular weight of full-length TRPM7 is around 250kDa. (UF=unfractionated lysate; Palm=enriched palmitoylated protein; Neg=negative control). Flot2, as a housekeeping gene, was presented as a standard to evaluate the efficiency of Acyl-Rac assay. (n=1) B) Representative western blot of Palmitoylation of TRPM7 in HEK293 cells. Wild type mouse TRPM7 was expressed as a fusion protein with yellow fluorescent protein (YFP) at the C terminus. GFP antibody and TRPM7 (human specific, Abcam) antibody revealed that transfected and endogenous TRPM7 are both palmitoylated in HEK293 cells. (n=9-14) C) Representative western-blot of TRPM7 palmitoylation in mouse Cardiac fibroblasts. (n=3) D) Western blot of palmitoylation of TRPM7 in ventricular muscle cells. The ventricular muscle cells are derived from different species, including neonatal rats, adult rats, and rabbit. Alomone TRPM7 antibody (detects all species) was used. (n=13-20) E) Western blot of TRPM7 palmitoylation in normotensive (NT) human vascular smooth muscle cells (hVSMCs); (n=6-9).

3.4.2 TRPM6 is also palmitoylated in HEK293 cells

TRPM6 and TRPM7 both belong to the melastain-related subfamily of TRP channel which are the only known fusions of a divalent ion channel pore with a

serine/threonine kinase domain in their C terminus (Schmitz et al., 2005). TRPM7 is ubiquitously expressed but TRPM6 is primarily an epithelial-associated channel (Zou et al., 2020). Both proteins regulate Mg homeostasis in vertebrates. In addition, TRPM6 is the closest homologue of TRPM7 which sharing approximately >50% sequence identity (Zhang et al., 2014). It can heteromultimerize with TRPM7 forming tetrameric structure to contribute the biological role of TRPM6 in epithelial magnesium absorption (Chubanov et al., 2004). TRPM7 homomeric ion channels are inhibited by intracellular Mg, but TRPM6/TRPM7 heteromeric complexes are insensitive to Mg as a result of the TRPM6 kinase domain (Zhang et al., 2014). We evaluated palmitoylation of TRPM6, but the majority research of this project is investigating the influence of palmitoylation on TRPM7 activity.

As shown in figure3.4, TRPM6-YFP is also highly palmitoylated in human embryonic kidney cells (Figure 3.4A), as it is captured using thiopropyl Sepharose resin in the presence of hydroxylamine. Mean palmitoylation data of TRPM6 from 11 independent experiments were demonstrated in figure 3.4B. In addition, palmitoylation of TRPM6-YFP is approximately twice compared to TRPM7-YFP (Figure 3.4B). Flot2, as a housekeeping gene, is known to be constitutively palmitoylated, acting as a standard for evaluating efficiency of Acyl-Rac assay (Figure 3.4A, C). The results suggested palmitoylation might be a crucial post-translational modification to TRPM6 and TRPM7, even including other TRPM family members in mammals. Therefore, we set out to map the palmitoylation site(s) of TRPM7.

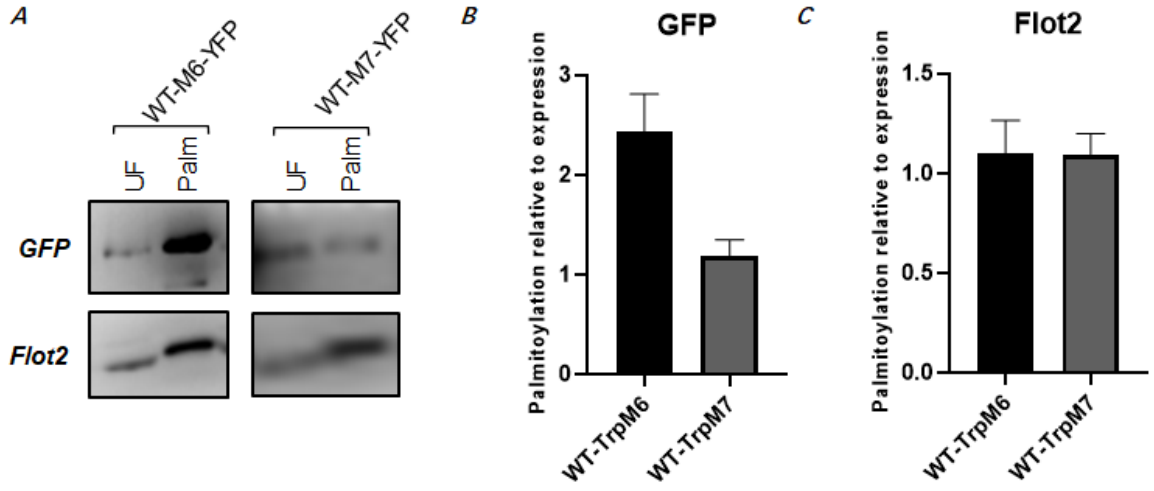

Figure 3.4 TRPM6 is palmitoylated in HEK cells.
A) Representative western-blot of palmitoylation of TRPM6 in HEK293 cells. Flot2, as a housekeeping gene, was used as a standard to evaluate the efficiency of Acyl-Rac assay. (UF=unfractionated lysate, HA=enriched palmitoylated protein). B, C) Summarizing western blot analyst of palmitoylation ratio relative to expression of wild type TRPM6 and Flot2 (n=11-14).

3.4.3 TRPM7 N-terminus and C-terminus alone are not palmitoylated

To identify the region of TRPM7 containing the palmitoylated cysteine(s), we firstly established two constructs of TRPM7-N-terminus (amino acid 1-755) and TRPM7-C-terminus (amnio acid 1096-1863) without the transmembrane domain. From representative western-blot (Figure 3.5A), it illustrated that neither N-termini nor C-termini of TRPM7 is significant palmitoylated when they were transfected in HEK293 cells. However, wild-type TRPM7 is robustly palmitoylated. GFP antibody was used to detected transfected TRPM7 because of YFP fusion to all proteins. Mean palmitoylation values of transfected TRPM7 from 5 individual experiments are presented in Fig 3.5B, which shows neither N-terminus nor C-terminus are palmitoylated when expressed alone ($P<0.0001$). It suggested that palmitoylation of TRPM7 may need presence or participation of the transmembrane domain.

We further tested the hypothesis that overexpressing N- or C- terminus of TRPM7 might overwhelm the cellular palmitoylation which might explain why these fragments were not significantly palmitoylated. If this were the case, we predicted overexpressing those proteins would reduce palmitoylation of endogenous TRPM7. However, when we detected endogenous TRPM7 palmitoylation in human embryonic kidney cells, there was so significant

difference among WT, N- or C-termini of TRPM7 transfected HEK293 cells (P>0.05, n=5) (Figure 3.5 A, C). This result further supports that transmembrane domain may be necessary for TRPM7 palmitoylation. Besides, there is no significant difference in Flot2 palmitoylation (P>0.05, n=5), which robust data confirm the efficiency of Acy-RAC experiments (Figure 3.5 D).

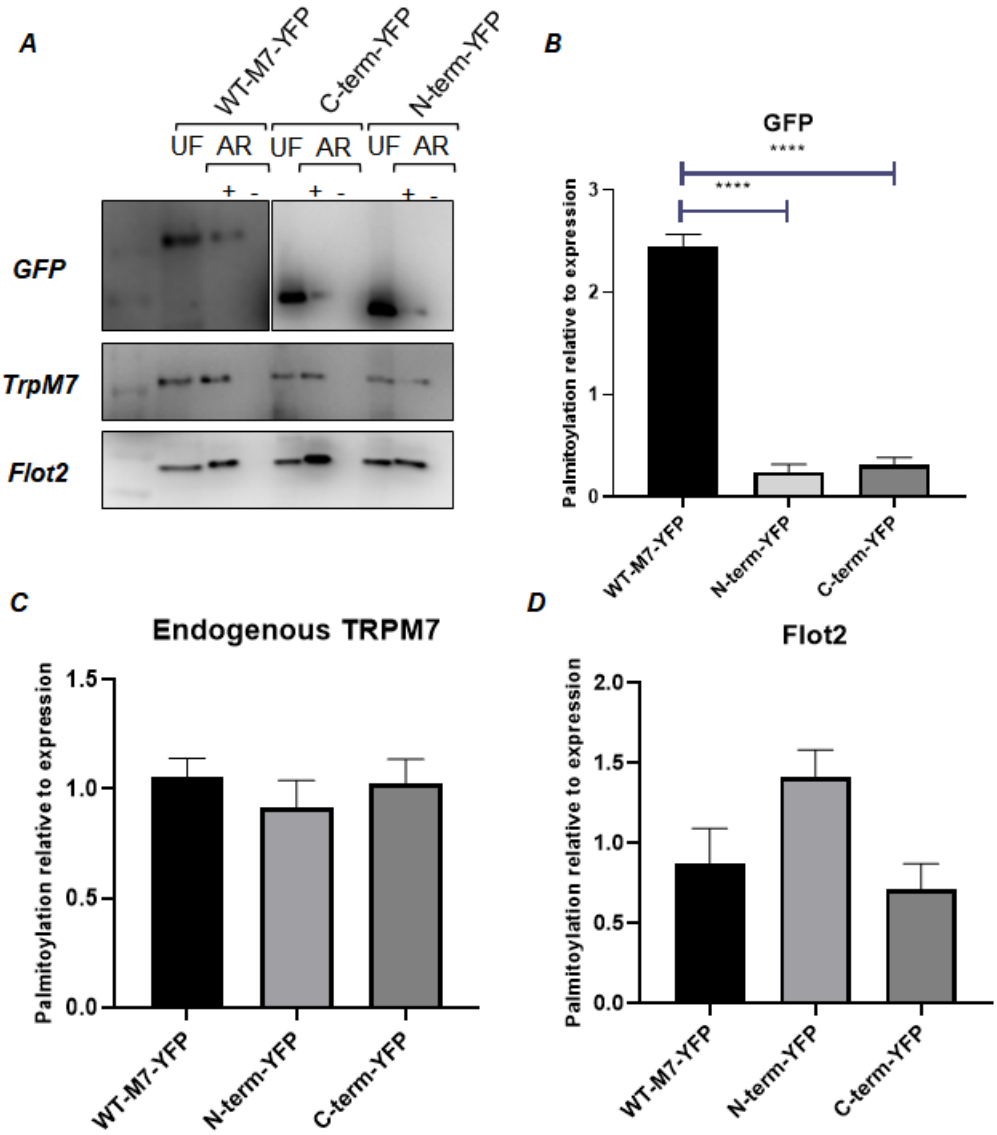

Figure 3.5 Palmitoylation of TRPM7 N-terminus and C-terminus regions in HEK293 cells. Wild type TRPM7, N- terminus and C-terminus of TRPM7 were all fused with YFP. A) Representative western-blot of palmitoylation of wild-type TRPM7, N-terminus and C-terminus of TRPM7, which were all fused with YFP. Flot2 was used as a standard to evaluate the efficiency of Acyl-Rac assay. UF is unfractionated lysate, +: acyl-Rac in the presence of hydroxylamine, -: acyl rac in the absence of hydroxylamine (NaCl was used as a negative control for Acyl-Rac). B) summarizing imaging data of palmitoylation level among wild-type TRPM7, N-terminus and C-terminus of TRPM7. N-terminal and C-terminal of TRPM7 regions are fused YFP without transmembrane domain. (P<0.0001, n=5). C) Summarizing image data of endogenous TRPM7 palmitoylation among WT-M7-YFP, N-terminal and C-terminal of TRPM7 (n=5). D) Summarizing image data of palmitoylation ratio of Flot2 among WT-M7-YFP, N-terminal and C-terminal of TRPM7 (n=5).

3.4.4 TRPM7 N-terminus or C-terminus deletions are not expressed

Since neither large cytosolic N nor C terminal domains of TRPM7 fused to YFP were robustly palmitoylated when we expressed them in HEK cells. We assumed that palmitoylation of TRPM7 may need transmembrane domain. So, we generated two new mutants of N-terminal domain deletion (amino acid C16-C738) and C-terminal domain deletion (amino acid C1143-C1814) of full length TRPM7. Both plasmids encoded truncated TRPM7 with YFP at the C terminus, neither of those plasmids expressed a YFP-tagged protein when they were transfected into HEK cells (Figure 3.6 A). The DNA sequence of plasmids was confirmed by sequencing with Eurofins Genomics and plasmid integrity was checked using an agarose gel. From Figure 3.6B, we found that after N- or C-termini deletion, the plasmids' size was around ~2000bp smaller than wild-type TRPM7. Meanwhile, gradient co-transfections of YFP plasmids with N-terminal or C-terminal deletion of TRPM7 were performed to estimate the efficiency of transfection in HEK cells. Specifically, the YFP expression corresponded well to the amount transfected, with it decrease by 0.5ug each time from 2ug to 0ug as the amount of TRPM7 N- or C- termini deletion mutants increasing (Figure 3.6 C). The total plasmid amount for co-transfection was consistent 2ug. However, there was no expression of either N or C terminal deletions of TRPM7 in any transfection conditions (Figure 3.6 C). In addition, we also performed transfection into an alternative host cell line, fibroblast-derived Cos7 cells (CV-1 in Origin with SV40 genes), which are known as non-steroidogenic cells because they are derived from kidney cells. Neither deletion mutant was detected following transfection of Cos7 cells (Figure 3.6 D). Since the sequences of recombinant constructs were correct and the plasmids were intact, the underlying reason why N- termini and C-termini deletion of TRPM7 would not express is unclear. It might suggest either the N or C terminus or both must be required for protein stability or oligomerization. Therefore, to identify the palmitoylated cysteines of TRPM7, we aimed to identify the location of all cysteines in experimentally derived TRPM7 structures.

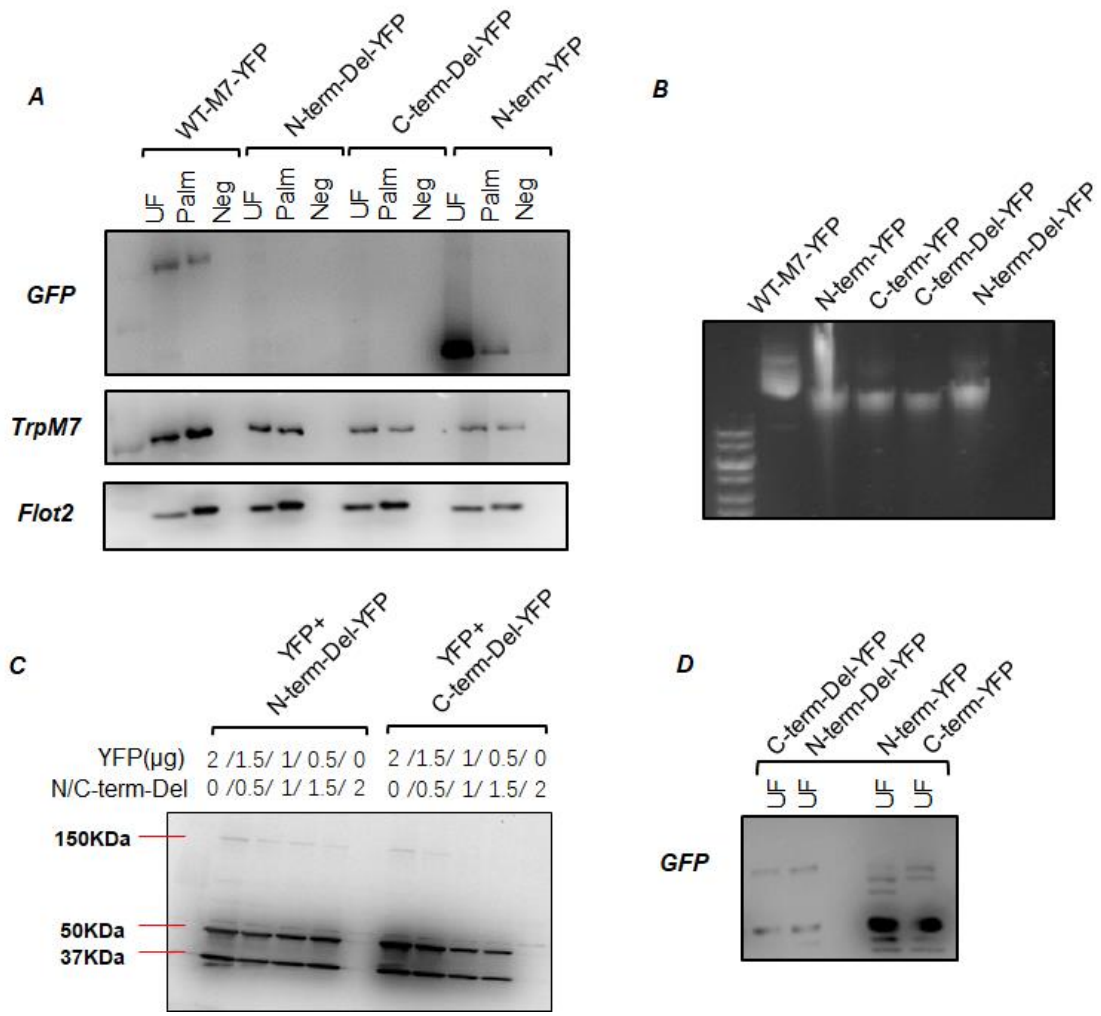

Figure 3.6 Palmitoylation of N terminus deletion and C terminus deletion of full length TRPM7 in HEK293 cells.
N-terminal and C-terminal deletion of wild-type TRPM7 were not expressed after transfection in HEK293 cells. A) Representative western-blot of wild-type, N-terminal deletion, C-terminal deletion, and N terminal fusion of TRPM7 fused to YFP. UF was unfractionated lysate, HA was enriched palmitoylated protein, NaCl was used as negative control (Neg) for Acyl-Rac. Flot2 was used as housekeeping gene to evaluate efficiency of Acyl-Rac assay. B) Plasmids integrity was confirmed via Agarose Gel Electrophoresis (1.5%). After N-terminal or C-terminal deletion, the plasmids size should be around ~2000bp smaller than wild-type TRPM7 plasmid. C) western-blot of gradient co-transfections of YFP with N-terminal deletion or C-terminal deletion of TRPM7. Total transfected DNA mass is 2µg.D) Representative western-blot of N-terminal deletion, C-terminal deletion, N-terminal fusion, and C-terminal fusion of TRPM7 transfected with COS7 cells. (UF=unfractionated lysate).

3.4.5 Cryo-EM structure of TRPM7 to identify positions of cysteines

The crystal structure of TRPM7's C-terminal isolated kinase domain was solved by Kuriyan et.al (Yamaguchi et al., 2001) and its N-terminal has marked structural similarity with classical protein kinases. Additionally, cryogenic electron microscopy (Cryo-EM) reconstruction structure of mammalian TRPM7 channel domain in different ionic conditions, including high external Mg and in

the presence of EDTA to remove most free cations, has been reported by Duan,et al (Duan et al., 2018).

To identify the cysteine residues that could be palmitoylated in TRPM7, we mapped all cysteines in a single subunit of TRPM7 through its cryo-EM structure. Using PyMOL software, we presented Ribbon diagram (Left) and surface representation (Right) of one subunit of TRPM7 (Figure 3.7 A). Each domain was labelled with different color-coding, for which N-terminus in yellow, C terminus in red and transmembrane domain (TMD) in cyan. Several surface cysteine residues (green) were revealed in its subunit structure viewed from different angles (Figure 3.7 B), including Cys526, Cys656 in N-termini, Cys1177 in C-termini, and a cluster of Cysteines in the TRP domain. In addition, structures between amino acids from 1 to 466 and 1139-1155 in TRPM7 are still not resolved. The cluster of cysteines are separately C1143, C1144 and C1146, which localise close to transmembrane domain (Top view without TMD in Figure 3.7C). The cluster of cysteines are solvent exposed and/or in close proximity to the membrane in TRPM7 which makes them strong candidates to be palmitoylation site(s), because active sites of DHHC (Asp-His-His-Cys) palmitoyl transferases resides at the membrane-cytosol interface (Rana et al., 2018). Hence, we first concentrated on investigating the group of cysteines which lie in the unstructured loop at the C-terminal end of TRPM7 TRP domain.

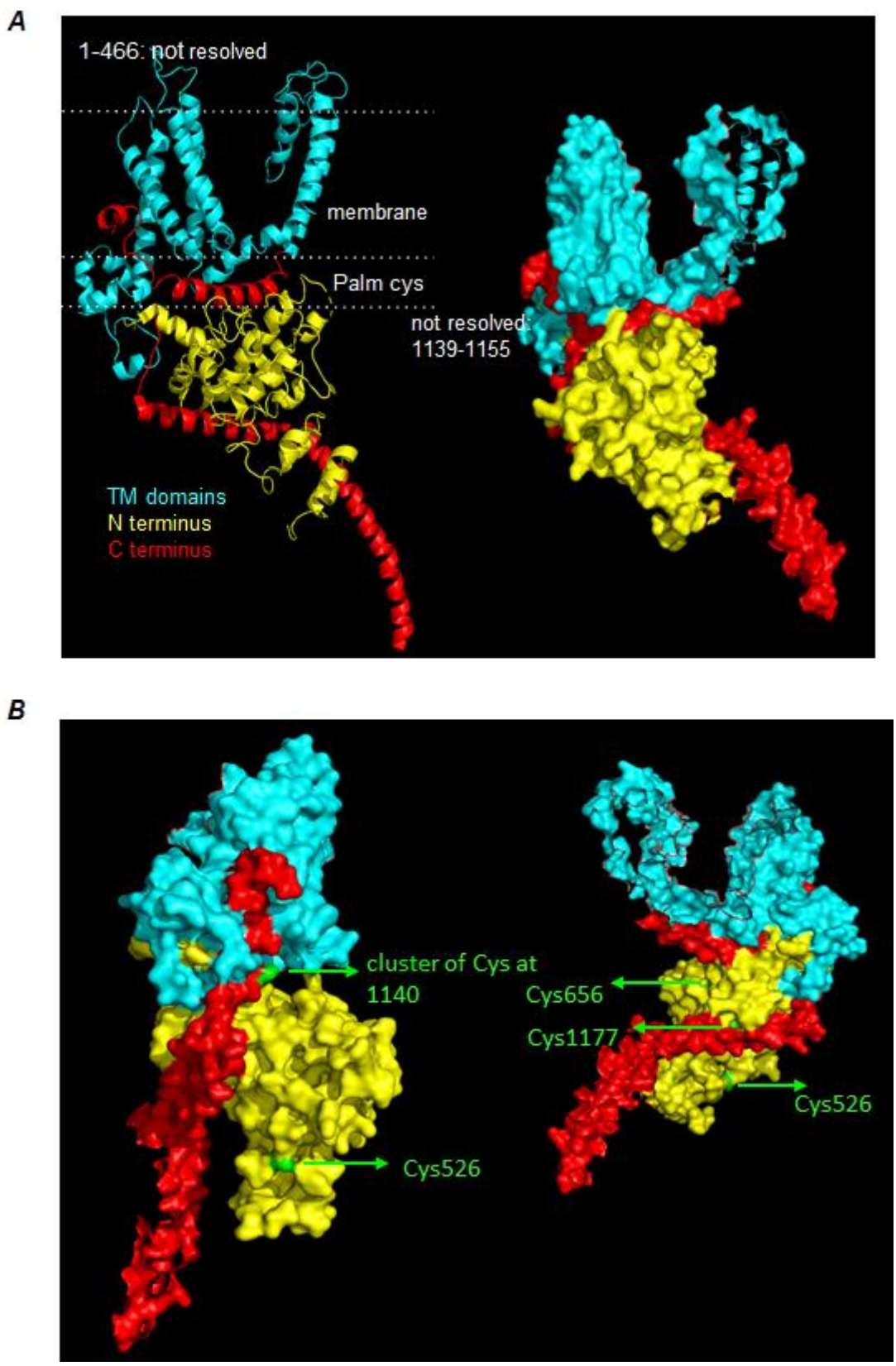
A
1-466: not resolved
membrane
Palm cys
not resolved:
1139-1155
TM domains
N terminus
C terminus
B
cluster of Cys at
1140
Cys656
Cys1177
Cys526
Cys526

C

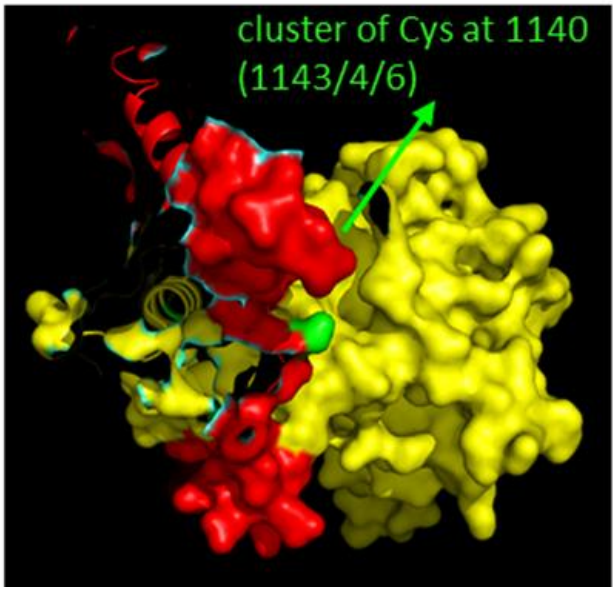

Figure 3.7 CryoEM structure of TRPM7 single subunit (bases on PDB structure 5ZX5) to identify potential palmitoylated cysteines in proximity to the membrane.
A) Ribbon diagram (left) and surface representation (right) of one subunit of TRPM7. Each domain was color-coded (N terminus yellow, transmembrane domains cyan, C terminus red). No structure is resolved between 1-466 and 1139-1155. (TM=transmembrane domains; the boundaries of the membrane are indicated by a white dotted line, and a second dotted line indicates likely proximity of palmitoylated cysteines to the membrane) B) Surface cysteine residues (green) revealed in subunit structure of TRPM7. A Cluster of Cysteines around 1140, was located close to the transmembrane domain. C) CryoEM structure of single subunit of TRPM7 from top view of membrane without TM domain highlighting the cluster cysteines in positions 1143, 1144 and 1146.

3.4.6 TRPM7 is palmitoylated among Cysteines 1143, 1144 and 1146

Site-directed mutagenesis was performed to replace the cluster cysteines of 1143, 1144 and 1146 to alanines (details in section 2.4.1), achieving mutants 1146_A (1CA), 1143/1144_AA (2CA) and 1143/1144/1146_AAA (3CA). Mutants of 1CA and 2CA did not change overall TRPM7-YFP palmitoylation assessed using acyl-RAC, but mutation of all three cysteines 1143/4/6_AAA (3CA) of TRPM7 almost completely abolished TRPM7 palmitoylation (Figure 3.8 A) when they were expressed in HEK cells. Mean palmitoylation values of transfected Wild type TRPM7 and its mutants from 13 individual experiments illustrated that palmitoylation level of TRPM7-3CA mutant dramatically reduced by 86.5% comparing with WT-TRPM7 ($P<0.001$, $n=13$) (Figure 3.8 B). YFP tag was fused at the C-terminal of WT-TRPM7 and its mutations, so GFP antibody was used for detecting transiently transfected TRPM7. Meanwhile, overexpressing TRPM7 and its 1CA, 2CA, 3CA mutants has no significant effect on endogenous full length TRPM7 palmitoylation in human embryonic kidney cells ($P>0.05$, $n=7$) (Figure 3.8

A, D). Flot2, as the identified robust palmitoylated protein, was applied to confirm the efficiency of Acyl-RAC assay (Figure 3.8 A, C). In conclusion, once we silenced all three cysteines (C1143, C1144 and C1146), it abolished palmitoylation of TRPM7 to large extent. Cluster of Cysteines 1143, 1144 and 1146 which localized at TRP domain and closed to membrane are the palmitoylation sites of TRPM7. With the mapped palmitoylation sites, we can further research the influence of palmitoylation on TRPM7's channel activity.

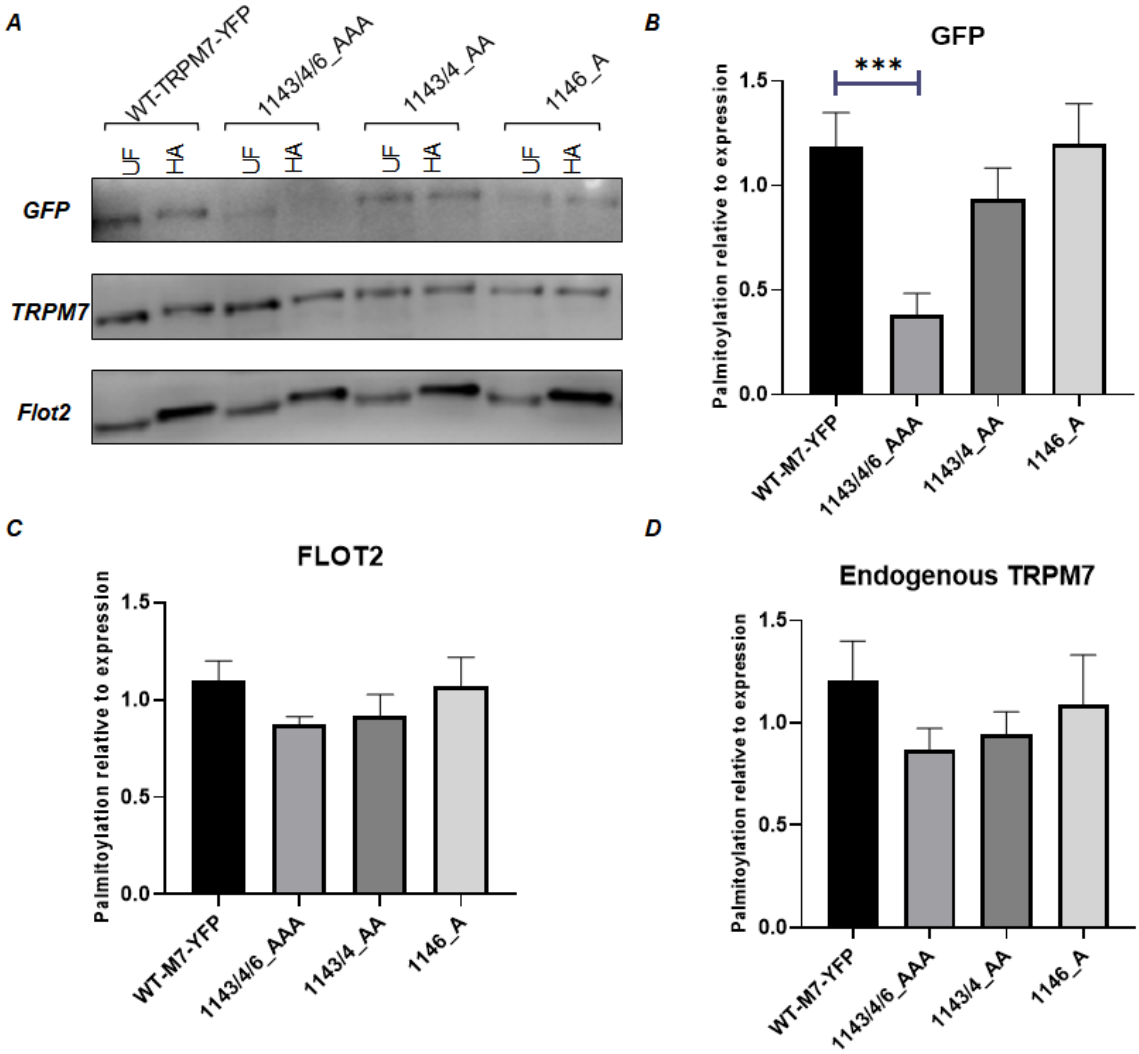

Figure 3.8 TRPM7 palmitoylated site(s) localize among cysteine1143, 1144 and 1146.
A) Representative western-blot of palmitoylation of wild-type TRPM7, as well as 1143/4/6_AAA, 1143/4_AA and 1146_A mutants. Palmitoylation of TRPM7 was significantly decreased once Cys1143, 1144 and 1146 were all replaced with Alanine. Hence, TRPM7 palmitoylation sites localize among cys1143/4/6. Flotillin-2, as a housekeeping gene, was used as a standard to evaluate the efficiency of Acyl-RAC. UF: unfractionated cell lysate. HA: purified palmitoylated proteins. B) summarizing imaging data of palmitoylation of wild-type TRPM7 and its 1143/4/6_AAA, 1143/4_AA ,1146_A mutants. Palmitoylation level of 1143/4/6_AAA mutant was reduced by 86.5% compared to wild-type TRPM7 (P=0.0009, n=13). C, D) summarizing imaging data of palmitoylation of endogenous TRPM7 and Flot2 in the presence of wild-type TRPM7 and its 1143/4/6_AAA, 1143/4_AA and 1146_A mutants (n=7).

3.4.7 Clustal Alignments of TRPM7 in all species and all TRPM family members in human and mouse

From the previous data, we found that palmitoylation cysteines (C1143, C1144 and C1146) of mouse-TRPM7 reside at the C terminal end of the TRP domain close to membrane. Since the TRP domain is highly conserved in TRPM, TRPN, TRPC, TRPS and TRPV subfamilies (Huang et al., 2020), we hypothesised that TRPM7 palmitoylated cysteines would also conserved in many different species. TRPM7 sequences in TRP domain were collected from a variety of vertebrate species (Phylum Chordata) with different classes, including mammalian (Homo sapiens; Mus; Ailuropoda melanoleuca; Physeter catodon; Eptesicus fuscus), Birds (Gallus; Columba livia; Falco peregrinus; Calypte anna) Reptiles (Chelonia mydas; Notechis scutatus), Amphibians (Xenopus tropicalis), and Fish (Danio rerio; Oryzias melastigma; Lates calcarifer; Nothobranchius furzeri). Multiple sequence alignment of those TRP domain of TRPM7 from different species were conducted in Clustal Omega Tool (EMBL-EBI in Hinxton). We found that potential palmitoylated cysteines of TRPM7 are highly conserved in all the species, with most of them have similar cluster of cysteines in relevant sequences (Figure 3.9). Moreover, the relatedness of chosen species is disclosed with phylogenetic Tree (Figure 3.9), which also illustrates the evolution of TRPM7 in various species.

```
NOTHOBRANCHIUS      WKYQRYHFIMAYHEKPVLPPPFIFLFHVYSLFC-MCSKRKK-ESTYGPKLFLSEEDQKKL    58
ORYZIAS             WKFQRYHFIMAYHDKPVLPPPFIFLCHVYSLFC-MCRKRKK-ESTYGPKLFLTEEDQKKL    58
LATES               WKYQRYHFIMAYHEKPVLPPPFILLCHIYSLFC-MCRKRKK-ENTYGPKLFLTEEDQKKL    58
DANIO               WKYQRYHFILAYHDKPILPPPLILLSHAASLLSSICRKRKKDSSTYGPKLFLTEEDQKKL    60
XENOPUS             WKYQRYHFIMAYHEKPVLPPPLIILSHLASLFGFVCKRRKKDKTSHGPKLFLTEEDQKKL    60
NOTECHIS            WKYQRYHFVMAYHEKPILPPPLIVLSHMASLCYCICKRRKKDKNSDGPKLFLTEEDQKKL    60
CHELONIA            WKYQRYHFIMAYHEKPVLPPPLIILSHMASLCCCICKRRKKDKTSDGPKLFLTEEDQKKL    60
GALLUS              WKYQRYHFIMAYHEKPVLPPPLIILSHMASLLCCICKRRKTDKTSDGPKLFLTEEDQKKL    60
COLUMBA             WKYQRYHFIMAYHEKPVLPPPLIILSHMASLFCCICKRRKTDKTSDGPKLFLTEEDQKKL    60
CALYPTE             WKYQRYHFIMAYHEKPVLPPPLIILSHMASLFCCICKRRKTDKTSDGPKLFLTEEDQKKL    60
FALCO               WKYQRYHFIMAYHEKPVLPPPLIVLSHMASLFCCICKRRKTDKTSDGPKLFLTEEDQKKL    60
HOMO SAPIENS        WKYQRYHFIMAYHEKPVLPPPLIILSHIVS-FCCICKRRKKDKTSDGPKLFLTEEDQKKL    59
MUS                 WKYQRYHFIMAYHEKPVLPPPLIILSHIVSLFCCVCKRRKKDKTSDGPKLFLTEEDQKKL    60
EPTESICUS           WKYQRYHFIMAYHEKPVLPPPLIILSHIASLFCCICKRRKKDKTSDGPKLFLTEEDQKKL    60
AILUROPODA          WKYQRYHFIMAYHEKPVLPPPLIILSHIVSLFCCICKRRKKDKTSDGPKLFLTEEDQKKL    60
PHYSETER            WKYQRYHFIMAYHEKPVLPPPLIILSHIVSLFCCICKRRKKDKTSDGPKLFLTEEDQKKL    60
                    **:*****::***:**:****:*.* *  *    :* :**. ..: ******:*******
```

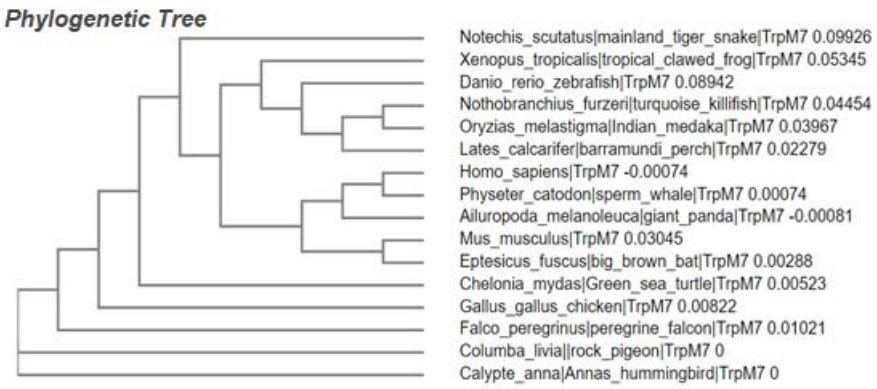

Figure 3.9 Clustal alignments of TRPM7's TRP domain in different species.
Clustal alignments and phylogenetic tree of TRPM7 in different species. Palmitoylated cysteines of TRPM7 which are located at the C terminal end of the TRP domain are conserved in a variety of species.

In addition, we found that TRPM6, which shares high homology with TRPM7, has cluster sof double cysteines (C1146/C1147) in its TRP domain, we hypothesised that palmitoylation cysteines are highly conserved in all mammalian TRPM family members. Clustal alignments was conducted with multiple sequences comparison of TRP domain from all TRPM family members in human and Mouse. This clearly demonstrated that majority of TRPM family members have conserved potential palmitoylated cysteine(s) in TRP domain except TRPM2 and TRPM5 (Figure 3.10). Canonically, the mammalian TRPM gene family members (TRPM1-TRPM8) could be roughly divided into 2 subgroups: TRPM1/3/6/7 (alpha branch) TRPM2/4/5/8 (beta branch) and according to sequence homology and functional similarity (Duan et al., 2018). As mammalian TRPM channel evolved, the ability of TRPM channels to conduct Ca was likely determined by the acquisition of the QIP motif within a proximal segment of the putative pore loop through TRPM2-like Ancestor (Schnitzler et al., 2008), ranging from Ca impermeable TRPM4/5 to highly Ca and Mg permeable like TRPM6/7. This finding hinted us it is valuable to assess the influence of palmitoylation to TRPM7 permeability to divalent cation especially Ca especially when we abolish palmitoylation (TRPM7-M2/TRPM7-M5) (details in section 3.4.8) by splicing relevant motifs in TRP domain.

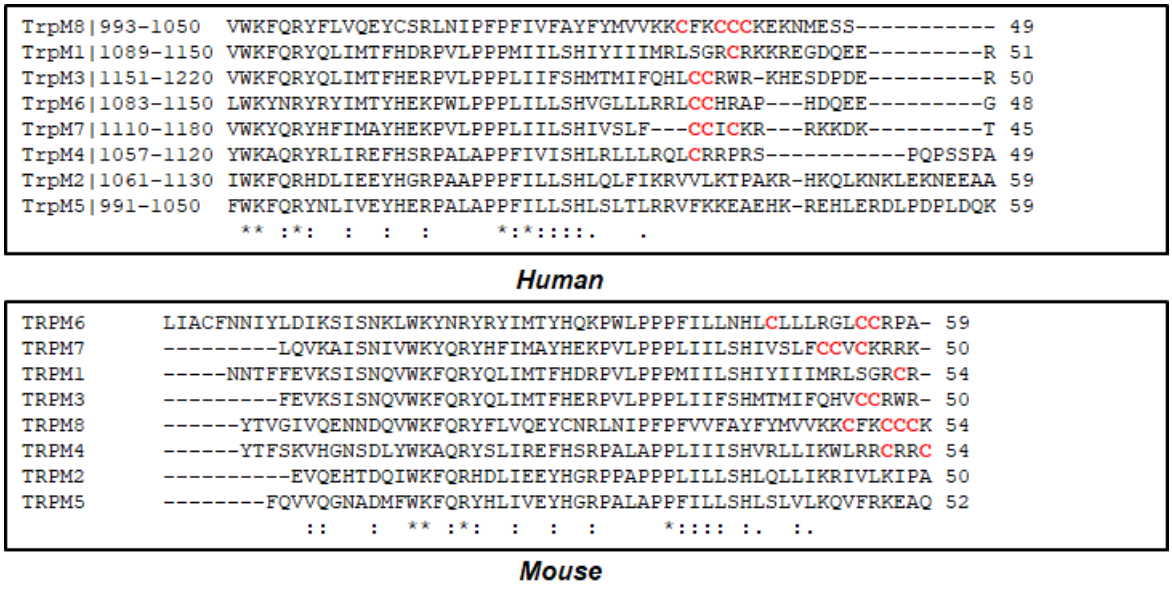

Figure 3.10 Clustal alignments of TRPM family members 1-8 in mammalian.
Clustal alignments of all TRPM family members in human and mouse. The TRPM7 palmitoylated cluster cysteines (1143/4/6) located after the TRP domain are highly conserved in almost TRPM family members in Human and Mouse, expect TRPM2 and TRPM5.

3.4.8 TRPM7-M5 and TRPM7-M2 chimaeras are non-palmitoylated

In accordance with Clustal alignments comparison, palmitoylated cysteines are highly conserved in all Alpha TRPM family members as well as TRPM4 and TRPM8 in the beta branch of the family (Figure 3.10). Notably, TRPM2 and TRPM5 are the only TRPM family members lacking palmitoylation sites, but they can still operate at cell surface membrane. TRPM2 is Ca permeable non-selective cation channel opened simultaneous binding of three obligate co-activators, separately cytosolic ADP-ribose, Ca and membrane phosphatidylinositol4,5-bisphosphate (PIP2) (Zhang et al., 2018). Whereas TRPM5 are nonselective monovalent-specific cation channel conducting Na and K, but it could also be activated by PIP2 and transiently responding to rapid changes in [Ca]i (Prawitt et al., 2003).An alignment of only TRPM2, TRPM5 and TRPM7 reveals that the palmitoylated cysteines in TRPM7 are replaced with positively charged and hydrophobic amino acids in TRPM2 and TRPM5 (Figure 3.11A). Therefore, we replaced the palmitoylated region “CCVC” in TRPM7 with the “KRIV” of TRPM2 or “KQVF” of TRPM5 to generate two chimaeras TRPM7-M2 and TRPM7-M5. All plasmids expressed TRPM variants with a C terminal YFP tag.

Both TRPM7-M2-YFP and TRPM7-M5-YFP chimaeras were non-palmitoylated when expressed in HEK cells ($P < 0.001$, $n=4$) (Figure 3.11B). Mean palmitoylation

relative to protein expression data from 4 repeated Acyl-Rac experiments suggested that palmitoylation of TRPM7-M2-YFP and TRPM7-M5-YFP were respectively diminished approximately 84% and 81% comparing with the WT-TRPM7-YFP (Figure 3.11C). Flot2, as the identified palmitoylated protein provided a standard for Acyl-RAC efficiency, with robust similar palmitoylation levels in lysates from cells expressing WT-TRPM7-YFP and non-palmitoylated chimaeras in individual experiment.

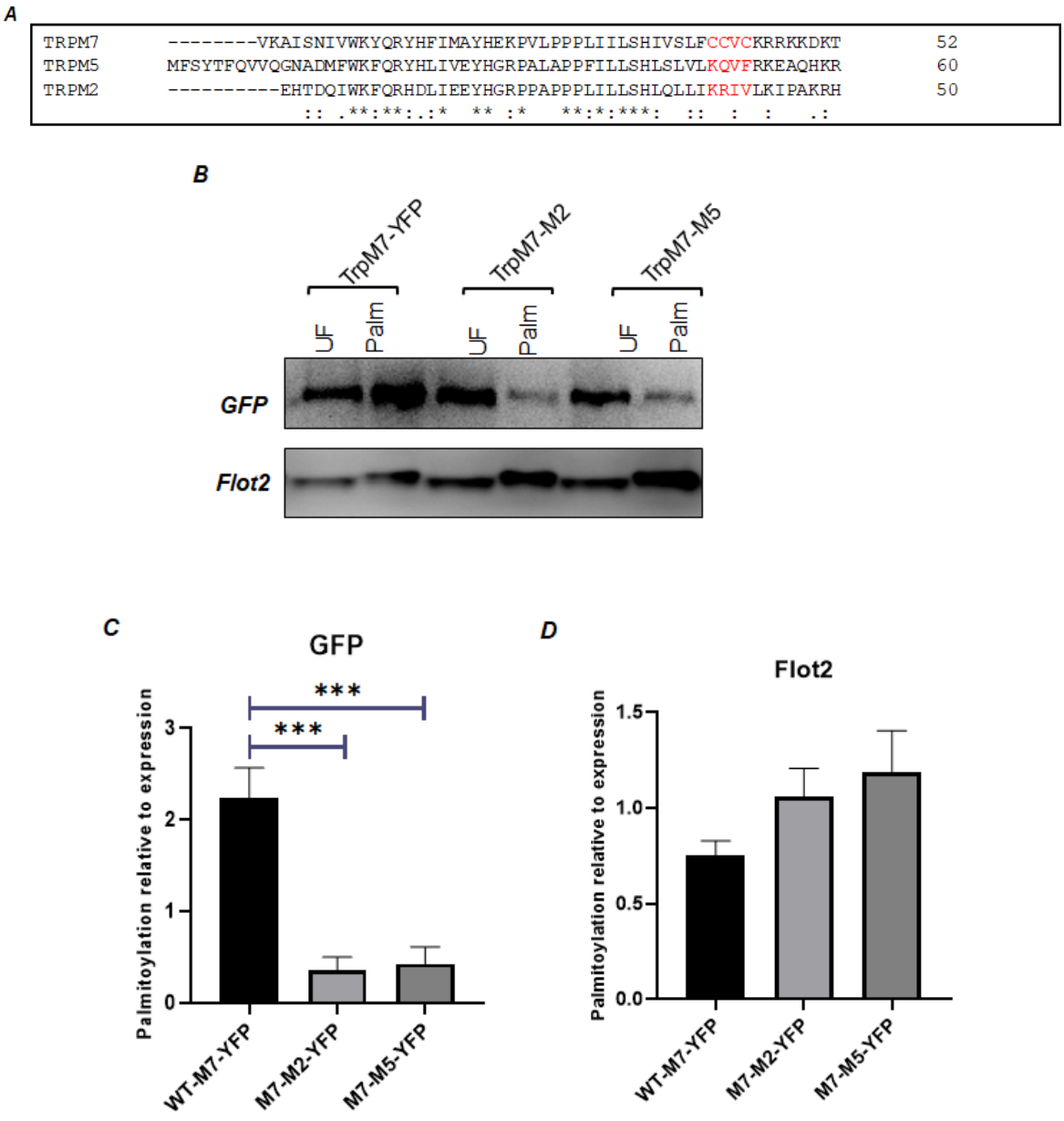

Figure 3.11 Palmitoylation of TRPM7-M2-YFP and TRPM7-M5-YFP expressed in HEK293 cells.

A) Clustal alignments of the TRP domain from mouse TRPM2, TRPM5 and TRPM7. From Figure 3.10, TRPM7 cluster palmitoylated cysteines (1143/4/6) are highly conserved in all TRPM family members except TRPM5 and TRPM2. The region of TRPM7 containing cysteines (CCVC) was replaced with the analogous regions of TRPM5 (KQVF) and TRPM2 (KRIV). B) Representative western-blot of palmitoylation of wild-type TRPM7, TRPM7-M2-YFP and TRPM7-M5-YFP

chimaeras. Palmitoylation of TRPM7-M2 and TRPM7-M5 chimaeras were significantly decreased. C) Summary imaging data of palmitoylation of wild-type TRPM7, TRPM7-M2 and TRPM7-M5. GFP antibody was to detect yellow fluorescent protein (YFP) fused proteins. Palmitoylation was decreased by 84% and 81% respectively for TRPM7-M2 and TRPM7-M5, compared to WT-TRPM7 ($P<0.001$, $n=4$). D) Summary imaging data of palmitoylation of Flot2 among WT-TRPM7, TRPM7-M2 an TRPM7-M5. Flot2 as a housekeeping gene for evaluate Acyl-Rac efficiency.

3.4.9 TRPM6 palmitoylation sites are identified by TRPM6-AA, TRPM6-M5 and TRPM6-M2 chimaeras

With 2011 amino acid residues, TRPM6 is the longest member of the TRP family, additionally sharing 60% sequence identity with TRPM7 and also contains a [alpha]-kinase domain at carboxy termini (Clapham et al., 2001). From alignments of all TRPM family members in mammalian, we found TRPM6 have the highly conserved palmitoylated cysteines in TRP domain. We therefore hypothesised that those double cysteines are TRPM6 palmitoylation sites. This hypothesis was confirmed via Acyl-RAC assay, TRPM6 palmitoylation was distinctly decreased when we were silencing the double cysteines to alanines (Figure 3.12B). Similarly, a clustal alignment of TRPM2, TRPM5 and TRPM6 disclosed that the palmitoylated cysteines in TRPM6 are replaced with positively charged and hydrophobic amino acids in TRPM2 and TRPM5 (Figure 3.12A). Hence, we produced similar chimaeras TRPM6-M2-YFP and TRPM6-M5-YFP by replacing the palmitoylated region “CC” in TRPM6 with the corresponding regions of TRPM2 (VL) and TRPM5 (FR). Both chimaeras demonstrated significantly reduced TRPM6 palmitoylation (Figure 3.12B). Quantification of several Acyl-RAC experiments illustrated that TRPM6 palmitoylation was dramatically reduced by ~87% with TRPM6-AA-YFP, ~77% with TRPM6-M2-YFP and ~72% with TRPM6-M5-YFP. ($P<0.0001$ and $P<0.001$, $n=11$) (Figure 3.12C). There is no significant difference in Flot2 palmitoylation in lysate from cells expressing wild-type TRPM6 and its non-palmitoylated mutants ($P>0.05$, $n=11$), which confirmed the efficiency of the acyl-RAC assay used in these experiments (Figure 3.12D).

The highly conserved double cysteines in TRP domain have been confirmed as the palmitoylation sites of TRPM6, which means it is highly likely that palmitoylation regulates all mammalian TRPM family members except TRPM2 and TRPM5.

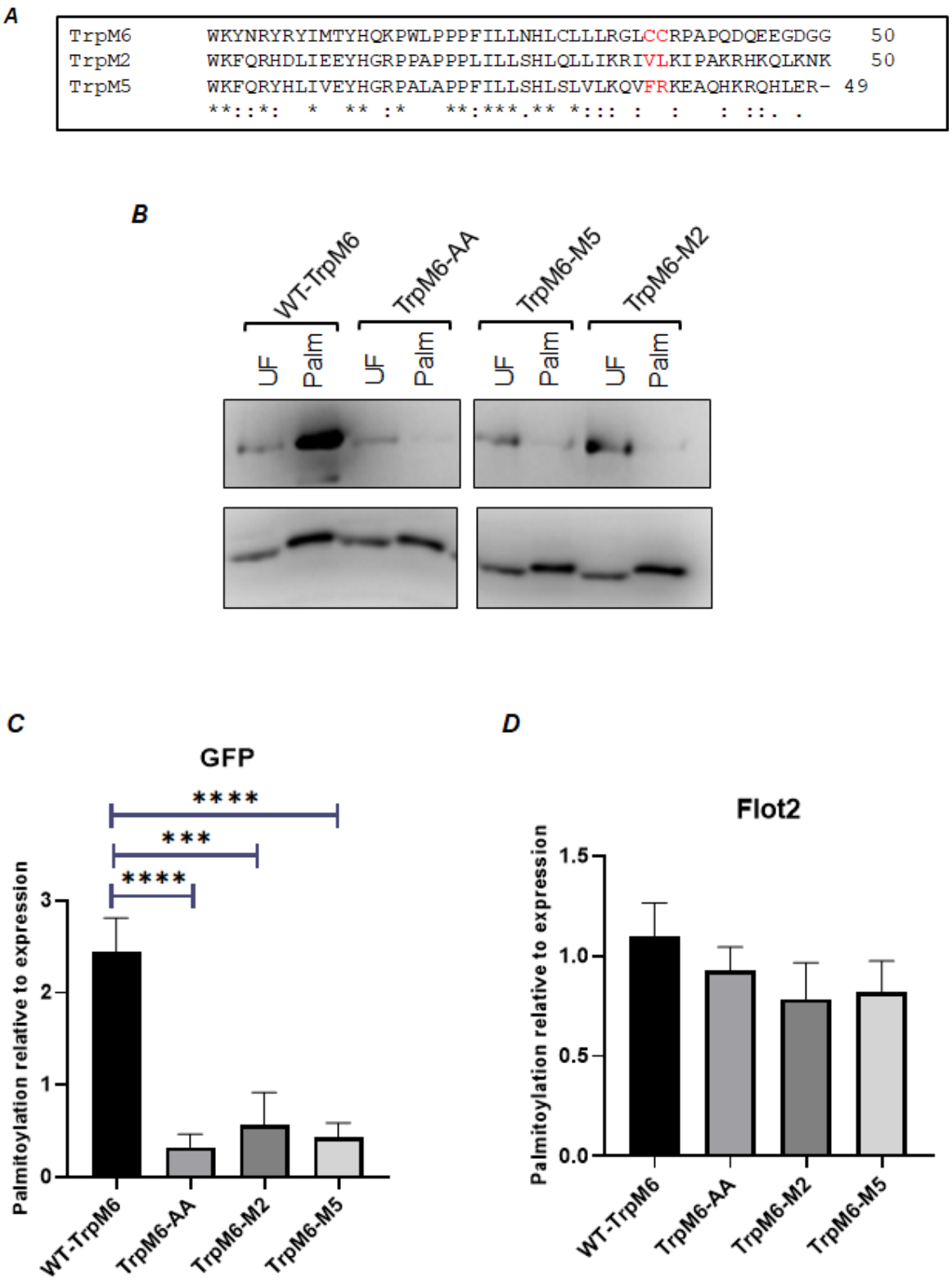

Figure 3.12 Palmitoylation of TRPM6-AA-YFP, TRPM6-M2-YFP and TRPM7-M5-YFP expressed in HEK293 cells.

A) Clustal alignments of TRP domain of TRPM2, TRPM5 and TRPM6 in mouse. The cluster of cysteines palmitoylated in TRPM7 (1143/4/6) is highly conserved in all TRPM family members including TRPM6 (1143/4) (Figure 3.10). Both cysteines of TRPM6 were mutated to alanine to eliminate palmitoylation. The region of TRPM6 cysteines (CC) was replaced analogous regions of TRPM5 (FR) and TRPM2 (VL). B) Representative western-blot of palmitoylation of WT-TRPM6, TRPM6-AA mutant, TRPM6-M2 and TRPM6-M5 chimaeras. Palmitoylation of WT-TRPM6 was significantly decreased with all mutants. C) Summarizing imaging data of palmitoylation of WT-TRPM6, TRPM6-AA, TRPM6-M2 and TRPM6-M5. GFP antibody was to detect yellow fluorescent

protein (YFP) fused proteins. Mutagenesis significantly reduced palmitoylation of TRPM6-AA, TRPM6-M2 or TRPM6-M5 compared to WT. ($P<0.01$, $n=11$). D) Summarizing imaging data of palmitoylation of Flot2 among WT-TRPM6, TRPM6-AA, TRPM6-M2 an TRPM6-M5. Flot2 as a housekeeping gene for evaluate Acyl-Rac efficiency.

3.5 Discussion

This chapter set out to identify the palmitoylated cysteines in TRPM7 and TRPM6. Several different mutants were created and found to have significantly reduced palmitoylation status. The palmitoylated cysteines in TRPM7 are highly conserved in other TRPM mammalian family members and TRP superfamily, TRPVs and TRPCs included.

3.5.1 Palmitoylation of TRPM7 and TRPM6

TRPM7 is the most abundantly expressed TRPM channel, which is essential in embryonic development. Absence of TRPM7 leads to embryonic lethality before embryonic day 7 in mice (Jin et al., 2012). It also plays a key role in cytoskeletal regulation, adhesion and migration (Visser et al., 2014). For instance, TRPM7 expression is positively correlated with migration processes in several tumor cell lines like neuroblastoma, breast adenocarcinoma and prostate cancer(Visser et al., 2014, Middelbeek et al., 2012).Moreover, TRPM7 may be required for vesicular trafficking, membrane reorganization, and neurotransmitter release (Sun et al., 2015b). TRPM7 which localizes in acetylcholine (ACh)-secreting synaptic vesicles of sympathetic neurons, forms a molecular complex with vesicular fusion proteins to stimulate neurotransmitter release (Krapivinsky et al., 2006). Palmitoylation exerts a large extent effect on protein life cycle, trafficking, stability, micro-domain compartmentalization and protein-membrane association (Sobocińska et al., 2018). In our report, TRPM7 is highly palmitoylated in many different cell types, including vascular smooth cells, cardiac ventricular tissues, cardiac fibroblasts, and human embryonic kidney cells. Similarly, TRPM6 as its homologue, is also palmitoylated. As an integral membrane protein, palmitoylation might play important role in TRPM7 trafficking and distribution in cellular micro-compartments. Previously research found that TRPM7 not only acts as an ion transporter on plasma membrane but also serves as also regulates Zn storage in unique intracellular vesicles (Abiria et al., 2017b). Therefore, in the following chapters we investigated the impact of

palmitoylation on TRPM7 sorting and its influence on intracellular ionic homeostasis.

3.5.2 Palmitoylated cysteines of TRPM7 and TRPM6

As we mentioned in section 3.1.3, proteomics research has been applied in discovering various putative palmitoylated proteins. After analyzing 906 putative palmitoylation sites, the common feature of palmitoylated cysteines in transmembrane protein are enriched with di-cysteines and surrounding with hydrophobic residues (Collins et al., 2017).The cluster of cysteines 1143,1144 and 1146 (CCVC motif) in TRPM7 and double cysteines in TRPM6 are in accordance with this principle. Meanwhile, these cysteines are localised close to the TRP domain which is parallel and close to membrane as well as being exposed in TRPM7's homologous or heterologous tetramers. This positions these cysteines appropriately for palmitoylation by their DHHC enzyme (Figure 3.13). Palmitoylation may occur throughout the secretory pathway, and TRPM7 may palmitoylated by different DHHCs enzymes in different cellular organelles. Other integral membrane proteins are palmitoylated in multiple cellular compartments (Gök et al., 2021). The next step of our project is defining DHHC acyltransferases of TRPM7.

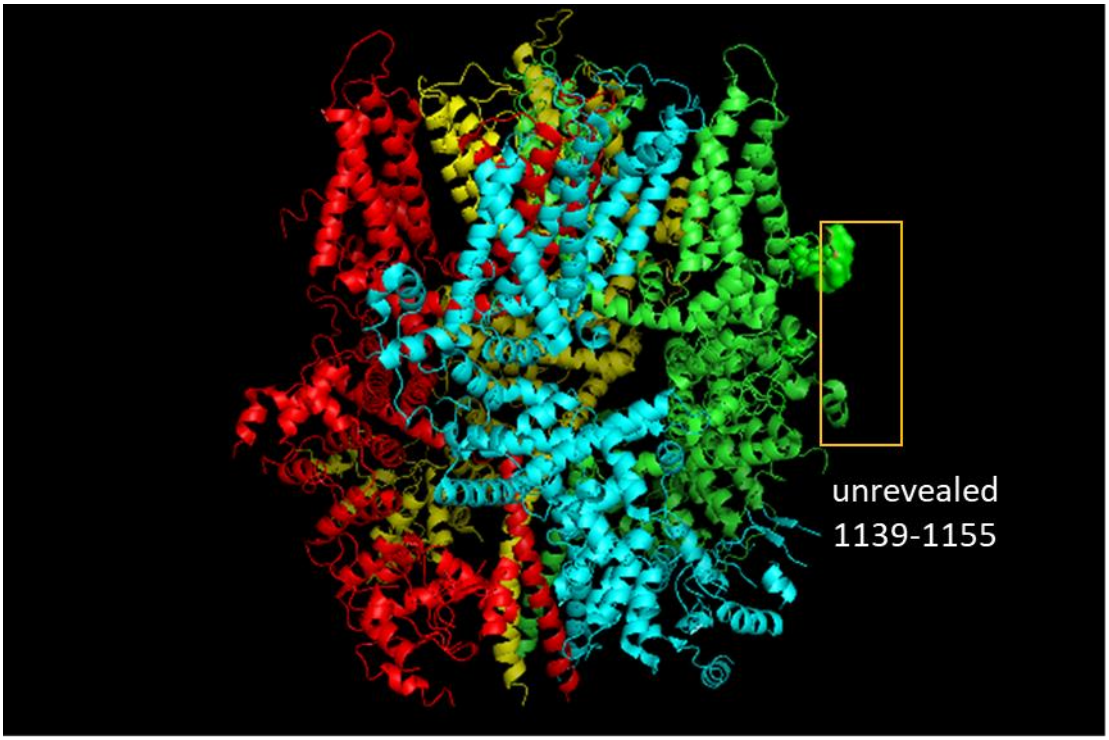

Figure 3.13 Cluster of palmitoylated cysteines localization in TRPM7 tetrameric structure (bases on PDB structure 5ZX5)
The crystal structure between 1139-1155 are still unrevealed. The palmitoylated cysteines (1143, 1144 and 1146) reside on the outside of the tetramer structure and close to the transmembrane where is convenient for DHHC enzyme reaction.

Furthermore, clustal alignments of multiple TRP domain from mammalian TRPM family members in human and mouse revealed that palmitoylated cysteines are conserved in all members except TRPM2 and TRPM5. The relevant motifs are separately 'KRIV' (TRPM2) or 'KQVF' (TRPM5), for which are mixture of hydrophobic and basic amino acids. These motifs may have an affinity for the membrane which may substitute for palmitoylation.

3.5.3 TRPM7 palmitoylated cysteines are conserved in TRPM evolution

As the palmitoylated cysteines were conserved in Human and Mouse TRPM family members, we expanded to investigate TRPM family evolutionary history. Accordingly, to the evolutionary research of TRPM channels, the TRPM family is widely conserved in all phyla except Tardigrada (Himmel et al., 2020). Previously published phylogenies have demonstrated that during evolution the TRPM family developed into two distinct clades, separately α-TRPM and ß-TRPM branches (Himmel et al., 2019). Figure 3.14A shows the consensus topologies in reconciled maximum likelihood trees generated against TRPM database

sequences from Himmel et.al (Himmel et al., 2020), including duplicated α- and ß- branches without Xenacoelomorpha (Figure 3.14A). We extracted a series of species of TRPM duplication branches belonging to the 11 classes of phylograms (with the exception of Xenacoelomorpha and Cephalochordata), which are listed in Figure 3.14B. A clustal alignment of TRP domain sequences of those species illustrated that potential palmitoylated cysteines are conserved in almost all phyla of both branches. (Figure 3.14C). Moreover, the phylogenetic tree of the selected sequences supports two branches of TRPM family members (Figure 3.14D).

Therefore, the TRPM7 palmitoylation sites are retained in most TRPM family members and exist in the duplicated evolutionary history of mammalian TRPM α- and ß- clades before the Cnidaria–Bilateria split. Palmitoylation may regulate key aspects of TRPM family function at all stages of evolution, providing a mechanism to reversibly control protein behaviour.

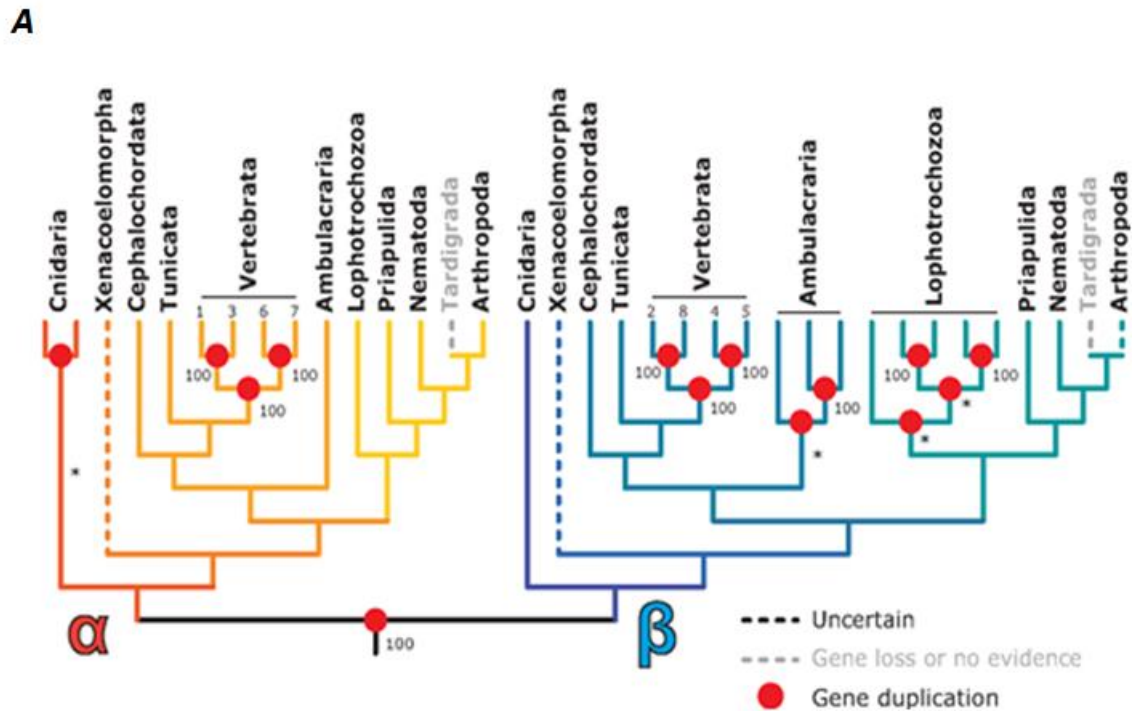

B

Cnidaria:	Hydra vulgaris
Nematoda:	Caenorhabditis elegans
Ambulacraria:	Strongylocentrotus purpuratus
Arthropoda:	Drosophila melanogaster
Lophotrochozoa:	Octopus vulgaris
Chordata:	Branchiostoma_belcheri
Priapulida:	Priapulus caudatus
Vertebrata:	Homo-species-Human
Tunicata:	Ciona_intestinalis


C
TRP Box
Hydra_vulgaris|Fresh-water-polyp|XP_012561335|alpha ---------VQANADTIWKFERFNLVLEYANRPPLIPPFILLCHLYMLGNYLNSLIR--- 918
Hydra_vulgaris|Fresh-water-polyp|XP_012554388|alpha ---------VQANAEQIGKFERYSLILEYATRPPLIPPFILLCHFYMLVNFFKDLYL--- 1047
Hydra_vulgaris|Fresh-water-polyp|XP_012565257|alpha ---------IIEDSDKVWKFQRFDLILEFHNRPAFCPPFIIISHLYLLIKWFLKICF--- 828
Caenorhabditis_elegans|Nematode|gon-2_CE30390|alpha ---------TDEMSQQIWLFQRYKQVMEYESTPFLPPPLTPLYHGVLILQFVRTRLSCSK 1612
Caenorhabditis_elegans|Nematode|gtl-1_CE33754|alpha ---------HIQSTREIFLFERYGQVMEYESTPWLPPPFTIIYHVIWLFKLIKS---SSR 1384
Caenorhabditis_elegans|Nematode|gtl-2_CE40563|alpha ---------SIEKSKEIWLFQRYQQLMEYHDSPFLPPPFSIFAHVYHFIDYLYNLRR--- 1183
Strongylocentrotus_purpuratus|Purple_sea_urchin|XP_794425.3|alpha ---------VMPIANQLWKFQRYHVVMKYEQKPILVPPFTIIYYLYSLFKFVACQCR--- 609
Ciona_intestinalis|Vasetunicate|XP_018667443|alpha ---------VKTYSDRIWKFQRYLMIVEYELRPVLPPPLILISYISMIIGRIFKKRK--- 1183
Drosophila_melanogaster|Common_fruit_fly|Trpm|alpha ---------VNSVSHQVWMFQRFTVVMEYQQKPVLPPPFIALCHFYSLLKYC-V----RK 1210
Octopus_vulgaris|Common_octopus|XP_029641654.1|alpha ---------NNANSREIWKFQRYQLIIVYELRPLLPPPLILLSHLFLTLKFIKRR----- 1171
Branchiostoma_belcheri|Lancelet|XP_019640450|alpha ---------IKAISNQVWKFQRFHLIMEYEQRPMLPMPLTILYHIYMLLKYLVCVCS-R- 982
Priapulus_caudatus|Penis_worm|XP_014671784|alpha ---------VNAVAQQVWKFQRYSVILEYEQRPVLAPPLIILCHMYQLVK-YCNRRY--- 1223
Homo_sapiens|Human|TRPM6_CCDS6647.1|alpha ---------MESISNNLWKYNRYRYIMTYHEKPWLPPPLILLSHVGLLLRRLCCHRA--- 1123
Homo_sapiens|Human|TRPM7_CCDS42035.1|alpha ---------VKAISNIVWKYQRYHFIMAYHEKPVLPPPLIILSHIVSLFCCICKRRK--- 1150
Homo_sapiens|Human|TRPM1_CCDS10024.2|alpha ---------VKSISNQVWKFQRYQLIMTFHDRPVLPPPMIILSHIYIIIMRLSGRCR-KK 1131
Homo_sapiens|Human|TRPM3_CCDS6634.1|alpha ---------VKSISNQVWKFQRYQLIMTFHERPVLPPPLIIFSHMTMIFQHLCCRWR--K 1026
Branchiostoma_belcheri|Lancelet|XP_019638014|beta ---------VQERAGMYWSYYRYDMIQEYQDRPLGPGPLLVFGLLWKLWEVFRG------ 562
Homo_sapiens|Human|TRPM4_CCDS33073.1|beta ---------VQGNSDLYWKAQRYRLIREFHSRPALAPPFIVISHLRLLLRQLCRRPR-S- 1098
Homo_sapiens|Human|TRPM5_CCDS31340.1|beta ---------VQGNADMFWKFQRYNLIVEYHERPALAPPFILLSHLSLTLRRVFKKEA-E- 1033
Homo_sapiens|Human|TRPM2_CCDS13710.1|beta ---------VQEHTDQIWKFQRHDLIEEYHGRPAAPPPFILLSHLQLFIKRVVLKTP-A- 1103
Homo_sapiens|Human|TRPM8_CCDS33407.1|beta ---------VQENNDQVWKFQRYFLVQEYCSRLNIPFPFIVFAYFYMVVKKCFKCCC-K- 1034
Branchiostoma_belcheri|Lancelet|XP_019640471|beta ---------IQDESEVHWKYQRYFVIEEYVSRPWGPPPLILLGHVWRLAYFMYRRRG-SC 1015
Strongylocentrotus_purpuratus|Purple_sea_urchin|XP_011661004.1|beta ---------IQANSLVIWRYEYYFLVMEFKDKSWLPPPFNVLVHLYKSLQWVFRCCI-KA 1131
Ciona_intestinalis|Vasetunicate|XP_026692588|beta ---------LVEKTDSLYKYQRYELLEVYYQRSSIVTPFSILSYGRQLILYCV---R-GC 612
Octopus_vulgaris|Common_octopus|XP_029647149.1|beta ---------VQVNTDLHWHFQRYSLIFEFYTRPPLPPPLILLNNIYLLFRYLYKKKR-HL 1044
Octopus_vulgaris|Common_octopus|XP_029646813.1|beta ---------VQEKSRLHWSFQRYELIFEFSIRPPLPPPFILLCNIYQACRYLCEKAS-RK 1167
Octopus_vulgaris|Common_octopus|XP_029646968.1|beta ---------VQERSYHHWSFQRYELIYEFSVRPPLPPPFILLSNIYQFCHYLHKKTR-NA 996
Strongylocentrotus_purpuratus|Purple_sea_urchin|XP_011674872.1|beta ---------VQENTDVVWKFQRYSLIKDYYNRPILAPPFIIISHFFILYSFILRCWC-G- 1106
Priapulus_caudatus|Penis_worm|XP_014669422|beta LPNLVICETGESTSGSLWSCFKS---------- 340

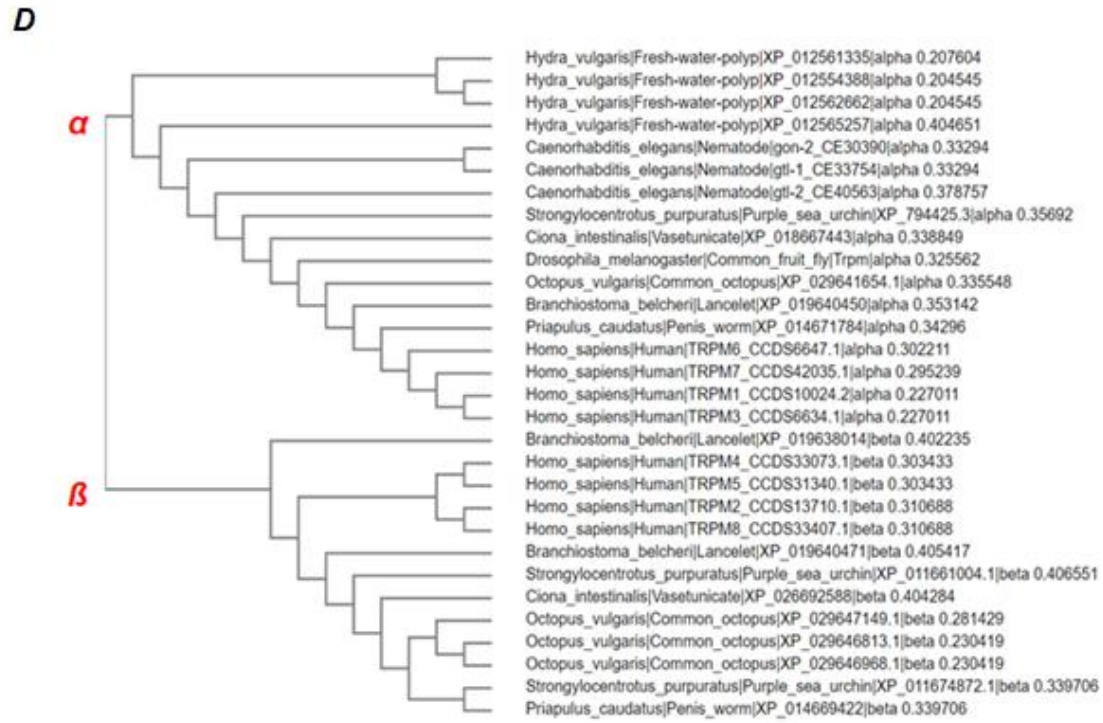

Figure 3.14 Clustal alignments of TRP domain of various species in different phyla.
A) Phylogenetic tree of sequences of representative species were applied for clustal alignment (Himmel et al., 2020). The variety of species of TRPM channels were chosen from of the 11 main classes, including Cnidaria, Xenacoelomorpha, Cephalocordata, Tunicata, Vertebrata, Ambulacraria, Lophotrochozoa, Priapulida, Nematoda, Tigrada (no genes found), Arthropoda. B) Selective species of TRPM family from all classes in panel A. C, D) Clustal alignments and phylogenetic tree of multiple TRPM TRP domain sequences sourced from a variety of species of both branches in all classes. Red text denotes the species with cysteines analogous to TRPM7.

3.5.4 Clustal Alignments of TRP superfamily and TRPM subfamily

Analysis with 136 TRP channel structures available via Cryo-EM microscopy illustrates that classical TRP channels consist of 6 transmembrane (TM) helices (S1-S6) which tetramerise to form a channel, with a pore loop between S5 and S6 (Huffer et al., 2020). In addition, TRP domain is a short hydrophobic stretch conserved in the TRPC, TPV and TRPM subfamilies with localization at C-terminal end of the S6 helix (Liedtke, 2006).Secondary structure predication algorithms predict that S6 helix extends beyond the membrane bilayer in the cytosolic side, including the TRP box (Liedtke, 2006). The TRP box which resides parallel to membrane is thought to co-operate with S6 to control channel gating (Huffer et al., 2020, Clapham et al., 2001). Also deletion of TRP domain disturbs tetramerization of TRPV1 channel (García-Sanz et al., 2004).

As TRPM7 palmitoylated cysteines conserved in most TRPM family members during evolution, we developed another clustal alignments of members from wider TRP superfamily which also identified analogous cysteines in most TRPV

and TRPC families except TRPC6, TRPV3, and TRPV4 (Figure 3.15A). Notably, although TRPV6, TRPV3 and 4 channels lack similar cysteine residues, they all have basic/hydrophobic amino acids motifs similar to those present in TRPM2 and TRPM5. In addition, we visualized the potential palmitoylated cysteine of TRPV6 on its Cryo-EM structure using PyMOL software. Ribbon diagram (Left) and surface representation (Right) of one subunit of TRPV6 show that Cys611 localized in an unstructured region just after the alpha helix containing the TRP domain (Figure 3.15B). This localization has high similarity with the cluster of TRPM7 palmitoylated cysteines, also exposed on the external surface of the tetramer, close to zDHHC-PAT active site.

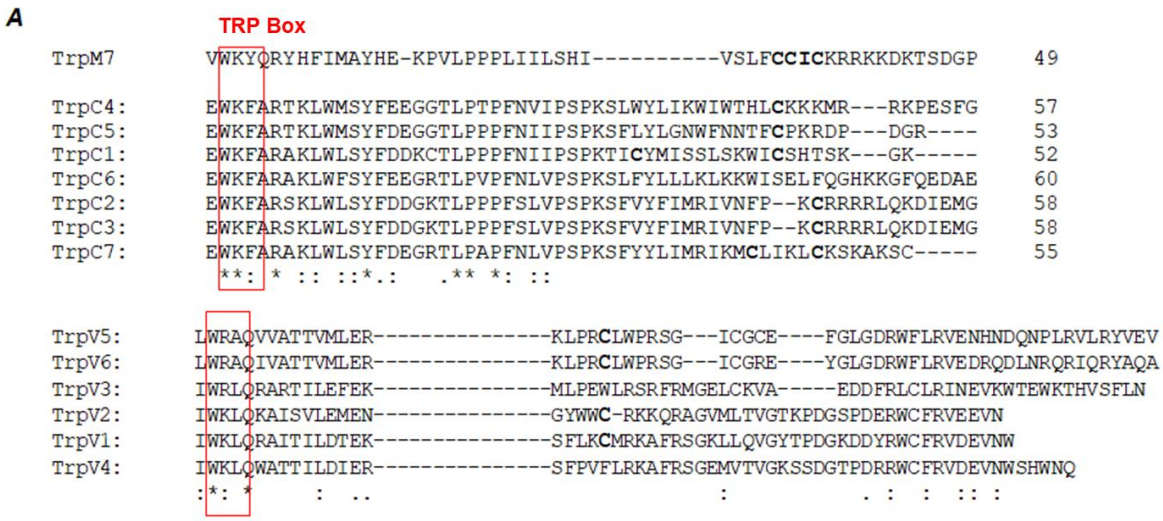

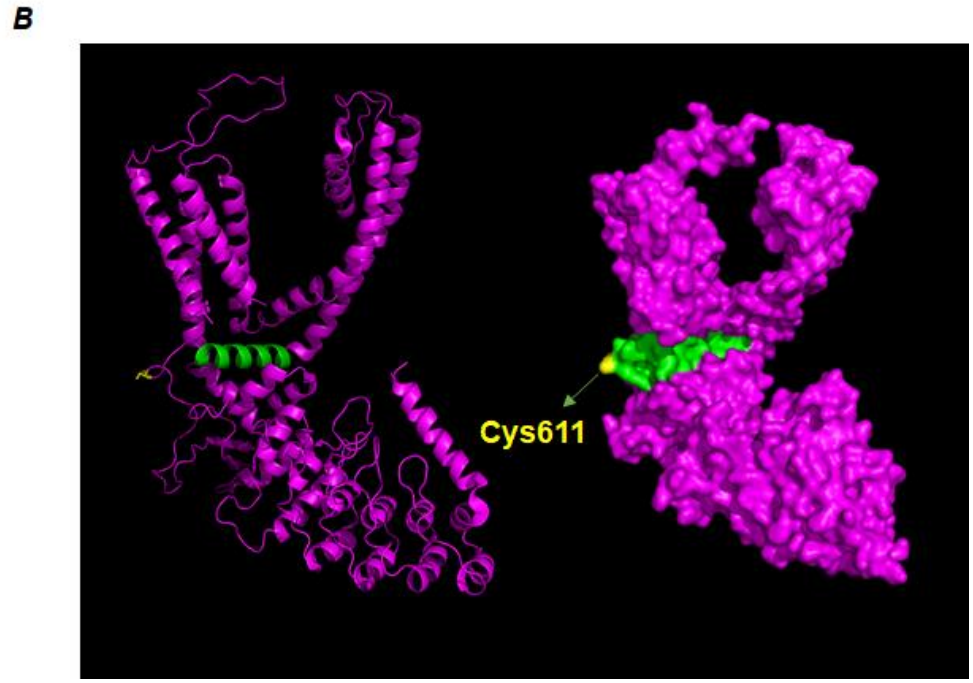

Figure 3.15 Clustal Alignments of TRP domain of TRPV and TRPC family members in human and TRPV6 Cryo-EM structure.
A) Clustal alignments of TRP domain among TRPC and TRPV channels. The sequences are all sourced from homo sapiens. Cysteines (bold) are conserved in most of the TRP domains. B) Cryo-EM structure of TRPV6 (PDB code 6bo8) subunit to reveal the potential palmitoylated cysteine. TRP domain helix were coloured Green and the Cys611, which is potential palmitoylated site for TRPV6 were labelled yellow.

The mechanisms controlling TRP superfamily members are diverse, but one common regulator is anionic lipid phosphatidylinositol 4,5 bisphosphate (PIP2) (Brauchi et al., 2007). It binds to the positively charged amino acids in TRP box to activate TRP channels (Rohács et al., 2005). Multiple channels are inhibited when PIP2 is hydrolysed, including TRPM7 (Runnels et al., 2002). The mobility and flexibility of TRP box, which is a key determinant of channel gating may be regulated by PIP2 binding. TRPM7 palmitoylation sites lie at the C-terminal end of the TRP domain, a region for which no structure is revealed, but whose conformational flexibility may influence TRP domain movement and therefore effect channel activity.

3.6 Summary

In conclusion, TRPM7 and TRPM6 are both highly palmitoylated in human embryonic kidney cells, whereas the former is also palmitoylated in many different cell types like vascular smooth muscle cells (human and rat), cardiac ventricular tissues. Palmitoylation sites of TRPM7 localized among cysteines cluster of Cys1143, Cys1144 and Cys1146 in the C-terminal end of TRP domain.

Additionally, TRPM6 palmitoylation sites lie in similar regions with a double cysteines cluster. Palmitoylated cysteines are highly conserved in all mammalian family members except TRPM2 and TRPM5. Comprehensive clustal alignments were conducted in wider TRP superfamily, we found that TRPV and TRPC channels also retain the conserved cysteines except TRPC6, TRPV3 and TRPV4. However, these channels contain basic/hydrophobic amino acids residues in the relevant regions. These findings support the notion that common features of potential palmitoylation cysteines are near the membrane and/or hydrophobic amino acids, and/or close to positively charged amino acids. With the non-palmitoylated mutants of TRPM7, we can further investigate the influence of palmitoylation on its trafficking, ion channel activity and kinase domain functions.

Chapter 4 Functional effect of TRPM7 palmitoylation

4.1 Introduction

4.1.1 TRPM7 localisation and its movement through the secretory pathway

Ubiquitously expressed TRPM7 is well-characterised as an ion channel and cytoplasmic kinase, which is required for organ development but also mediates oxidative stress-induced anoxic neuronal death (Aarts et al., 2003). Recording TRPM7 activity using the patch clamp technique only reveals the behaviour of the channel at the plasma membrane (Chokshi et al., 2012b). However, research has already demonstrated that TRPM7 is distributed in intracellular membranes. For instance, TRPM7 resides in the membrane of synaptic vesicles of sympathetic neurons, forming complexes with synapsin I and synaptotagmin I, exerting essential impacts on neurotransmitter release (Brauchi et al., 2008). Recently an investigation conducted by Abiria et.al. (Abiria et al., 2017a) detected TRPM7 largely expressed in intracellular vesicles in multiple cell types such as HEK293 cells and LN-18 glioma cells. TRPM7 punctate distribution in cytoplasmic vesicles of unknown origin, showing no colocalization with markers of several known cellular compartments, including endoplasmic reticulum, peroxisomes, lysosomes, endosomes and ER-Golgi intermediate compartments (Abiria et al., 2017a).

There are a variety of routes for transport and modifications of protein in the secretory pathway in cells due to the diversity of compartments and plasma membrane subdomains (Hanus and Ehlers, 2008, Rodriguez-Boulan et al., 2005). To comprehensively understand the mechanisms and dynamics of cargo sorting in the secretory pathways, several approaches are currently established to specifically investigate cargo secretory trafficking. For example, a classical method to visualise cargo protein traffic relies on thermosensitive viral glycoprotein, vesicular stomatitis virus glycoprotein ts045 (VSVGts045). It normally accumulates in the endoplasmic reticulum (ER) at 39.8° C but rapidly cross through Golgi apparatus to the cell surface after lowering the temperature to 32° C (Arnheiter et al., 1984). However, temperature restriction for the system is not fully physiological. To dissect control of TRPM7 distribution to vesicles and cell membranes, we applied the retention using selective hooks (RUSH) system (Boncompain et al., 2012). It relies on the selective retention and

release of target proteins from the donor compartment. To be specific, the system is based on expression of two fusion proteins: one is the core streptavidin fused to a hook which is stably expressed in the donor compartment, the other one is the streptavidin binding protein (SBP) fused to the protein of interest. SBP binds to streptavidin with high affinity, but the interaction is outcompeted by biotin, releasing the protein of interest from the donor compartment (Figure 4.1A). We chose li for ER retention and Golgin-84 for Golgi retention, and fused SBP to the N-terminus of wild TRPM7-YFP and non-palmitoylated TRPM7-1143/4/6_AAA-YFP mutant (Figure 4.1B). Therefore, we can detect the impacts of palmitoylation of TRPM7 on its passage through the secretory pathway from ER or Golgi to destination compartments consisting of surface membrane and intracellular vesicles.

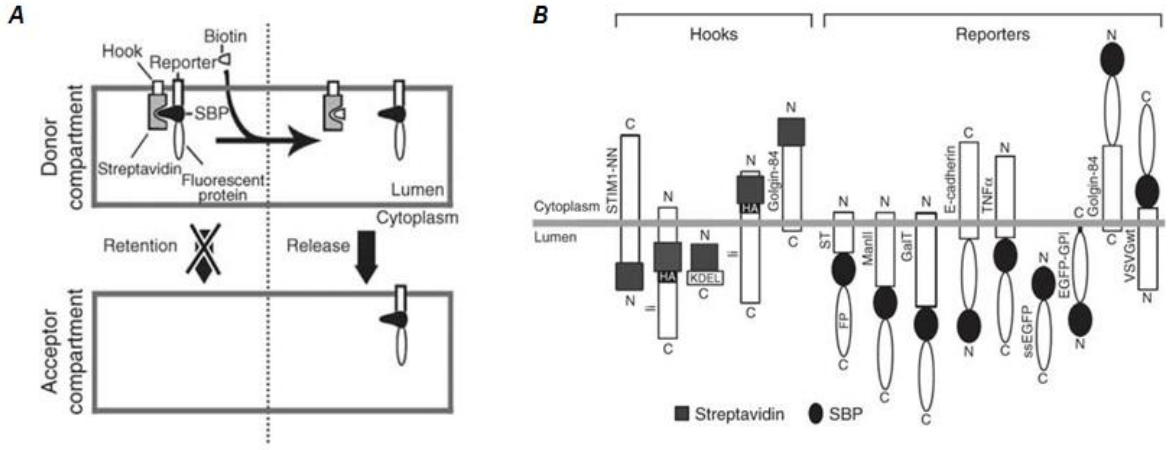

Figure 4.1 A diagram of the principles of RUSH system (Boncompain et al.)
Reporters is retained in the donor compartment by interaction with the hook, which is mediated by the core streptavidin and the SBP. Addition of Biotin would release reporter from the hook and allow trafficking to its acceptor compartment. B) Schematics of selections for hook, containing STIM1-NN, Ii or KDEL for ER retention or Golgin-84 for Golgi retention fused to streptavidin. And SBP fusion with multiple reporters. Golgi proteins ST, ManII, GalT or Golgin-84; plasma membrane proteins VSVGwt, E-cadherin, TNFα or EGFP-GPI and secreted protein SBP-ssEGFP. HA is hemagglutinin tag; FP is fluorescent protein.

4.1.2 TRPM7 ion channel activity

Alterations of intracellular calcium concentration regulate diverse physiological and biological functions including signal transduction, proliferation, motility, transcription and the cell cycle (Berridge et al., 1999). Intracellular Ca is regulated by releasing Ca from the endoplasmic reticulum (ER) or sarcoplasmic reticulum storage or opening Ca conduction channels within the plasma membrane (PM). Those two mechanisms normally are coupled in many

electrically non-excitable cells. This process is known as store-operated calcium entry (SOCE), and relies on Ca released from the ER engaging with the calcium release-activated calcium channels (CRAC) (Faouzi et al., 2017b).TRPM7 has been identified to regulate Ca entry via SOCE via its kinase domain, which suggested that SOCE might be a new mechanistic target of TRPM7 channel kinase (Faouzi et al., 2017b). Furthermore, Ca influx through N-methyl-D-aspartate glutamate receptors (NMDARs) is one key damaging process cause by excitotoxic glutamate receptor activity in brain ischemia (Lipton, 1999). Oxygen-glucose deprivation (OGD) leading to neuronal death via NMDAR activation is associated with a lethal cation current I_{OGD} generated by TRPM7 (Nadler et al., 2001, Goldberg and Choi, 1993). Blocking I_{OGD} or suppressing TRPM7 expression prevents anoxic neuronal death, which suggests that TRPM7-mediated Ca entry is responsible for Ca overload and cell death during anoxia (Aarts et al., 2003). In addition, recently published research found that Ca influx through TRPM7 is essential to regulate synaptic vesicle endocytosis in neurons thereby influencing short-term plasticity of synaptic strength (Jiang et al., 2021).Generally, TRPM7 also contributes to Ca homeostasis by maintaining the filling state of intracellular Ca stores in resting cells (Faouzi et al., 2017b).

As the second most abundant mineral in the body, magnesium plays a fundamental role in the physiological functions of human brain, heart and skeletal muscle (De Baaij et al., 2015). Mg is involved in more than 600 enzymatic reactions, which control diverse physiological functions including protein synthesis, nerve transmission, signal transduction, energy metabolism, cardiac excitability, and blood pressure (Gröber et al., 2015, Matsuda-Lennikov et al., 2019). Mg binds to adenosine triphosphate (ATP) forming the enzymatically active Mg·ATP complex, which is crucial for catalytic activity of protein kinases by contributing to the transfer of phosphoryl group. Mg balance in human body and intracellular magnesium homeostasis require the balanced interplay between intestinal absorption and renal excretion, additionally multiple transporters across cell membrane to regulate Mg influx and efflux (Jahnen-Dechent et al.). It is well recognized that TRPM7 and TRPM6 play an important role in Mg homeostasis, for which TRPM7 is also sensitive to the cellular Mg and Mg·ATP levels (Nadler et al., 2001, Schmitz et al., 2003). TRPM7 is strongly activated when Mg·ATP levels fall below 1mM, thereby producing a

current designated as MagNuM for magnesium-nucleotide-regulated metal ion current (Nadler et al., 2001, Himmel et al., 2020). The kinase domain is not required for ion channel activation but it influences sensitivity of the channel to Mg inhibition (Schmitz et al., 2003).Besides, mutations of TRPM6 causes hypomagnesemia with secondary hypocalcaemia, for which symptoms could be improved by additional high does Mg supplementation (Schlingmann et al., 2002). Heteromeric TRPM6/TRPM7 channel relieves homomeric TRPM7 from tight inhibition of Mg·ATP (Ferioli et al., 2017).

Apart from Ca and Mg , heterologous overexpression of TRPM7 in HEK-293 cells also conducts a range of trace metal ions with high preference for Zn and Ni (Monteilh-Zoller et al., 2003). These trace metal ions are required cofactors for many fundamental cellular enzymes. For example, Zinc is required for over 300 enzymes' activity with the major roles of directly participating in catalysis, co-catalysis and maintaining protein structure and stability (McCall et al., 2000). Increasing evidence revealed that Zn-induced neuronal injury was largely suppressed by TRPM7 channel inhibition or silencing TRPM7 using interfering RNA (Inoue et al., 2010). In addition, as previously discussed, the population of TRPM7 that localises to intracellular vesicles releases Zn in a TRPM7-dependent manner leading to Zn overload triggered by reactive oxygen species (ROS) (Abiria et al., 2017a). Consequently, cytosolic free [Zn] is controlled in a TRPM7-dependent manner and also regulates TRPM7 cleaved kinase (M7CK) binding to transcription factors containing zinc-finger domains (Krapivinsky et al., 2014).

TRPM7 palmitoylation sites, cysteines 1143, 1144 and 1146, are localized in the TRP domain, which resides parallel to membrane and co-operates with transmembrane segment6 to control channel gating (Huffer et al., 2020). Accordingly, we probed the influence of palmitoylation on TRPM7 ion channel activity.

4.1.3 Protein interactions with TRPM7

Accumulating research indicates that TRPM7 kinase domain is essential for a variety of cellular processes including proliferation, survival, differentiation, migration, and growth. The TRPM7 kinase is proteolytically cleaved from the channel domain in a cell specific manner, after which cleaved kinase fragments

(M7CKs) translocate into the nucleus and participate in multiple components of chromatin remodelling complexes (Krapivinsky et al., 2014). A few proteins have already been identified binding the TRPM7 kinase domain such as phospholipase C (PLC), annexin I, myosin II heavy chain, and elongation factor 2 (eEF2) (Clark et al., 2006, Dorovkov et al., 2008, Dorovkov and Ryazanov, 2004, Perraud et al., 2011). Specifically, TRPM7 kinase domain is directly associated with the C2 domain of phospholipase C (PLC). Hydrolysis of phosphatidylinositol 4,5-bisphosphate (PIP 2) leads to inactivation of the TRPM7 channel (Runnels et al., 2002). Recent published research by Kollewe et.al., demonstrated endogenous TRPM7 channels formed high-molecular-weight multiple protein complexes consisting of putative metal transporter proteins (CNNM1-4) and a small G-protein ADP-ribosylation factor-like protein 15 (ARL15) (Kollewe et al., 2021a). On one hand, ARL15 acts as a negative regulator of TRPM7 channel with transient expression of ARL15 in HEK293 cells inhibits endogenous TRPM7 current. On the other hand, CNNM3 to a large extent serves as a negative regulator of TRPM7 kinase activity (Kollewe et al., 2021a).

Notably, TRPM7 is highly overexpressed in cell lines and tissues of a variety of cancers (Yee, 2017). For instance, TRPM7 is overexpressed 13-fold in pancreatic cancer comparing with healthy tissue, and mediates migration of the human pancreatic cancer cell line BxPC-3 via an Mg-dependent mechanism (Hantute-Ghesquier et al., 2018). In addition, TRPM7 expression is required for tumour metastasis via regulation of cell tension and adhesion by its substrate myosin II (Middelbeek et al., 2012). Hence TRPM7 and its interaction partners might be involved in many signalling pathways with clinical significance. Consequently, we sought to determine whether palmitoylation influences protein interactions with TRPM7.

4.2 Aims

The aim of this chapter is to investigate the influence of palmitoylation on TRPM7 function. Having identified the palmitoylated cysteines in TRPM7, we can make comparison to explore the impact of palmitoylation on TRPM7 distribution between surface membrane and intracellular vesicles as well as its movement thought the secretory pathway. In addition, we try to illustrate how

palmitoylation influences TRPM7 protein interactions, and three important divalent cation conduction including Mg, Ca and Zn.

4.3 Methods

4.3.1 Endoplasmic reticulum (ER) and Golgi retention hook system

As previously mentioned in section 4.1.1, we chose Str-li_neomycin (#65312) for ER-Hook and Str-Golgin84_VSVG-SBP-EGFP (#65305) for Golgi-Hook via Addgene(Boncompain et al., 2012). Those cDNAs encoding these hooks were subcloned into pcDNA™5/FRT vector or pc pcDNA™5/FRT/TO vector to generate constitutive/inducible stably expressed 293 T-Rex cell line. Flp-In™ 293 T-Rex cell line contains a single stably integrated FRT site in a transcriptionally active genomic locus which allows targeted integration with Flp-In™ vector (e.g., pcDNA™5/FRT, pcDNA™5/FRT/TO) to ensure high expression of Golgi-hook and ER-hook protein. For ER-hook constitutive/inducible cell lines, we amplified streptavidin-HA-Ii from Str-li_neomycin then ligated it into pcDNA5-FRT/pcDNA5-FRT/TO. For Golgi-hook lines ones, we amplified streptavidin-HA from Str-li_neomycin, and Str-Golgin84_VSVG-SBP from Golgi-hook then ligated them together into pcDNA5-FRT/pcDNA5-FRT/TO. Details of primers sequences are demonstrated as following Table 4.1. Oligo sequences of primers for engineering ER-hook and Golgi-Hook stable cells (inducible).

Table 4.1. Oligo sequences of primers for engineering ER-hook and Golgi-Hook stable cells (inducible).
Primers were designed by Takara primer design software. HA tag is existing in both vectors.

PCR reaction	Template	Oligo Name	Sequence
1	pcDNA5-FRT/TO	pcDNA5-FRT/TO HOOK For pcDNA5-FRT/TO HOOK Rev	GCTCGAGTCTAGAGGGCCC GGCCGCCACTGTGCTGGATA
2	Str-li_neomycin	Streptavidin-HA-Ii For Streptavidin-HA-Ii Rev	AGCACAGTGGCGGCCaccATGCACC GGAGGAGATCACG CCTCTAGACTCGAGCTCACATGGG GACTGGGCC
3	Str-li_neomycin	Streptavidin-HA For Streptavidin-HA Rev	TATCCAGCACAGTGGCGGCCaccAT GCACCGGAGGAGATCACG CAAACCAAGATGCGTAGTCTGGTA CGTCG
4	Str-Golgin84_VSVG-SBP-EGFP	Str-Golgin84_VSVG-SBP For Str-Golgin84_VSVG-SBP Rev	AGACTACGCATCTTGGTTTGTTGA TCTTGCTGG CGGGCCCTCTAGACTCGAGCTCAT TTGCCATATGGTTGGTCG

Wild type TRPM7-YFP and non-palmitoylated 1143/4/6_AAA-TRPM7-YFP were fused with streptavidin binding protein (SBP), to enable capture by hooks in the ER or Golgi compartment. SBP was inserted in the N-terminus of TRPM7, immediately after the translation start site. We amplified SBP from Str-Golgin84_VSVG-SBP-EGFP and TRPM7-YFP from WT-TRPM7-YFP and TRPM7-1143/4/6_AAA-YFP mutant separately. The details of oligo sequences of primers are showed in Table 4.2.

Table 4.2. Oligo sequences of primers for generation of wild type SBP-TRPM7-YFP and non-palmitoylated SBP-1143/4/6_AAA-YFP plasmids.

PCR reaction	Template	Oligo Name	Sequence
1	WT-TRPM7-YFP	TRPM7-YFP vector For TRPM7-YFP vector Rev	GCCCAGAAATCCTGGATAGAG AGC CATGGTGGTCACGGGGCG
2	TRPM7-1143/4/6_AAA-YFP	TRPM7-YFP vector For TRPM7-YFP vector Rev	GCCCAGAAATCCTGGATAGAG AGC CATGGTGGTCACGGGGCG
3	Str-Golgi84_VSVG-SBP-EGFP	Streptavidin-HA For Streptavidin-HA Rev	TATCCAGCACAGTGGCGGCCa ccATGCACCGGAGGAGATCAC G CAAACCAAGATGCGTAGTCTG GTACGTCG

All the amplifying and ligation procedures followed the In-fusion cloning kit instructions (Table 2.4), for which PCR cloning parameters details are provided in section 2.5.1. The procedures of engineering 293 T-Rex cells stably expressed ER-hook and Golgi-hook were illustrated in Chapter.2 (section 2.7.2). Expression of the gene of interest in stably transfected cells was tested with relevant antibody via western blot before experiments.

4.4 Results

4.4.1 TRPM7-AAA-YFP is trapped in the endoplasmic reticulum

TRPM7 has been identified as being highly palmitoylated in primary and immortalised cells using resin assisted capture of acylated proteins (Acyl-RAC) (section 3.4.1). In addition, we mapped palmitoylation sites of TRPM7 and found localization at a cluster of cysteines 1143/1144 and 1146 at the C terminal end of the characteristic TRP domain near transmembrane domain. Palmitoylation occurs throughout the secretory pathway and controls the subcellular

localisation of numerous ion channels and transporters(Essandoh et al., 2020, Linder and Deschenes, 2007, Tulloch et al., 2011). Therefore, we visualised the subcellular location of wild type, 1143A, 1143/1144_AA and un-palmitoylated 1143/1144/1146_AAA TRPM7 in transiently transfected HEK cells. YFP tag was fused to the C terminus of WT-TRPM7 and its mutants. Wild type TRPM7 localised to intracellular vesicles (Figure 4.2A) which conform to Abiria et al.'s finding that the majority of TRPM7 is distributed in abundant unknown intracellular vesicles (Abiria et al., 2017a). TRPM7-1143/4/6_AAA mutant was localised only to a perinuclear compartment that we identified as the endoplasmic reticulum (ER) using the marker protein DsRED-ER (Figure 4.2B). TRPM7-1143A and TRPM7-1143/4_AA mutants displayed intermediate localisation, with some observed in punctate intracellular vesicles and some in the ER (Figure 4.2A). In addition, we also performed transient transfections of WT-TRPM7 and non-palmitoylated TRPM7 in WKY Vascular smooth muscle cells (VSMCs). Similarly, wild type TRPM7-YFP localised in punctate intracellular vesicles and non-palmitoylated 1143/4/6_AAA mutant was trapped in the ER (Figure 4.2B).

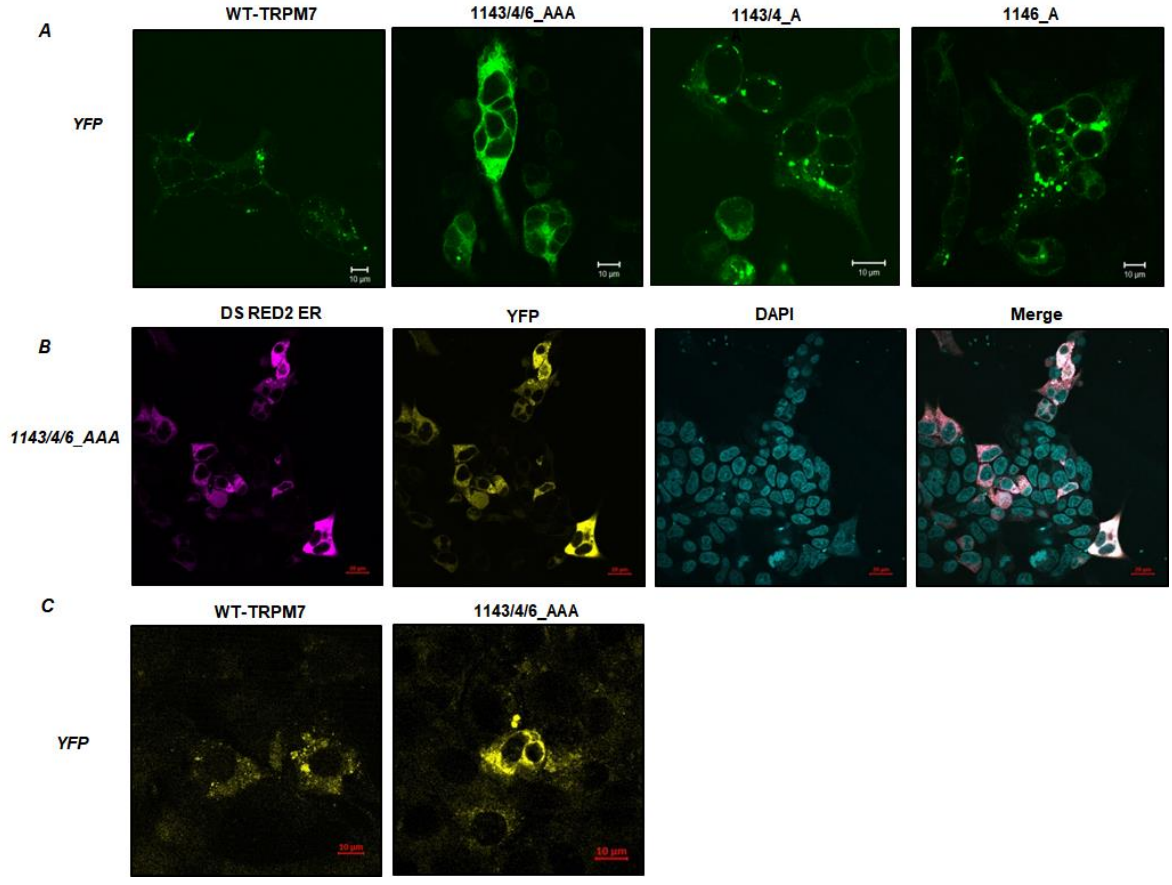

Figure 4.2 TRPM7-1143/4/6_AAA non-palmitoylated mutant is trapped in endoplasmic reticulum in HEK cells and VSMCs.

A) Confocal imaging of WT-TRPM7, 1143/4/6_AAA, 1143/4_AA and 1146_A mutants transfected in HEK293 cells. All plasmids were fused with YFP and TRPM7-1143/4/6_AAA mutant is non-palmitoylated. 514nm laser wavelength was applied for generating peak excitation of YFP for Zeiss LSM520 microscope. B) Confocal imaging of TRPM7-1143/4/6_AAA-YFP mutant co-transfected with ER marker (DS RED2 ER). Non-palmitoylated TRPM7 was trapped in endoplasmic reticulum and colocalized with DS RED2 ER plasmid. 543nm laser wavelength was applied for peak excitation of DS RED2 ER in Zeiss LSM 880 microscope. DAPI was used for staining cell nuclear (405nm). C) Confocal images of WT-TRPM7-YFP and TRPM7-1143/4/6_AAA-YFP transfected in rat WKY vascular smooth muscle cells (VSMCs). Scale bar: 10 μm

4.4.2 Subcellular location of palmitoylated and non-palmitoylated TRPM6

We also explore palmitoylation of TRPM6. investigated the subcellular localization of wild type TRPM6 and its non-palmitoylated TRPM6-AA-YFP mutant. Unlike 1143/4/6_AAA TRPM7 which was trapped in the ER, TRPM6-AA mutant could exit the ER freely (Figure 4.3). previously research indicated that TRPM6 must from a hetero-oligomer with TRPM7 for trafficking to the cell surface (Boncompain et al., 2012). It might be interesting to investigate if alteration of TRPM6 would influence its co-trafficking with TRPM7 to cell surface.

In conclusion, we found that palmitoylation is required for TRPM7 to exit the ER, which implies that TRPM7 is palmitoylated by an ER resident zDHHC-PAT. However, non-palmitoylated TRPM6-AA-YFP was not trapped in the ER. Palmitoylation is not only necessary for TRPM7 to traverse the secretory pathway in HEK cells but also important in other cell types like VSMCs which influence its biological significance.

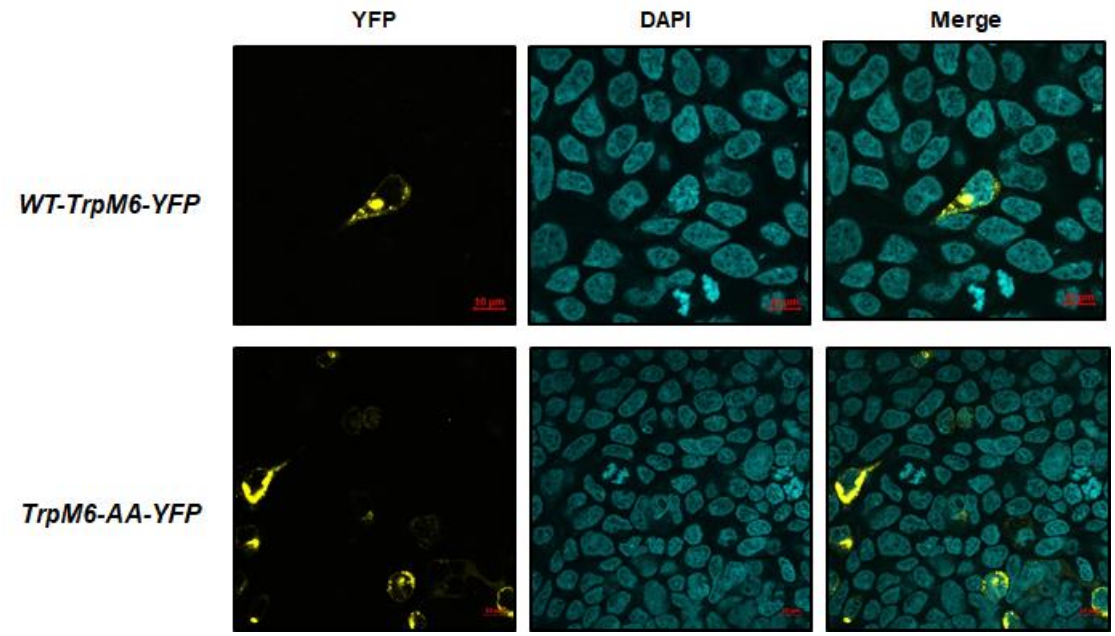

Figure 4.3 TRPM6-AA-YFP non-palmitoylated mutant could exit the ER in the HEK cells. Transiently transfection of wild type TRPM6 and its non-palmitoylated mutant localization in HEK cells were visualized by confocal microscope. YFP tag fused on all plasmids. WT-TRPM6 distributed in the ER/Golgi which was quite similar with the TRPM6-AA-YFP mutant. Scale bar: 10 µm

4.4.3 RUSH system for TRPM7 in the endoplasmic reticulum cell line (Constitutive)

The retention of the1143/6/7_AAA TRPM7 in the endoplasmic reticulum prevented us working with this mutant for functional studies. To investigate the role of palmitoylation in the life cycle of TRPM7 after it leaves the ER, we used the retention using selective hooks (RUSH) system to control the localisation of TRPM7 in the secretory pathway (Boncompain et al., 2012). RUSH systems relies on the interaction of a core streptavidin fused “hook”, which is confined to a specifc subcellular compartment, with a streptavidin binding protein (SBP) fused to the protein of interest. The interaction between SBP and core streptavidin would be disrupted by addtion of biotin due to its high affinity to streptavdin.

We engineered HEK-derived 293 T-REx cells stably expressing the ER hook (streptavidin-CD74) and the Golgi hook (streptavidin- Golgi 84). The expression of the hooks in stable cells was tested alongside the overexpression of ER-Hook transiently transfected into HEK cells, which demonstrated all cell lines expressed effienicently (Figure 4.4). Next we fused SBP to the N terminus of wild type TRPM7-YFP and its non-palmitoylated 1143/4/6_AAA-YFP. Fusion to SBP to not change TRPM7 behaviour in HEK cells. SBP-WT-TRPM7-YFP localised in the unknown punctate intracellular vesicles when expressed in HEK cells (Figure 4.5)

but was retained in the ER when expressed in ER-hook stably expressing 293 T-REx cells (Figure 4.6A), which was confirmed by co-localisation with DsRED2-ER marker. Biotin treatment released the protein from the hook in the ER (Figure 4.6B). Meanwhile, SBP-1143/4/6_AAA-YFP mutant remained confined to the ER in both cell types (Figure 4.5and Figure 4.6A),and was not released following biotin treatment in engineered ER-hook stable cells (Figure 4.6B). Non-palmitoylated TRPM7-1143/4/4_AAA mutant was continuously trapped in the ER, which prevented us working with this non-palmitoylated mutant.

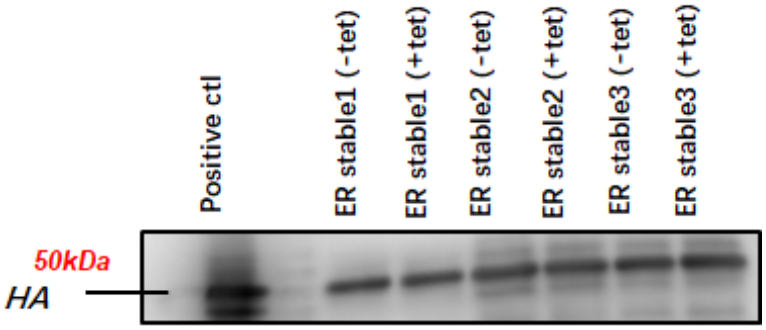

Figure 4.4 ER-hook stable cell lines expression test.
Transiently trasnfected HA tagged ER hook (Strepatavidin-CD74) in HEK 293 cells was positive control. The 3 engineered ER-Hook stable cell lines (1:high ratio, 2:medium ratio, 3:low ratio) were tested alongside it. All cell lines have ER-hook encoded gene expression regardless of the presence of tetracycline or not and we choose medium ratio one as the following expriments.

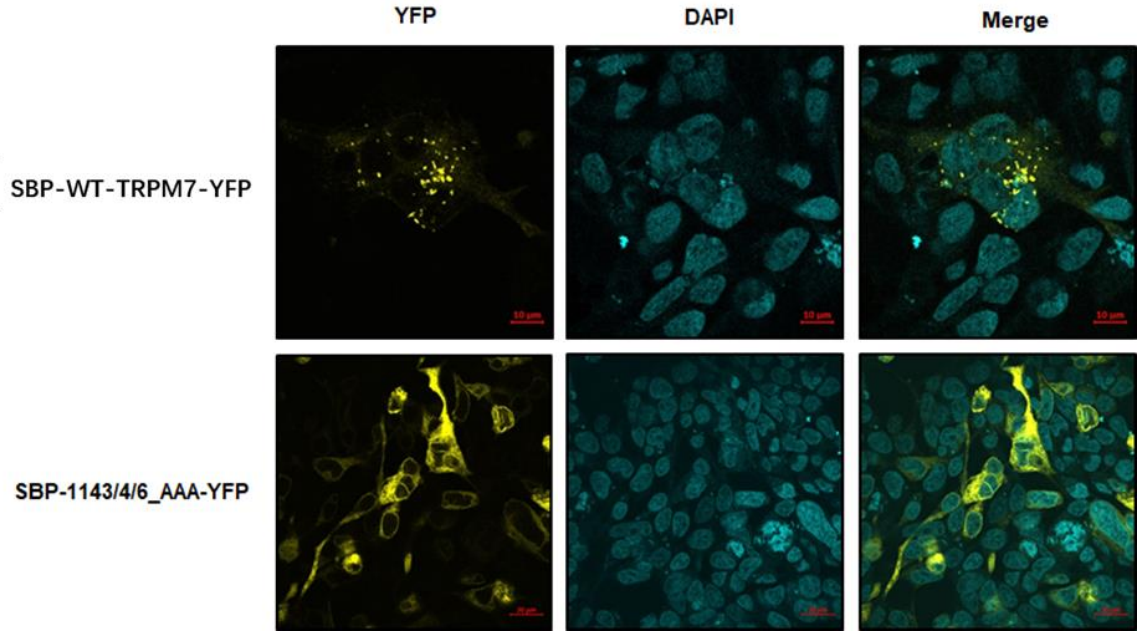

Figure 4.5 Confocal images of SBP fused wild type TRPM7-YFP and non-palmitoylated 1143/4/6_AAA-YFP localization in HEK cells
SBP was fused to the TRPM7 N terminus. SBP-WT-TRPM7-YFP localised at punctate intracellular vesicles which was same with WT-TRPM7 expressed in HEK cells. 1143/4/6_AAA mutant with SBP fusion was trapped in the ER. Scale bar: 10 µm

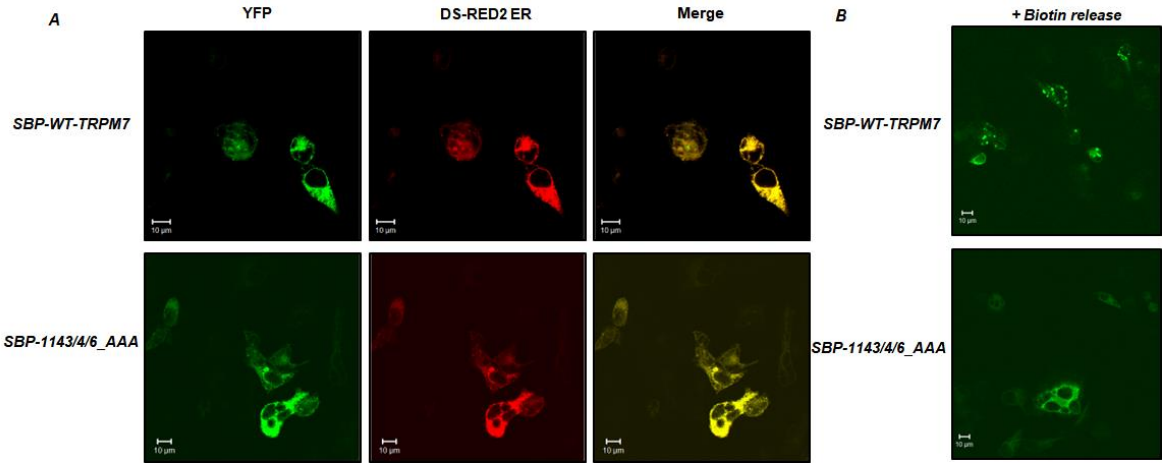

Figure 4.6 Localization of WT-TRPM7 and 1143/4/6_AAA mutant in constitutive endoplasmic reticulum (ER) retention cell line
A) Co-transfection of WT-M7/1143/4/6_AAA and DS-RED2 ER marker in ER-Hook constitutive cells. Both were colocalized with ER marker confirming they were retained in ER. The ER-hook cell line was generated with Ii for ER retention, fused with core streptavidin. Streptavidin binding protein (SBP) fused in the N-termini of WT-TRPM7 and 1143/4/6_AAA allowed them retaining in ER via interaction with core streptavidin. YFP was fused on WT-M7 and 1143/4/6_AAA plasmids. YFP excitation filter was 514nm (wavelength range 519-580nm) and DS RED2 ER excited filter was 543nm (wavelength range 575-644nm). B) SBP-WT-TRPM7-YFP but not SBP-1143/4/6_AAA-YFP were released from ER by addition of biotin. Biotin concentration was 40µM and treatment duration was 1hour. Scale bar: 10 µm

4.4.4 RUSH system of TRPM7 in Golgi Hook cell line (Constitutive)

In a related series of experiments, we investigated the behaviour of SBP-WT-TRPM7-YFP and SBP-1143/4/6_AAA-YFP transiently transfected in the engineered Golgi-hook (streptavidin-Golgi 84) stably expressed 293 T-REx cells. Expression of the hook was confirmed by western blotting alongside a transiently transfected control (Figure 4.7). All generated constitutive cell lines have streptavidin- Golgi 84 expression. SBP-WT-TRPM7-YFP was arrested in the Golgi when expressed in the engineered Golgi hook stably expressing 293 T-REx cells and reached punctate vesicles after incubation with Biotin (Fig 4.8A). In contrast, SBP-1143/4/6-AAA-YFP mutant always localised in the ER whether treated with biotin or not (Figure 4.8A).

We sought to label the Golgi apparatus in cells expressing the Golgi-hook using GRASP65-mCherry marker, which was identified as a Golgi stacking factor that links adjacent Golgi cisternae (Boncompain et al., 2012). Overexpression of GRASP65-mCherry disrupted the Golgi-hook efficiency (Zhang and Seemann, 2021) and TRPM7 failed to traffic to vesicles after treatment with biotin (Figure

4.8B). The dynamic and unique structure of Golgi critically depends on its structural proteins, which can be categorized into two major protein families, GRASPs and Golgins (Ramirez and Lowe, 2009). On one hand, Golgins such as GM130, Glogin-97, Golgin-84, and Golgin-45 are the long rod-like coiled-coil proteins that act as vesicles tethers at distinct cisternae (Gillingham and Munro, 2016). On the other hand, GRASPs, composed of GRASP55 and GRASP65, are firstly identified Golgi peripheral protein that linked adjacent Golgi cisternae by forming mitotically regulated trans-oligomers (Tang et al., 2010). Notably, members of GRASP and Golgin families normally function as subcomplexes with each other. For example, the second PSD95-DlgA-zo-1 (PDZ) domain in N-termini of GRASP65 interacts with GM130, which maintain the integrity of Golgi ribbon and function in membrane trafficking (D'Angelo et al., 2009, Zhang and Seemann, 2021). Golgin-84 is a membrane-anchored Golgin which comprehensively distributed throughout Golgi stack with an increasing gradient towards the trans-side (Satoh et al., 2003). Expression of Golgin-84 stabilized trans-cisternae stacking, which lack the GRASP proteins implicated in cis/medial-stacking (Satoh et al., 2003). Meanwhile, non-regulated GRASP65 extends the cell cycle by delaying mitotic entry via inhibition of Golgi fragmentation. The underlying reason GRASP65-mCherry disrupted the behaviour of the hook in the streptavidin-Golgi-84 stable cell line is unclear. However, when GRASP65 was not expressed (Zhang and Seemann, 2021), the constitutive streptavidin Golgi-hook stably expressing 293 T-REx cells arrested/released WT-TRPM7 normally.

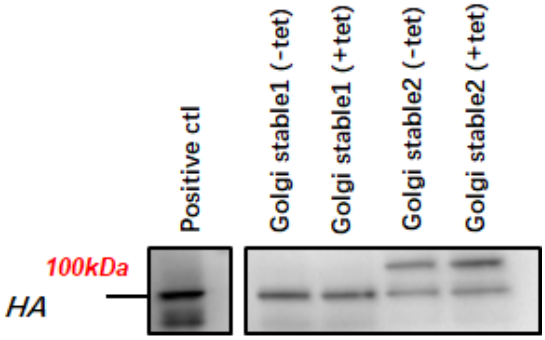

Figure 4.7 Golgi-Hook stable cells expression test.
Over-expressing HA tagged Golgi-hook gene (streptavidin-Golgi 84) in HEK cells by transiently transfection serves as the positive control. Two generated Golgi-hook stable cells (1: medium ratio, 2: low ratio) were tested whether in presence of tetracycline or not. All stable cells have Golgi-hook gene expression, but we chose medium ratio one for following experiments since the hook protein was expressed with greater efficiency. HA tag was encoded in the streptavidin-Golgi 84 and the protein size around 100kDa.

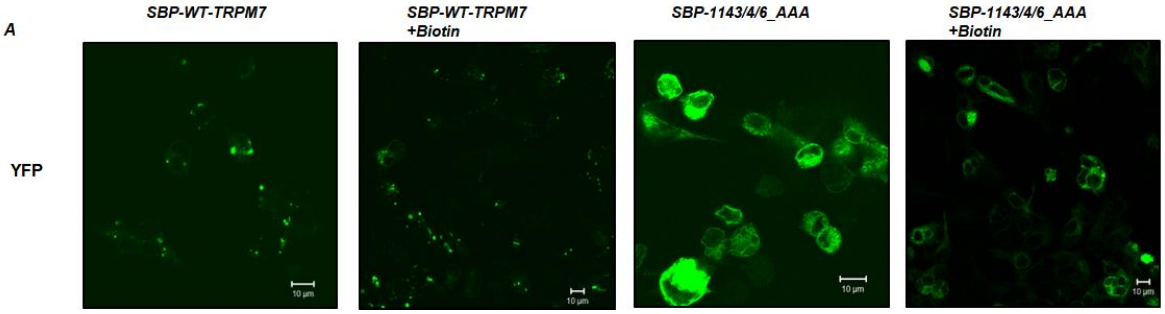
A
SBP-WT-TRPM7
SBP-WT-TRPM7 +Biotin
SBP-1143/4/6_AAA
SBP-1143/4/6_AAA +Biotin
YFP

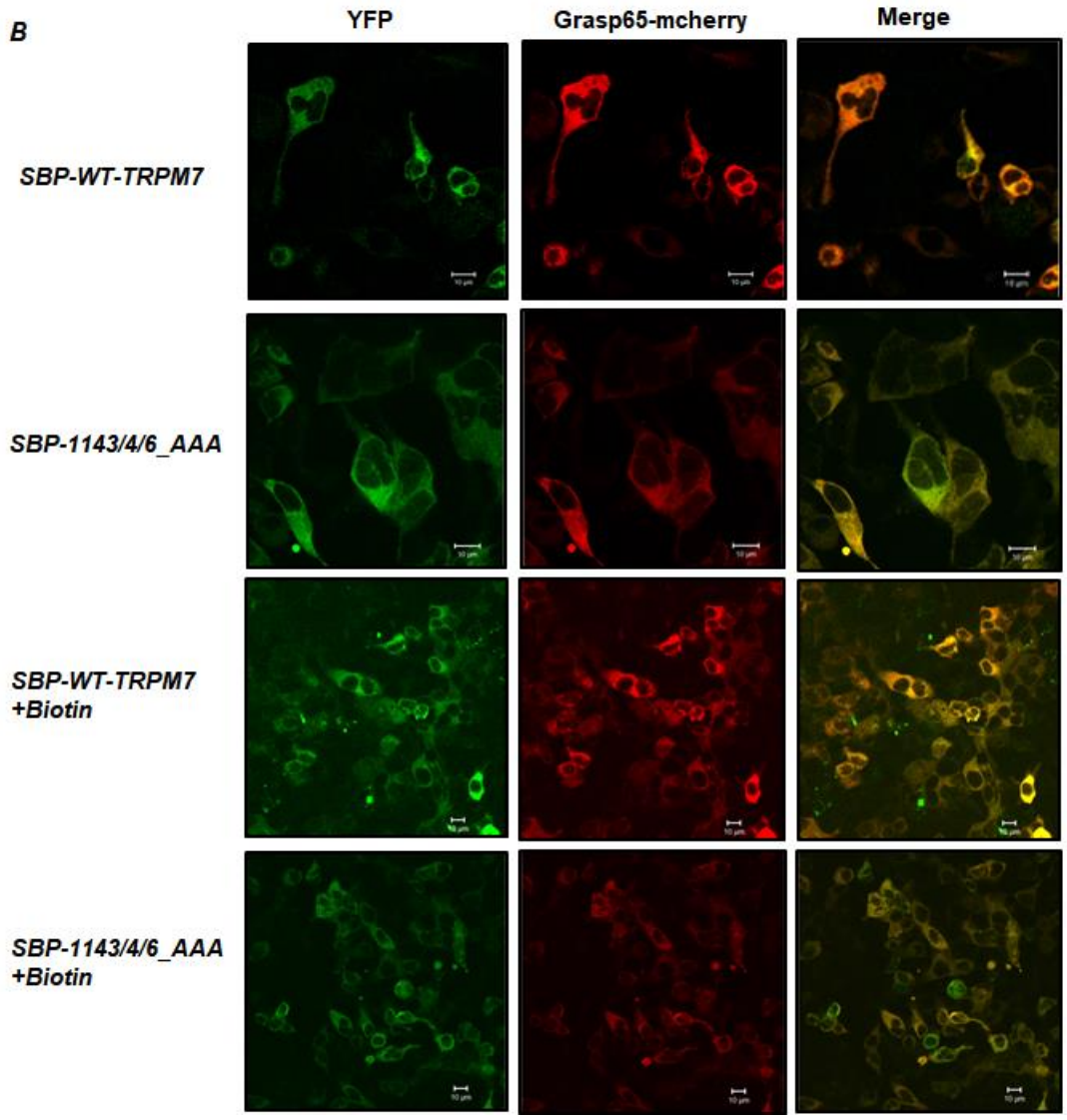
B
YFP
Grasp65-mcherry
Merge
SBP-WT-TRPM7
SBP-1143/4/6_AAA
SBP-WT-TRPM7 +Biotin
SBP-1143/4/6_AAA +Biotin

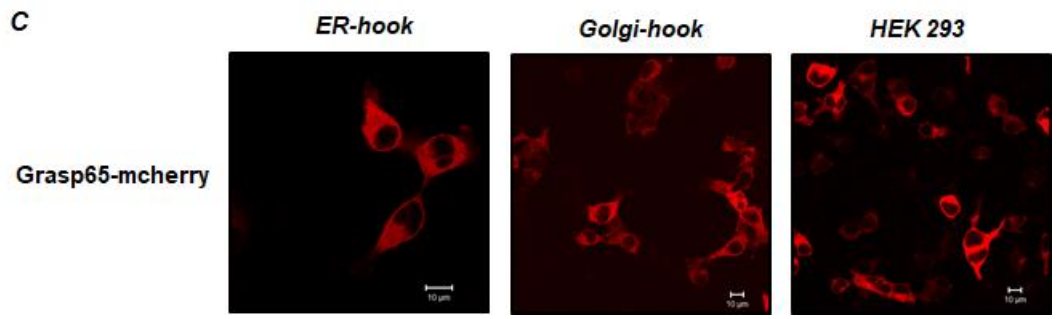
C
ER-hook
Golgi-hook
HEK 293
Grasp65-mcherry

Figure 4.8 Localization of WT-TRPM7 and 1143/4/6_AAA mutant in constitutive Golgi retention cell line.
A) Confocal images of WT-TRPM7 and 1143/4/6_AAA mutant transfected in Golgi-Hook cells. The hook cells was used with Golgin-84 for Golgi retention fused to core streptavidin. WT-TRPM7 and its 1143/4/6_AAA mutant were fused with strepatavidin binding protein (SBP) in their N-termini, as well as YFP at C-termini. The interaction between Streptavidin and SBP functions as golgi retention system for WT-TRPM7. TRPM7-1143/4/6_AAA, the non-palmitoylated mutant, was retained in endoplasmic reticulum (ER). B) Co-transfection of WT-TRPM7 /1143/3/6_AAA mutant and GRASP65 in Golgi-hook cells. GRASP65 (mCherry) was used as Golgi marker. The efficiency of Golgi-hook system would be disrupted when golgi-marker protein was present. Biotin (40μM) was applied for 1 hour to outcompete SBP binding to Streptavidin. 514nm laser wavelength was applied for generating peak excitation for YFP and 543nm for Grasp65-mcherry. C) Confocal images of GRASP65 (mCherry) transfected in different cell types including ER-Hook, Golgi-hook and HEK293 cells. The GRASP65 (mCherry) marker protein behavior is robust in all cell lines. Scale bar: 10 μm

4.4.5 Manipulating palmitoylation in the constitutive Golgi Line- 2-BP, PalmB

Confocal imaging demonstrated that SBP-WT-TRPM7-YFP was arrested in Golgi then released to punctate vesicles by biotin addition in Golgi-Hook (streptavidin-Golgi-84) stably expressed 293 T-REx cells (Figure 4.7A). Therefore, we manipulated palmitoylation of SBP-WT-TRPM7 confined in the Golgi by treating cells with the broad-spectrum zDHHC-PAT inhibitor 2-bromopalmitate (2-BP) and the broad-spectrum thioesterase inhibitor palmostatin B (PalmB). 2-BP is a non-metabolizable palmitate analog that binds to palmitoyl acyltransferases enzymes which blocks palmitate incorporation onto proteins (Alonso et al., 2012). And palmostatin B is a broad-spectrum cell-permeable inhibitor of numerous thioesterase enzymes (ATP1). TRPM7 palmitoylation was reduced by 2-BP but was not enhanced with palmostatin B after 4 hours treatment (Figure 4.9A). This suggests that TRPM7 is depalmitoylated by a thioesterase which is insensitive to palmostatin B. Mean palmitoylation relative to its expression data from three repeated Acyl-RAC experiments illustrated that TRPM7 palmitoylation was significantly decreased by around 60% following treatment with 2-BP (**$P<0.01$, $n=3$) (Figure 4.9B). Meanwhile, we also treated SBP-WT-TRPM7 transfected Golgi-Hook cells with biotin for 4hours. Interestingly palmitoylation of TRPM7 after biotin release was reduced compared to when it was held in the Golgi (*$P<0.05$, $n=3$), which implies TRPM7 is de-palmitoylated in post-Golgi compartments. Flot2, as the identified highly palmitoylated protein, was performed to evaluate the efficiency of Acyl-RAC assay (Figure 4.9C).

After manipulating TRPM7 palmitoylation in Golgi, SBP-WT-TRPM7 was released by treatment with Biotin for 2 hours followed by cell surface biotinylation assay. This assay purifies cell surface protein via membrane-impermeable biotinylation

reagents (details in 2.8.2). Representative western-blot illustrated that less TRPM7 was delivered to the surface membrane in cells pre-treated with 2-BP before it was released from the Golgi (Figure 4.10A). Mean data also disclosed that inhibition of TRPM7 palmitoylation with 2-BP was significantly reduced its abundance in surface membrane (*P<0.05, n=3) but palmostatin B treatment did not change TRPM7 enrichment in cell surface (n=3). Glyceraldehyde-3-phosphate dehydrogenase (GAPDH) mainly localise cytoplasm fractions (Figure 4.10A). Additionally, Na pump was used as standard for estimating the efficiency of cell surface biotinylating assay due to its evenly disturbing in cell surface membrane and intracellular compartments (Figure 4.10C)

In conclusion, TRPM7 palmitoylation was significantly reduced by the broad-spectrum zDHHC-PAT inhibitor 2-bromopalmitate (2-BP) which subsequently led to reduced delivery of TRPM7 to the cell surface membrane. TRPM7 is de-palmitoylated after leaving the Golgi, but the de-palmitoylating thioesterase is insensitive to palmostatin B. These experiments suggest that palmitoylation in the Golgi determines whether TRPM7 is sorted to intracellular vesicles or the cell surface membrane.

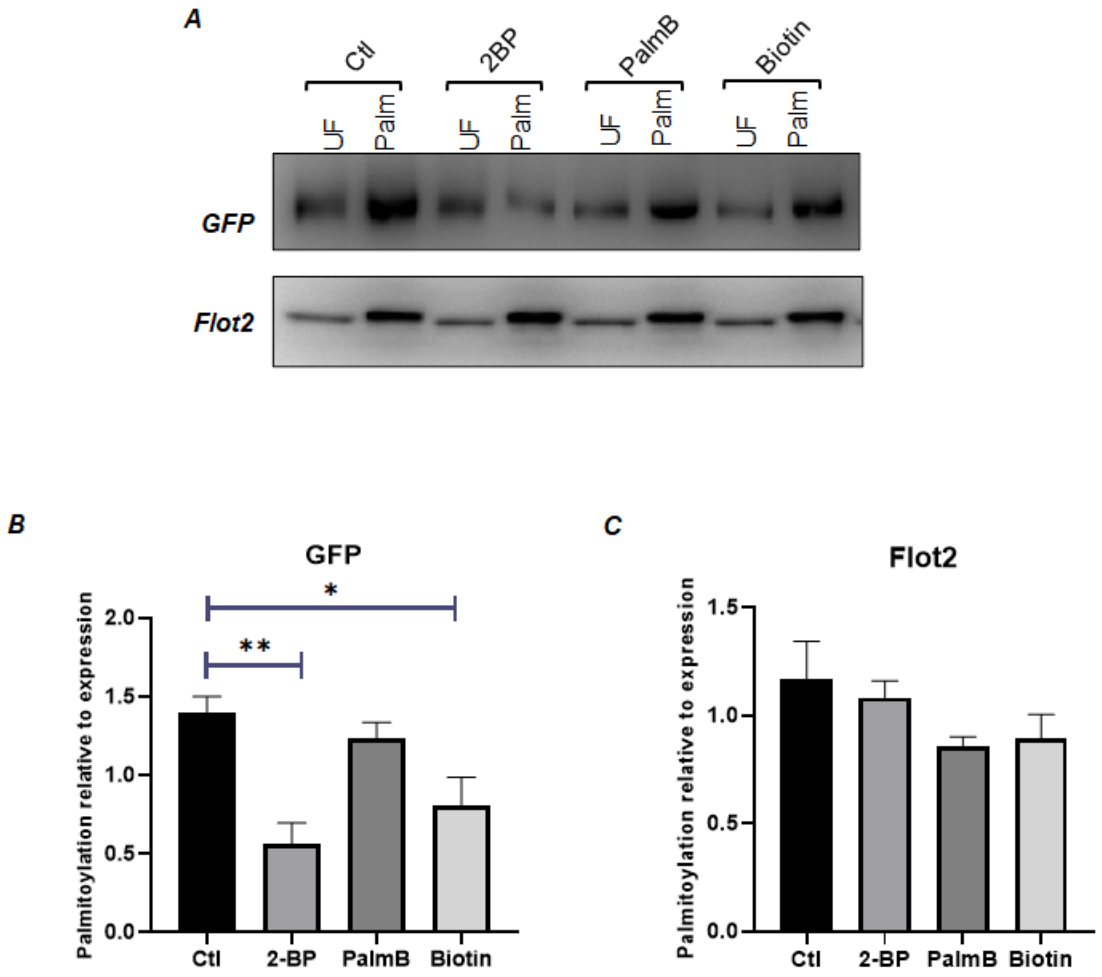

Figure 4.9 Manipulation of WT-TRPM7 palmitoylation in constitutive Golgi-Hook cell line. A) Representative western-blot of manipulating palmitoylation of WT-TRPM7 when it was transfected in Golgi-hook cells. SBP was fused on N-termini of WT-TRPM7 as well as YFP fused with C-termini. 2-bromopalmitate (2-BP) was used as palmitoylation inhibitor and Palmostatin B was used as a cell membrane permeable acyl protein thioesterase inhibitor, with both incubated for 4 hours. 2-BP=100μM; PalmB=100μM; biotin=40μM. Flot2, as a standard for evaluating the efficiency of Acyl-Rac assay. *B)* Summarizing of quantification of western-blots of manipulating WT-TRPM7 palmitoylation in Golgi-hook constitutive cell line. 2-BP reduced palmitoylation level of WT-TRPM7 to a large extent around 60% (**P<0.01, n=3). In addition, comparing with the WT-TRPM7 group, its palmitoylation had been decreased around 42% after releasing by Biotin (*P<0.05, n=3). *C)* summarizing quantification imaging data of Flot2 in transfected Golgi-hook cells. Flot2 palmitoylation was robust among different groups (n=3).

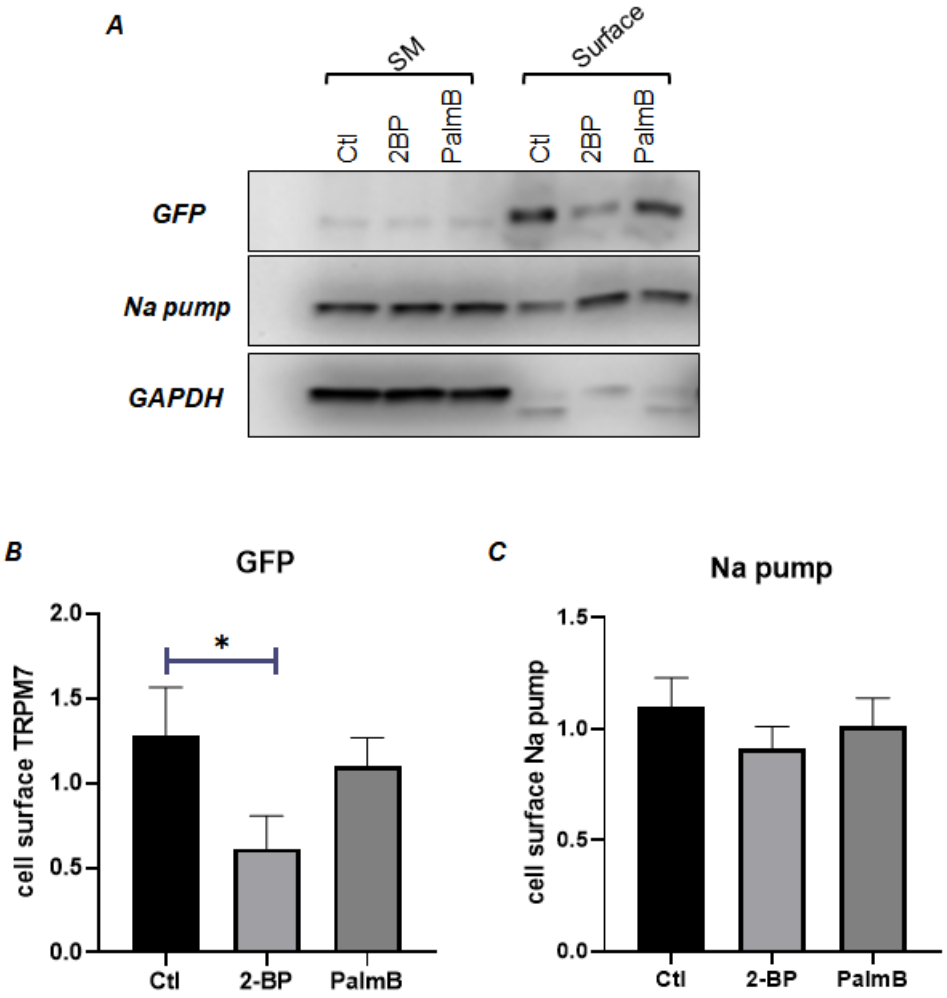

Figure 4.10 Inhibition of Palmitoylation of WT-TRPM7 in the Golgi reduces delivery of TRPM7 to the cell surface.
A) Representative western-blot of TRPM7 distribution after altering palmitoylation status in Golgi-hook cells followed by biotin release. After SBP-WT-TRPM7-YFP plasmids transfected in constitutive golgi-hook cells, 2-BP (100μM) and PalmB (100μM) were applied for incubation with 4 hours followed by Bitoin (40μM) treatment for 2 hours before cell surface biotinylation assay. YFP and SBP were fused on C- and N- terminal of WT-TRPM7. Na pump was used as a housekeeping protein localized on plasma membrane and subcellular compartments; GAPDH was served as a cytoplasmic protein. SM=starting material (whole lysate); Surface= purified cell surface protein by Streptavidin beads. B) Summarizing quantification data of several repeated cell surface biotinylation experiments which were measuring the amount of TRPM7 distribution on cell surface after manually reducing its palmitoylation. Decreasing TRPM7 palmitoylation led to less amount distributing on cell surface (*P<0.05, n=3). C) summarizing quantification of imaging data on Na pump distribution on cell surface. The amount of Na pump localized on cell surface was similar among different groups (n=3).

4.4.6 RUSH system of TRPM7 in Golgi Hook cell line (Inducible)

Similarly, we engineered an inducible Golgi Hook stably expressed cell line which derived from Flp-In 293 T-REx cells. These cells contain tetracycline repressor in the promoter of the pcDNA5/FRT/TO vector, which allows high expression of streptavidin-Golgi 84 after treatment with tetracycline. Immunofluorescence was used to detect HA tag which engineered into the hook of streptavidin-Golgi 84. From Figure 4.11A, the Golgi hook gene was only highly

expressed after treating with tetracycline for with 24 hours incubation, for which detected by two different wavelength secondary antibodies for HA tag (546nm and 633nm).

Meanwhile, SBP-WT-TRPM7 was retained in the Golgi effectively in Golgi hook stably expressing 293 T-REx cell line treated with tetracycline incubation and released from the Golgi after biotin treatment for 2 hours (Figure 4.11B). In contrast, SBP-WT-TRPM7 localisation in Golgi Hook cells without tetracycline incubation was as normal as it transfected in HEK cells (Figure 4.11B). In addition, SBP-TRPM7-1143/4/6_AAA remained confined to the ER following induction of hook expression (Figure 4.11B). The co-localization of HA tag in Golgi and YFP tag in SBP-WT-TRPM7 generated from immunofluorescence evaluated the efficiency of retention using Golgi-hook system.

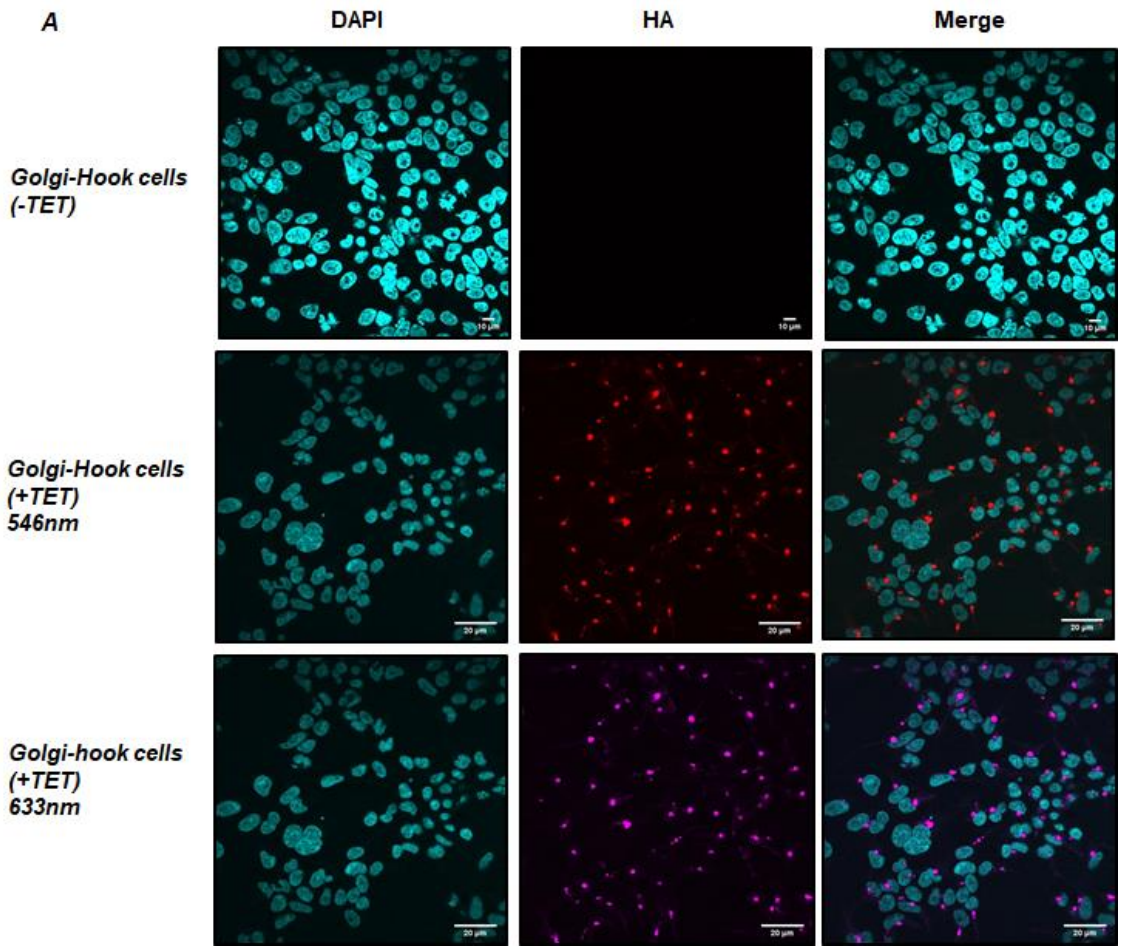
A
DAPI
HA
Merge
Golgi-Hook cells (-TET)
Golgi-Hook cells (+TET) 546nm
Golgi-hook cells (+TET) 633nm

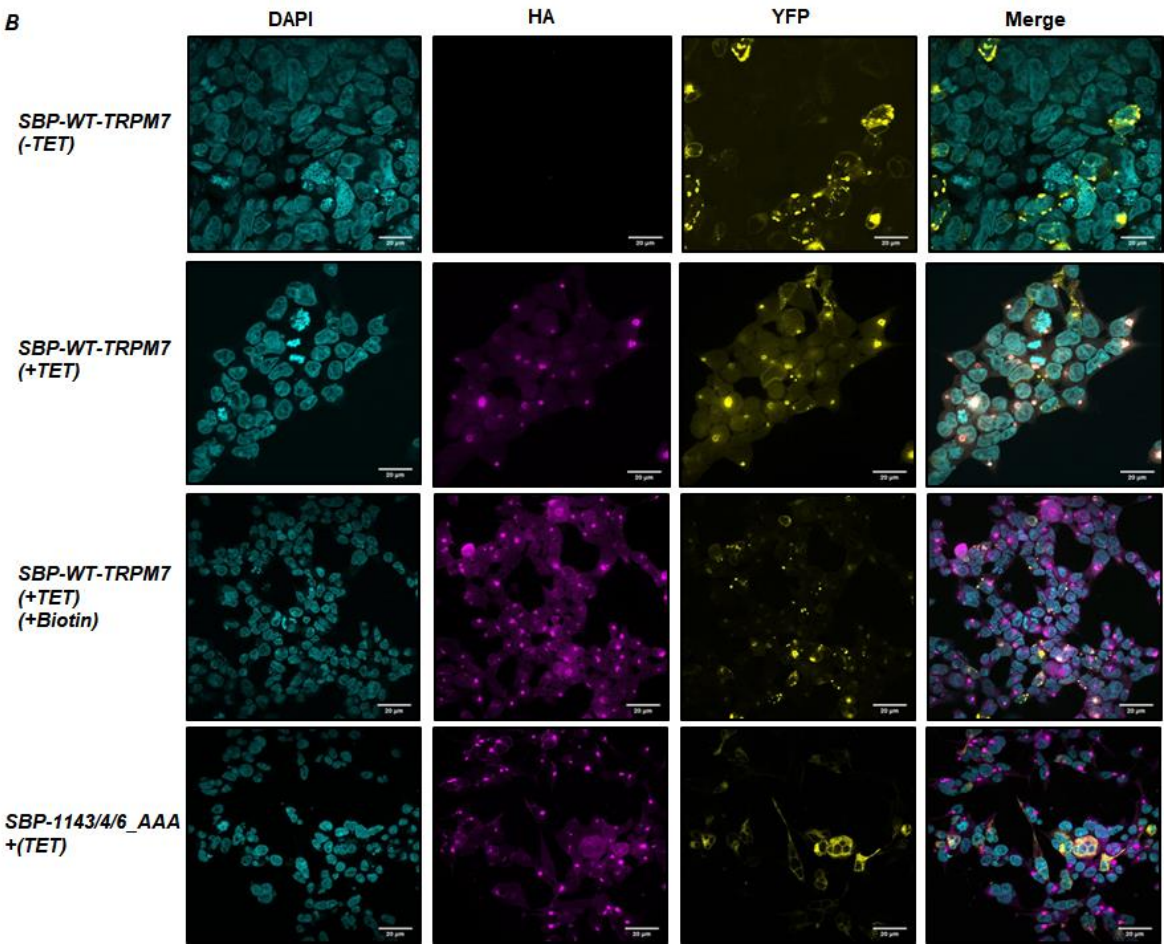
B
DAPI
HA
YFP
Merge
SBP-WT-TRPM7 (-TET)
SBP-WT-TRPM7 (+TET)
SBP-WT-TRPM7 (+TET) (+Biotin)
SBP-1143/4/6_AAA +(TET)

Figure 4.11 Immunofluorescence on inducible Golgi hook cells to detect WT-TRPM7 and non-palmitoylated mutant distribution.
A) HA-Tag staining in Golgi-Hook inducible cells. The hook cells line was generated with FRT/TO parental cells which used Golgi-84 assembled into pcDNA5-FRT/TO vector for Golgi retention. Core streptavidin and HA Tag were coded in FRT-TO-Golgi-84 plasmid. Tetracycline was used as antibiotics to allow the gene expression. The cells were stained with immunofluorescence which primary anti-HA antibody was used 1:200 and secondary antibody (1:400) was fluorescent anti-rat (546nm/636nm). Both wavelengths worked well for evaluating the efficiency of Golgi-hook cell line. Scale bar: 10 µm and 20 µm B) Fluorescent confocal images of transfected WT-TRPM7 and non-palmitoylated 1143/4/6_AAA mutant in inducible Golgi-gook cells. Streptavidin binding protein (SBP) was fused on N-termini of both plasmids and YFP tagged at C-termini. TRPM7 was retained in Golgi apparatus via interaction between Core streptavidin and SBP. Meanwhile, it was released from streptavidin by addition of Biotin (40µM). Tetracycline (10µMg/ml) was added every 24 hours to maintain Golgi-84 retention gene expression. Biotin treatment duration was 2 hours. Non-palmitoylated 1143/4/6_AAA mutant was always confined to the endoplasmic reticulum (ER). Excited filter for YFP was 514nm and for HA was 543/633nm. Scale bar: 20 µm

4.4.7 Manipulating palmitoylation in the inducible Golgi Line- 2-BP, PalmB

Similarly with manipulating TRPM7 palmitoylation in constitutive Golgi Hook cells, we controlled its palmitoylation when confined in the Golgi in tetracycline inducible Golgi hook cells. SBP-WT-TRPM7 palmitoylation was reduced following treatment with zDHHC-PAT inhibitor 2-bromopalmitate (2-BP) (Figure 4.12A) but palmostatin B was without effect after 4 hours treatment. Mean data of seven repeated Acyl-Rac experiments illustrated that TRPM7 palmitoylation had been significantly inhibited by 2-BP (*$P<0.05$, $n=7$) (Figure 4.12B). Palmitoylation of Biotin released WT-TRPM7 was not significantly different compared to TRPM7 held in the Golgi (Figure 4.12A, B).

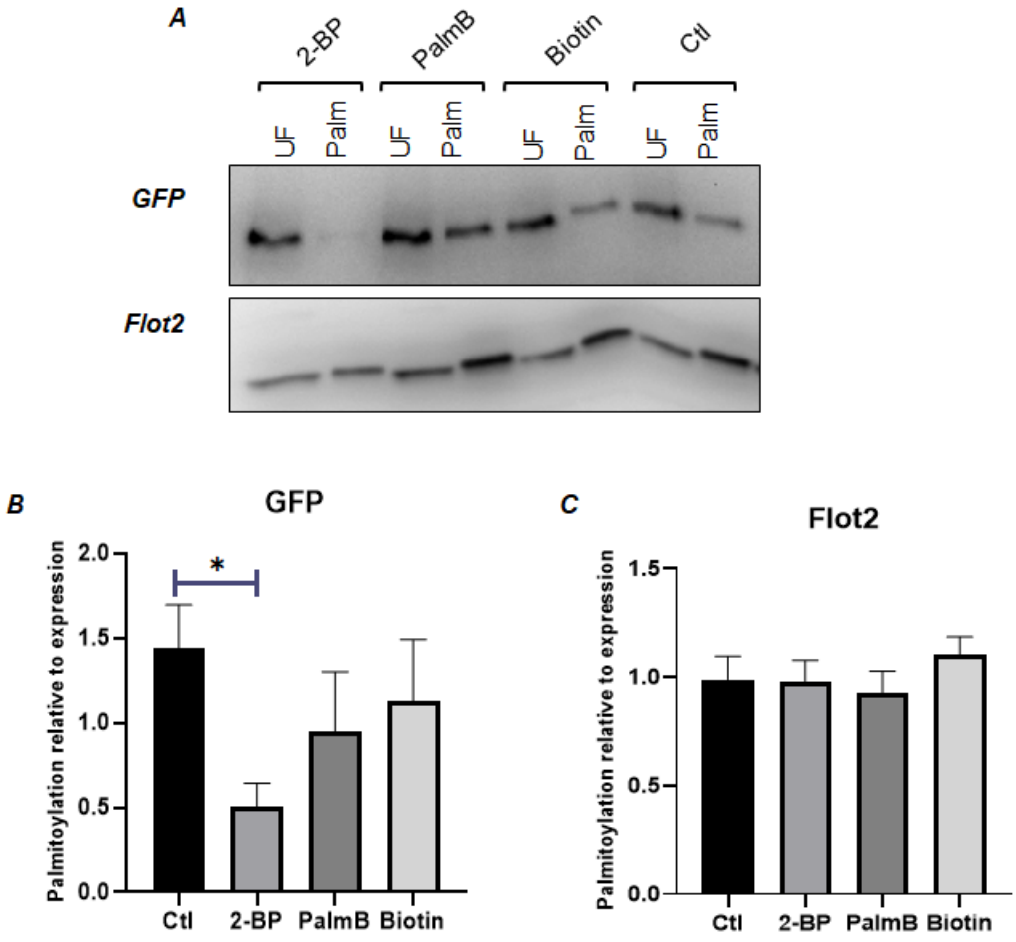

Figure 4.12 Manipulation WT-TRPM7 Palmitoylation in inducible Golgi-Hook cell line.
A) Representative western-blot of palmitoylation of WT-TRPM7 transfected in Golgi-hook inducible cells. SBP was fused on WT-TRPM7 N-termini and YFP tagged at its C-termini. 2-bromopalmitate (2-BP) was used as palmitoylation inhibitor and Palmostatin B (Broad-spectrum thioesterase inhibitor) was used as membrane-permeable inhibitor of acyl protein thioesterase, which were both incubated for 4hrs before Acyl-RAC.2-BP=100μM; PalmB=100μM; Biotin=40μM. Tetracycline (10μg/ml) was added every 24 hours to maintain expression of Golgi retention hook. Flot2, as a standard for evaluating the efficiency of Acyl-Rac assay B) Summarizing quantification of imaging data about manipulating palmitoylation of WT-TRPM7 in Golgi-hook inducible cells. Comparing with WT-TRPM7, 2-BP treatment decreased its palmitoylation approximately 65% (*P<0.05, n=7). PalmB treatment did not increase WT-TRPM7 palmitoylation. C) summarizing imaging data of Flot2 in SBP-WT-TRPM7-YFP transfected inducible Golgi-hook cells. Palmitoylation of Flot2 were broadly similar among different groups (n=7).

To assess the impact of palmitoylation on TRPM7 localization, SBP-WT-TRPM7 was released from the Golgi by treating with biotin after incubation with 2-BP or PalmB inhibitor for 4 hours. Cell surface protein were purified by membrane impermeable amine reactive biotinylation reagent sulfo-NHS-SS-biotin. Approximately 40% less TRPM7 was delivered to surface membrane after pre-treating with 2-BP (Figure 4.13B). Surprisingly there was no significant difference in the amount of TRPM7 which localised on cell surface between control and 2-BP treated groups (Figure 4.13B). These experiments include blank group of cells which transfected with SBP-TRPM7, treated with tetracycline, but

not treated with drugs to manipulate TRPM7 palmitoylation and not released using biotin. The amount of TRPM7 localised in the surface membrane was similar between this blank group and after biotin release (Control group), suggesting the behaviour of inducible Golgi-hook cells might be interrupted by multiple factors. Na pump distributed on cell surface were similar among all groups demonstrating that the reliable quality of cell surface biotinylation assay (n=5-6).

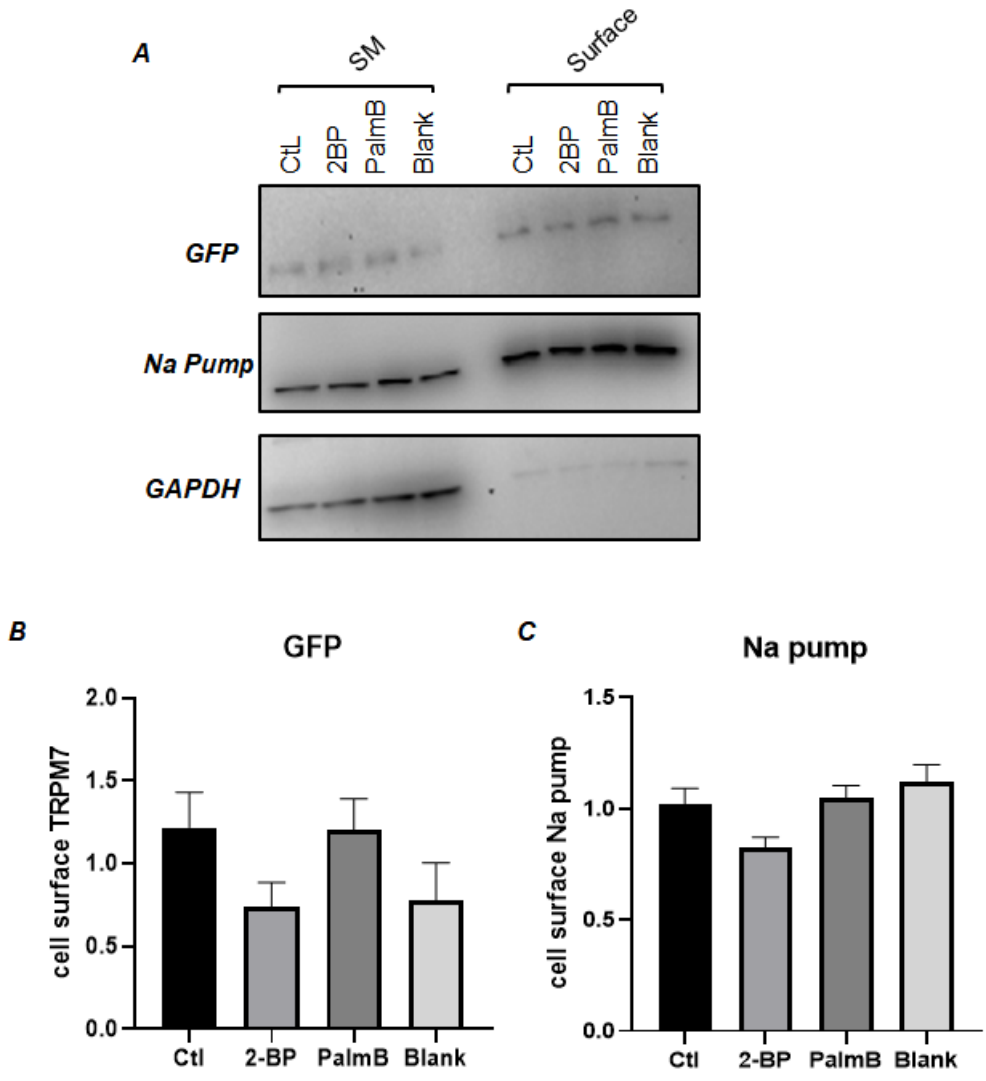

Figure 4.13 Inhibition of Palmitoylation of WT-TRPM7 resulting less amount of TRPM7 distribution on cell surface.
A) Representative western-blot of TRPM7 distribution after palmitoylation changes in Golgi-hook cells followed by biotin release. After SBP-WT-TRPM7-YFP plasmids were transfected into inducible golgi-hook cells, 2-BP (100μM) and PalmB (100μM) were applied for incubation with 4 hours followed by Biotin (40μM) treatment for 2 hours before cell surface biotinylation assay. YFP and SBP were fused on C- and N- terminal of WT-TRPM7. Na pump was used as a housekeeping protein localized on plasma membrane and subcellular compartments; GAPDH was served as a cytoplasmic protein. SM=starting material (whole lysate); Surface= enriched cell surface protein by Streptavidin beads; Control (ctl), 2-BP and PalmB treated groups were treated with biotin. 'Blank' refers to no biotin release. B) Summarizing quantification data of several repeated cell surface

biotinylating experiments which were measuring the amount of TRPM7 distribution on cell surface after manually reducing its palmitoylation. There were no significant differences detected between experimental groups (n=5-7). C) Summarizing quantification of imaging data of Na pump distribution on cell surface. The amount of Na pump localized on cell surface are roughly similar among different groups (n=5-6).

4.4.8 TRPM7-M5 and TRPM7-M2 chimaeras behaviour in transfected cells

In chapter 3 the comparison of palmitoylation sites conservation among the TRPM7 family members found that TRPM2 and TRPM5 are the only TRPM family members lacking potential palmitoylated cysteines. The TRPM7-M5-YFP and TRPM7-M2-YFP chimaeras are non-palmitoylated when expressed in HEK cells (details in section 3.4.8). Notably, TRPM2 and TRPM7 are established to operate at the cell surface membrane (Lange et al., 2009, Hofmann et al., 2003), suggesting that some TRPM family members can traverse the secretory pathway without being palmitoylated. Confocal images of TRPM7-M2-YFP and TRPM7-M5-YFP chimaeras revealed that their gross subcellular localisations were not different from WT-TRPM7 (Figure 4.14A). This suggested we can use the non-palmitoylated chimaeras to overcome the restriction of TRPM7-1143/4/6_AAA trapped in the ER. We assessed the abundance of TRPM7-M2 and TRPM7-M5 on the cell surface membrane using the same membrane-impermeable reagent (sulfo-NHS-SS-biotin). Representative western-blot showed that significantly less non-palmitoylated chimaeric TRPM7 was delivered to the cell surface compared to WT-TRPM7 (Figure 4.14B). Multiple comparison with one-way ANOVA illustrated that dramatic decrease of non-palmitoylated TRPM7-M2 and TRPM7-M5 distribution on surface membrane (****$P<0.0001$, n=6) (Figure 4.14C).

TRPM7-M2 and TRPM7-M5 chimaeras were respectively replacing the “CCVC” palmitoylated region with “KRIV” (TRPM2) or “KQVF” (TRPM5). Both contains positively charged and hydrophobic amino acids which might substitute for palmitoylation and facilitate ER exit. Overall, we concluded that palmitoylation is one principal determinants of the fate of TRPM7 in cells. Inhibiting TRPM7 palmitoylation would induce less abundance on cell surface membrane.

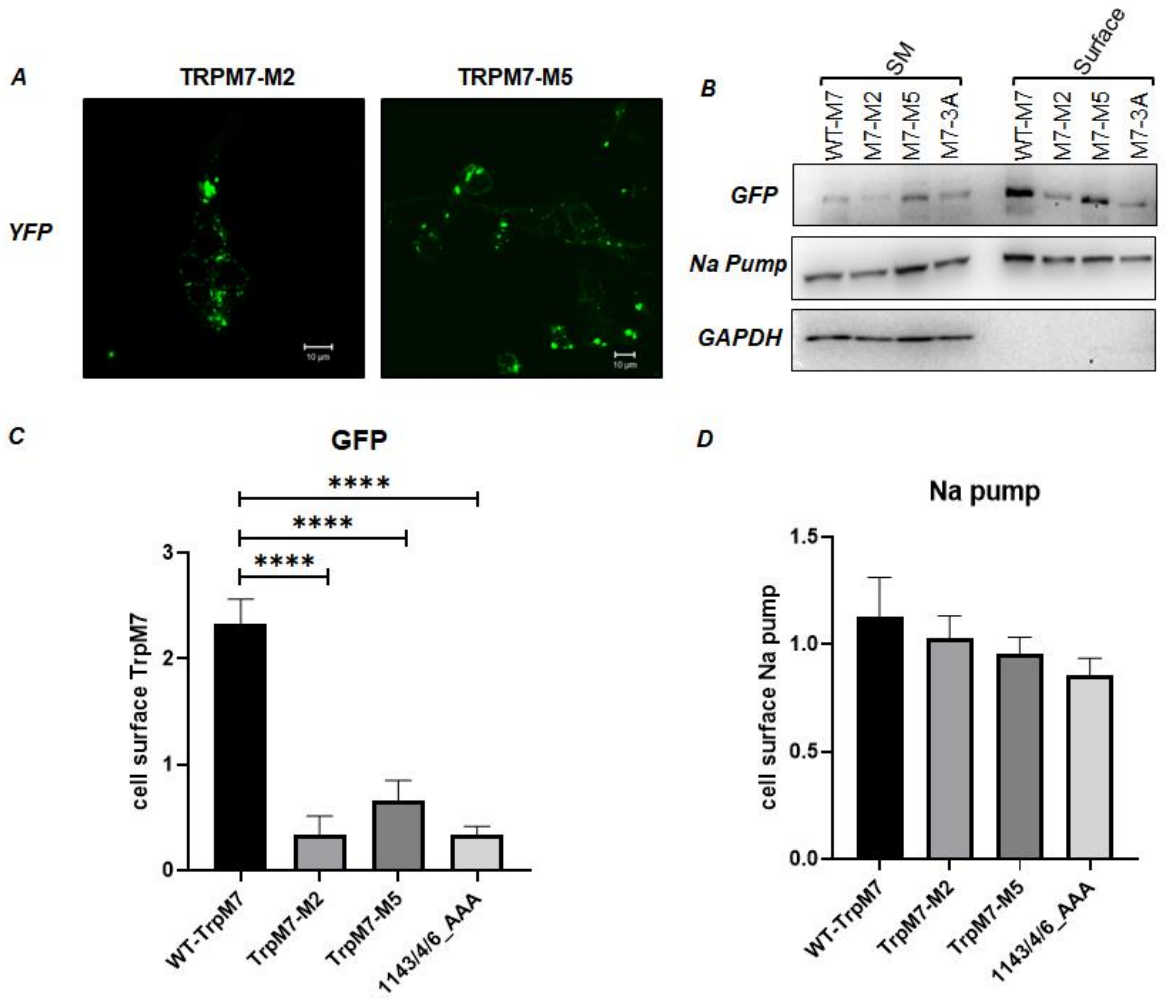

Figure 4.14 TRPM7-M2 and TRPM7-M5 behaviour in transiently transfected HEK293 cells. A) Confocal images of TRPM7-M2 and TRPM7-M5 transfected in HEK293 cells. YFP was fused on both plasmids. Non-palmitoylated TRPM7-M2 and TRPM7-M5 were not trapped in endoplasmic reticulum (ER). Scale bar: 10 µm B) representative western-blot of cell surface biotinylation of WT-TRPM7, TRPM7-M2, TRPM7-M5 and 1143/4/6_AAA transfected in HEK293 cells. Comparing with WT-TRPM7, non-palmitoylated mutants have less amount abundant on cell surface. Na pump was used as a housekeeping protein localized on plasma membrane and subcellular compartments; GAPDH was served as a cytoplasmic protein. SM=starting material (unfractionated lysate); Surface= enriched cell surface protein by streptavidin beads. C) Quantification of the amount of TRPM7 distributed on cell surface among WT-TRPM7 and its non-palmitoylated mutants, TRPM7-M2, TRPM7-M5 and 1143/4/6_AAA. Abundance of cell surface TRPM7 was dramatically decreased when inhibiting TRPM7 palmitoylation (****P<0.001, n=4-6). D) Summarizing images data of cell surface Na pump distribution in WT-TRPM7, TRPM7-M2, TRPM7-M5 and 1143/4/6_AAA mutants. Na pump displayed as a standard for cell surface protein which is equally distributed among those groups (n=3-4).

4.4.9 TRPM7-M5 and TRPM7-M2 behaviour in stable cells-biochemistry

To be convenient for further research, we generated cell lines stably expressing inducible wild type TRPM7, TRPM7-M2 and TRPM7-M5 derived from 293 T-REx cells. These cells are tetracycline inducible because of existence of tetracycline-sensitive transcriptional repressor at pcDN5/FRT/TO vector. TRPM7 were not

expressed without tetracycline incubation (Figure 4.15A). There was no gross difference in the subcellular distribution of WT and chimeric TRP-M7 assessed using confocal microscopy (Abiria et al., 2017a) (Figure 4.15B).

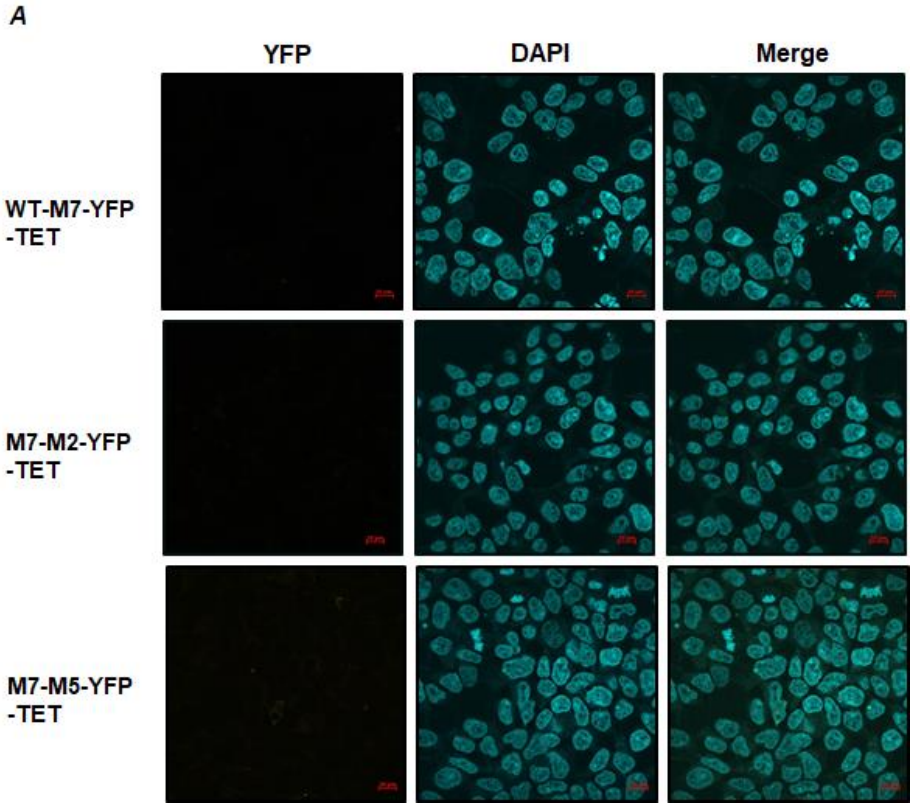

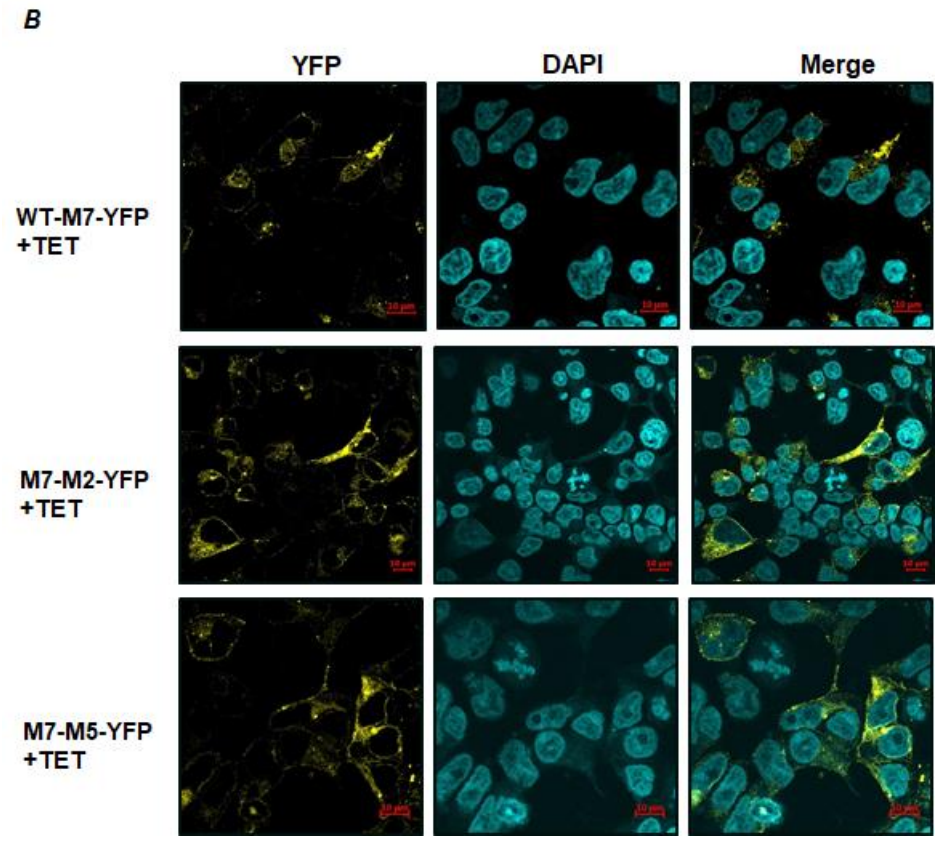

Figure 4.15 Confocal images of TRPM7 localization among WT-TRPM7, TRPM7-M2, and TRPM7-M5 stable cells.
All stable cells were generated with FT parental cells and the stably transfected gene contained tetracycline in vectors. Tetracycline (10µg/ml) was served every 24 hours as selective antibiotics allowing gene expression. A) Cells behavior without addition of tetracycline. YFP (wavelength 519nm-580nm) had not been detected in all cell lines. Scale bar: 10 µm B) Localization of non-palmitoylated TRPM7-M2 and TRPM7-M5 were similar with WT-TRPM7. YFP fused with C-termini of all plasmids and its excited filter was 514nm. Scale bar: 10 µm

Acyl-Rac assay was used to measure palmitoylation meanwhile cell surface biotinylation assay was used to evaluate TRPM7 distribution between two pools among WT-TRPM7, TRPM7-M2-YFP and TRPM7-M5-YFP inducible cell lines. Tetracycline incubation was in 2 different durations, 24 hours and 48 hours separately for each cell line, to permit adequate expression of TRPM7. On one hand, representative western-blot of Acyl-Rac demonstrates that WT-TRPM7 was highly palmitoylation however TRPM7-M2 and TRPM7-M5 were essentially non-palmitoylated (Figure 4.16A). One-way ANOVA followed by Dunnett's post-hoc multiple comparison test reveals significantly reduced palmitoylation of TRPM7-M2 and TRPM7-M5 compared to WT-TRPM7 in these stable cells (****P<0.0001, n=5) (Figure 4.16B). On the other hand, representative western-blot, and mean data shows that the abundance of TRPM7 on membrane surface in TRPM7-M2-YFP and TRPM7-M5-YFP stable cells was significantly less than in cells expressing WT-TRPM7-YFP (****P<0.0001, n=7) (Figure 4.16E). These results suggests that

palmitoylation controls TRPM7 distribution between the two distinct cellular populations. Specifically, decreasing palmitoylation reduced TRPM7's abundance in cell surface membrane.

TRPM7 has been identified to play important role in Mg homeostasis. It acts as a cellular Mg uptake mechanism and that Mg-dependent channel inhibition is modulated via functional coupling between the channel gating and the kinase domain(Ryazanova et al., 2010, Schmitz et al., 2003).In neurons, TRPM7-mediated Ca influx causes cellular Ca overloaded and cell death during anoxia (Aarts et al., 2003). TRPM7 also localizes to intracellular vesicles which have been proposed as an intracellular zinc reservoir, which release zinc from vesicle when stimulated by reactive oxygen species (ROS)(Linder and Deschenes, 2007). Since TRPM7 ion channel activity controls conduction of multiple ions, we speculate that by controlling its distribution between surface membrane intracellular vesicles, TRPM7 palmitoylation may influence cellular ion concentrations in multiple scenarios.

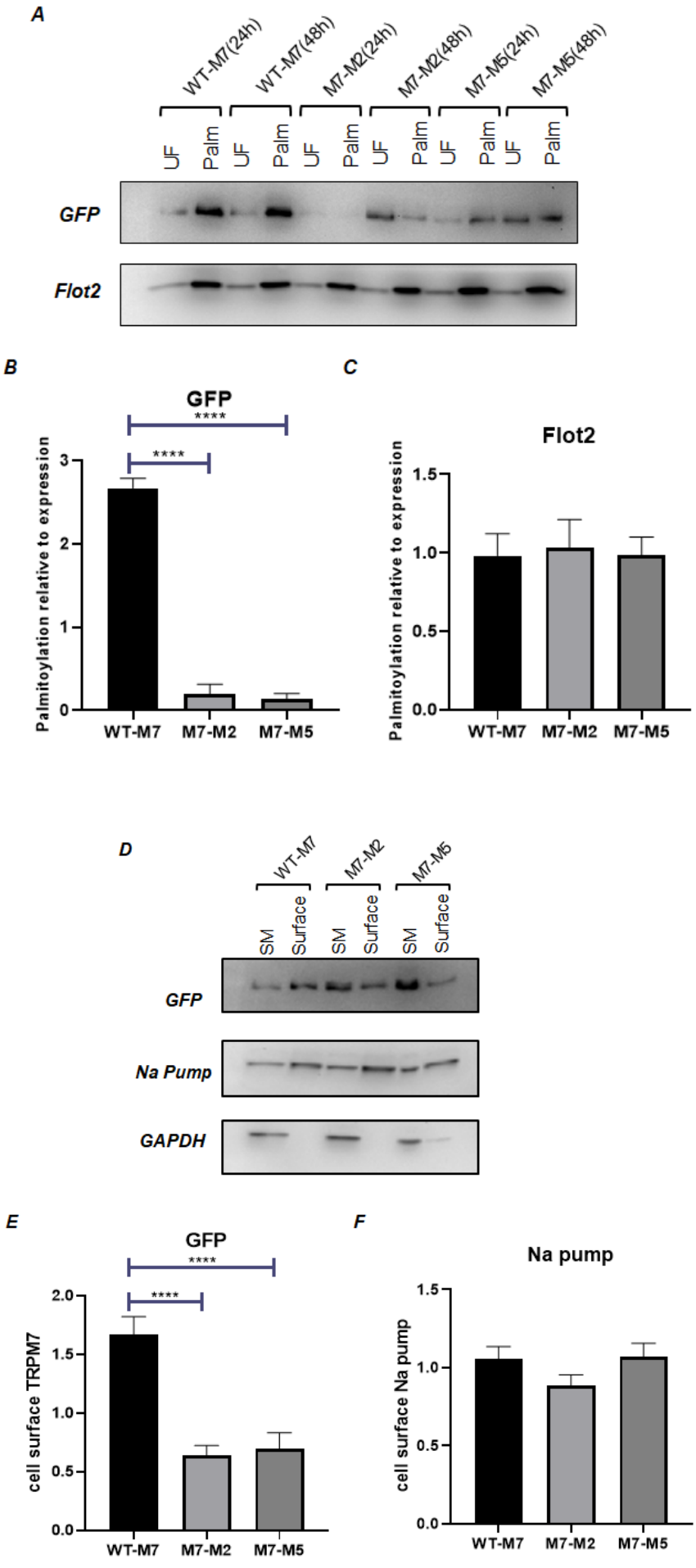
A
WT-M7(24h)
WT-M7(48h)
M7-M2(24h)
M7-M2(48h)
M7-M5(24h)
M7-M5(48h)
UF
Palm
GFP
Flot2
B
GFP
****
****
Palmitoylation relative to expression
WT-M7
M7-M2
M7-M5
C
Flot2
Palmitoylation relative to expression
WT-M7
M7-M2
M7-M5
D
WT-M7
M7-M2
M7-M5
SM
Surface
GFP
Na Pump
GAPDH
E
GFP
****
****
cell surface TRPM7
WT-M7
M7-M2
M7-M5
F
Na pump
cell surface Na pump
WT-M7
M7-M2
M7-M5

Figure 4.16 TRPM7-M2 and TRPM7-M5 behavior in stable cells.
A) Representative western-blot of Acyl-Rac assay to measure palmitoylation of WT-TRPM7, TRPM7-M2 and TRPM7-M5 inducible stable cells. The inducible cells were grown with 24 hours and 48 hours separately with addition of tetracycline (10µg/ml) every 24 hours. YFP was fused on C-terminus of all proteins Flot2 was used as housekeeper gene to evaluate Acyl-Rac efficiency. B, C) summarizing western-blots quantification data to make comparison of palmitoylation of TRPM7 and Flot2 among WT and mutants cell lines. TRPM7 palmitoylation level was significantly decreased in TRPM7-M2 and TRPM7-M5 inducible stable cell lines (****P<0.0001, n=5). D) Representative western-blot of cell surface biotinylation of WT-M7, TRPM7-M2 and TRPM7-M5 in stable cell lines. Na pump was used as a housekeeping protein localized on plasma membrane and subcellular compartments; GAPDH was served as a cytoplasmic protein. SM=starting material; surface=enriched cell surface protein captured by Streptavidin beads. E, F) Summarizing quantification of images data of cell surface enrichment TRPM7 and Na pump in stable cell lines. Inhibiting palmitoylation on TRPM7 would lead to less amount of TRPM7 abundant on cell surface (****P<0.0001, n=7). And there is no significant difference in Na pump distribution among WT-TRPM7, TRPM7-M2 and TRPM7-M5. All mean data was analysed by one-way ANOVA, Dunnet's post-hoc multiple comparisons test.

4.4.10 Protein interaction and gene ontology enrichment in WT-TRPM7 and TRPM7-M5 cell components

We first undertook some pilot experiments to assess the efficiency of capture of TRPM7-YFP and co-purification of plasma membrane marker proteins. Western-blotting of GFP-Trap immunoprecipitated TRPM7 revealed that Flot2 has associated with TRPM7 (Figure 4.17B). Representative western-blot and mean data show that significant less Flot2 enrichment in non-palmitoylated TRPM7-M5/TRPM7-M2 comparing with WT-TRPM7 (****P<0.0001, ****P<0.001, n=3) (Figure 4.17B, C).

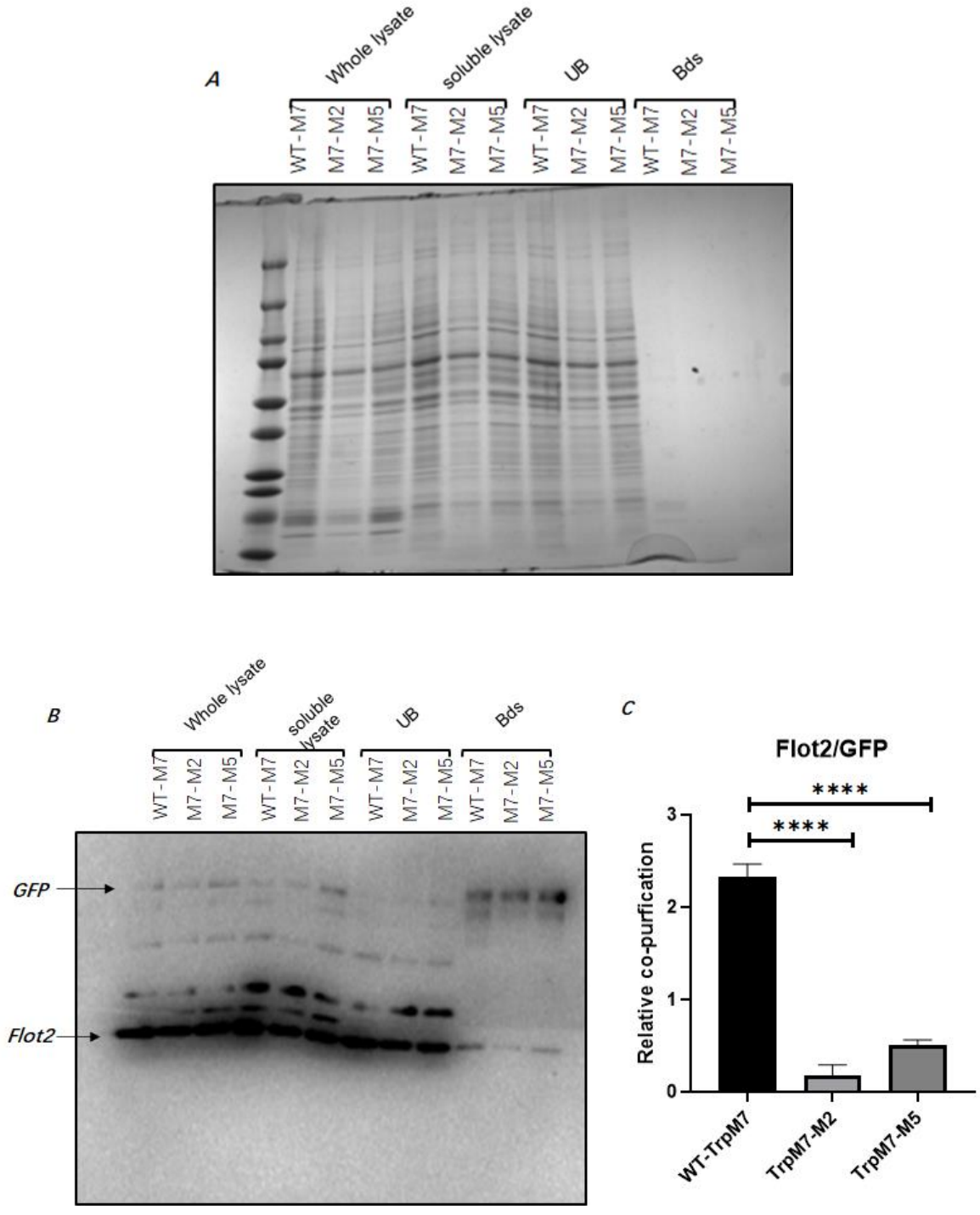

Figure 4.17 Palmitoylation controls association of TRPM7 with Flot2.
A) Coomassie blue staining polyacrylamide gel of GFP-Trap immunoprecipitated wild type TRPM7 and non-palmitoylated TRPM7-M2/ TRPM7-M5 stable cells. Tetracycline incubated for 24 hours. B) Representative western-blot of GFP-Trap immunoprecipitated TRPM7. Flot2 was less enriched in immunoprecipitation reactions from TRPM7-M2 and TRPM7-M5 expressing cells. C) Summarizing images data of Flot2 co-purification relative to TRPM7-YFP (Flot2/GFP). Flot2 abundance was significantly decreased in non-palmitoylated TRPM7 stable cells (****P<0.0001, n=3). one-way ANOVA followed by post-hoc Dunnett's multiple comparison.

In order to understand how palmitoylation impacts TRPM7 protein interactions we set out to evaluate TRPM7 protein interactions in cells expressing wild type and non-palmitoylated TRPM7. Proteomics is an effective analysis of the entire

protein complement of a cell, tissue, or organism under specific and defined conditions. The complete process of proteomics is dependent on a series of advanced technologies including protein fractionation technique which is a method to fractionate complex protein or peptides mixtures, mass spectrometry (MS) acquiring data to identify individual peptide/protein and bioinformatics to analyse and assemble MS data (Yu et al., 2010). In the early days of proteomics, protein mixtures were separated using two-dimensional polyacrylamide gel electrophoresis, however this approach has largely been superseded as instruments can measure more complex mixtures of protein (O'Farrell, 1975). Meanwhile, Mass spectrometry technology have been the most popular and efficient method to characterize trypsin-digested proteins (Henion, 1978, McLafferty, 1981). Liquid chromatography has enabled complex mixtures, which fragments mostly obtained by enzymatic digestion, to be fractionated prior to mass spectrometry (Yu et al., 2010). LC-MS could efficiently detect thousands of peptides within a few hours. In addition, bioinformatics is critical to convert the raw experimental mass spectral data into protein data according to match with specific proteome database. For our experiment, Wild type TRPM7-YFP and non-palmitoylated TRPM7-M5-YFP immunoprecipitated with GFP-Trap agarose resin (Chromotek) were fractionated via 10% polyacrylamide gels. Afterwards, Trypsin was applied to the digest gel pieces and tryptic peptides were identified using LC-MS analysis (LTQ Velos Qrbitrap). Mass spectral data was analysed comparing with Uniprot-proteome human database and CRAPome database (Abiria et al., 2017a) via MaxQuant (v1.6.5.0).

In total 1572 protein groups were identified from the immunoprecipitation reactions with GFP-Trap immunoprecipitated of WT-TRPM7-YFP and TRPM7-M5-YFP stable cells. After filtration of proteins with potential contaminants, reverse sequence, single peptide identified, etc., 1143 protein were detected by 2 unique peptides, for which peptides are not shared with another protein group [additional online data 1]. This data was filtered to remove proteins identified in HEK negative control (Abiria et al., 2017a) [additional online data 2]. These 667 proteins were designated high confidence. TRPM7 was identified with 85 peptides and 44.3% sequence coverage, which is the second topmost hit protein. The top hit was DNA-dependent protein kinase catalytic subunit (Gene name PRKDC) with 94 peptides identification, which encodes Serine/threonine-protein

kinase that acts as a molecular sensor for DNA damage. Numerous protein groups have been proven to interact with TRPM7, including our familiar phosphorylation substrate of α-kinase domain, annexin1 (gene name ANXA1) (Dorovkov and Ryazanov, 2004), and the novel characterized protein forming high-molecular-weight-multi-protein complexes with TRPM7, metal transporter protein CNNM1-4 (Kollewe et al., 2021a).

[Additional online data 1]: http://dx.doi.org/10.5525/gla.researchdata.1357

[Additional online data 2]: http://dx.doi.org/10.5525/gla.researchdata.1357

With further studies, we generated the Volcano plot showing the quantification of proteins copurified with WT or non-palmitoylated TRPM7 (Figure 4.18). This scatterplot illustrates the relationship of statistical significance (p-value) versus magnitude of protein intensity change (fold change shown with Log2). The protein that was most enriched with TRPM7-M5 in comparison to WT was NGLY1 with 535-fold enriched. This encodes Peptide-N (4) -(N-acetyl-beta-glucosaminyl) asparagine amidase (PNGase), a de-N-glycosylating enzyme. Subsequently, Gene ontology (GO) analysis of the proteins more enriched either with WT-TRPM7 or TRPM7-M5 mutant was used to investigate the cell components where those proteins reside. All the proteins that are significantly more or less co-purified with WT-TRPM7 are described in Figure 4.19 and Figure 4.20 separately. For instance, Flot2 is approximately 4-fold less enriched from TRPM7-M5 cells (*P<0.05), while annexin-1 is roughly 8-fold more enriched from TRPM7-M5 cells (*P<0.05). The majority of proteins co-purifying more abundantly with WT-TRPM7 were from nuclear lumen (N.of Gene=34), however the most enriched proteins co-purifying with TRPM7-M5 were from vesicles (N.of Gene=25). This finding is in accordance with our previous results that non-palmitoylated TRPM7 is more abundant in intracellular vesicles. It also suggests that when non-palmitoylated, cleavage and nuclear localization of the TRPM7 kinase may be reduced. In addition, comparing our proteomics analysis of genes co-purified with TRPM7-YFP with the one of gene enriched in TRPM7 vesicles (Abiria et al., 2017a), there are in total 76 genes might be the candidates which were localized in vesicles and interacted with TRPM7 as well (Figure 4.21, details in appendix Table S1**).**

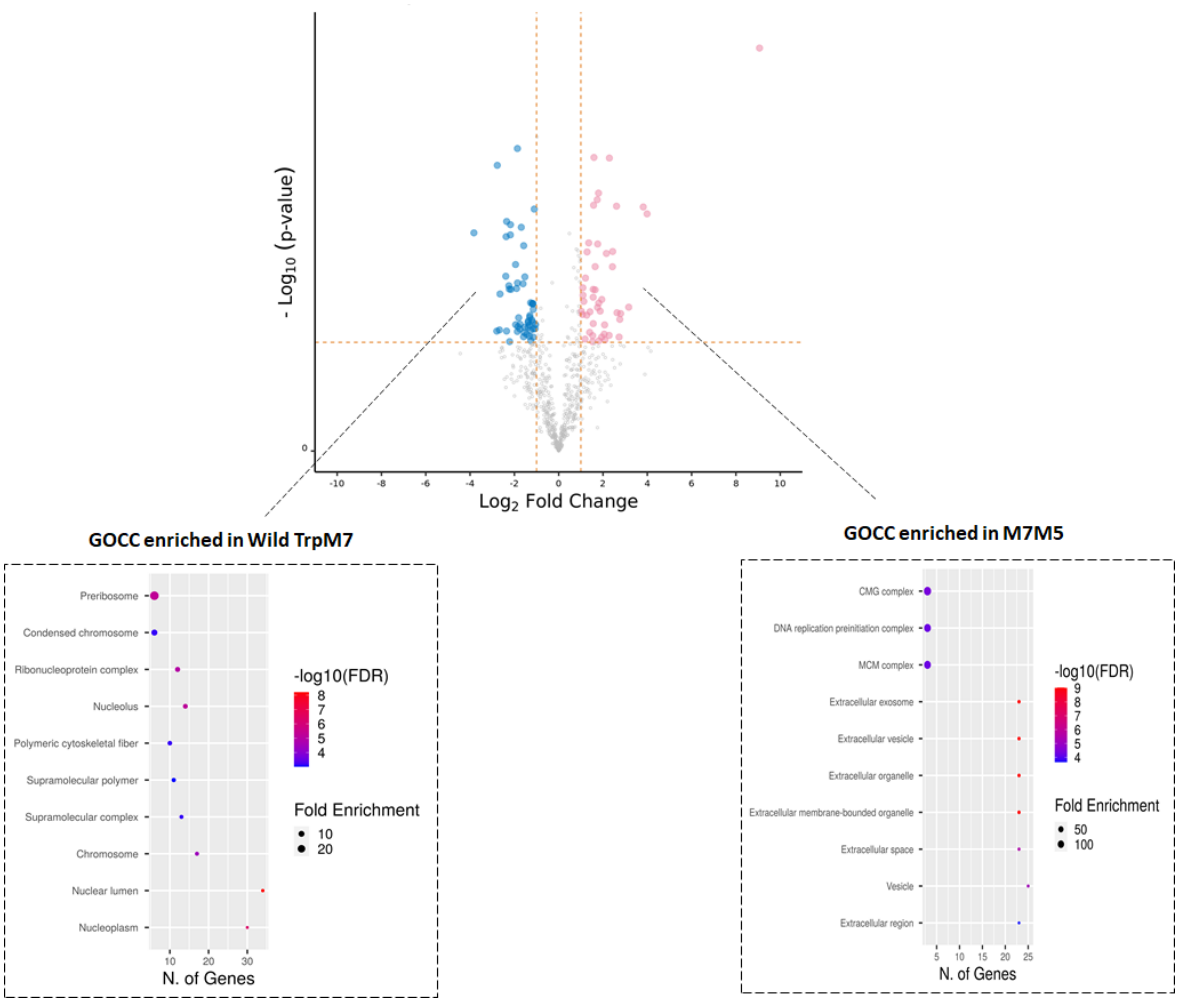

Figure 4.18 Gene ontology for cellular components of differentially expressed genes between WT-TRPM7 and TRPM7-M5 stable cells.
The upregulated proteins in TRPM7-M5 were mainly from vesicles and the one from upregulated in WT-TRPM7 were from nuclear lumen. Blue spots represent gene enriched in WT-TRPM7 and Pink spots represents those enriched in TRPM7-M5 in significant difference. The orange dotted line P value =0.05. (n=3). N.of Genes =number of genes enriched in different cell components.

In conclusion, our proteomics data presents a list of potential candidates of protein interacted with TRPM7, with different enrichment when it is not palmitoylated. The gene ontology of cell components (GOCC) enrichment in WT-TRPM7 and TRPM7-M5 are involved in many pathways, which may inspire us to identify novel regulators of TRPM7 that interact according to its palmitoylation status.

DEP upregulated in WT-TrpM7					
Enrichment FDR	nGenes	Pathway Genes	Fold Enrichment	Pathway	Genes
6.29E-09	34	4885	2.993623144	Nuclear lumen	FOXC1 PKP2 DHX8 HLTF NLE1 KIF22 KIF4A CDC5L BYSL RRP9 HEATR1 TRIM25 KHDRBS1 DEK GTF2F1 SMARCA4 ASH2L DNMT1 TUBG1 TOP2A RBM17 WDR36 MKI67 SSRP1 SCAF4 LMNA PPIB TSR1 PA2G4 CKAP5 RRS1 USP7 ABCF1 EPPK1
4.84E-07	30	4519	2.855365396	Nucleoplasm	FOXC1 PKP2 DHX8 HLTF NLE1 KIF22 KIF4A CDC5L BYSL RRP9 HEATR1 TRIM25 KHDRBS1 DEK GTF2F1 SMARCA4 ASH2L DNMT1 TOP2A RBM17 WDR36 MKI67 SSRP1 SCAF4 LMNA PPIB TSR1 RRS1 USP7 ABCF1
3.70E-05	17	1918	3.812265135	Chromosome	FOXC1 KIF22 KIF4A TOX4 CDC5L BYSL SMARCA4 DNMT1 TUBG1 TOP2A MKI67 SSRP1 LMNA CHAF1A CKAP5 RRS1 USP7
6.33E-06	14	1067	5.643472264	Nucleolus	HLTF NLE1 BYSL RRP9 HEATR1 SMARCA4 TOP2A WDR36 MKI67 SSRP1 TSR1 PA2G4 CKAP5 RRS1
0.000692932	13	1455	3.842935875	Supramolecular complex	CSDE1 PKP2 KIF22 KIF4A TRIM25 DEK TUBG1 LMNA CKAP5 YES1 PLEC KIFC1 EPPK1
1.07E-05	12	792	6.516866781	Ribonucleoprotein complex	DHX8 CDC5L BYSL RRP9 HDLBP HEATR1 TOP2A RBM17 WDR36 TSR1 RRS1 ABCF1
0.000957436	11	1110	4.262383138	Supramolecular polymer	PKP2 KIF22 KIF4A DEK TUBG1 LMNA CKAP5 YES1 PLEC KIFC1 EPPK1
0.000692932	10	856	5.024687004	Polymeric cytoskeletal fiber	PKP2 KIF22 KIF4A TUBG1 LMNA CKAP5 YES1 PLEC KIFC1 EPPK1
5.16E-06	6	89	28.99639601	Preribosome	BYSL RRP9 HEATR1 WDR36 TSR1 RRS1
0.000692932	6	245	10.53338467	Condensed chromosome	KIF22 TUBG1 TOP2A MKI67 CKAP5 RRS1

Figure 4.19 GOCC upregulated in WT-TRPM7 stable cells.
The various gene enriched in WT-TRPM7 are from nuclear lumen (nGenes=34)

DEP upregulated in Mutant TrpM7-M5					
Enrichment FDR	nGenes	Pathway Genes	Fold Enrichment	Pathway	Genes
6.04E-06	25	4396	2.818273529	Vesicle	MDH1 VCL GPC1 EZR DPYSL2 TPI1 PARK7 CTSD GOT2 PCNA AP3B1 ANXA1 LAMC1 ATIC NPEPPS TTN PIP AP2M1 PIGR CAPN2 PRDX2 UMOD PSMD2 PPIA SIAH1
9.36E-10	23	2339	4.873022659	Extracellular organelle	MDH1 VCL GPC1 EZR DPYSL2 TPI1 PARK7 CTSD GOT2 PCNA ANXA1 LAMC1 ATIC NPEPPS TTN PIP AP2M1 PIGR CAPN2 PRDX2 UMOD PSMD2 PPIA
9.36E-10	23	2339	4.873022659	Extracellular membrane-bounded organelle	MDH1 VCL GPC1 EZR DPYSL2 TPI1 PARK7 CTSD GOT2 PCNA ANXA1 LAMC1 ATIC NPEPPS TTN PIP AP2M1 PIGR CAPN2 PRDX2 UMOD PSMD2 PPIA
9.36E-10	23	2314	4.925669836	Extracellular exosome	MDH1 VCL GPC1 EZR DPYSL2 TPI1 PARK7 CTSD GOT2 PCNA ANXA1 LAMC1 ATIC NPEPPS TTN PIP AP2M1 PIGR CAPN2 PRDX2 UMOD PSMD2 PPIA
9.36E-10	23	2337	4.877192982	Extracellular vesicle	MDH1 VCL GPC1 EZR DPYSL2 TPI1 PARK7 CTSD GOT2 PCNA ANXA1 LAMC1 ATIC NPEPPS TTN PIP AP2M1 PIGR CAPN2 PRDX2 UMOD PSMD2 PPIA
3.03E-06	23	3550	3.210704225	Extracellular space	MDH1 VCL GPC1 EZR DPYSL2 TPI1 PARK7 CTSD GOT2 PCNA ANXA1 LAMC1 ATIC NPEPPS TTN PIP AP2M1 PIGR CAPN2 PRDX2 UMOD PSMD2 PPIA
0.000220991	23	4658	2.446972954	Extracellular region	MDH1 VCL GPC1 EZR DPYSL2 TPI1 PARK7 CTSD GOT2 PCNA ANXA1 LAMC1 ATIC NPEPPS TTN PIP AP2M1 PIGR CAPN2 PRDX2 UMOD PSMD2 PPIA
3.81E-05	3	10	148.6695652	CMG complex	MCM6 MCM3 MCM7
5.42E-05	3	12	123.8913043	DNA replication preinitiation complex	MCM6 MCM3 MCM7
5.42E-05	3	12	123.8913043	MCM complex	MCM6 MCM3 MCM7

Figure 4.20 GOCC upregulated in TRPM7-M5 stable cells.
The various gene enriched in TRPM7-M5 are from vesicles (nGenes=25). The most enrich genes with 123-fold are which in preinitiation complex and MCM complex.

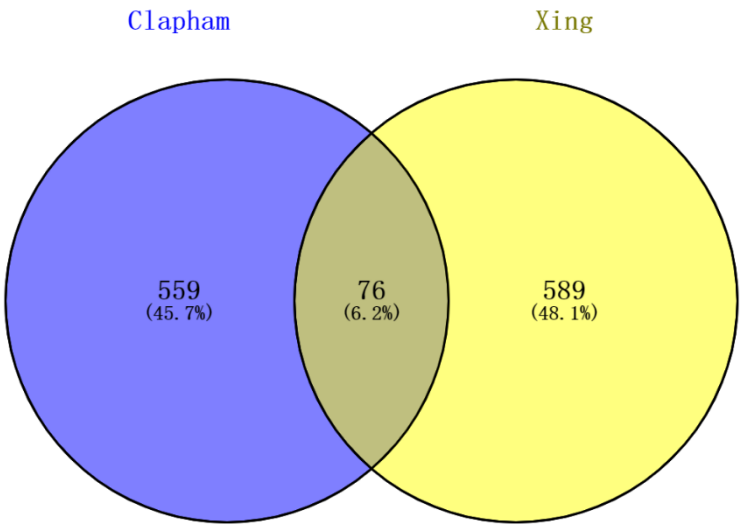

Figure 4.21 Proportion of gene of interacted with TRPM7 overlapped with gene enriched in TRPM7 vesicles.
Proteomics analysis with Abiria et.al., which all the gene from the TRPM7 enrichment vesicles. Our proteomics analysis included 665 genes interacted with TRPM7. There are 76 genes were overlapped, indicating that those are candidates localized in vesicles and interacted with TRPM7.

4.4.11 TRPM7-M5 and TRPM7-M2 behaviour in stable cells-physiology

Chanzyme TRPM7 is generally known as a predominantly divalent cation permeable ion channel conducting Ca, Mg and Zn, whose activity is regulated by intracellular Mg and Mg•ATP (Monteilh-Zoller et al., 2003). The majority of research to date has investigated the influence of the kinase domain on its ion channel activity. However, to investigate palmitoylation impacts on TRPM7 ion channel activity, we conducted a series of experiments to measure the intracellular ion concentrations and cation influx in wild-type TRPM7 and non-palmitoylated TRPM7, including Mg, Ca and Zn.

4.4.11.1 Influence of palmitoylation on TRPM7-mediated intracellular Mg

Mg is the second most abundant cellular divalent cation which is involved in over 600 enzymatic reactions (De Baaij et al., 2015). Previously research found that TRPM7-dependent currents were strongly suppressed in high [Mg], and completely blocked with 3mM [Mg] (Nadler et al., 2001).

To investigate the impacts of altering palmitoylating of TRPM7 on intracellular free Mg concentration and Mg conduction, we used a fluorescent Mg indicator to

measure free Mg levels in WT-TRPM7-YFP, TRPM7-M2-YFP and TRPM7-M5-YFP stable cells. In pilot experiments we confirmed that the yellow fluorescent protein (YFP) tag fused at the C terminus of TRPM7 did not interfere with the Mg green indicator. YFP fluorescence was 20-40 weaker than Mg green. The intracellular free Mg level was the same when inducing TRPM7 expression compared with uninduced 293 T-REx cells (Figure 4.22A, TRPM7 -/+; Mg add:-/-). Meanwhile, the static cellular free Mg was no different between WT-TRPM7 and two non-palmitoylated TRPM7 expressing cells (Figure 4.22A, TRPM7: + Mg add:-). We evaluated Mg influx after adding 5mM extracellular MgCl2 to three different cell lines. Again, there was no significant difference in Mg concentration after Mg incubation (Figure 4.22A, TRPM7: +; Mg add: +).

The extent to which Mg changed on induction of TRPM7 was estimated by subtracting Mg levels in uninduced cells from Mg levels in induced cells ('delta': Figure 4.22B). In the presence of 5mM extracellular Mg, the delta changes of intracellular Mg level triggering by non-palmitoylated TRPM7-M2 and TRPM7-M5 were lowered compared with WT-TRPM7. The net delta entry of Mg was obviously lower in TRPM7-M2 stable cells, with a negative mean value (-3.20%) representing free Mg concentration was less after incubation with MgCl2. The delta changes of Mg in TRPM7-M5 was quite similar with its in WT-TRPM7 stable cells, which mean values are 8.04% and 9.87% separately with no significant difference.

Free Mg level in mammalian cells is maintained tightly in a narrow range, specifically 0.7-1.1mmol/L(Antunes et al., 2016). Probably there are other magnesium regulators in 293 T-REx cells that impact on Mg homeostasis. The underlying reason for the very different behaviour of TRPM7-M2 and TRPM7-M5 stable cells in Mg influx is unclear, but it is unlikely to be related to differences in palmitoylation of TRPM7.

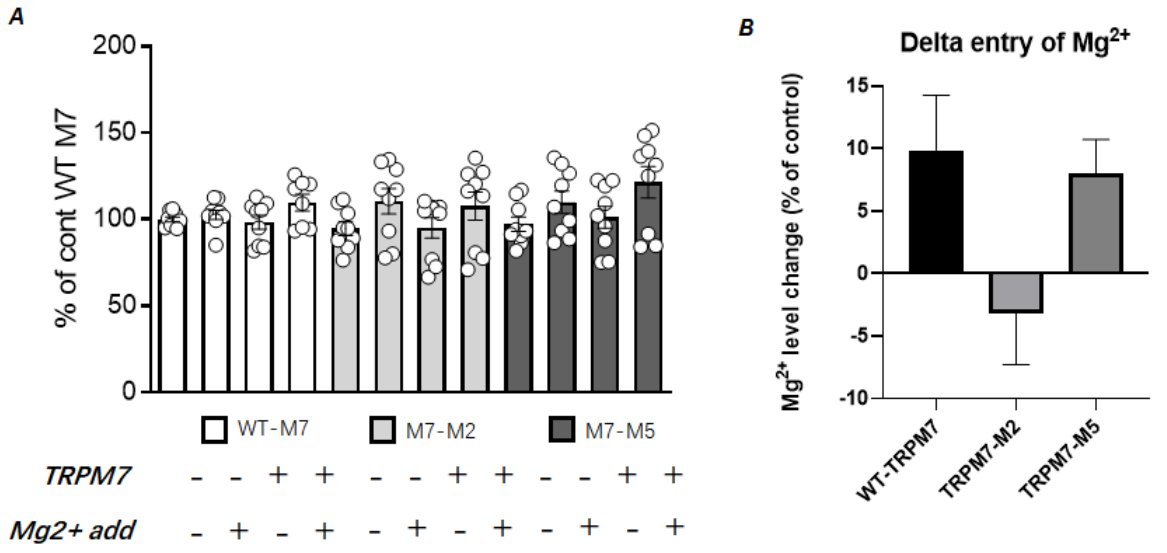

Figure 4.22 Intracellular Mg concentration and Mg influx in WT-TRPM7, TRPM7-M2 and TRPM7-M5 stable cells.
Tetracycline(10μg/ml) added to induce gene expression. A) Summary of Mg level measurement via flow cytometry about intracellular free Mg level and Mg influx among WT-TRPM7, TRPM7-M2 and TRPM7-M5 stable cells (n=9). The basal intracellular Mg concentration among all cell lines has no difference (TRPM7: -; Mg add: -). In addition, the intracellular free Mg level in non-palmitoylated TRPM7-M2 and TRPM7-M5 are similar with WT-TRPM7 (TRPM7: +; Mg add: -). Besides, there is no significant difference in Mg influx ability between WT-TRPM7 and TRPM7-M2/TRPM7-M5 stably expressed cells when 5mM MgCl2 added extracellularly (TRPM7: +; Mg add: +). B) Delta changes of Mg influx when WT-TRPM7, TRPM7-M2 and TRPM7-M5 were induced. Average changes of Mg entry when we induced WT-TRPM7 and non-palmitoylated TRPM7-M2 and TRPM7-M5 expression in stable cells(n=9). TRPM7-M2 reduced Mg entry but TRPM7-M5 only slightly reduced Mg influx level.

4.4.11.2 Influence of palmitoylation on TRPM7-mediated cellular Ca uptake

As well as measuring palmitoylation influence on TRPM7 ion channel activity by evaluating uptake of Mg, we also measured its influence on Calcium uptake. The Fluo-4 Direct™ Calcium Assay was used as fluorescent indicator for cellular Ca level applied within 293 T-REx cells stably expressing either tetracycline inducible WT-TRPM7-YFP or TRPM7-M5-YFP (Chubanov et al., 2012). Notably, these experiments were conducted in the absence of extracellular Mg because of the ability of Mg to block TRPM7 ion channel. In these stably transfected cells TRPM7-M5-YFP was not palmitoylated and less abundant at the surface membrane compared to WT-TRPM7 (Figure 4.16B, E). Ca uptake in the presence of 1mM or 5mM extracellular Ca was measured in cells loaded with the fluorescent Fluo-4 AM indicator (Chubanov et al., 2012). In cells not treated with tetracycline and not expressing TRPM7, Ca uptake was identical in either 1mM or 5mM extracellular Ca (Figure 4.23A, B). In contrast, Ca uptake was significantly increased when TRPM7 expression was induced both in wild type and non-

palmitoylated TRPM7-M5 cells in presence of 1mM (*** P<0.001, ** P<0.01) and 5Mm Ca (**** P<0.0001, **** P<0.0001) (Figure 4.23 A, B). In addition, TRPM7-mediate Ca uptake was significantly less in cells expressing non-palmitoylated TRPM7-M5-YFP compared to WT-TRPM7-YFP (** p<0.01 in 1mM; * P<0.05 in 5mM). Delta changes of Ca influx on induction of TRPM7 also confirmed that changes of Ca uptake were significantly reduced when TRPM7 was not palmitoylated (Figure 4.23C, D). We conclude that palmitoylation controls TRPM7-mediated divalent Calcium cation transport, specifically inhibiting its palmitoylation would supress Ca influx, which might be associated with its distinct subcellular distribution controlled by palmitoylation.

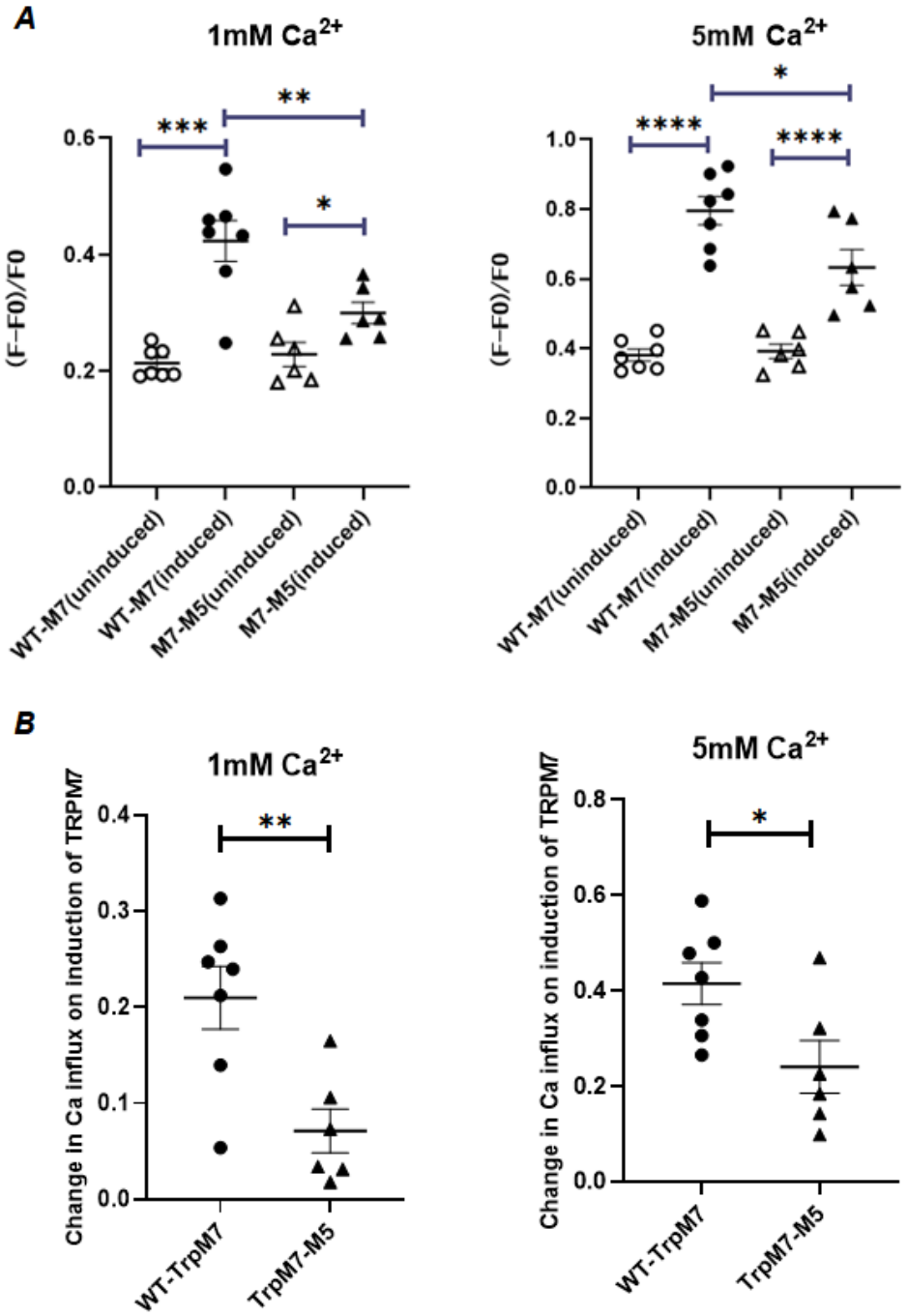

Figure 4.23 TRPM7 palmitoylation mediate intracellular Ca uptake.
A) Comparing with WT-TRPM7, Ca influx was significantly decreased in non-palmitoylated TRPM7-M5 stable cells when 1mM (left) and 5mM (right) extracellular Ca was added (**P<0.01, n=6-7) (*P<0.05 n=6-7). The basal level of Ca uptake was equal between WT-TRPM7 and TRPM7-M5 in the absence of tetracycline (uninduced) in 1mM Ca and 5mM Ca. Tetracycline added for allowing gene expression. One-way ANOVA followed by post-hoc Tukey's test (n=6-7) B) TRPM7-mediated (Tet-induced) Ca influx in cell lines expressing WT or M7-M5 TRPM7. Delta changes of Ca influx was significantly reduced in WT-TRPM7 compared to non-palmitoylated TRPM7-M5 expressing cells (**: P<0.01 in 1mM Ca, *: P<0.05 in 5mM Ca). Unpaired t-test was applied (n=6-7).

4.4.11.3 Ion transporter activity in intracellular vesicles for Zn

Since TRPM7 localises to intracellular vesicles which serve as a Zn reserovir (Abiria et al., 2017a), we encoded the eCLAWY4ic Zn sensor between transmembrane doamin S1-S2 loops of WT-TRPM7-YFP, TRPM7-M2-YFP and

TRPM7-M5-YFP.Since the loop between S1 and S2 faces the vesicle lumen, we hypothesised that this sensor would measure intravesicular Zn levels. Zn binding to the sensor reduces FRET efficiency. Palmitoylation of engineered Flag-eCLAWY4ic-WT-TRPM7-YFP, Flag-eCLAWY4ic-M7-M2-YFP and Flag-eCLAWY4ic-M7-M5-YFP Zn sensor was assessed by Acyl-Rac assay. Representative western-blot and mean data revealed that Flag-M7-M2 Zn sensor and Flag-M7-M5 Zn sensor were signficantly less palmitoylated compared the WT-TRPM7 Zn sensor (* $P<0.05$ and ** $P<0.01$; Figure 4.24A, B).

Intravesicular free Zn level was measured with trasnsiently trasnfected TRPM7 Zn sensor in HEK cells via fluorescence resonance energy transfer (FRET) assay. The basal Zn concentration assessed by WT-TRPM7-ZN sensor and non-palmitoylated M7-M5-Zn sensor were similar in Zn-free conditions (Figure 4.25). FRET ratio was recorded continuously after additon of extracellular 0.5mM extracellular $ZnCl_2$, the Zn ionophore Zn/pyrithione, and the Zn chelator TPEN. FRET ratio declined immediately on adding extracellular Zn with WT-TRPM7-YFP which represents the intravesical Zn level increasing (Figure 4.26A). However, the M7-M5-Zn sensor responding to Zn addition was slow, with Zn influx slightly lower compared to WT-M7 (Figure 4.26A). Mean values of delta changes of FRET ratio during first 300s after adding Zn are displayed as Figure 4.26.B, Vesicular Zn entry is reduced by 70% in non-palmitoylated TRPM7-M5 transiently transfected HEK cells compared to WT-TRPM7 ones but without significant difference after statistical analysis. Addition of the ionophore Zn/Pyr did not trigger significantly increased vesicular Zn entry according to the TRPM7-M5 Zn probe. Finally, membrane-permeable zinc chelator TPEN (50μM) was applied after Zn/Pyr treatment but surprisingly did not decrease intravascular zinc level (Figure 4.26A). Delta changes of FRET ratios after 600s, 900s and 1200s illustrates that although intravesicular Zn uptake is slightly higher in WT-TRPM7 but without significant difference with TRPM7-M5 (Figure 4.26C, D, E).

In conclusion, compared with the WT-TRPM7-Zn sensor, the TRPM7-M5-Zn sensor is less palmitoylated. Those encoded eCLAWY4ic Zn sensor inserted in the S1-S2 loops of TRPM7 found that the basal intravesicular Zn concentration was similar at rest condition when they were transiently transfected in intact HEK cells. Zn uptake in vesicles might be lower in non-palmitoylated TRPM7-M5 in presence of extracellular ZnCl2. But the underlying reasons why TRPM7-M5 Zn sensor did not

respond to Zn/pyr, or why neither sensor responded to Zn Chelation with TPEN is unclear, which may indicate that the encoded Zn sensor might not be a reliable method to investigate vesicular Zn level.

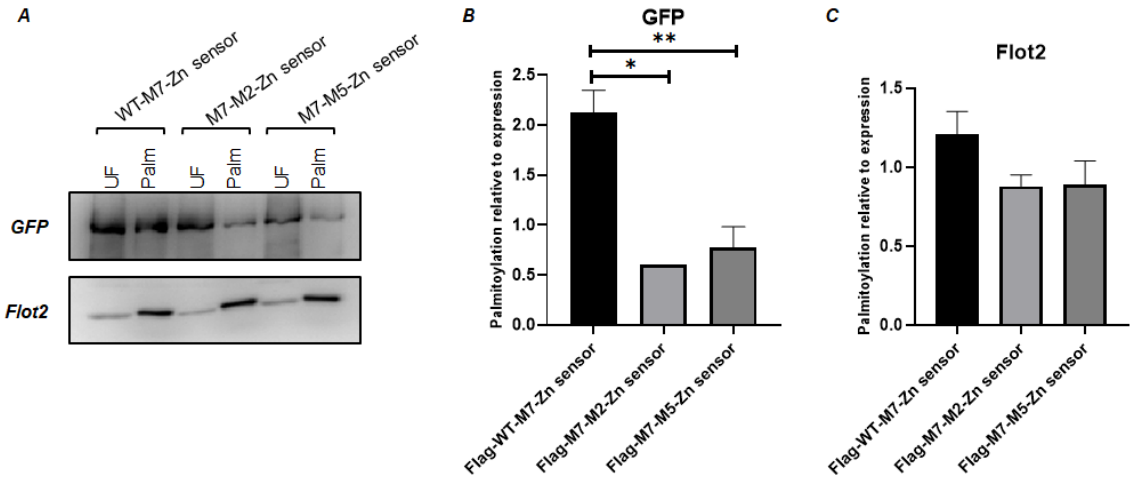

Figure 4.24 eCALWY4 sensors of WT-TRPM7, TRPM7-M2 and TRPM7-M5 targeted at measuring vesicular Zn level.
A) Representative western-blot of palmitoylation status in assembled WT-TRPM7, TRPM7-M2 and TRPM7-M5 Zn sensor. Flot2, a palmitoylated protein, as the standard for evaluating Acyl-RAC assay efficiency. B) Summarizing quantifications of several western-blots data of palmitoylation levels among WT-TRPM7, TRPM7-M2 and TRPM7-M5 Zn sensor. M7-M5 and M7-M2 Zn sensor has distinctly reduced TRPM7 palmitoylation (*P<0.05; **P<0.01). One-way ANOVA followed by Dunnett's multiple comparisons test (n=5-6). *C)* Summarizing images data of Flot2 Palmitoylation in different Zn sensor. Flot2 palmitoylation was robust and no difference among all groups. One-way ANOVA followed by Tukey's multiple comparisons test (n=5-6).

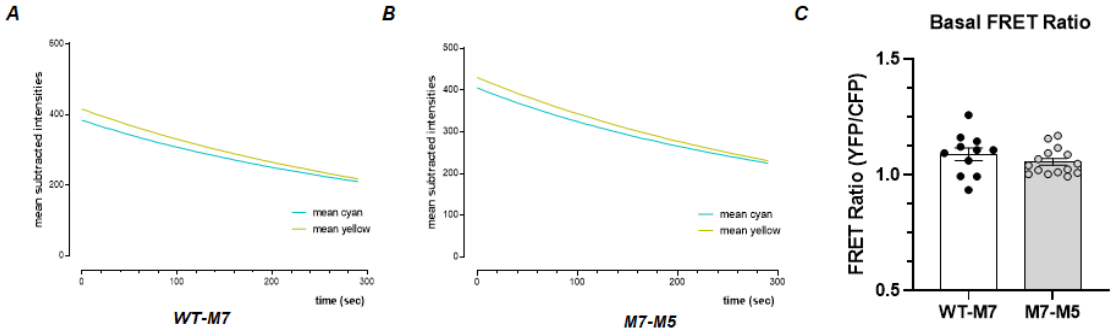

Figure 4.25 Basal FRET ratio of eCLAWY4ic Flag-WT-M7-Zn sensor and Flag-M7-M5-Zn sensor.
A, B) YFP and CFP signal records of transfected Flag-WT-M7-Zn sensor (left) and Flag-M7-M5-Zn sensor (right) in HEK cells. C) Summary of quantification of basal FRET ratios in WT-M7 and M7-M5 Zn senor. Every single cell with transfected Zn sensor was recorded approximately 500s. The basal FRET ratio of WT-M7 and non-palmitoylated M7-M5 Zn sensor was similar which implies resting intravesicular Zn concentration was not different (n=11-15).

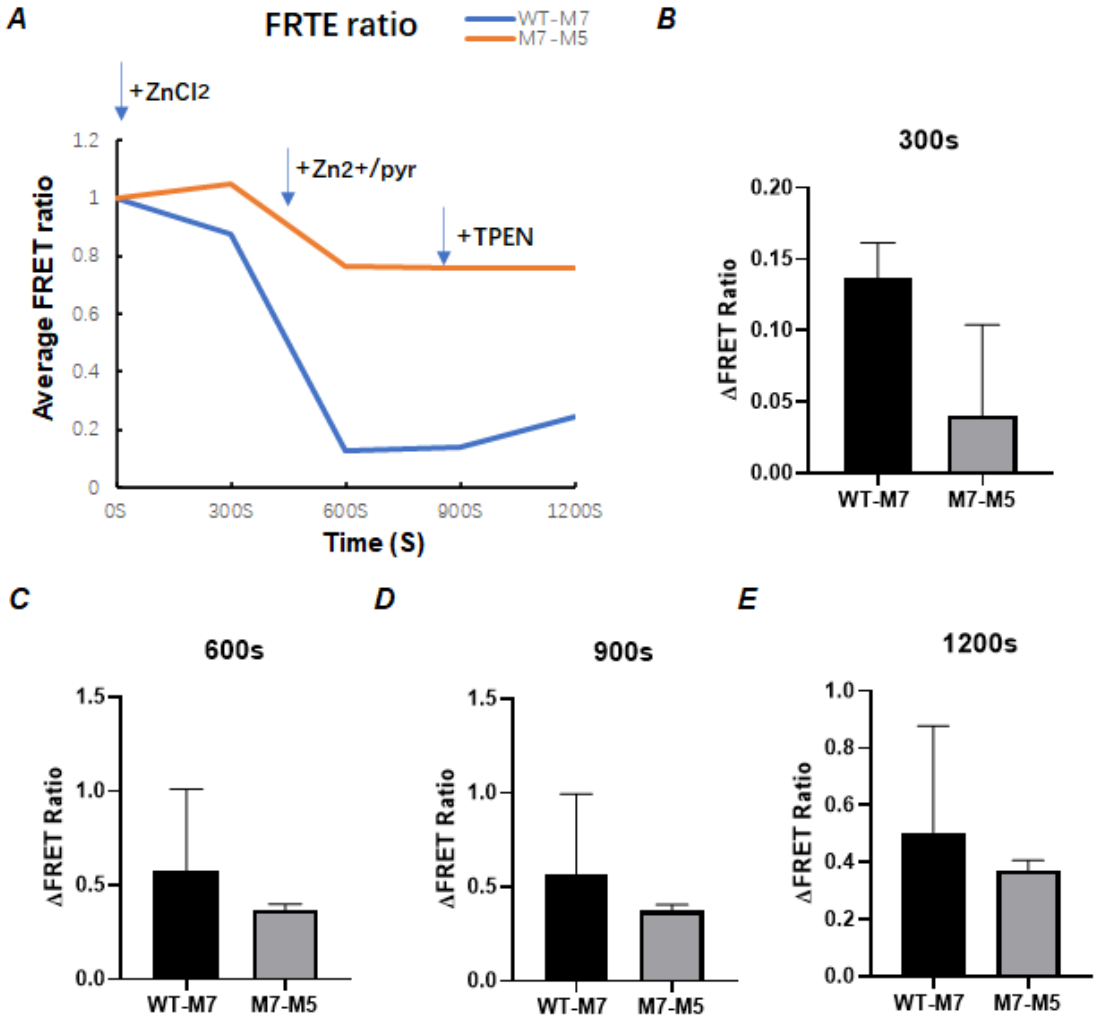

Figure 4.26 FRET ratio changes responding to extracellular Zn alterations.
A) HEK293 cells were transfected with either Flag-WT-M7 or Flag-M7-M5 eCALWY4 Zn sensor and then were incubated with 500 µM Zn, followed by 50 µM Zn/20 µM pyrithione and TPEN (50µM). Shown were time course of Zn entry and 95% CIs of 30-45 cells representative of multiple similar experiments, which illustrated that Zn entry to WT-M7 was quicker and concentration of Zn in WT-M7 is higher than M7-M5. however, both Zn sensor did not respond to Zn/pyrithione neither TPEN. B, C, D, E) Average changes of FRET ratio in WT-M7 and M7-M5 eCLAWY4 sensor among different time duration, 300s, 600s, 900s, and 1200s separately after adding extracellular Zn. All the changes showed that M7-M5 had slightly less Zn entry but without significant difference (n=30-45).

4.5 Discussion

This chapter is set out to identify how palmitoylation controls TRPM7 distribution between membrane surface and intracellular vesicles. We find non-palmitoylated TRPM7 less abundant in the cell surface membrane. Besides, gene ontology (GO) of proteins co-purified with wild type and non-palmitoylated TRPM7 identifies more vesicular proteins associated with TRPM7-M5, which suggests that non-palmitoylated TRPM7 is preferentially directed to intracellular

vesicles. Palmitoylation controls TRPM7-mediated cellular Ca uptake but has no influence on Mg conduction.

4.5.1 Palmitoylation of TRPM7 in the secretory pathway

The retention of the non-palmitoylated TRPM7 mutant 1143/4/6_AAA in the ER in many cell types demonstrated that palmitoylation initially occurs in the early stage in its life cycle. We conclude that a zDHHC palmitoyl acyltransferase residing in ER is necessary for ER export. Previous research on lipid raft and viral membrane protein suggested that palmitoylation can control membrane curvature and vesicle budding (Yurtsever and Lorent, 2020). To be specific, palmitoylation could control the distribution of proteins in membrane based on their curvature, indicating that palmitoylated protein tend to cluster at sites of vesicle budding. But since the non-palmitoylated chimaeras TRPM7-M5 and TRPM7-M2 could exit the ER, therefore it indicates that palmitoylation is required to stabilise TRPM7 structure by anchoring the C-terminal end of TRP domain to the membrane, rather than for clustering TRPM7 into ER export vesicles. The replaced hydrophobic amino acids “KRIV” (TRPM2) and “KQVF” (TRPM5) might be sufficient to engage to membrane and substitute for palmitoylation in stabilising nascent TRPM7 in the ER.

Furthermore, palmitoylation controls the distribution of TRPM7 between surface and intracellular vesicles. The gene ontology of cell components (GOCC) enrichment analysis also found that significantly enriched genes associated with non-palmitoylated TRPM7-M5 stable cells are from the vesicles, which suggested the vesicular TRPM7 are likely non-palmitoylated. Our findings indicates that TRPM7 may be palmitoylated and de-palmitoylated several times in the secretory pathway. For example, TRPM7 was less palmitoylated after releasement by biotin from Golgi-hook retention cells (section 4.4.4), which suggested that TRPM7 was de-palmitoylated after leaving the Golgi. However, TRPM7 palmitoylation status was not changed by the broad-spectrum thioesterase inhibitor, which suggests that TRPM7 is de-palmitoylated by a PalmB-insensitive enzyme. The palmitoylation and de-palmitoylation enzymes responsible for TRPM7 need further investigation but were notably not identified using co-immunoprecipitation. We attempted to use live cell imaging to visualize

biotin-induced TRPM7 release from the ER and Golgi using the RUSH system but these experiments were not successful.

4.5.2 Palmitoylation and TRPM7 protein interactions

Protein partners of TRPM7 were purified with GFP-Trap agarose beads then analysed via Liquid Chromatography - Mass spectrometry (LC-MS). The gene ontology of cell components (GOCC) enrichment revealed that most proteins showing increased co-purification with non-palmitoylated TRPM7-M5 are vesicular. In contrast, PKP2 is more abundantly associated with WT-TRPM7. This cell-surface localised protein is expressed in cardiac muscle desmosomes, and links cadherins to intermediate filaments in the cytoskeleton, for which mutations are associated with arrhythmogenic cardiomyopathy (Awad et al., 2006). Moreover, PKP2 is required to maintain the gene transcription that control intracellular calcium cycling which encoding Ryanodine receptor 2, Ankyrin-B and Cav1.2 (Cerrone et al., 2017). In hence, shortage of PKP2 disrupts intracellular calcium homeostasis and leads to isoproterenol-induced arrhythmias (Cerrone et al., 2017). Transcriptional changes in PKP2 have also been found to change expression of TRPM7, reinforcing the functional link between these proteins (Montnach et al., 2018).

Emerging evidence suggests a relationship between TRPM7 and epidermal growth factor (EGF), specifically EGF upregulated membrane protein expression and current of TRPM7 via its receptor as well as enhanced the migration of A549 cells (Gao et al., 2011). Further evidence shows that TRPM7 channel activity was inhibited by EGF signalling involving PLCγ and PIP2 (Runnels et al., 2002). Meanwhile, the most unique aspect of TRPM7 is its C-terminal active serine/threonine kinase, which is proteolytically cleaved from the channel domain in cell type-specific manner then translocated to the nucleus (Krapivinsky et al., 2014). TRPM7-cleaved kinases (M7CKs) binds multiple components of chromatin remodelling complexes, PRC1 and PRC2 and INO80 (Krapivinsky et al., 2014), and phosphorylates histones to mediate gene expression. A series of substrates identified for TRPM7 kinase domain consisting of annexin-1, myosin IIA heavy chain, eEF2, SMAD2, and PLCγ2 (Zou et al., 2019). Annexin-1 association with TRPM7 was increased in cells expressing TRPM7-M5 compared to wild type. We speculate that this increased association

with substrate may indicate TRPM7 palmitoylation can regulate both kinase activity and proteolysis of the chanzyme.

Two novel types of interaction proteins with TRPM7, putative metal transporter proteins CNNM1-4 and a small G-protein ADP-ribosylation factor-like protein 15 (ARL15), have been found to form ternary ternary complexes with TRPM7 (TRPM7/CNNM/ARL15) (Kollewe et al., 2021a). ARL15 inhibits TRPM7 current in a concentration dependent manner, and CNNM3 functions as a negative regulator of TRPM7 kinase (Kollewe et al., 2021a).Those two proteins also have been discovered in our proteomics analysis but without significant difference in co-purification between wild type TRPM7 and non-palmitoylated TRPM7-M5. Research conducted by Abiria et.al., demonstrated the proteomics analysis of TRPM7 vesicles (Abiria et al., 2017a). We compared our intact cells proteome with vesicular one, discovering the potential proteins in unique vesicles which are associated with TRPM7. Many mitochondrial related genes have been identified in the overlapped 76 genes (Table S1), suggesting the vesicular TRPM7 are associated with cellular ATP source.

4.5.3 Palmitoylation and TRPM7 ion channel activity

TRPM7-mediated cellular Ca uptake is substantially decreased when TRPM7 is non-palmitoylated. We suggest this reduction is largely caused by the reduced distribution of non-palmitoylated TRPM7-M5 on surface membrane. But notably, we found that substantial reduced delivery of TRPM7-M5 to cell surface compared to wild type TRPM7 (approximately 70% less, details in section 4.4.8). This reduced delivery is not entirely matched by the decline in cellular Ca uptake in the same cells compare to WT-TRPM7 with a 50% reduction in the presence of 5mM extracellular Ca (section 4.4.11.2). This may suggest that the single channel activity of palmitoylated TRPM7 is different from the non-palmitoylated TRPM7. Meanwhile, since non-palmitoylated TRPM7 predominantly resides in intracellular vesicles, the channel activity or regulatory pathways of the vesicular pool maybe distinct from those in cell surface TRPM7.

Aside from Ca uptake, TRPM7-mediated Mg and Zn influx were also investigated. The Mg concentration and influx measurement via cell flow cytometry suggested that there is no difference between wild type and non-palmitoylated TRPM7. As

TRPM7 activity could be negatively regulated by free intracellular Mg and Mg·ATP levels (Nadler et al., 2001, Schmitz et al., 2003), our protocol from measuring Mg might have some limitations. The addition of 5mM extracellular Mg may have completely blocked the TRPM7 channel. The failure of the assay to detect significant Mg influx when extracellular Mg was increased to 5mM may indicate it lacks the sensitivity to detect changes in intracellular Mg. Intracellular free Mg concentration is regulated by many other factors which may efficiently maintain the Mg level stable. Finally, FRET measurement for WT-TRPM7 -eCALWY4ic and TRPM7-M5- eCALWY4ic Zn sensors revealed slightly lower vesicular Zn influx in the presence of non-palmitoylated TRPM7. However, the underlying reason why those sensors did not respond to fully responded to TPEN membrane-permeable chelation and Zn/Pyr are still unclear.

The mechanisms of controlling channel activation of TRP superfamily members are diverse, but a common feature of TRP channel gating is regulated by the anionic lipid phosphatidylinositol 4,5 bisphosphate (PIP2) which normally binds to positively charged amino acids in the TRP box (Brauchi et al., 2007, Rohács et al., 2005). A variety of TRP channels are inhibited when PIP2 is hydrolysed including TRPM7 (Runnels et al., 2002). TRPM7 palmitoylation sites residents at the C-terminal end of the TRP domain, in the region where the protein structure is not resolved (Duan et al., 2018). The mobility and flexibility of TRP domain likely regulated by PIP2 binding, is a key determinant of channel gating. It is conceivable that palmitoylation may influence the ability of the TRP domain to move relative to the membrane, which might affect the channel behaviour consequently affect channel behaviour. Interestingly, several other ion transporters regulated by PIP2 are palmitoylated to change their PIP2 sensitivity such as NCX1 and ATP-sensitive potassium channels (Gök et al., 2020, Yang et al., 2020).

4.6 Summary

In conclusion, non-palmitoylated 1143/4/6_AAA mutant of TRPM7 was retained in the endoplasmic reticulum (ER) in HEK cells and vascular smooth muscle cells (VSMCs). However, non-palmitoylated TRPM7-M5 and TRPM7-M2 chimaeras could exit ER which indicated that palmitoylation is required to stabilise the TRPM7 structure by anchoring the C terminal end of the TRP domain to the membrane,

rather than for clustering TRPM7 for ER export. We found inhibiting TRPM7 palmitoylation reduced the abundance of TRPM7 in membrane surface. TRPM7 is likely processed by multiple palmitoylating and de-palmitoylating enzymes in different compartments during passage through the secretory pathway. Our data indicates that TRPM7 is palmitoylated by some ER-resident zDHHCs enzymes and de-palmitoylated by some enzyme(s) that are not inhibited by broad-spectrum thioesterase ATP 1 inhibitor (palmostatin B) after leaving the Golgi. We identified a series of protein candidates which interacted with TRPM7, and proteomics analysis also revealed that gene enriched in co-purifications with non-palmitoylated TRPM7-M5 are mainly from the vesicles. For ion channel activity, palmitoylation controls TRPM7-mediated divalent cation transport through controlling its subcellular distribution. Specifically, reducing palmitoylation inhibits TRPM7-mediated cellular Ca influx.

Chapter 5 Regulation of TRPM7 palmitoylation

5.1 Introduction

5.1.1 Palmitoylating and de-palmitoylating enzymes and their regulators

S-palmitoylation refers to the attachment of 16 carbon-fatty acid to cysteine residues through a thioester linkage (Guan and Fierke, 2011). Two mechanisms have been proposed to mediate palmitate transfer to proteins : one is through the enzymatic reaction of protein acyltrasnferases (PATs), the other is non-enzymatic spontaneous auto-acylation in presence of lipid vesicles and long-chain acyl-coenzyme A (acyl-CoAs) (Smotrys and Linder, 2004a). Three important factors that control whether a cysteine residue becomes palmitoylated are the local concentration of fatty acyl-CoA, co-localisation with a zDHHC enzyme, and the reactivity of that cysteine (which is controlled by its proximity to basic residues) (Shipston, 2011, Bélanger et al., 2001). As we previously described, almost all s-palmitoylation reactions in mammals are mediated by more 20 zDHHC enzymes with highly conserved Asp–His–His–Cys cysteine-rich domain (DHHC-CRD) (Malgapo and Linder, 2021). Palmitoylation may act at distinct stages of protein secretory/trafficking pathways to contribute to target protein's surface expression and clustering.

The intracellular localization of DHHCs has been revealed by Ohno et.al. (Ohno et al., 2006). Most zDHHCs are localised to the endoplasmic reticulum (ER) and Golgi membranes. In addition, Palmitoylation often couples with N-myristoylation or prenylation to regulate membrane interactions of soluble proteins, so some zDHHC enzymes are closely associated with the enzymes that mediate N-myristoylation and prenylation (Shahinian and Silvius, 1995). As well as controlling stability, palmitoylation can influence surface expression and intrinsic activity of ion channels as well as controlling many adaptor and signalling proteins that regulate macromolecular ion channel complex (Shipston, 2011). For example, zDHHC5 controls synaptic plasticity in learning and memory by palmitoylating delta-catein (Li et al., 2010). zDHHC2 palmitoylates lck (lymphocyte-specific protein tyrosine kinase or p56 lck) which belongs to a non-receptor tyrosine kinase of the Src-family subsequently affecting its phosphorylation and downstream signalling activation (Zeidman et al., 2011). In addition, DHHC9 and GCP16, the Golgi-resident protein, are responsible for

palmitoylating H- and N-Ras family (Swarthout et al., 2005). However, the subcellular localization of native zDHHCs is poorly characterized and the majority of current research has focussed on localisation of overexpressed zDHHCs (Shipston, 2011). It is likely that several zDHHC-PATs are responsible for palmitoylating TRPM7, as palmitoylation controls TRPM7 exit from the ER and the Golgi. Using Retention Using Selective Hooks (RUSH) system in the Golgi, we also found that palmitoylated TRPM7 traffics from the Golgi to surface membrane and non-palmitoylated TRPM7 was sequestered in intracellular vesicles. Additionally, recent high-resolution proteomic characterization of TRPM7 found a potential interaction with zDHHC17, which suggests zDHHC17 as a putative palmitoylation acyltransferase of TRPM7 (Kollewe et al., 2021a).

As a dynamic reversible post-translational modification, many soluble proteins undergo continuous cycles of palmitoylation and de-palmitoylation(Salaun et al., 2010). However, the process of protein de-palmitoylation is less well characterized. There are 3 classes of de-palmitoylating enzymes currently recognized, the acyl-protein thioesterases (APTs), the α/ß hydrolase domain-containing protein 17 (ABHD17), and the palmitoyl-protein thioesterases (PPTs)(Koster and Yoshii, 2019). APTs shuttling from the Golgi and cytoplasm are two interconverting thioesterase pools achieving substrate de-palmitoylation (Vartak et al., 2014). ABHD17 is a recently discovered N-Ras de-palmitoylase (Lin and Conibear, 2015) and which also de-palmitoylates neuronal and synaptic proteins microtubule-associated protein 6 (MAP6) (Tortosa et al., 2017). Besides, PPT1 is a lysosomal thioester hydrolase exerting important effects on morphological development of neurons, and synaptic function in mature cells (Koster and Yoshii, 2019). Disruption of PPT1 function causes infantile neuronal ceroid lipofuscinosis which is the first de-palmitoylating enzyme associated to genetic disorder (Vesa et al., 1995). The bulk of studies of protein de-palmitoylation rely on dual APT1/APT2 inhibitor palmostatin B (Dekker et al., 2010). Although this reagent was developed as a specific inhibitor only targeting these APTs, it is now established to target ABHD17 (Lin and Conibear, 2015). Specific inhibitors of APT1 (ML-348) and APT2 (ML-349) are available (Adibekian et al., 2012). It is widely accepted that the Golgi is the predominant hub for palmitoylation and de-palmitoylation, although these reactions can occur rapidly throughout the cell (Salaun et al., 2010).

5.1.2 Phosphorylation and Kinase domain interaction with TRPM7 palmitoylation

Emerging evidence has proposed interplay between palmitoylation and other PTMs especially phosphorylation, co-ordinating regulation of channel activity and signalling transduction (Shipston, 2011). For instance, the growth-associated protein GAP43 must be palmitoylated to be associated with the membrane, and requires phosphorylation at ser-41 to be locally sorted to the plasma membrane (Gauthier-Kemper et al., 2014). Besides, in BK channels, PKA-dependent phosphorylation on a serine residue immediately upstream of the palmitoylated cysteines leads to detachment of its C-terminal STREX (stress-regulated exon) domain from the plasma membrane (Shipston, 2011).

TRPM7 as a bifunction cation channel/kinase protein, which is palmitoylated at the cluster of cysteines at the C-terminal end of its TRP domain. Meanwhile, palmitoylation controls the abundance of TRPM7 on plasma membrane. TRPM7 C-terminal kinase is homologous to the atypical serine-threonine kinases called α-kinases which is similar to protein kinase A (PKA) in structure (Yamaguchi et al., 2001). The interaction between ion channel and kinase domain of TRPM7 is still incompletely understood. To be specific, the phosphotransferase activity of TRPM7 kinase is not necessary for ion channel activation nor required for its inhibition by [Mg]i (Schmitz et al., 2003, Matsushita et al., 2005). But the nucleotide-dependent regulation of TRPM7 is mediated by the nucleotide binding site on its intrinsic kinase domain, and physiological Mg·ATP collaborates with intracellular free Mg to enhance its inhibition efficacy of TRPM7 channel (Demeuse et al., 2006). In addition, TRPM7 is involved in signalling transduction through autophosphorylation and phosphorylation of exogenous substrates. For example, TRPM7 kinase domain controls expression of Eukaryotic elongation factor 2 (eEF2) cognate kinase eEF2-k and its phosphorylation at Ser77 thereby enhancing Thr56 phosphorylation of eEF2, which is a regulator of ribosomal translocation (Perraud et al., 2011). Meanwhile, TRPM7 phosphorylates annexin A1 at Ser5 within an N-terminal α-helix which alters the conformation of amphipathic α-helix and blunts its interaction with membranes and S100A11 protein (Dorovkov et al., 2011). Apart from annexin-A1 and eEF2, there are many other identified phosphorylated substrates of TRPM7 kinase domain,

including myosin IIA (Thr1800, Ser1803 and Ser1808),SMAD2 (Ser465/467) and phospholipase Cγ2 (PLCγ2) (Ser1164) (Zou et al., 2019) (Figure 5.1).

In addition, a recent investigation also has revealed the interaction between Epidermal growth factor receptor (EGFR) and TRPM7 through c-Src dependent pathway subsequently influences TRPM7 expression and phosphorylation, thereby modulating ERK1/2 signalling pathway in vascular smooth muscle cells (VSMCs) functions(Zou et al., 2020). Therefore, it is worthwhile to investigate the relationships between palmitoylation and phosphorylation of TRPM7, as well as the inference of TRPM7 palmitoylation on downstream signalling cascades via kinase domain.

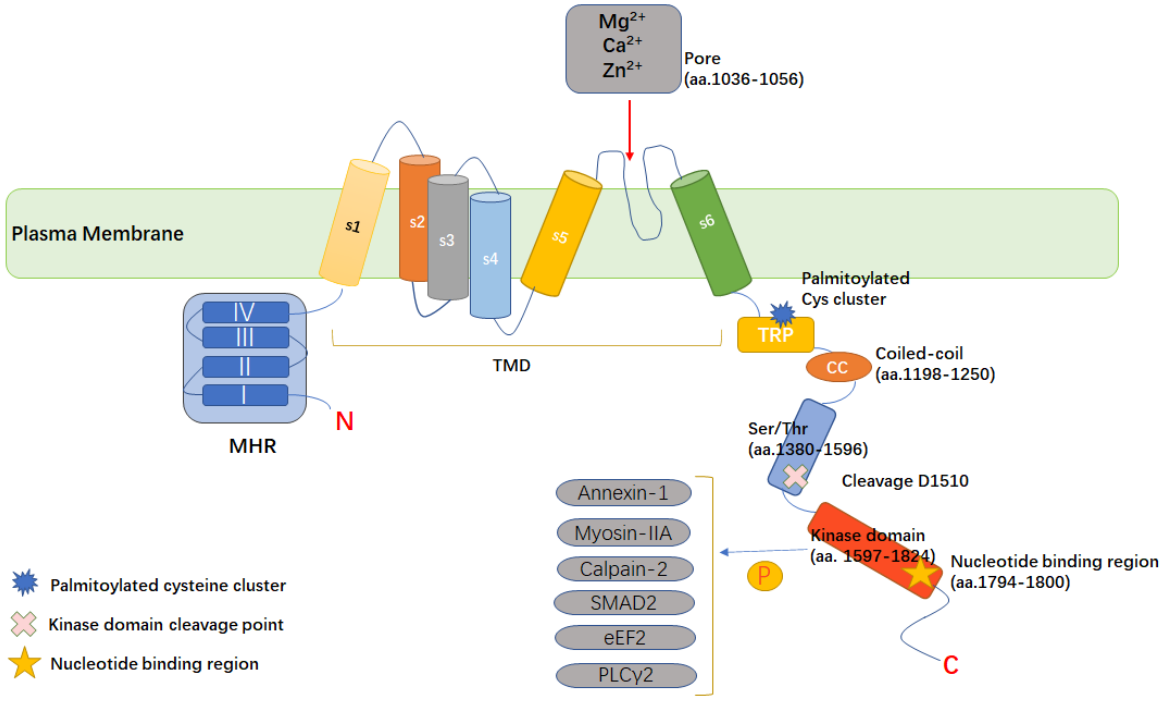

Figure 5.1 Schematic subunit structure of TRPM7 channel and kinase.
Each subunit contains 6 transmembrane domains (TMDs) and ion pore formed between S5-S6. Its palmitoylated cysteines cluster localizes in the TRP domain. The C-terminal end also contains a α-kinase domain which could phosphorylate itself and substrates, including Annexin-1, myosin-IIA, Calpin-2, SMAD2, Eef2, and PLC γ 2. The kinase domain could be cleaved at D1510 by caspases and released into nucleus to regulate gene transcription. MHR: Melastatin Homologous Regions.

5.1.3 TRPM7 regulation in disease

In addition to its role as an ion channel, the TRPM7 kinase domain is released from the ion channel by proteolysis at D1510 (Desai et al., 2012) and phosphorylates histones in nucleus to regulate gene expression (Krapivinsky et al., 2014). TRPM7 regulates numerous cellular processes, such as interaction

with receptor tyrosine kinase signalling, cell motility, survival and differentiation (Meng et al., 2013, Zou et al., 2020, Zhang et al., 2012c), which is crucial to embryonic development. Consequently, TRPM7 is a key player in multiple pathologies. For example in the nervous system TRPM7 has been implicated in neurodegenerative disorders (Sun et al., 2015b). TRPM7 channels activated by reactive oxygen species (ROS) induced increase in [Ca]i concentrations in neuronal cells. Besides, in primary cortical neurons, TRPM7 knockdown is also accompanied by knockdown of TRPM2, another TRPM channel which can be activated by either oxidative stress or TNFalpha, suggesting TRPM7 and TRPM2 may cooperate in modulation of oxidative-stress-induced cell death (Miller, 2006). Phosphatidyl 4,5-bisphosphate (PIP2) is an important regulator of TRPM7 activity. PIP2 metabolism is altered in cells expressing mutants of presenilin, which causes familial Alzheimer disease (Landman et al., 2006). TRPM7-mediated currents are suppressed in the presence of mutated presenilin but restored by supplementing with PIP2.

Beyond the nervous system, TRPM7 is highly expressed in human heart and vascular system. Cardiac-targeted TRPM7 deletion brings different physiological consequences in different time points during cardiogenesis (Sah et al., 2013). Early cardiac TRPM7 deletion (before embryonic day9) causes heart failure (HF) and death by embryonic day 11.5 triggered by myocardial fragility (Sah et al., 2013). During the intermediate and late stage of cardiogenesis (embryonic day 11.5 to 13), cardiac-specific TRPM7 deficient mice display significant interstitial ECM deposition and interstitial fibrosis in hearts at 6-8 months (Sah et al., 2013). Therefore, TRPM7 is important in myocardial proliferation during early cardiogenesis and fibrosis during intermediate-and-late cardiogenesis (Hu et al., 2021). Recently, TRPM7 has been identified as novel protector in aldosterone-salt induced cardiovascular damage, such as hypertension, preventing cardiac hypertrophy, fibrosis and inflammation in an Mg-dependent fashion (Rios et al., 2020, Antunes et al., 2016). In contrast, leptin-induced elevation of TRPM7 expression and ion channel activity in carotid body is required for development of obesity-induced resistant hypertension (Shin et al., 2019). Therefore, as TRPM7 emerged as new target in a variety of clinical diseases, the mechanisms controlling its palmitoylation and whether TRPM7 palmitoylation is remodelled in different diseases requires further investigation.

5.2 Aims

The aim of this chapter is to investigate the regulating factors of TRPM7 palmitoylation. We were mainly focus on the palmitoyl-acyltransferases as responsible for TRPM7 palmitoylation, the relationships between phosphorylation and palmitoylation. In addition, we investigated whether EGFR signalling pathway crosstalk with TRPM7, and Kinase domain cleavage would influence its palmitoylation. Finally, by evaluating TRPM7 palmitoylation status in different disease models we aimed to determine whether palmitoylation is a new determinant of TRPM7 in clinical diseases.

5.3 Methods

5.3.1 DHHC5 KO stable cell line

DHHC5 KO cell line was kindly provided by Dr. Jacqueline Howie in Fuller Lab. According to their previous publications (Plain et al., 2020, Gök et al., 2020), z DHHC5 knockout HEK cells was generated using guide RNAs (gRNA) targeted against zDHHC5 provided by Horizon Discovery. Cells were frozen in liquid nitrogen for storage and retrieved in accordance with previously described procedures (section 2.6.5).

5.3.2 Primer sequences of P586W, P769W and P1131W of TRPM7

TRPM7-YFP acted as parental DNA template for mutant strand synthesis. The oligos sequences of primers for silencing potential zDHHC17 binding sites in TRPM7 are described in Table 5.1. Master mix for DNA amplification were prepared according to the relative manufacturers from In-fusion HD cloning Kit (Takara) (details in section 2.5.1). Mutations were achieved through programming several thermal cycling with the recommended PCR parameters (details in section 2.5.1).

Table 5.1. Oligos primer sequences of TRPM7-P586W, P769W and P1131W.

Mutagenesis reaction	Plasmids	Targeted mutations	Primer sequence
1	TRPM7-P586W	586 P-W	AGCCCAATGGTACAGACCAAAGATGGATGCATC (33) **-Forward**

			CTGTACCATTGGGCTGTTTTAATGAAATGATTG (33) **-Reverse**
2	TRPM7-P769W	769 P-W	AGTTCCATGGGCCATATTAATGCTAGAGTATAAAA (35) **-Forward** ATGGCCCATGGAACTAAAATGCTTAATATGACC (33) **-Reverse**
3	TRPM7-P1131W	1131 P-W	GCCTCCTTGGCTTATCATCCTCAGCCATATAGTTT (35) **-Forward** ATAAGCCAAGGAGGCAGGACTGGTTT (26) **-Reverse**

5.3.3 Cardiac fibroblasts samples

Cardiac fibroblasts were kindly provided by Dr.Francisco Rios. Cells were derived from male wild type TRPM7+/- mice (C57BL/6J and SV129 mixed background) with 18- to 22- week-old mice. Mouse hearts were cut into pieces and digested in collagenase II. Adherent, low passage cells were cultured using Dulbecco's modified Eagle's medium/20% fetal bovine serum (Rios et al., 2020). Animal experiments were performed in accordance with the United Kingdom Animals Scientific Procedures Act 1986 and ARRIVE guidelines and, which approved by the institutional ethics review committee.

5.4 Results

5.4.1 Palmitoylation of endogenous TRPM7 in cells overexpressing selected zDHHC-PATs

Ohno et al. revealed the intracellular localization of DHHC acyltransferases (Ohno et al., 2006), for which most of DHHCs are localized in the endoplasmic reticulum (ER) and/or Golgi and a few ones resident in the plasma membrane. This investigation has established that TRPM7 palmitoylation occurs throughout the secretory pathway and controls its intracellular distribution. Since non-palmitoylated TRPM7-1143/4/6_AAA-YFP mutant was trapped in the ER, we firstly measured palmitoylation of TRPM7 following overexpression of all the ER-resident DHHCs, including DHHC-1,2,6,9,11,12,13,14,16,19,22,23,24. Meanwhile, Golgi-resident DHHC-7 were involved in the measurement (Figure 5.2A). Endogenous TRPM7's palmitoylation was evaluated with Acyl-Rac assay after transient transfection of DHHCs in HEK 293 cells and detected via Abcam TRPM7 antibody. Mean data of palmitoylation of endogenous TRPM7 relative to expression illustrates that there was no significant difference when these DHHCs were over-expressed in HEK cells (Figure 5.2B). Flot2, as the identified

palmitoylated protein, was performed as the standard to evaluate the efficiency of Acyl-Rac assay (Figure 5.2C).

The retention of non-palmitoylated TRPM7-1143/4/6_AAA-YFP in the ER suggested that TRPM7 palmitoylation occurs in the early stage of its lifetime. However, none of the ER-resident DHHC acyltransferases enhanced palmitoylation of TRPM7. The underlying reason might be the native zDHHC-PATs have already efficiently palmitoylated TRPM7. Future experiments should address the impact of DHHC-PAT silencing on ER exit of TRPM7.

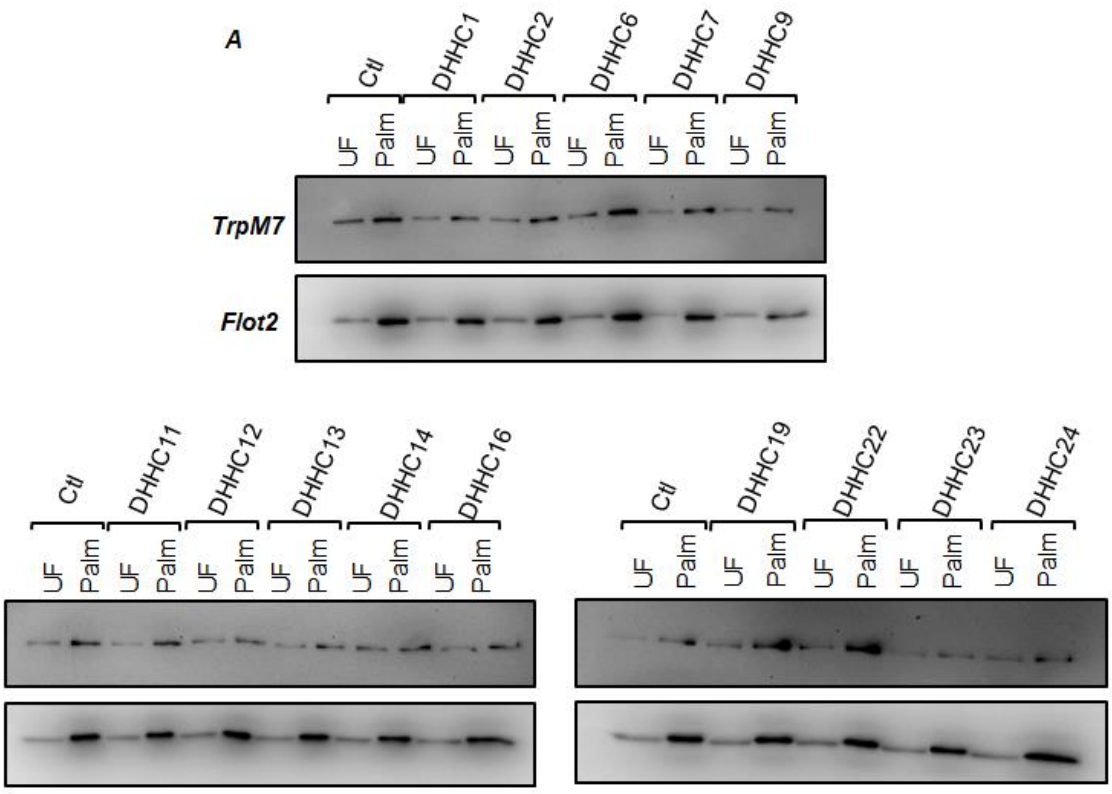

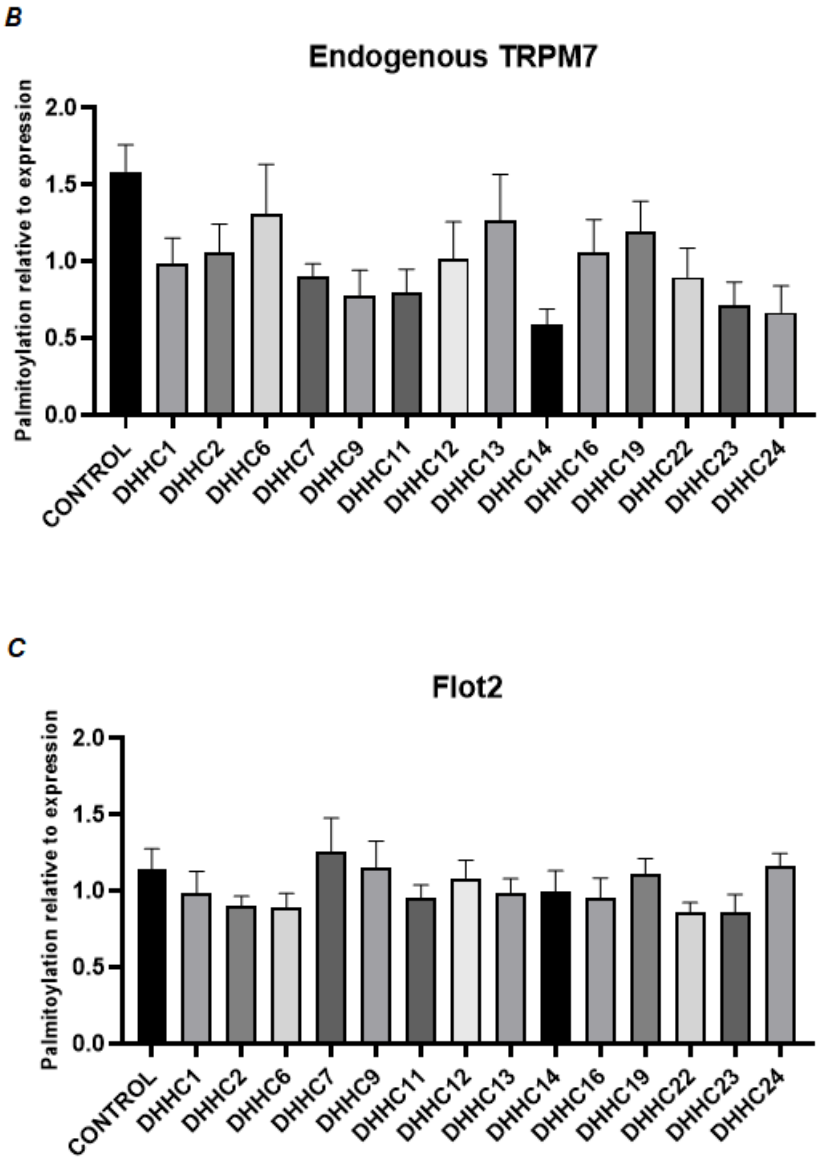

Figure 5.2 Palmitoylation of endogenous TRPM7 after overexpressing selected DHHC-PATs. A) Representative western-blot of palmitoylation relative to expression in the HEK293 cells overexpressed with a variety of DHHCs enzymes, including ER-resident DHHC-1, 2,6,9,11,12,13,14,16,19,22, Golgi-resident DHHC-7,23 and membrane-resident DHHC-24. Control= Untransfected HEK cells. B) Mean data of endogenous TRPM7 palmitoylation after quantification of western-blot data. Overexpression of DHHCs palmitoyl transferases did not alter endogenous TRPM7 palmitoylation level. (n=9-12) C) Mean data of flot2 palmitoylation in overexpressed DHHC-PATs HEK293 cells. Flot2, the previously confirmed palmitoylation protein, serves as a standard for evaluating efficiency of Acyl-Rac assay. (n=9-12)

5.4.2 TRPM7 palmitoylation is decreased in DHHC5 KO cells

It is widely recognized that DHHC5, as one of the few cell-surface localized palmitoyl acyltransferases (PATs) has been involved in a series if physiological processes, especially in synaptic plasticity (Ohno et al., 2006, Brigidi et al., 2015). DHHC5 is stabilized at the synaptic membrane dependent on its association with postsynaptic density protein 95 (PSD-95) and Fyn kinase, although itself is not substrate of DHHC5 (Li et al., 2010). Interruption of

DHHC5/PSD-95/Fyn kinase complex would enhances the internalization of DHHC5 from spines to dendritic shafts where it binds and palmitoylates δ-catenin (Brigidi et al., 2014, Brigidi et al., 2015). Then recycling endosomes (Res) recruit DHHC5 to be re-trafficked back into spine synapses together with δ-catenin. In addition, dynamic surface membrane protein palmitoylation catalyzed by DHHC5 is fundamental for a novel form of endocytosis, massive endocytosis (MEND) trigged by large Ca transients (Hilgemann et al., 2013). Mitochondrial permeability transition pore (MPTP) transiently opened by calcium overload would release CoA into the cytoplasm, subsequently synthesizing acyl CoA by DHHC5 to palmitoylate surface membrane proteins (Hilgemann et al., 2013).

With widespread distribution in nervous system, Ca influx-dependent on TRPM7 is critical to synaptic vesicle endocytosis (Jiang et al., 2021). From our previous results, intracellular trafficking of TRPM7 in Golgi-Hook retention cell line after manipulating its palmitoylation with 2-BP suggested that TRPM7 palmitoylation promotes its trafficking from the Golgi to surface membrane. Meanwhile, palmitoylation of TRPM7 was reduced after biotin release compared to when it was held in the Golgi (Figure 4.9B), suggesting TRPM7 is de-palmitoylated in post-Golgi compartments. Therefore, we firstly assessed the contribution of DHHC5 acyltransferases to TRPM7's palmitoylation.

We used zDHHC5 knockout HEK cells which was generated by guide RNAs (gRNA) targeted against zDHHC5 provided by Horizon to evaluate the impacts of DHHC5 to TRPM7 palmitoylation (Gök et al., 2020).Comparison of palmitoylation of TRPM7 between DHHC5 KO cells and DHHC5 KO cells in which DHHC5 was overexpressed suggested that endogenous TRPM7 palmitoylation has been significantly enhanced by transient transfection of DHHC5 (*** $P<0.001$; Figure 5.3B). Therefore, we conclude that DHHC5 localized at cell surface membrane might be one of potential palmitoyl acyltransferases for TRPM7.

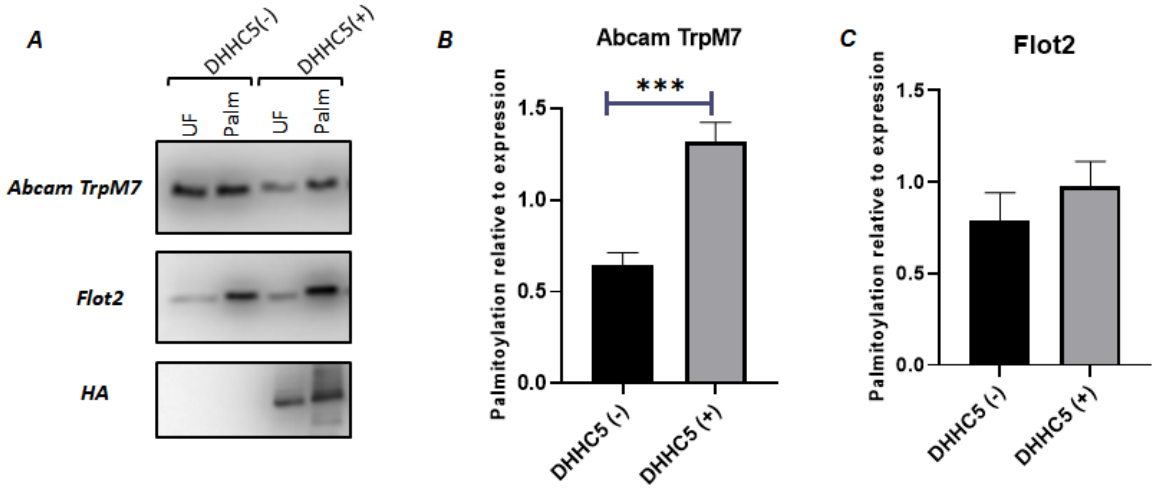

Figure 5.3 TRPM7 palmitoylation in DHHC5 KO cells.
A) Representative western-blot of endogenous TRPM7 palmitoylation in DHHC5 KO cells (-) and following re-expression of DHHC5 (+). DHHC5 was transiently transfected into KO cells 24 hours before lysis for 24 hours before measurement. (-): DHHC5 KO cells; (+) DHHC5 transfected DHHC5 KO cells. Transfection efficiency was confirmed with HA antibody (HA tag was fused on DHHC5) Flot2 as evaluation of acyl-RAC efficiency. B) Summary of imaging data of endogenous TRPM7 palmitoylation in DHHC5(-) cells and DHHC (+) cells. Endogenous TRPM7 palmitoylation was significantly increased after DHHC5 overexpressed ($P<0.001$, n=6). C) Mean data of Flot2 palmitoylation in absence (-)/presence (+) of DHHC5. There was no difference between flot2 palmitoylation levels confirming reliable acyl-RAC efficiency. (n=6)

5.4.3 Palmitoylation of TRPM7 after overexpression of surface-membrane resident DHHC-PATs

Palmitoylation of endogenous TRPM7 relative to its expression was inhibited in the DHHC5 KO cells compared to those transfected with DHHC5. In addition, we have already identified that the amount of TRPM7 trafficked to surface membrane was significantly reduced when we suppressed palmitoylation with broad-spectrum zDHHC-PAT inhibitor 2-bromopalmitate in Golgi-hook confined cells (section 4.4.4). In addition, experiments with non-palmitoylated chimaeras TRPM7-M2-YFP an TRPM7-M5-YFP suggested that palmitoylation is one of principal determinants of TRPM7 distribution in cells, and that palmitoylated TRPM7 was delivered to the surface membranes (section 4.4.8). We therefore investigated whether overexpressing selected surface membrane resident DHHC-PATs alters palmitoylation of TRPM7. According to the classification of localization of DHHCs, only a few of DHHC-PATs localized at plasma membrane which included DHHC-2, DHHC-5, DHHC-20, and DHHC-21 (Greaves et al., 2011, Ohno et al., 2006, Milnerwood et al., 2013). DHHC17 is a Golgi-resident PAT acting as a non-plasma membrane acyl-transferase control. We measured palmitoylation of TRPM7 (by immunoblotting for GFP) when it co-expressed with

those surface membrane-resident DHHC-PATs in engineered WT-TRPM7-YFP inducible cells derived from HEK-293 T-REX cells (Figure 5.4A). However, the statistical analysis suggested that none of those DHHC-PATs was able to significantly enhance palmitoylation of TRPM7 (Figure 5.4B). Flot2, as the well-known palmitoylated proteins revealed the reliable efficiency of Acyl-RAC assay (Figure 5.4C).

These results suggest that no surface-membrane localised DHHC-PATs palmitoylate TRPM7. The underlying reason might be TRPM7 has been sufficiently palmitoylated by endogenous DHHCs-PATs in HEK-derived 293 T-REx cell line. Compared to the circumstance of in absence of DHHC5, TRPM7's palmitoylation was not significantly facilitated in WT-TRPM7-YFP inducible cell line transfected with DHHC5. In conclusion, our experiments with DHHC5 KO cells indicate that when DHHC5 is absent, TRPM7 palmitoylation can be enhanced by over-expression of this enzyme. However, our experiments using overexpressed DHHC5 in HEK cells indicates that endogenous expression levels and activity of DHHC5 are not rate-limiting for TRPM7 palmitoylation.

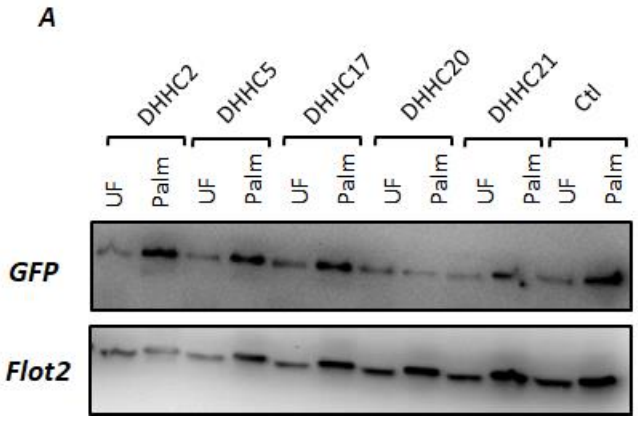

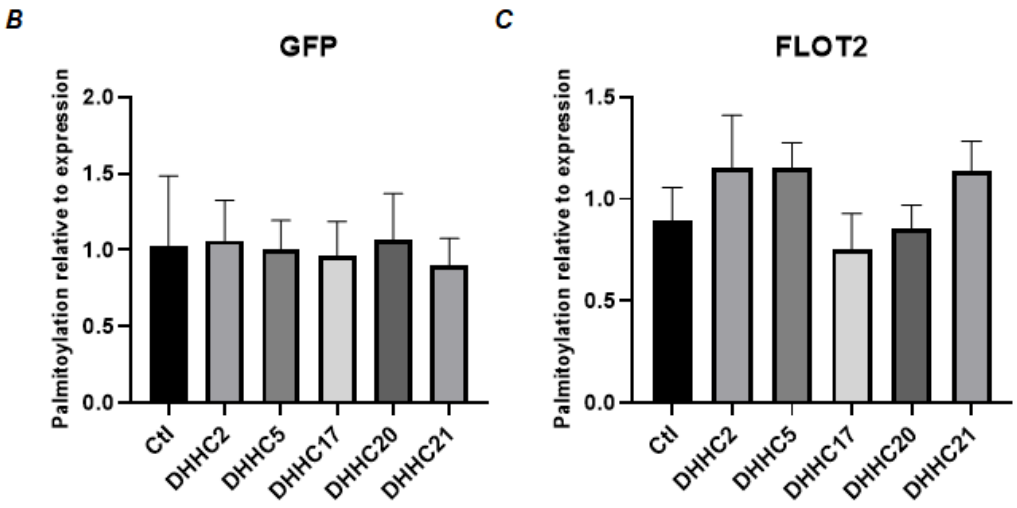

Figure 5.4 Palmitoylation of TRPM7by surface membrane-resident DHHC-PATs enzyme overexpressed WT-TRPM7-YFP stable cells.
A) Representative western-blot of palmitoylation of TRPM7 in WT-TRPM7-YFP stable cells transfected with membrane-resident DHHC-PATs, including DHHC-2, -5, -20, -21, and Golgi-resident DHHC17. WT-TRPM7-YFP stable cells was treated with tetracycline for 24 hours. GFP antibody was used to detect TRPM7. Control= WT-TRPM7-YFP stable cells with tetracycline induced only. B) Summary imaging data of TRPM7 palmitoylation in WT-TRPM7-YFP stable cells transfected with membrane-resident DHHC-PATs. None of those DHHCs increased TRPM7 palmitoylation significantly (n=4-6). C) Summary imaging data of Flot2 palmitoylation between DHHCs transfected WT-TRPM7-YFP stable cells and control group (n=4-6). Flot2 is the standard for evaluating Acyl-Rac assay efficiency.

5.4.4 zDHHC17 palmitoyl-transferase palmitoylates TRPM7

Recently, a high-resolution proteomic characterization of TRPM7 identified palmitoyl acyltransferase zDHHC17 as a putative interaction partner (Kollewe et al., 2021a). DHHC17 (PAT HIP14) is mainly enriched in brain as well as primarily localized to Golgi and to palmitoylate a series of synaptic substrates including PSD-95 (postsynaptic density-95), GAD-65, SNAP-25 (synaptosome-associated protein 25), Synaptotagmin and Huntingtin (HTT) in mammalian neurons (Singaraja et al., 2002). Alongside Golgi localization, DHHC17 also exists in presynaptic terminals and some of them co-localized with a synaptic vesicle marker (Stowers and Isacoff, 2007).

zDHHC17 contains an ankyrin repeat (AR) domain in its cytosolic N-terminus which is involved in numerous interactions including facilitating substrate recruitment for S-acylation and participating in S-acylation-independent activity (Lemonidis et al., 2015, Yang and Cynader, 2011). To date, zDHHC17 has been proved to recruit and subsequently S-acylate several neuronal proteins such as SNAP25 (Lemonidis et al., 2014) and HTT (Huang et al., 2011) via zDHHC ankyrin repeat-binding motif sequences (zDABM) consensus (VIAP)(VIT)XXQP in these

substrates (Lemonidis et al., 2015). The final proline in this motif is constant and indispensable to the interaction with zDHHC17 ankyrin repeats (Lemonidis et al., 2015, Verardi et al., 2017). Lemonidis et al constructed a position-specific scoring matrix (PSSM) to identify zDABM sequences in human proteins using Scansite 3 (Lemonidis et al., 2017). The six highest scoring matches to the zDABM in TRPM7 are separately P586, P26, P1131, P21, P1068 and P769 (Table 5.2). We excluded P1068 because it is extracellular and P26 and P21 because peptide arrays demonstrated that neighboring amino acid D (in position 25) and I (in position 20) are strongly disfavored immediately N-terminal to the zDABM proline (Lemonidis et al., 2017). Therefore, we evaluated whether P586, P769 or P1131 are critical to TRPM7 palmitoylation. These three residues reside in regions of TRPM7 that are either disordered or were not resolved in its cryoEM structure (Duan et al., 2018), but they are all surface exposed therefore may engage in protein interactions. Tryptophan is strongly disfavoured in most positions in the zDABM (Lemonidis et al., 2017) so we generated the mutants P586W, P769W and P1131W of TRPM7. From Figure 5.5, palmitoylation of TRPM7 was significantly reduced in P769W and P1131W mutants (but not P586W) compared to wild type TRPM7 (**P<0.01 and ***P<0.001; n=4-6). We therefore conclude that zDHHC17 mediates palmitoylation of TRPM7 and therefore sorting of TRPM7 delivery or trafficking in the Golgi.

Table 5.2. Potential zDHHC17 binding motif on TRPM7.
Top six position in TRPM7 based on Scansite in Lemonidis et al (Lemonidis et al., 2017).

Scansite Score	Modified z-score	SwissProt ID (2011_11)	Pro position	Peptide	Comments
0.8609	4.797	TRPM7_HUMAN	P586	HFIKTAQpYRPKIDT	Include.
1.138	3.140	TRPM7_HUMAN	P26	IIPSSKDpHRCLPGC	'D' strongly disfavoured next to P
1.1609	3.003	TRPM7_HUMAN	P1131	EKPVLPPpLIILSHI	Include.
1.2109	2.704	TRPM7_HUMAN	P21	RECVYIIpSSKDPHR	'I' strongly disfavoured next to P
1.2479	2.483	TRPM7_HUMAN	P1068	VIPQICGpGTWLTPF	Extracellular
1.2572	2.427	TRPM7_HUMAN	P769	ILSILVPpAILLLEY	Include.

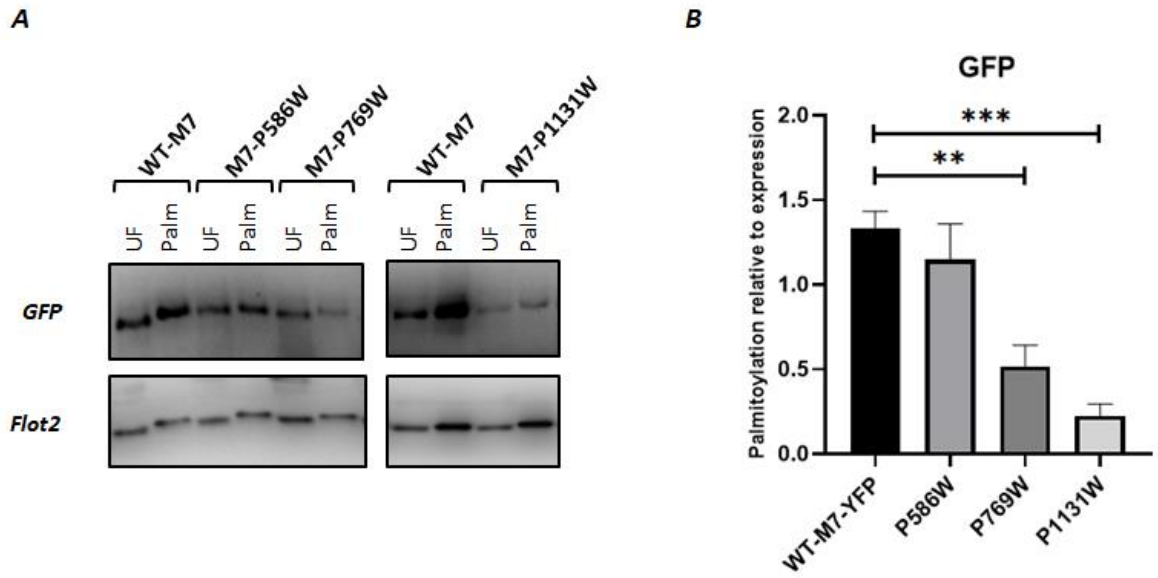

Figure 5.5 zDHHC17 is a candidate palmitoyl-transferase for TRPM7.
A) Representative western-blot of wild type (WT) TRPM7-YFP and selected potential zDHHC17 ankyrin repeat (AR)-binding motif (zDABM) mutants in transfected HEK cells. UF: unfractionated cell lysate; Palm: purified palmitoylated proteins. B) Relative enrichment of TRPM7-YFP in the palmitoylation assay. **:P<0.01 ***:P<0.001 compared to WT-TRPM7-YFP. one-way ANOVA followed by post-hoc Dunnett's multiple comparisons test (n=4-6).

5.4.5 Impacts of de-palmitoylating amphiphile compounds on palmitoylation of TRPM7 in VSMCs

As protein palmitoylation is a reversible process, the rates of palmitoylation and de-palmitoylation can vary widely among protein types, from minutes to hours. It is increasing acknowledged that S-palmitoylation turns over rapidly in minutes for certain proteins, allowing proteins to be facilely shuttled between the plasma membrane and cytoplasmic compartments like lysosome and Golgi apparatus to execute many cellular functions (Martin et al., 2012, Zhang et al., 2010, Guan and Fierke, 2011). Currently, there are three classes of identified protein thioesterases, separately the acyl-protein thioesterases (APTs) (Vartak et al., 2014), the α/β hydrolase domain-containing 17 proteins (ABHD17s) (Lin and Conibear, 2015), and the palmitoyl-protein thioesterases (PPTs) (Vesa et al., 1995).

As the number of investigations into protein palmitoylation has increased, more and more palmitoylation and de-palmitoylation inhibitors have been identified. However, methods for remodeling of protein lipidation are limited in vivo because the palmitoylation inhibitor cannot cleave the palmitoyl groups from currently lipidated proteins and some reagents irreversibly inhibit several enzymes involved in lipid biosynthesis (Yeste-Velasco et al., 2015). For example,

The most commonly used palmitoylation inhibitor 2-bromopalmiytate (2-BP) not only widely inhibited the DHHC-PATs activity in vivo but also inhibit APT1 and APT2 enzymatic activities in vitro through uncompetitive mechanism (Pedro et al., 2013). Another similar covalent pan-DHHC inhibitor with an acrylamide warhead, PATi, has been reported, which possesses more potency as well as less toxicity and inhibition for S-acylation thioesterases than 2-BP (Azizi et al., 2021). In contrast, a novel de-palmitoylation compounds have been recently designed by Rudd A K et al (Rudd et al., 2018), Amphiphile-mediated de-palmitoylation (AMD) compound which directly cleaved S-palmitoylated groups from endogenous proteins using an approach that is harmless to the rest of the protein (Figure 5.6). Its structure is based on the native chemical ligation (NCL) (Dawson et al., 1994) between N-terminal cysteines with thioesters, specifically a small, membrane-anchored, cysteine-containing amphiphile compound which could react with lipidation under physiological conditions spontaneously and rapidly (Brea et al., 2016). These reagents have already proved the efficiency of cleavage of AMD from the native GTPase HRas and successfully de-palmitoylate mis-localised proteins in an infantile neuronal ceroid lipofuscinosis (INCL) disease model (Rudd et al., 2018).

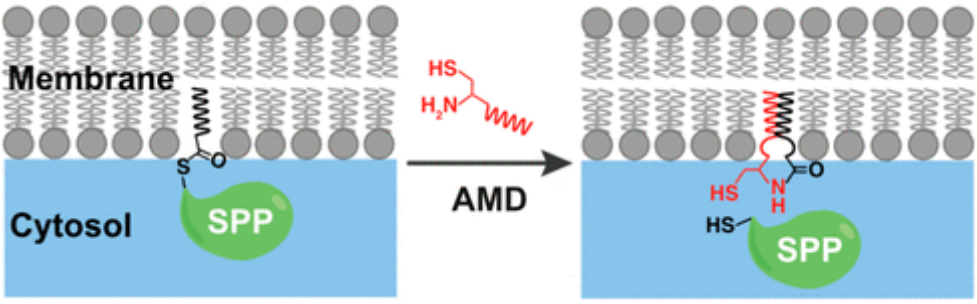

Figure 5.6 Diagram of Amphiphile-mediated de-palmitoylation (AMD) function (Rudd et al., 2018).
Schematic of de-palmitoylating of S-palmitoylated protein (SPP) by AMD which allows releasement of palmitoyl groups as well as it is nondestructive toward the remained protein.

We investigated whether AMD could serve as an efficient de-palmitoylation compound for TRPM7. We applied AMD-7 with two different concentrations on rat vascular smooth muscle cells (rVSMCs), 10μM and 50μM, and made comparison with traditional pan-palmitoylation inhibitors, 2-BP and PATi (all treatment for 7 hours). From Figure 5.7, Both broad-spectrum zDHHC-PAT inhibitor 2-BP and PATi significantly diminished palmitoylation of endogenous

TRPM7 (**P<0.01 and *P<0.05, n=4-5). However, the Amphiphile-mediated de-palmitoylation 7 (AMD7) did not successfully de-palmitoylate TRPM7 in rVSMCs. It suggested that AMD7 may not selectively de-palmitoylate endogenous TRPM7. Other experiments in the Fuller lab found that AMD7 effectively de-palmitoylated singly palmitoylated proteins such as NCX1, but not multiply palmitoylated proteins such as caveolin 3. The acyl-RAC assay cannot distinguish between multiply and singly palmitoylated proteins, so it is possible that TRPM7 was partially de-palmitoylated in these experiments.

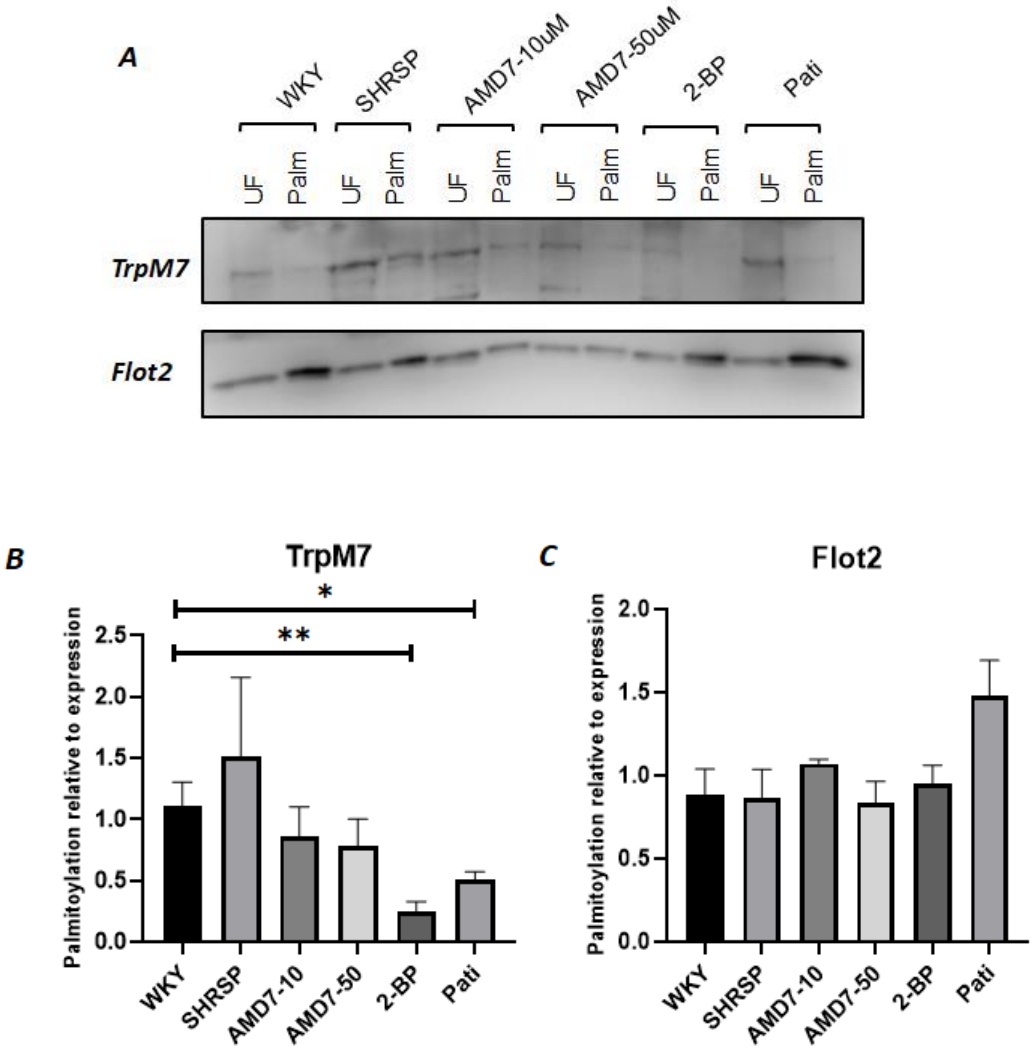

Figure 5.7 Impacts of de-palmitoylation compounds on palmitoylation of endogenous TRPM7 in rat vascular smooth muscle cells (rVSMCs).
A) Representative western-blot of endogenous TRPM7's palmitoylation in VSMCs with treatments of different de-palmitoylated compounds for 7 hours. WKY: Wistar Kyoto rat; SHRSP: Spontaneously Hypertensive Stroke Prone Rat. 2-BP was used 100μM and Pati was used 20μM. AMD7 was used 10μM and 50μM separately. B) summary of mean data of endogenous TRPM7's palmitoylation among different groups. 2-BP and Pati has significantly decreased palmitoylation of TRPM7 (**P<0.01 and *P<0.05; n=4-5). Two-tails unpaired t-test was applied. C) summary of mean data about palmitoylation of Flot2 in VSMCs with different de-palmitoylated compounds treatments (n=5-6).

5.4.6 Influence of changes in Mg levels on TRPM7 palmitoylation

Accumulating research demonstrates TRPM7 serves as a regulator in Mg homeostasis, however, increased intracellular free Mg inhibits ion channel activity. As we previously mentioned, there is a general consensus that TRPM7 ion channel is suppressed or de-activated in response to free intracellular Mg or Mg-nucleotide complexes (Nadler et al., 2001). Specifically, the nucleotide-dependent regulation of TRPM7 relies on the nucleotide binding site in the intrinsic kinase, which interacts synergistically with Mg binding site extrinsic to that domain (Demeuse et al., 2006). From the Cryo-EM structure of TRPM7 raised by Duan et al (Duan et al., 2018), the selectivity filter of TRPM7 is formed by the backbone carbonyls of Phe1045/Gly1046 AND Glu1047s side chain and the structure of this filter has no difference in the presence of EDTA or high [Mg]. however, in the TRPM7-Mg structure, a nonprotein density that they speculate Mg was identified with two hydration shells.

Since TRPM7 ion channel is regulated by [Mg]i, we questioned whether alterations of extracellular Mg levels might influence endogenous TRPM7 palmitoylation status. We conducted measurement of palmitoylation of endogenous TRPM7 in HEK293 cells after supplementing with external MgCl2 or chelator ethylenediaminetetraacetic acid (EDTA) for two different durations, 1 hour and 3 hours separately. Interesting, incubation extracellular Mg (5mM) and EDTA (3mM) for 1 hour had no effects on TRPM7 palmitoylation, but incubation for 3 hours both lead to its suppression (**P<0.01 and ***P<0.001; n=4-6) (Figure 5.8B, C). This suggests that inhibition of TRPM7 palmitoylation in response to circumstance of Mg supplement/withdrawal required long duration in HEK cells. Besides, Nadler et.al (Nadler et al., 2001) also proposed that high concentration of divalent cation would block the channel pore. Meanwhile, previous research identified that high extracellular magnesium could decrease the levels of TRPM7 by activation of calpains whereas the low extracellular magnesium would stimulate TRPM7 accumulation as well as promoting endothelial dysfunction (Baldoli et al., 2013). At the time these experiments were conducted we lacked knowledge regarding the influence of altering palmitoylation of TRPM7 in Mg conduction (details in 4.4.11.1). Therefore, either the conformation adopted by TRPM7 in the presence of EDTA or Mg is more readily de-palmitoylated / less readily palmitoylated, or the activities of the palmitoylating or de-

palmitoylating enzymes are influenced by cellular Mg levels still need further investigation.

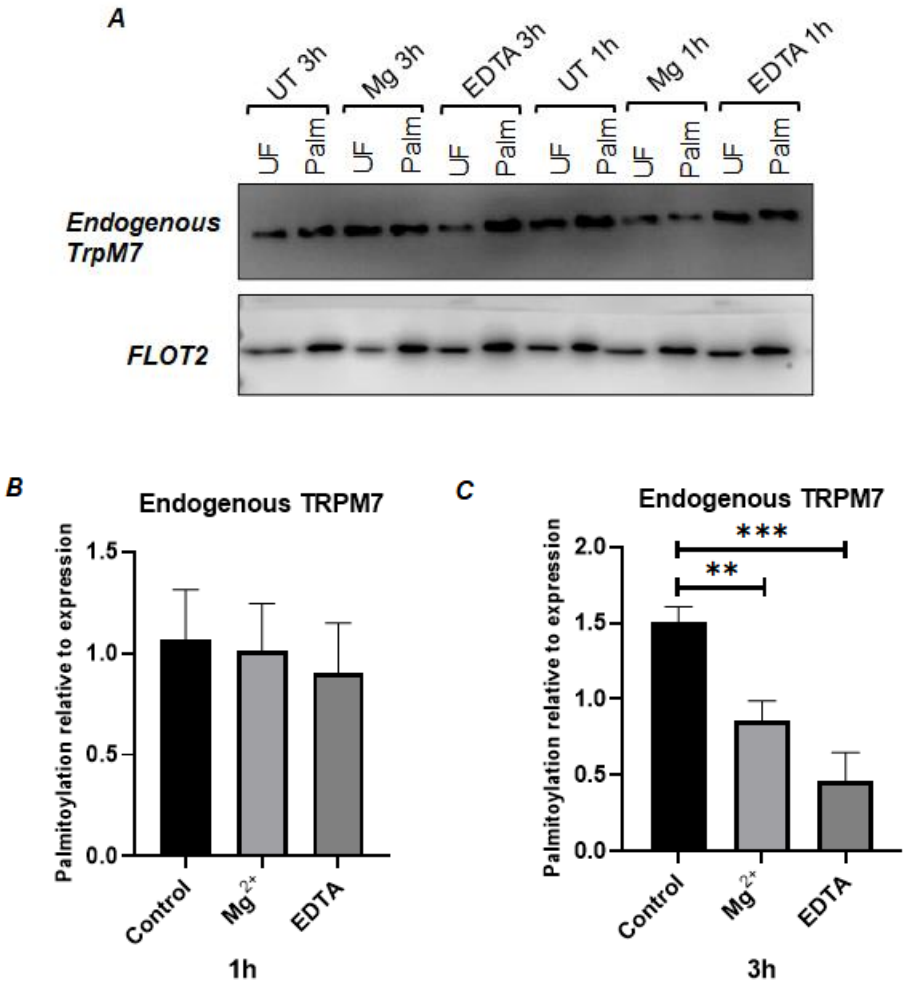

Figure 5.8 Endogenous TRPM7 palmitoylation of Mg supplement and withdrawal in HEK293 cells.
A) Representative western-blot of endogenous TRPM7 palmitoylation in HEK293 cells with supplements of 5mM MgCl2 and 3mM EDTA separately for 1 hour and 3 hours. Control group was untreated HEK293 cells. B, C) Summary imaging data if endogenous TRPM7 palmitoylation levels of Mg supplement or withdrawal in HEK293 cells incubating for 1hour and 3 hours. There was no significant difference of TRPM7 palmitoylation between Mg supplement/withdrawal and untreated HEK cells. However, incubation of 5mM Mg supplement and 3mM EDTA for 3 hours both reduced the endogenous TRPM7 palmitoylation ($P<0.01$ and $P<0.001$). One-way ANOVA with Tukey's multiple comparisons test (n=4-6).

5.4.7 EGF, VEGF and aldosterone effects on palmitoylation of TRPM7 in vascular smooth muscle cells (VSMCs)

Accumulating evidence illustrate that TRPM7 exerts critical physiological functions in vascular smooth muscle cells (VSMCs) (He et al., 2005). For instance, TRPM7 is widely expressed in endothelial cells isolated from the umbilical vein (HUVEC), where TRPM7 levels were increased following exposure to oxidative stress generated by the addition of hydrogen peroxide (Baldoli et

al., 2013). TRPM7 plays an important Mg-dependent role in VSMCs proliferation in response to vasoactive agents such as epidermal growth factor (EGF) or angiotensin II (Ang II) (Montezano et al., 2008) and overexpression of TRPM7 is proposed to impair endothelial function (Baldoli et al., 2013). In addition, Angiotensin II (Ang II) and aldosterone upregulates TRPM7 plasma membrane expression(He et al., 2005, Valinsky et al., 2016) and the TRPM7 kinase domain has been proposed to be involved in Ang II-induced hypertension (Antunes et al., 2016). Aldosterone, a steroid hormone with mineralocorticoid activity, regulates renal ion handling and conduction through the mineralocorticoid receptor (MR) and mediates tissue remodeling, inflammation, and fibrosis(Cat and Jaisser, 2012, Montezano et al., 2008, Nguyen Dinh Cat et al., 2011). Meanwhile, a non-genomic signalling pathway of aldosterone upregulates c-Src signaling pathway and MAPKs activation in spontaneously hypertensive rat (SHR) (Grossmann and Gekle, 2007). This suggests that aldosterone-induced VSMC proliferation is a consequence of rapidly inducing ERK1/2 signaling through c-Src which is an established activator of epidermal growth factor (EGF) receptor (Callera et al., 2005). Additionally, recently research about the mechanism of Aldosterone signaling revealed that TRPM7 is involved (Yogi et al., 2013). Specifically, aldosterone stimulates Mg influx and NAPDH oxidase activity in a TRPM7 kinase-insensitive manner but modulate inflammatory responses in a TRPM7 α-kinase-sensitive way.

Clearly, the roles of TRPM7 in VSMCs include modulation of Mg homeostasis (He et al., 2005),vascular endothelial cell growth and proliferation(Baldoli and Maier, 2012, Inoue and Xiong, 2009), adhesion(Su et al., 2006). We therefore investigated whether TRPM7 palmitoylation in VSMCs was altered in respond to extracellular stimulation of EGF, VEGF and Aldosterone. Among those three factors, aldosterone reduced approximately 63% palmitoylation of endogenous TRPM7 compared to untreated WKY VSMCs but without significant difference (Figure 5.9). Furthermore, epidermal growth factor (EGF) and vascular endothelial growth factor (VEGF) had no influence on TRPM7 palmitoylation (n=5). We therefore conclude that although emerging evidence indicates that EGF and VEGF regulates VSMCs through TRPM7-dependent manner involving receptor tyrosine kinase (RTK) mediated pathway in vascular function (Zou et

al., 2019), it had no influence on palmitoylation levels of TRPM7 in vascular smooth muscle cells (VSMCs).

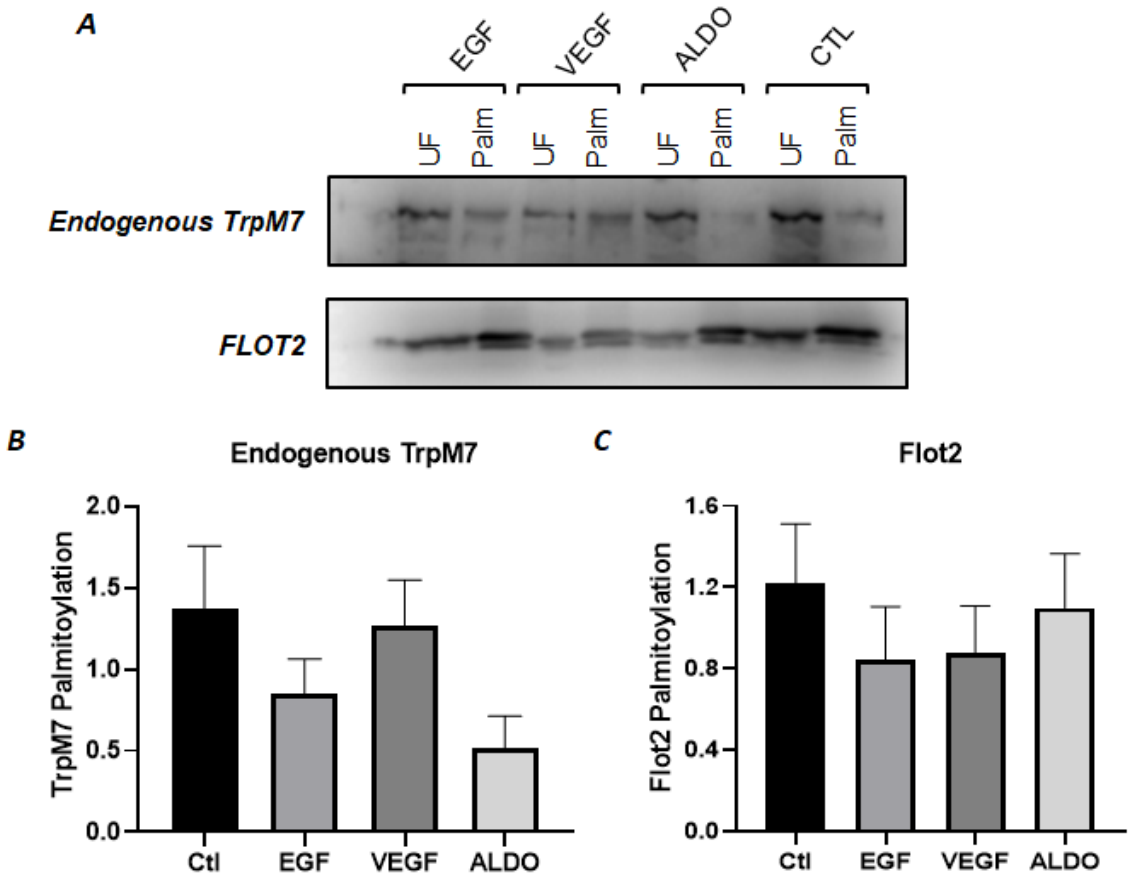

Figure 5.9 Palmitoylation of TRPM7 in vascular smooth muscle cells (VSMCs) isolated from Wistar Kyoto rat (WKY).
A) Representative western-blot of palmitoylation of endogenous TRPM7 in VSMCs. EGF, VEGF (50ng/ml) and Aldosterone (100nM) treated for 30 mins before harvesting for Acyl-Rac. Flot2 as a standard for evaluating the efficiency of Acyl-Rac assay. B, C) Summary of imaging data of palmitoylation of endogenous TRPM7 and Flot2 in VSMCs. TRPM7's palmitoylation was diminished by Aldosterone but without significant difference. One-way ANOVA followed by Dunnett's t-test. Flot2 was equally palmitoylated in all groups. (n=5).

5.4.8 EGF, VEGF and aldosterone have no effects on TRPM7 distribution in HEK293 cells

It has been demonstrated that EGF actives EGFR signalling and enhances the abundance of TRPM6 in plasma membrane via translocation from cytosol in kidney cells through the action of Src tyrosine kinases (Thebault et al., 2009). Aside from palmitoylation status of endogenous TRPM7 in VSMCs, we also investigated EGF, VEGF and Aldosterone effects on TRPM7 distribution in HEK 293 cells after two different treatment durations, separately 30 minutes for short one and 18 hour for long one. However, there was no significant difference

TRPM7 abundance on plasma membrane after treatment of EGF, VEGF and aldosterone neither after 30min or 18h (Figure 5.10B). Na pump was used as a housekeeping protein localized on plasma membrane and subcellular compartments and GAPDH was used as a cytoplasmic protein. The distribution of neither protein changed in any treatment group (Figure 5.10A, C). In conclusion, EGF, VEGF and aldosterone have no influence on TRPM7 abundance on cell surface. However, the crosstalk of signalling pathway between receptor tyrosine kinases (RTKs) and TRPM7 requires further investigation.

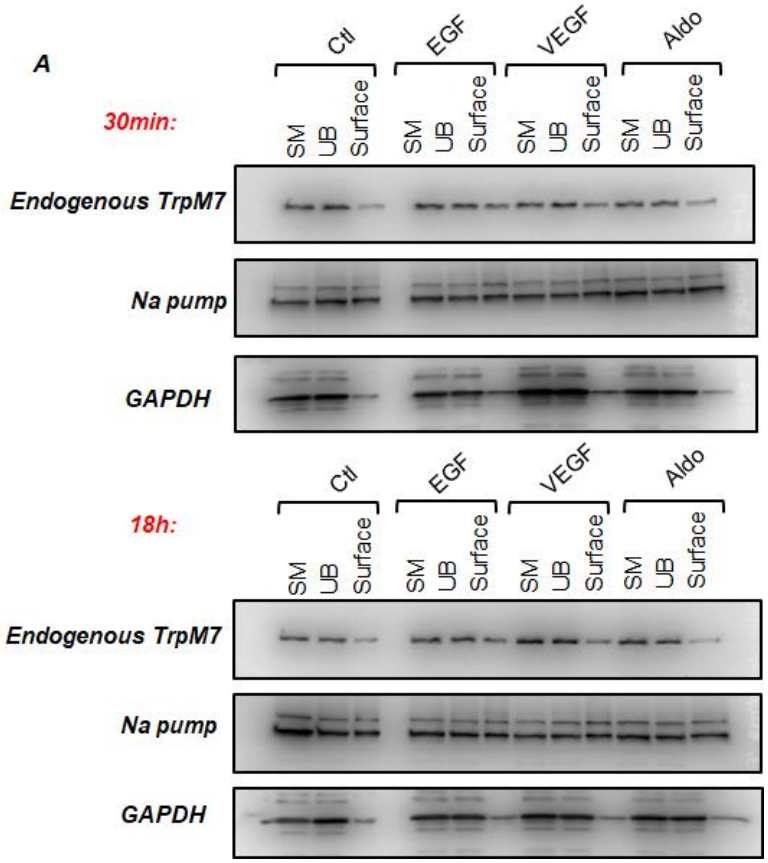

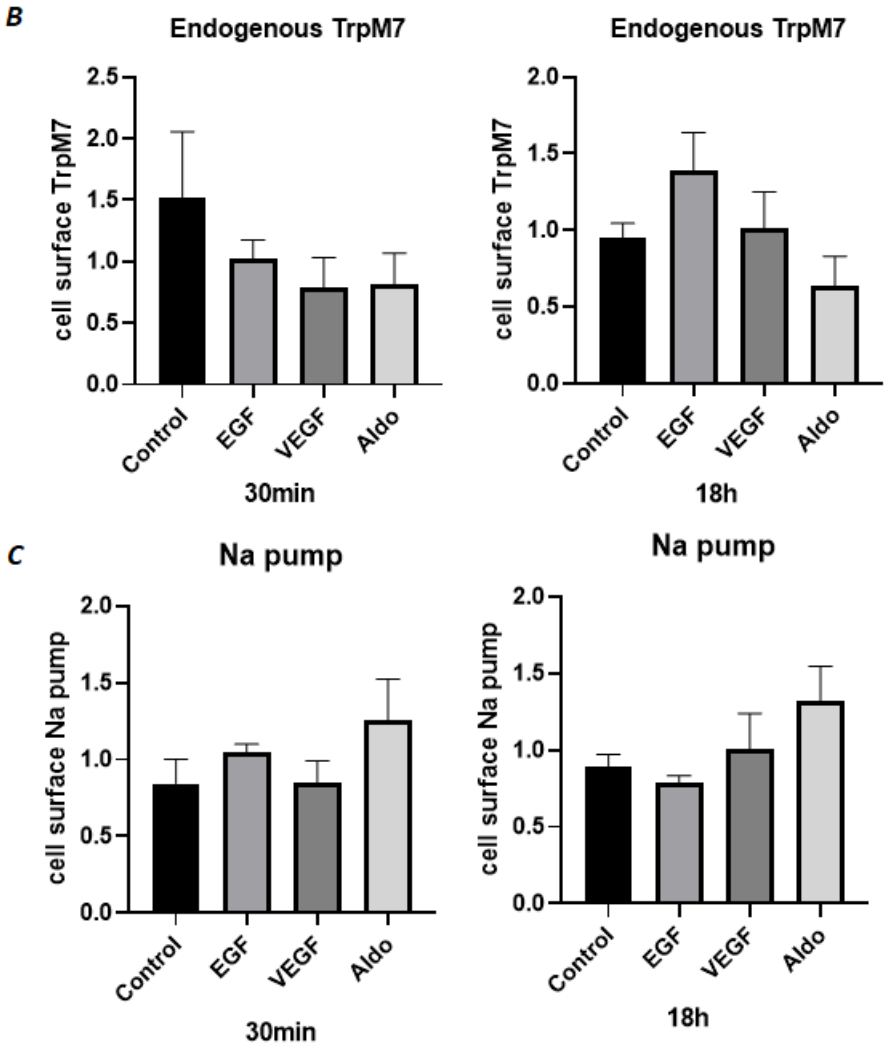

Figure 5.10 Cell surface biotinylation of HEK293 cells treated with EGF, VEGF and Aldosterone.
A) Representative western-blot of cell surface biotinylation on HEK cells treated with EGF, VEGF and Aldosterone for 30mins and 18 hours separately (EGF/VEGF= 50ng/ml and Aldosterone= 100nM). SM= unfractionated materials; UB=unbound materials; Surface=enriched cell surface protein by Streptavidin beads. Na pump was used as a cell standard protein of translocase on plasma membrane and GAPDH was served as a cytoplasmic protein. B) Summary of quantification of imaging data of cell surface localized endogenous TRPM7 after treatment with EGF, VEGF and Aldosterone (30mins and 18 hours). Neither of those growth factor nor Aldosterone changed endogenous TRPM7 distribution in HEK cells. (n=4-6) C) Summary of imaging data of cell surface-resident Na pump after treatment with EGF, VEGF and Aldosterone for 30mins and 18 hours separately (n=3-4).

5.4.9 EGF Signalling pathways with WT-TRPM7 and non-palmitoylated inducible stable cells

EGF binding epidermal growth factor receptor (EGFR) and its ligands serve as critical regulators in multiple cellular processes (Makki et al., 2013). Activation of EGFR leads to autophosphorylation at the key tyrosine residues, which has been implicated in numerous downstream signalling cascades such as Src family kinase and mitogen activated protein (MAP) kinase (Tomas et al., 2014). As we

mentioned before, TRPM7 also controls Mg homeostasis and mitogenic signalling in VSMCs. A signalling pathway between TRPM7 and EGF identified by Zou et.al (Zou et al., 2020) defined a novel signalling cascade linkage between EGF/EGFR and TRPM7 (Figure 5.11). Specifically, c-Src activation triggered by EGFR activation is required for TRPM7 phosphorylation and expression which subsequently contributes to physical interaction of EGFR and TRPM7 in the cell membrane and activation of ERK1/2 signalling pathway to promote VSMC proliferation and migration. In addition, EGF/EGFR induces phosphorylation of TRPM7 (Ser 1151) which is critical to Mg levels in VSMCs (Zou et al., 2020).

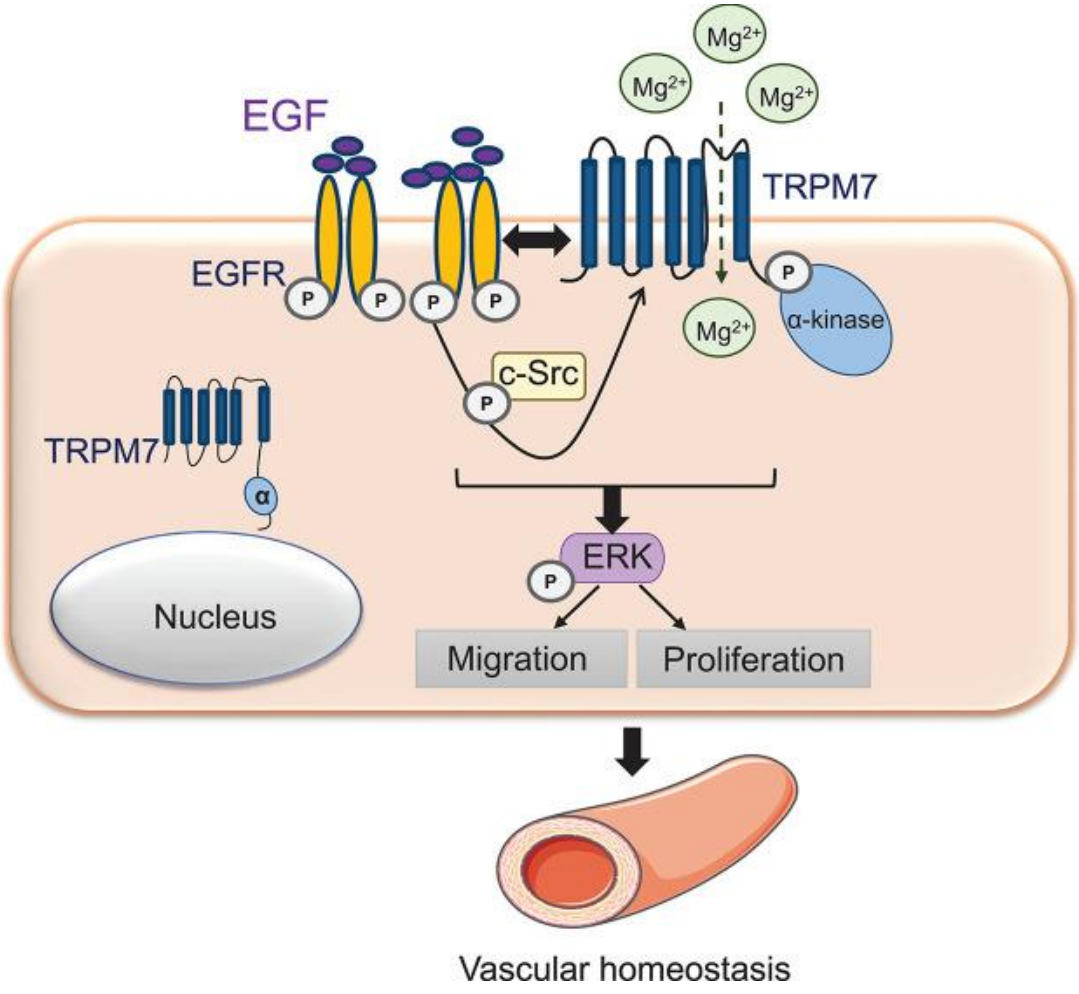

Figure 5.11 Schematic diagram demonstrating the novel signaling pathway involving EGFR − TRPM7 interaction in VSMCs (Zou et al., 2020).
TRPM7 is signaling target of EGF and EGFR and TRPM7 physically associated at cell membrane in a c-Src dependent manner. EGF/EGFR/c-Src signaling promotes VSMCs proliferation and migration through TRPM7-regulated ERK1/2 dependent processes.

Therefore, we explored the impacts of palmitoylation of TRPM7 on its signalling crosstalk with EGFR. We treated inducible cell lines expressing WT-TRPM7-YFP, non-palmitoylated TRPM7-M2-YFP and TRPM7-M5-YFP with EGF (50ng/ml for

30min) to make comparison. In the absence of EGF, phosphorylation of TRPM7 relative to its total expression (GFP for immunoblotting) was significantly decreased in cell expressing non-palmitoylated TRPM7-M2-YFP and TRPM7-M5-YFP cells (Figure 5.12B). EGF enhanced TRPM7 phosphorylation in cells expressing WT TRPM7 and M7-M5 TRPM7, but not M7-M2 TRPM7 (Figure 5.12C). EGF-induced phosphorylation of TRPM7 was significantly blunted in cells expressing TRPM7-M2. Surprisingly, there was only significant difference in phosphorylation of TRPM7 after treatment with EGF between WT-TRPM7-YFP and non-palmitoylated TRPM7-M2-YFP cells (Figure 5.12C). ERK1/2 are the downstream of EGFR activation and TRPM7 (Figure 5.12A, D). Erk1/2 phosphorylation was significantly increased after addition of EGF, but EGF-induced Erk phosphorylation was not different between cells expressing WT TRPM7 and the two non-palmitoylated mutants.

According to Zou et.al, research, TRPM7 has been identified co-localized with EGFR on cell membrane in VSMCs (Zou et al., 2020). We suggest the reduced phosphorylation of TRPM7 in TRPM7-M2-YFP And TRPM7-M5-YFP might be a consequence of lower abundance of TRPM7 on plasma membrane when it is not palmitoylated. But the following downstream signalling of ERK1/2 expression and phosphorylation was not affected by TRPM7 palmitoylation levels.

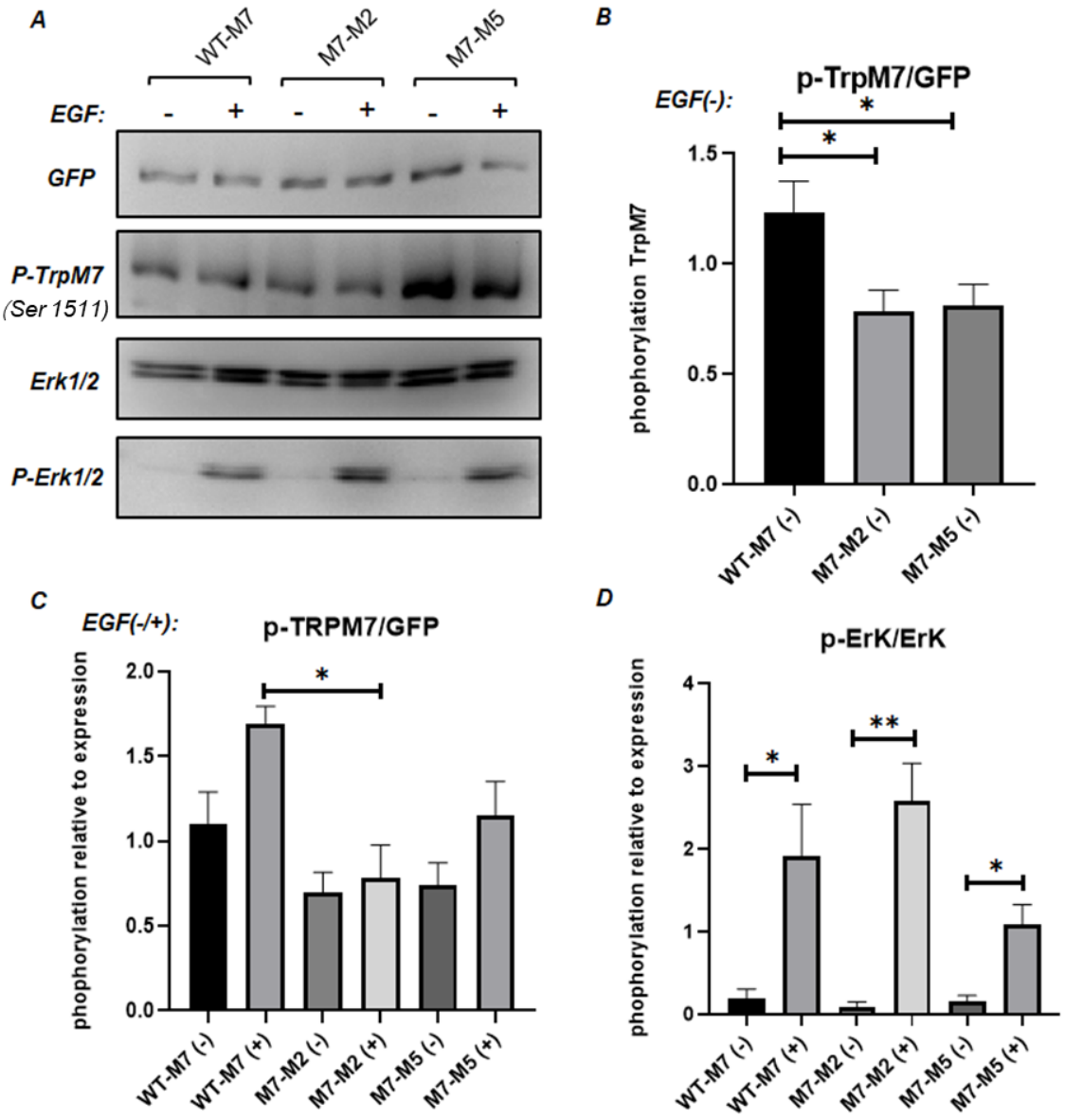

Figure 5.12 EGF signaling pathway in WT-TRPM7 and non-palmitoylated (TRPM7-M2 and TRPM7-M5) stable cells.

A) Representative western-blot of phosphorylated TRPM7 (p-TRPM7) and phosphorylated Erk1/2 (p-Erk1/2) levels in EGF stimulated TRPM7 stable cells. EGF (50ng/ml) treated for 15 minutes. GFP antibody was used for detecting total TRPM7 expressed in cell lysate. B) summarizing images data of quantifying phosphorylation TRPM7 relative to its expression among stable cell line. In comparison to the WT-TRPM7, non-palmitoylated TRPM7 (TRPM7-M2&TRPM7-M2) was less phosphorylated. (*P<0.05, n=10) C) Summarizing quantification data of EGF (-/+) stimulated p-TRPM7 levels in stable cells. EGF promotes TRPM7 phosphorylation slightly in all stable cells but without significant difference. P-TRPM7 stimulated by EGF was distinctly inhibited in TRPM7-M2 non-palmitoylated mutant cells but not in TRPM7-M5 (*P<0.05 n=4-5). D) summarizing images data of P-Erk1/2 levels among TRPM7 cell lines, with or without EGF treatment. Erk1/2 phosphorylation was induced by EGF in all stable cells (*P<0.05, **P<0.01, n=5). However, EGF-mediated Erk1/2 phosphorylation has no difference in WT-TRPM7 and non-palmitoylated TRPM7-M2/TRPM7-M5 stable cells.

5.4.10 Relationships between TRPM7 palmitoylation and phosphorylation

Phosphorylation is a critical post-translational modification (PTM) of TRPM7. Accumulating evidence has revealed the signalling mechanisms in which TRPM7 is implicated. Its kinase domain acts as a cellular sensor of physical and chemical stimuli such as mechanical stretch, oxidative stress, cell volume or osmotic gradient and alteration of extracellular/cytosolic pH, and triggers changes in ion channel activity and mitogen- and cytokine-induced signalling pathways (Yee et al., 2014). TRPM7 kinase domain auto-phosphorylates at multiple sites (Kim et al., 2012) and phosphorylates various substates such as annexin1 (Dorovkov et al., 2011), myosin IIA (Clark et al., 2008a), calpain II (Su et al., 2006), and PLCγ2 (Deason-Towne et al., 2012), allowing it to participate in numerous RTK signalling pathways modulate essential physiological responses and epigenetic modifications (Krapivinsky et al., 2014). Meanwhile, TRPM7 has been discovered co-localized with EGFR at cell membrane and EGFR-mediated c-Src activation is required for TRPM7 phosphorylation (Zou et al., 2020).

Since palmitoylation controls TRPM7 localisation in the cell, we investigated the association between palmitoylation and phosphorylation in TRPM7 after inducing expression of TRPM7 for 24hr and 48hr by tetracycline. To explore whether these PTMs interact with each other, we measured the phosphorylation levels in palmitoylated TRPM7 (phosphor-specific- immunoblotting for TRPM7) in samples prepared by acyl-RAC from WT-TRPM7-YFP, non-palmitoylated TRPM7-M2-YFP and TRPM7-M5-YFP inducible cells (Figure 5.13A). Specifically, we evaluated the enrichment of phosphorylated TRPM7 in the palmitoylation assay. Statistical analysis illustrated that total and phosphorylated TRPM7 were identically enriched in the palmitoylation assay from WT, M2-M5 and M2-M7 TRPM7 expressing cell lines. Furthermore, compared to WT-TRPM7-YFP, enrichment of the phosphorylated form of TRPM7 in the acyl-RAC assay was significantly attenuated in non-palmitoylated TRPM7-M5-YFP and TRPM7-M2-YFP inducible cells (****$p<0.0001$, $n=4$) (Figure 5.13B, C). In the acyl-RAC reactions, the phosphorylated form of TRPM7 was equally enriched in compared to total TRPM7 in all cell lines (Figure 5.13D). To conclude, this suggests phosphorylation and palmitoylation in TRPM7 are more likely two independent post-translational modification rather than competitive relationship.

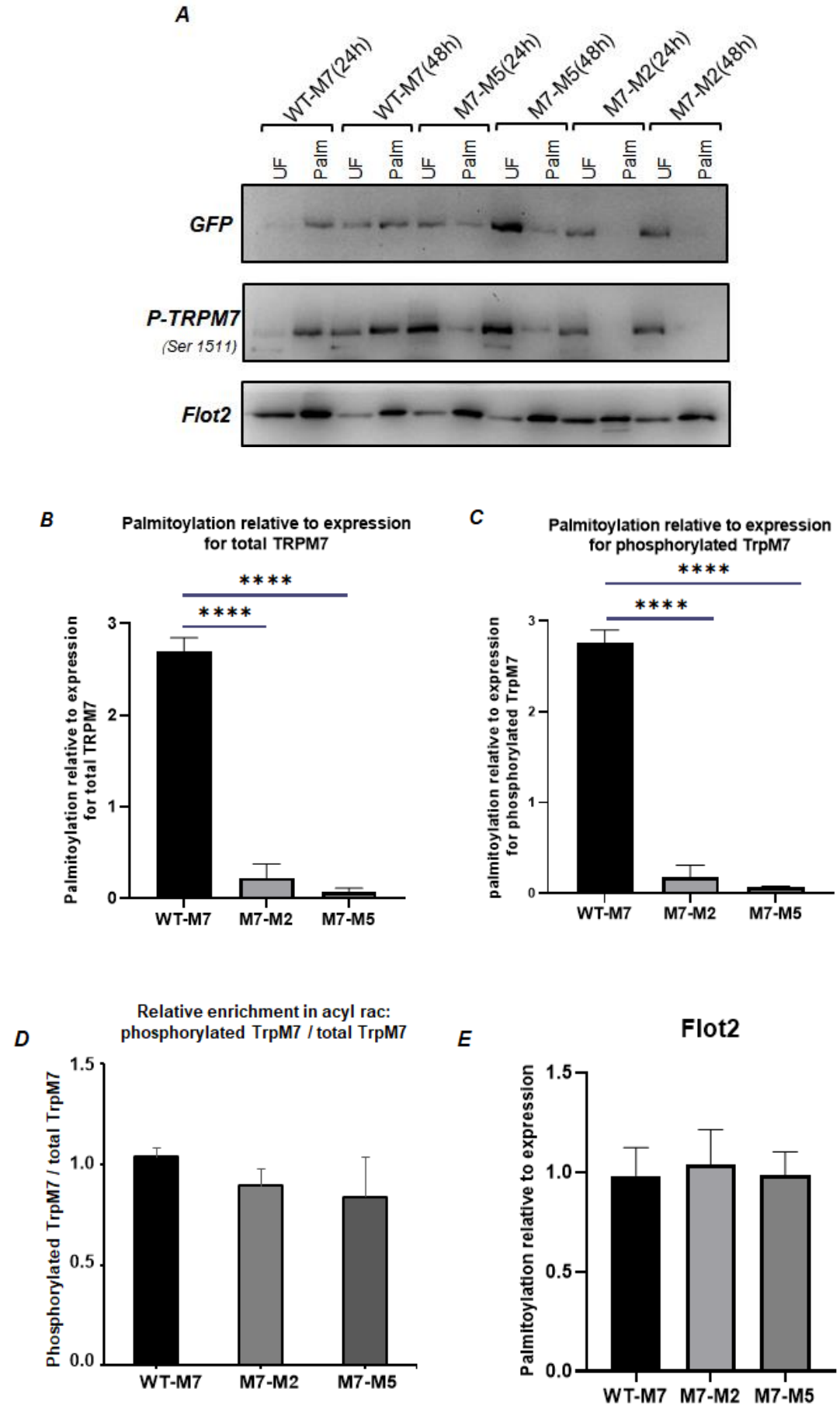
A
WT-M7(24h)
WT-M7(48h)
M7-M5(24h)
M7-M5(48h)
M7-M2(24h)
M7-M2(48h)
UF
Palm
GFP
P-TRPM7
(Ser 1511)
Flot2
B
Palmitoylation relative to expression for total TRPM7
****
****
Palmitoylation relative to expression for total TRPM7
WT-M7
M7-M2
M7-M5
C
Palmitoylation relative to expression for phosphorylated TrpM7
****
****
palmitoylation relative to expression for phosphorylated TrpM7
WT-M7
M7-M2
M7-M5
D
Relative enrichment in acyl rac: phosphorylated TrpM7 / total TrpM7
Phosphorylated TrpM7 / total TrpM7
WT-M7
M7-M2
M7-M5
E
Flot2
Palmitoylation relative to expression
WT-M7
M7-M2
M7-M5

Figure 5.13 Phosphorylation status of palmitoylated TRPM7.
A) Representative western-blots of phosphorylation TRPM7(p-TRPM7) in Acyl-Rac assay captured palmitoylated TRPM7 among different stable cell lines. Stable cells were incubated with tetracycline for 24 hours or 48 hours to allow gene expression. B) Summary of quantification of palmitoylation relative expression for total TRPM7 in WT, M7-M2 and M7-M5 stable cells (****:P<0.0001, n=4; Tukey's multiple comparisons test by ANOVA). C) Summary of quantification of palmitoylation relative to expression for phosphorylated TRPM7 in WT, M7-M2 and M7-M5 stable cells (****:P<0.0001, n=4; Tukey's multiple comparisons test by ANOVA). D) Summary of quantification of relative enrichment in Acyl-Rac with phosphorylated TRPM7 relative to total TRPM7 in WT and mutant TRPM7 stable cells (TRPM7-M2 and TRPM7-M5). (n=4; Tukey's multiple comparisons test by ANOVA). However, there is no significant difference among all groups suggesting that palmitoylation and phosphorylation are two independent post-translational modifications (PTMs) in TRPM7. E) Robust Flot2 palmitoylated data as the standard for Acyl-Rac efficacy. (n=4).

5.4.11 Palmitoylation of TRPM7 in Cardiac fibroblasts derived from mice

TRPM7-deficient mice display significant cardiac hypertrophy, and exhibited inflammatory phenotype characterized by increased production of chemokines and pro-inflammatory cytokines (Rios et al., 2020). The process of cardiac fibrosis is mostly attributed to excessive synthesis and accumulation of extracellular matrix (ECM) proteins by activated myofibroblasts (Ranjan et al., 2019). In the normal heart, the major cell population is composed of fibroblasts (Maisch, 1995) whose phenotype could be changed into myofibroblasts by external stress (Powell et al., 1999). The myofibroblasts are activated by cytokines including fibroblast growth factor (FGF) and transforming growth factor (TGF-ß), Angiotensin II (Ang II) or aldosterone, insulin-like growth factor-1 (IGF-1) (Booz and Baker, 1995, Powell et al., 1999, Stockand and Meszaros, 2003). Aldosterone (10nM) stimulates proliferation of isolated adult rat cardiac myofibroblasts (RDF) by activating Kirsten Ras (Ki-RasA) then MAPK1/2 cascade (Stockand and Meszaros, 2003). In hence, The finding that TRPM7 deficiency induces cardiac hypertrophy suggests TRPM7 mediates anti-inflammatory and anti-fibrotic action in the cardiovascular system (Rios et al., 2020).

To investigate whether TRPM7 palmitoylation is a determinant of myofibroblasts turnover from cardiac fibroblast, we measured TRPM7 palmitoylation levels in wild-type cardiac fibroblasts and those after EGF or Aldosterone stimulation (stimuli conducted by Dr.Rios). Representative western-blots illustrated palmitoylation of TRPM7 was inhibited after EGF (50ng/ml) and Aldosterone (50μM) stimulation for 10 minutes (Figure 5.14A). Statistical analysis for several experiments (Figure 5.14B) revealed that EGF stimulated CF showed significantly reduced TRPM7 palmitoylation by approximately 28.1% (*P<0.05) and

Aldosterone stimulated ones exhibited decrease by roughly 50.4% (**P<0.01) (n=3). Flot2, as a well-known palmitoylated protein, acting standard of efficacy of Acyl-rac assay (Figure 5.14B). To sum up, TRPM7 palmitoylation may play an important role in EGF/Aldosterone induced transformation of fibroblasts into myofibroblast. Francisco et.al. has revealed that genetically TRPM7-kinase deficient mice show pro-inflammatory and pro-fibrotic cardiovascular and renal phenotype (Rios et al., 2020). Previous results in chapter 4 have shown reduced palmitoylation of TRPM7 causing less TRPM7 abundance at the cell surface. Influence of TRPM7 surface abundance on hypertrophy development and the underlying mechanism of TRPM7 palmitoylation in cardiac fibrosis requires further investigation.

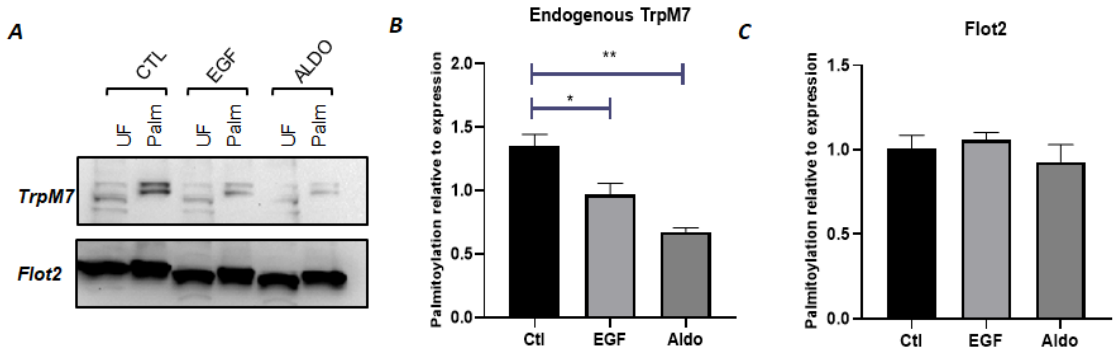

Figure 5.14 Palmitoylation of endogenous TRPM7 in cardiac fibroblasts cells (mice), is reduced following treatment with EGF and Aldosterone.
A) Representative western-blot of endogenous TRPM7 palmitoylation of cardiac fibroblasts (CF). Comparing the untreated control CF, palmitoylation of TRPM7 was decreased after incubation with EGF (50ng/ml) and Aldosterone (50μM) for 10 minutes. B) Mean ± SEM data of endogenous TRPM7 palmitoylation illustrated that both EGF and Aldosterone significantly reduced TRPM7's palmitoylation (*:P<0.05; **P<0.01). one-way ANOVA followed by Dunnett's t-test (n=3). C) Mean ± SEM data of palmitoylation of Flot2 among different groups. Flot2 was applied as a standard for Acyl-Rac assay and there is no significant difference in Flot2's palmitoylation. One-way ANOVA followed by Turkey's t-test (n=3).

5.4.12 Palmitoylation of TRPM7 in normotensive and hypertensive human VSMCs (hVSMCs)

Deficits in control of intracellular free [Mg]i affects vascular smooth muscle cell (VSMC) tone, proliferation and fibrosis, which are major determinants of vascular and endothelial dysfunction, remodeling in hypertension (Romani, 2018, Antunes et al., 2016). Mechanisms of regulating magnesium homeostasis in vasculature is still unclear but TRPM7 might plays an important role (Romani, 2007b). As we previously mentioned, TRPM7 is expressed in the vasculature meanwhile where it is regulated by many vasoactive agents including

bradykinin(Callera et al., 2009), aldosterone (Yogi et al., 2013), endothelin-1 and Angiotensin II (Ang II) (He et al., 2005, Touyz et al., 2006). TRPM7 has been regarded as a novel modulator in hypertension through regulating [Mg]i and many signaling pathways.

To investigate if palmitoylation of TRPM7 is a key factor in hypertension, we assessed its palmitoylation status in human VSMCs, including normotensive (NT) and hypertensive (HT) ones. From the representative western-blot (Figure 5.15A), the palmitoylation of TRPM7 was quite variant in individual human VSMC sample no matter NT or HT VSMCs. However, the statistical analysis of several Acyl-Rac experiments indicated the average of normalized palmitoylation levels between NT and HT VSMCs were approximately identical (Figure 5.15B). Flot2, with the similar palmitoylation ratio, representing acceptable efficiency of Acyl-Rac assay (Figure 5.15C). Therefore, defects in TRPM7 palmitoylation may not contribute to the hypertensive phenotype in vascular smooth muscle cells. This suggests that any TRPM7-mediated impairment in Mg transport in hypertension occurs in a palmitoylation-independent manner.

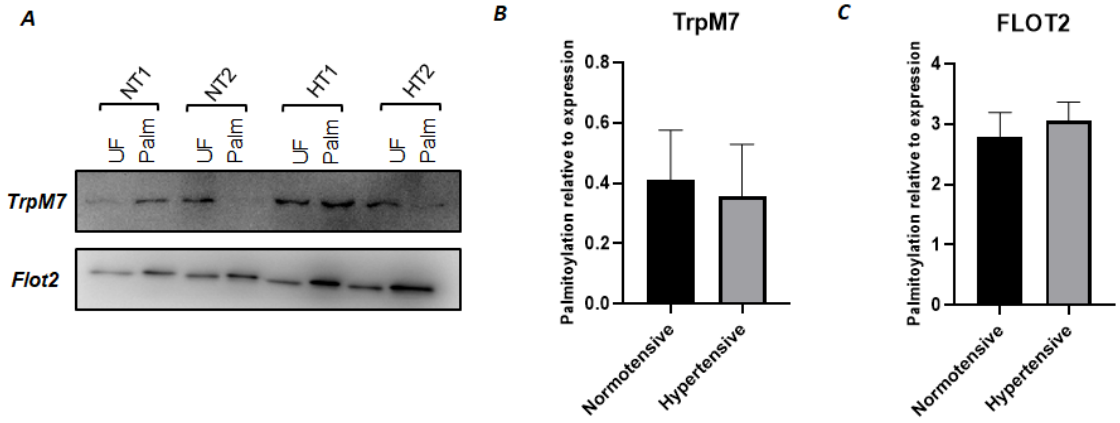

Figure 5.15 Palmitoylation of TRPM7 in human VSMCs derived from normotensive and hypertensive patients.
A) Representative western-blot of palmitoylation of TRPM7 in normotensive (NT) and Hypertensive (HT) human vascular smooth muscle cells (hVSMCs). NT and HT samples are derived from different participants. B, C) Summary of quantification of imaging data on TRPM7's palmitoylation in NT and HT hVSMCs. There is no significant difference in palmitoylation of TRPM7 between normotensive and hypertensive hVSMCs (n=6-9). Flot2 as the standard for evaluating Acyl-Rac efficiency which was quite similarly palmitoylated in NT and HT hVSMCs (n=5).

5.4.13 Palmitoylation of TRPM7 in human heart failure cardiac myocytes

Recently, expression of TRPM7 has been discovered in various cardiac tissue including in atrial and ventricular cardiomyocytes, conduction cells and in fibroblasts (Andriulė et al., 2021). However, the molecular and electrophysiological characterizations of TRPM7 in heart has predominantly focused on cardiac fibroblasts (Yu et al., 2014). To date, TRPM7 expression is upregulated in atria with atrial fibrillation (Zhang et al., 2012a) and TRPM7-current contributes to cardiac action potential (AP) profile. TRPM7 current in human atrial cardiomyocytes is highly dependent on pathology, and is significantly higher in cells from patients with coronary artery disease(Macianskiene et al., 2012). As previously results demonstrated, TRPM7 is palmitoylated in ventricular muscle cells in many species (details in section 3.4.1). So, we evaluated whether TRPM7 palmitoylation was modified in diseased cardiac tissue.

Therefore, we investigated the palmitoylation levels of TRPM7 in human cardiac myocytes which were obtained from normal organ donor (OD) (n=13) and heart failure (HF) patients (n=20). Although palmitoylation levels were relatively variant individually (Figure 5.16A), overall, there was no significant difference in TRPM7 palmitoylation levels between OD and HF samples (Figure 5.16B). Interestingly, Alomone TRPM7 antibody which raised against amino acids 1146-1165 of human TRPM7 could react with all species investigated and detected full length and cleaved TRPM7 (1-1281, the ion channel domain). As we know, TRPM7 is cleaved by caspases at D1510, releasing the carboxy-terminal kinase domain from the ion channel without disrupting its phosphotransferase activity (Desai et al., 2012). Palmitoylation of cleaved TRPM7 (~150KDa) detected by Alomone TRPM7 antibody (Figure 5.16A) was identical to palmitoylation of full length TRPM7 both in HF group and OD group (Figure 5.16D, E). This suggests that there is no direct relationship between palmitoylation and proteolytic processing.

As previously described, TRPM7 is dispensable in adult ventricular myocardium under basal conditions but is vital to myocardial proliferation during early cardiogenesis (Sah et al., 2013). TRPM7 has been implicated in pro-inflammatory and pro-fibrotic cardiovascular and renal phenotype (Rios et al., 2020). Both

pathologies might implicate in its role of Mg and/or Ca conduction. We have shown reducing TRPM7 palmitoylation induces decreased Ca influx but the underlying mechanism and whether palmitoylation participated in cardiac function need further investigation.

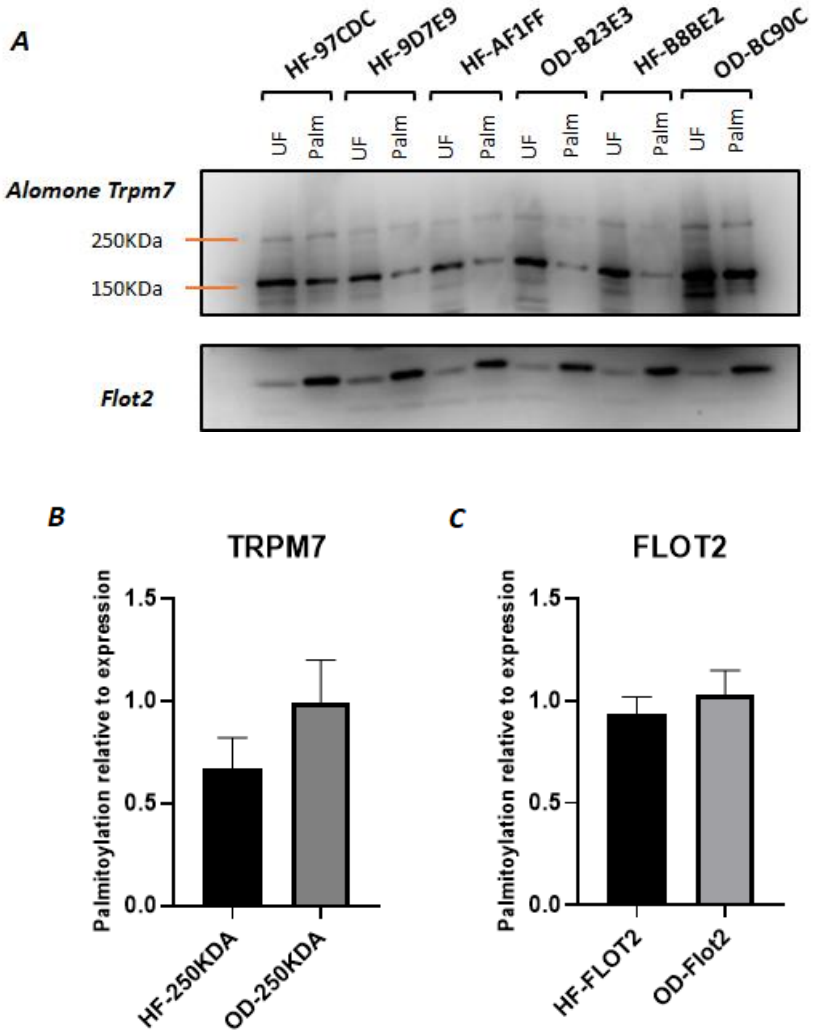

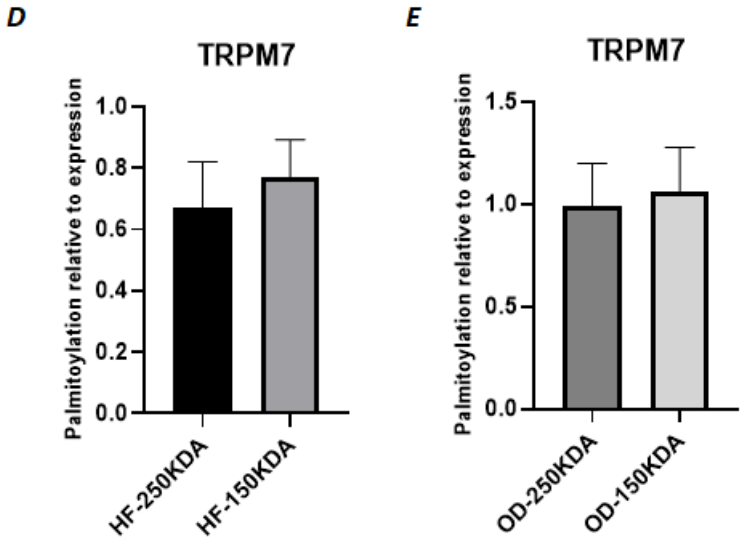

Figure 5.16 Palmitoylation of TRPM7 in cardiac myocytes derived from heart failure (HF) patients.
A) Representative western-blot of palmitoylation of TRPM7 in normal organ donor (OD) and Heart failure (HF) cardiac myocytes. Alomone TRPM7 antibody was applied for detection 150kDA represents TRPM7 from which the kinase domain has been cleaved. Palmitoylation of both kinase domain cleaved-TRPM7 and full-length TRPM7 had been measured. Flot2 as the housekeeping gene to evaluate Acyl-Rac assay. B) Summary of imaging data about palmitoylation of Full-length TRPM7 in HF and OD cardiac myocytes. TRPM7's palmitoylation has slight decreased trend in HF samples but without significant difference (n=13-20). C) Flot2 was equally palmitoylated between two types of cardiac samples. D, E) palmitoylation of full-length TRPM7 and kinase domain cleaved TRPM7 in OD and HF cardiac myocytes. Statistical analysis with unpaired t-test reveals that there is no significant difference in palmitoylation of full-length TRPM7 and Kinase domain cleaved TRPM7 in OD and HF samples separately (n=13-20).

5.5 Discussion

This chapter set out to investigate cellular mechanisms that control TRPM7 palmitoylation. We found that TRPM7 is palmitoylated by plasma-membrane resident zDHHC5 and Golgi-resident zDHHC17. Manipulating extracellular Mg concertation alters TRPM7 palmitoylation after 3 hours. Palmitoylation and phosphorylation are two independent forms of post-translational modifications without direct relationships. Non-palmitoylated TRPM7 shows reduced phosphorylation as well. Acute changes in TRPM7 palmitoylation in cardiac fibroblasts by agonists promotes fibroblast to myofibroblast transition. But we have not found significant alterations in TRPM7 palmitoylation in human hypertensive VSMCs and ventricular tissue from human heart failure patients.

5.5.1 TRPM7 is palmitoylated by zDHHC5 and zDHHC17

Similarly with other polytopic membrane proteins, TRPM7 is palmitoylated throughout the secretory pathway (Gök et al., 2021) by zDHHC-PATs confined to

individual cellular compartments. The fact that the non-palmitoylated TRPM7-1143/4/6-YFP mutant was retained in the ER indicates that palmitoylation occurs at the early stage of TRPM7's lifetime. But the other two non-palmitoylated chimeras TRPM7-M2-YFP and TRPM7-M5-YFP could both leave the ER. We therefore propose that palmitoylation is necessary for stabilising the TRPM7 structure by anchoring the C-terminal end of TRP domain to the membrane, rather than for clustering TRPM7 into ER export vesicles. The mixed basic/hydrophobic nature of replaced amino acids from TRPM2 (KRIV) and TRPM5 (KQVF) is sufficient to substitute membrane affinity and stability of palmitoyl fatty acids. In our investigation of overexpression of the ER-resident zDHHCs-PATs, none of them was significantly increased TRPM7 palmitoylation. The underlying reason might be TRPM7 was fully palmitoylated by endogenous DHHCs. However, in the DHHC5 KO cells, we found concomitant decrease of TRPM7 palmitoylation which was compensated by addition of DHHC5. DHHC5 is abundantly expressed in the cell surface which indicated TRPM7 is palmitoylated again in plasma membrane (Howie et al., 2014). Our finding that TRPM7 was de-palmitoylated when it was released from the Golgi is also consistent with the idea that palmitoylation of TRPM7 is dynamic following its release from the Golgi.

These experiments also identified zDHHC17 in the Golgi is identified as another principal determinant of TRPM7 palmitoylation. We discovered that two different prolines within consensus zDHHC AR-binding motifs (zDABMs) whose presence was required for TRPM7 palmitoylation, P769 and P1131. Notably, a large proportion (12/17, 70%) of proteins containing multiple potential zDABMs were found to interact with zDHHC17 through more than one of these motifs (Lemonidis et al., 2017). Since removal of one zDABM clearly impairs the ability of the other to direct TRPM7 palmitoylation, our data suggest some cooperativity to substrate recruitment and/or palmitoylation by zDHHC17. In contrast, P586 localises in the N-terminus of TRPM7 whereas the palmitoylation cysteines are resident in the C-terminus, which might be the potential reason why silencing P586 was not interfering its palmitoylation.

5.5.2 Alterations of [Mg]i concentrations impact TRPM7 palmitoylation

Our understanding of TRPM7 ion channel gating mechanisms are incomplete, with the current view mainly resting on two findings: one is that intracellular Mg(either free Mg or Mg-ATP) negatively regulating the TRPM7 channel (Nadler et al., 2001), the other is the plasma membrane phospholipid phosphatidylinositol-4,5-bisphophate (PIP2), the substrate of PLC, is required for TRPM7 channel activity (Runnels et al., 2002). Previously research unsuccessfully revealed the influence of palmitoylation inhibition to intracellular Mg conduction. Experiments presented in Chapter 4 failed to identify any influence of TRPM7 palmitoylation on Mg conduction. But when we altered the extracellular Mg concentrations, endogenous TRPM7 palmitoylation was decreased, but only after incubation for 3 hours. Surprisingly, TRPM7 palmitoylation was reduced in both conditions with supplement and withdrawal Mg.

The conformational changes of ion pore forming segments 5 and 6 of TRPM7 might be important for channel activity. However, the structure of TRPM7 in the presence of Mg and EDTA does not have distinct differences (Figure 5.17) (Duan et al., 2018).Accordingly, the underlying reason for palmitoylation reduction might be due to either the palmitoylating enzymes being less active or the de-palmitoylating enzymes being more active. In addition, since PIP2 regulator binding sites reside among some positively charged residues in the highly conserved TRP box of C-terminal end (Rohács et al., 2005), where is the same localization of palmitoylated cysteine cluster. The unrevealed crystal structure of this region might indicate its dynamic structure (Duan et al., 2018) has been involved in channel gating. Palmitoylation of TRPM7 might be implicated in PIP2 regulated channel activation, as well as the alterations of Mg ionic concentration affected its palmitoylation in turn.

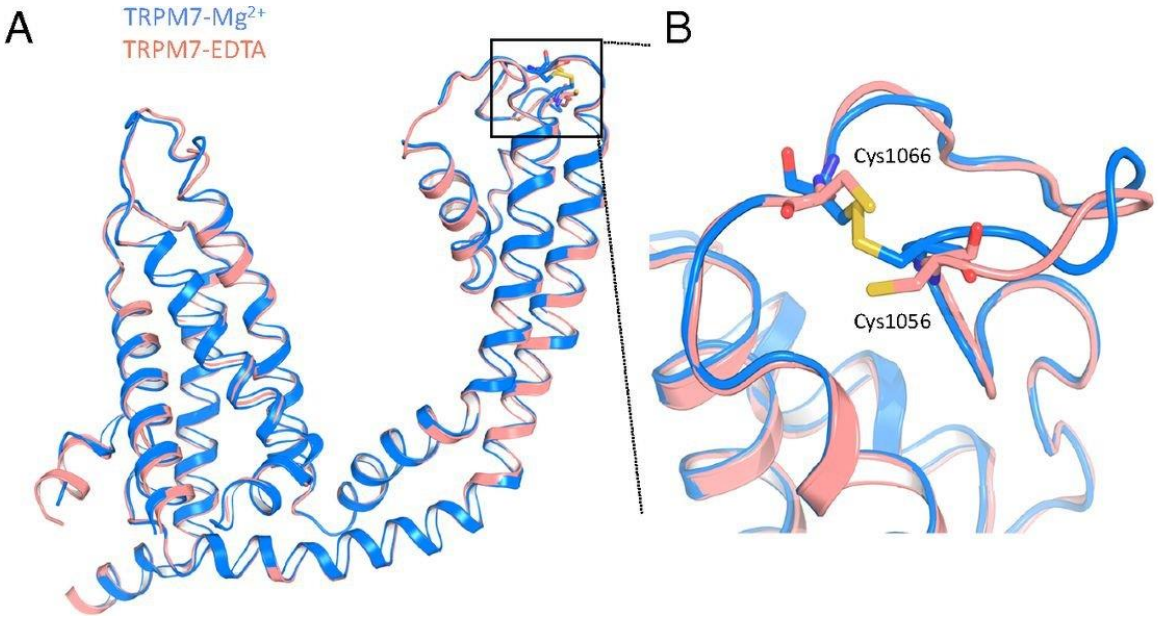

Figure 5.17 Structure of TRPM7-Mg and TRPM7-EDTA (Duan et al., 2018).
A) Superimposition of the transmembrane module from TRPM7-Mg (blue) and TRPM7-EDTA structures (pink). B) Site of the broken disulfide bond between Cys1056 and Cys1066 in the pore domain. Shown is superimposition of the disulfide bond between S5 and S6 in the TRPM7-Mg (blue) and TRPM7-EDTA (pink) structures.

5.5.3 TRPM7 palmitoylation and phosphorylation signalling pathways

In contrast to the relatively small amount of information about regulation of TRPM7 by palmitoylation, phosphorylation of TRPM7 is well-established and well understood. The TRPM7 C-terminal end contains a serine/threonine (Ser/Thr) enriched domain which is adjacent to its kinase domain. Autophosphorylation of TRPM7 is not a prerequisite for kinase's catalytic activity (Clark et al., 2008b). Interestingly, in the heteromeric TRPM6/TRPM7 complex, TRPM7 is trans-phosphorylated by TRPM6 as well as facilitating TRPM6 trafficking to the plasma membrane in turn (Cai et al., 2017). Many putative signalling mechanisms of TRPM7 signalling have been proposed (Zou et al., 2019, Yee et al., 2014). Here, we add to the mechanisms of TRPM7 regulation by adding palmitoylation modification (Figure 5.18).

In our study, we found that phosphorylation and palmitoylation are largely independent post-translational modification. The cleavage of kinase domain from the ion channel does not alter TRPM7 palmitoylation, and phosphorylated TRPM7 is equally well purified by acyl-RAC compared to total TRPM7. As TRPM7 has been identified co-localized with EGFR on the plasma membrane and c-Src induced by EGFR activation is necessary for TRPM7 phosphorylation (Zou et al.,

2020). Phosphorylation of TRPM7 was diminished in non-palmitoylated TRPM7-M2-YFP and TRPM7-M5-YFP stable cells which we suggest is likely to be due to the reduced abundance of TRPM7 in the plasma membrane. Signalling cascades downstream of TRPM7 were not affected by the inhibition of palmitoylation. Future experiments should address the role of PIP2, a primary regulator of the TRPM7 ion channel, whose influence on TRPM7 activity may be influenced by palmitoylation via regulating the ability of the TRP domain, a rigid α-helix, to move relative to the membrane consequently alter channel activity. The ability of PIP2 to regulate other transporters is established to be regulated by palmitoylation (Reilly et al., 2015, Yang et al., 2020). The consequent alteration ionic conduction by channel behaviour might be crucial to other crosstalk signalling pathways or kinase domain activities.

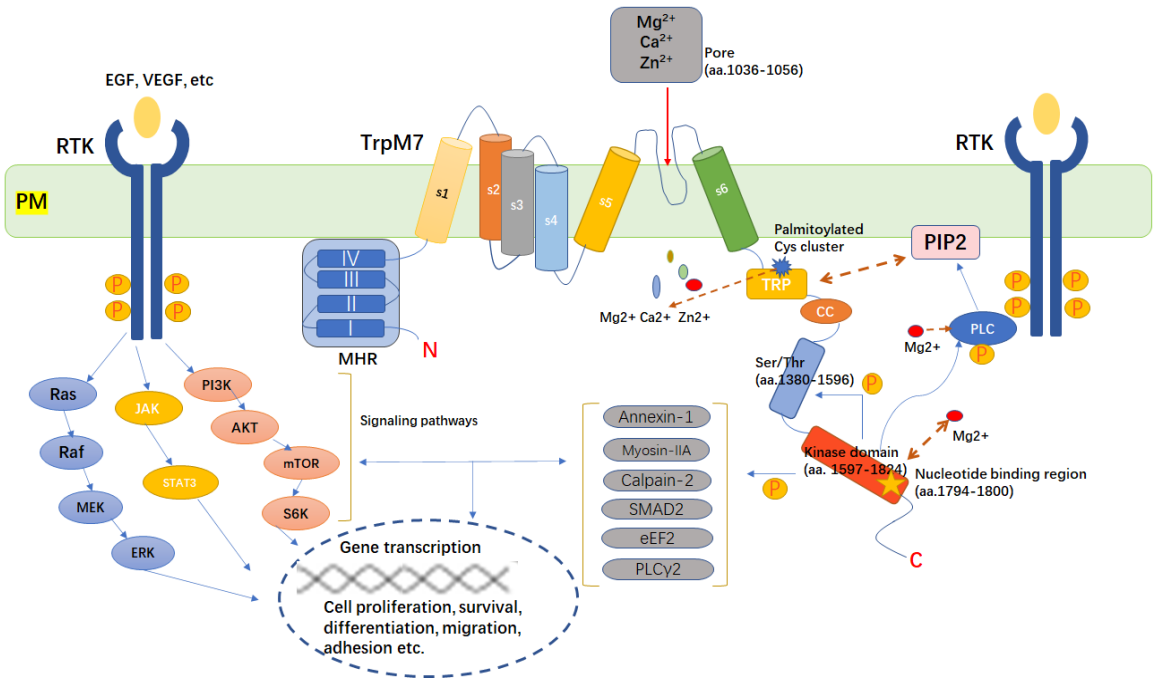

Figure 5.18 Schematic mechanisms of TRPM7 on plasma membrane.
TRPM7 as an ion channel mainly permeable to Zn, Mg and Ca and as cytoplasmic kinase which phosphorylates itself and identified substrates annexin-1, myosin IIA heavy chain, eEF2, SMAD2, and PLCγ2. Through the ionic alteration and kinase activities, TRPM7 could be involved in RTK downstream signalling pathways. TRPM7 palmitoylation may influence the ability of PIP2 to regulate channel gating. The alteration of ionic concentration triggered by palmitoylation might manipulate cascade signalling pathways, allowing it regulate cell cycle. PM: plasma membrane; RTK: receptor tyrosine kinase; MHR: melastatin Homologous Regions.

5.5.4 Palmitoylation of TRPM7 in cardiovascular disease models

TRPM7 exerts significant influence on many cardiovascular diseases through regulating Mg homeostasis and/or participating multiple signalling pathways. The

ubiquitous expression and unique biophysical characteristics of TRPM7 allow it to engage in the pathogenesis and development of fibrosis-related cardiac diseases, such as heart failure (HF), arrhythmia and hyperaldosteronism(Hu et al., 2021). Aldosterone stimulates proliferation of isolated adult rat cardiac fibrosis through Ki-RasA and MAPK1/2 cascade (Stockand and Meszaros, 2003). Since TRPM7 is the only Calcium flux channel found on the cell membrane of Cardiac fibroblasts (CFs) (Zhang et al., 2012a), it has the potential to influence the proliferation of these cells. Assessment of TRPM7 palmitoylation indicates it was inhibited in aldosterone-induced cardiac fibroblasts. Notably, the calcium influx was significantly reduced in the cells stably expressing non-palmitoylated TRPM7-M2-YFP and TRPM7-M5-YFP. Since TRPM7 emerged as a novel target in pathological processes in cardiac fibrosis, palmitoylation might be a new therapeutic target in this setting. Furthermore, palmitoylation of TRPM7 is not changed in Human hypertensive VSMCs and Human HF cardiac myocytes in general population. But the palmitoylation status was highly variable between individuals, which suggested TRPM7 function also varies considerably across the population.

5.6 Summary

In conclusion, we identified zDHHC5 in the plasma membrane and zDHHC17 in the Golgi as two candidate palmitoyl acyl transferases for TRPM7. Phosphorylation and palmitoylation are two independent post-translational modifications of TRPM7 and cleavage of TRPM7 kinase domain does not alter its palmitoylation. The phosphorylation of TRPM7 is diminished in cells stably expressing non-palmitoylated TRPM7-M2-YFP and TRPM7-M5-YFP which probably due to the reduced abundance of TRPM7 at the cell surface. In cardiovascular disease, palmitoylation might act as a new modulator of TRPM7's role in aldosterone-induced cardiac fibrosis.

Chapter 6 General conclusion and discussion

6.1 Key findings

The aims of this study were to investigate the influence of palmitoylation on TRPM7 ion channel activity and kinase domain as well as to understand the regulatory mechanisms of TRPM7 palmitoylation. In addition, we used several different clinical human samples to measure if TRPM7 palmitoylation is significantly changed in disease.

The key finding from this project are:

1. TRPM7 is palmitoylated in multiple cell types, including human embryonic cells (HEK), vascular smooth muscle cells (VSMCs) from human and rats, cardiac ventricular cells from (rat, mice, and human) etc. TRPM6, the closest homologue is also palmitoylated in HEK cells.

2. TRPM7 palmitoylation sites are among a cluster of cysteines (Cys1143, Cys1144 and Cys1146) in the TRP domain.

3. Non-palmitoylated 3CA-TRPM7-YFP mutant could not exit the endoplasmic reticulum (ER).

4. Using RUSH (retention using selective hooks) system we captured SBP-TRPM7 in the Golgi and reduced its palmitoylation using the zDHHC-PAT inhibitor 2-bromopalmitate. Following release with biotin, less TRPM7 was delivered to the cell surface when palmitoylation was reduced.

5. TRPM7 palmitoylation sites are highly conserved in most of TRP channels, including TRPM, TRPV, TRPC subfamilies.

6. Non-palmitoylated TRPM7-M5-YFP and TRPM7-M2-YFP could exit the ER meanwhile they are less abundant at the cell surface.

7. Palmitoylation regulates TRPM7 passage through the secretory pathway. Non-palmitoylated TRPM7 is delivered to intracellular vesicles whereas palmitoylated TRPM7 is delivered to the cell surface.

8. Inhibiting palmitoylation reduces TRPM7-mediated Ca influx but without significantly alters of TRPM7-mediated Mg influx.

9. Golgi-resident DHHC17 and Plasma membrane-resident DHHC5 are both responsible for TRPM7 palmitoylation

10. Gene ontology cellular compartment (GOCC) analysis of proteins co-purified with wild-type TRPM7 and non-palmitoylated TRPM7 reveals most genes enriched in WT-TRPM7 are from nuclear lumen whereas those enriched in TRPM7-M5 are from vesicles.

6.2 Palmitoylation regulates sorting in the TRPM7 secretory pathway

Most research of TRPM7 emphasis its functions at the plasma membrane where it regulates transmembrane cation flux, but TRPM7 also has been found localized at intracellular vesicles to regulate Zn storge (Abiria et al., 2017a). Our study has identified palmitoylation as an important determinant of TRPM7's fate in the secretory pathway. Firstly, non-palmitoylated TRPM7-1143/4/6_AAA mutant cannot exit the endoplasmic reticulum (ER) which indicates palmitoylation occurs at an early stage of its lifecycle, is mediated by ER-resident zDHHC-PATs and is required for ER export. With the Golgi-Hook retention cell line, we found once palmitoylation of WT-TRPM7 was inhibited by 2-BP in the Golgi, this led to reduced TRPM7 abundance at cell surface after release via biotin. This suggests that TRPM7 palmitoylation status in Golgi is a key determinant of its post-Golgi fate in the secretory pathway. Non-palmitoylated TRPM7 was delivered to the intracellular vesicles and palmitoylated TRPM7 was delivered to the cell surface. Interestingly, we found the palmitoylation level of WT-TRPM7 was decreased after biotin-induced release from the Golgi, which suggests it is de-palmitoylated by some acyl-thioesterase enzymes post-Golgi. In consequence, TRPM7 that is destined for the cell surface may need to be re-palmitoylated by Golgi-resident or plasma-membrane-resident zDHHCs-PATs. From our results (section 5.4.2 and 5.4.4), we confirmed two palmitoyl-transferase enzymes are responsible for palmitoylating TRPM7, respectively are DHHC17 residing in Golgi and DHHC5 residing in the plasma membrane. Hence, we conclude that palmitoylation occurs multiple times during TRPM7 life cycle and regulates its

trafficking in secretory pathway (Figure 6.1). In addition, preliminary experiments using sucrose gradient-based fractionation suggested more TRPM7 was present in intracellular vesicles from cells expressing the M7-M5 chimaera than wild type.

Palmitoylation has controls the distribution of proteins in membranes based on their curvature indicating that palmitoylated proteins tend to cluster at sites of vesicular budding (Yurtsever and Lorent, 2020, Larsen et al., 2015). Compared with the TRPM7-1143/4/6_AAA mutant, TRPM7-M2 and TRPM7-M5 chimaeras could exit the ER which suggests palmitoylation is required to stabilize the TRPM7 structure by anchoring the C terminal end of the TRP domain to the membrane, rather than for clustering TRPM7 into ER export vesicles. This suggests that the hydrophobic nature of 'KIRV' (TRPM2) and 'KQVF' (TRPM5) is sufficient to engage the membrane and substitute for palmitoylation in stabilising nascent TRPM7 in the ER. Notably, clustal alignments of members of the wider TRP superfamily also demonstrates analogous cysteines in most members of TRPV and TRPC families. Even the channels lacking cysteine residues analogous to TRPM7, TRPV6, TRPV3 and TRPV4, instead include clusters of basic and hydrophobic amino acids like those found in TRPM2 and TRPM5. Therefore, stabilizing the C-terminal end of TRP domain to membrane might be a common feature of TRP superfamily.

In addition, palmitoylation has been illustrated to accelerate the anterograde transport of proteins through the Golgi because palmitoylated protein tend to be concentrated in highly curved rims of Golgi (Ernst et al., 2018). However, the influence of palmitoylation on Golgi-resident TRPM7 is different. Palmitoylation seems plays a role in sorting TRPM7 to vesicles headed for the plasma membrane. In contrast, non-palmitoylated TRPM7 appears to leave the Golgi via different vesicle which predominantly act as a Zn storage organelle.

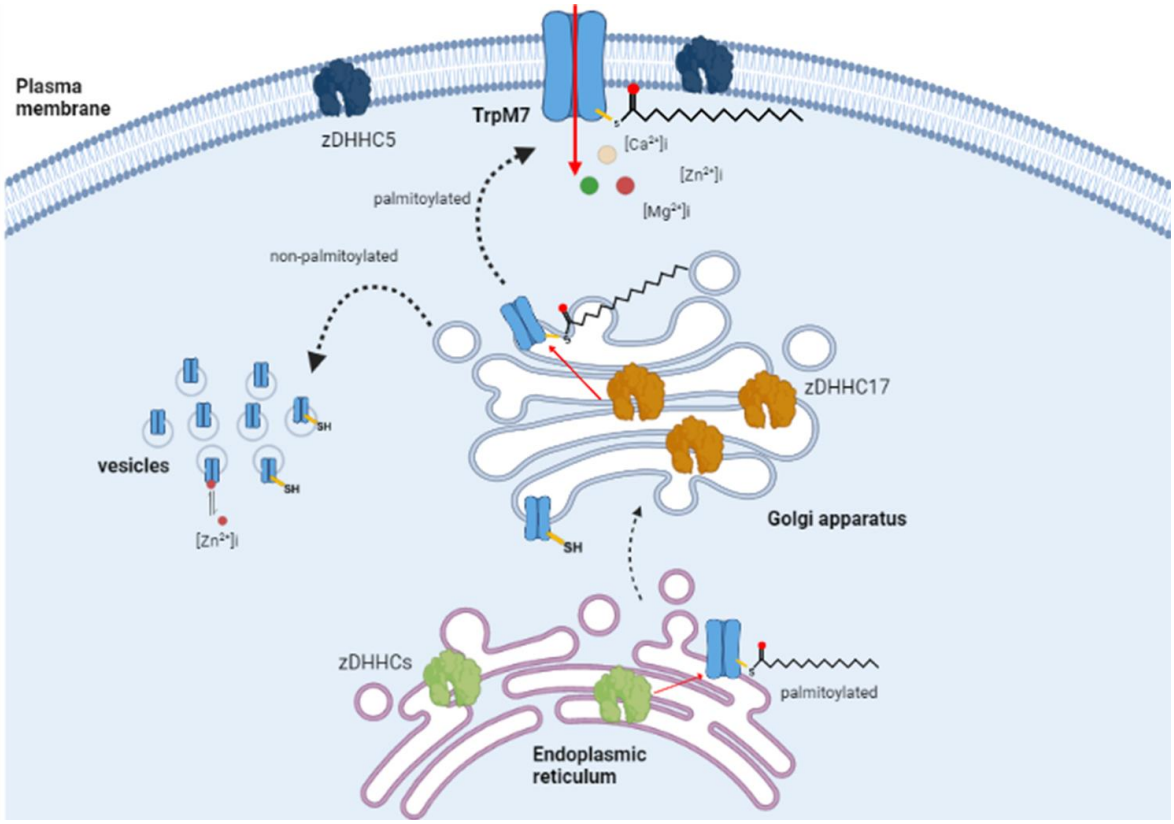

Figure 6.1 Palmitoylation regulates TRPM7 passage through secretory pathway. TRPM7 is required to be palmitoylated consequently enhancing their hydrophobicity and anchoring their C-terminal end of TRP domain to exit the ER. Subsequently, palmitoylation status in the Golgi determines its subsequent delivery to either intracellular vesicles or plasma membrane, specifically non-palmitoylated TRPM7 translocated into vesicles whereas the palmitoylated ones delivered to membrane.

6.3 Influence of TRPM7 palmitoylation on intracellular free [Mg]i

It is generally accepted that intracellular free [Mg]i and Mg·ATP serve as negative regulators of TRPM7 ion channel function. But the molecular mechanism determining TRPM7 sensitivity to intracellular Mg remains unclear. Kinase-dead mutation or kinase domain deficient variants of TRPM7 channel resulted in channels with modestly changed sensitivity to Mg (Demeuse et al., 2006, Matsushita et al., 2005). Mg and Mg·ATP inhibition of TRPM7 occur through engagement with different binding sites and Mg acts as channel blocker independently from the kinase domain (Schmidt et al., 2022). In accordance with the molecular dynamic (MD) analysis from Chubanov and colleagues, four side chains of N1097 in the TRPM7 tetrameric structure form an internal cation-binding pocket and consequently close the channel in the presence of Mg (Figure 6.2) (Schmidt et al., 2022). In contrast, removal of Mg assists transition to the channel open state. The adjacent N1098 most likely forms inter-subunit

hydrogen bonds stabilizing the closed state of the TRPM7 channel (Figure 6.2) whose mutation consequently leads to a constitutively active channel variant which is insensitive to physiological levels of free Mg and PIP2. Similarly, TRPM7-S1107E mutation in TRP domain consequently produces a constitutively active channel insensitive to intracellular Mg and PIP2 (Hofmann et al., 2014). The amino acids N1097 and N1098 of TRPM7 reside adjacent ahead of TRP helix and its palmitoylation cystines (C1143, C1144 and C1146) are also localizing quite close but after of TRP helix.

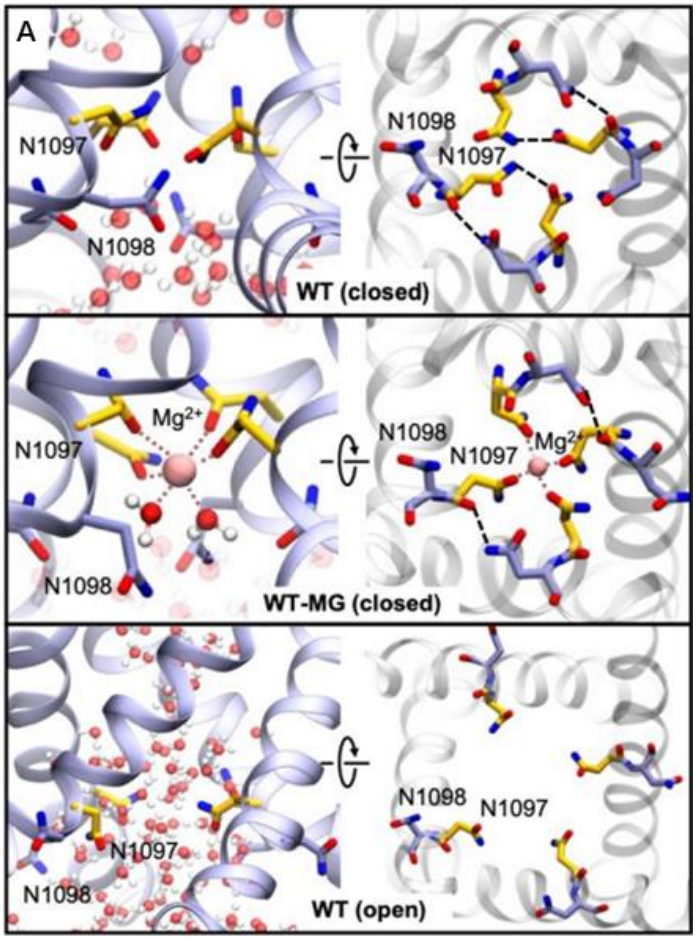

Figure 6.2 Molecular dynamic (MD) analysis of closed and open conformation of TRPM7 (Schmidt et al., 2022).
Structure of channel gated in the closed state in/out presence of Mg and open channel. Red: persistent water molecules; dashed line: hydrogen bonds formed between N1097 and N1098 residues and Mg.

The development of magnesium measurements has some intrinsic difficulty. One is the chemical nature of magnesium, the large difference in diameter between the dry and hydrated form making it difficult for Mg form high affinity complexes with indicators (Romani and Scarpa, 1992). Another is the large difference between free and total Mg in cytosol. The abundance of Mg masks even large

fluxes of Mg and measuring micromolar changes shows poor sensitivity and a high background (Romani and Scarpa, 1992). Compared to the calcium ions, changes of magnesium are smaller and slower to detect. For example, most studies use indicators based on APTPA (London, 1991), which are also sensitive to changes in Ca. The Magnesium indicator used for measuring Mg influx in our project is Magnesium Green™ Acetoxymethyl (AM) indictor, with Kd=1.0mM for Mg but Kd=6.0μM for Ca. Consequently, the limitation of this measurement is not suitable for buffers containing high concentrations of Mg. Electrophysiological technique, patch clamp, might be a better choice for measuring the influence of palmitoylation on TRPM7 ion channel conduction activity for Mg influx (Chokshi et al., 2012b, Monteilh-Zoller et al., 2003, Schmidt et al., 2022). In addition, ionized Ca: Mg ratio might be another useful value to consider which is more significant in clinical diseases, as Mg is a well-known antagonist of calcium (Ca) that can compete the binding sites of proteins and transporters (Li et al., 2020, Kousa et al., 2006).

6.4 Influence of palmitoylation on TRPM7 channel gating

Phosphatidylinositol-4,5-bisphophate (PIP2) is a key regulator of many TRP channels (Qin, 2007). It has been illustrated that PIP2 hydrolysis mediated by receptor-dependent phospholipase C (PLC) activation potently inactivates TRPM7 (Runnels et al., 2002). Through the investigation of TRPM6 ion channel gatekeeper, its closest homologue TRPM7 is proposed to bind PIP2 via positively charged residues K1112, R1115 and K1125, which are localized in the TRP domain (Xie et al., 2011) (Figure 6.3A). Meanwhile, the palmitoylation sites of TRPM7 have been identified resident in the cysteines cluster 1143, 1144 and 1146 at the C terminal end of the TRP domain. Saturated palmitic acids covalent attachment to cystine residues would enhance the protein hydrophobicity and stabilize its association to membrane. In addition, the mobility and flexibility of the TRP domain is likely regulated by PIP2 binding, which are crucial determinants of channel gating. The protein structure of the palmitoylated region is poorly resolved (Duan et al., 2018). It is conceivable that palmitoylation here may be influence the ability of the TRP domain, a rigid α-helix, to move relative to the membrane, which would consequently alter channel behaviour. Furthermore, some studies suggest that Mg interferes with the interaction of PIP2 and TRPM7 subsequently indirectly influences TRPM7

channel. However, high-resolution structures of closed TRPM7 channel via cryo-electron microscopy (cryo-EM) has not identified structural rearrangements associated with the Mg- and PIP2-dependent opening of the TRPM7 channel (Schmidt et al., 2022, Duan et al., 2018). Since the palmitoylation cysteine(s) are highly conserved in most TRPM family members and TRPM7 palmitoylation sites resides quite close to its TRP domain (Figure 6.3B). It may interfere with the PIP2 binding sites to affect the sensitivity or selectivity of ion channel activity. Therefore, palmitoylation might cooperate with PIP2 serving as the gatekeeper of TRPM7, which might be channel gating control mechanism for most TRPM members.

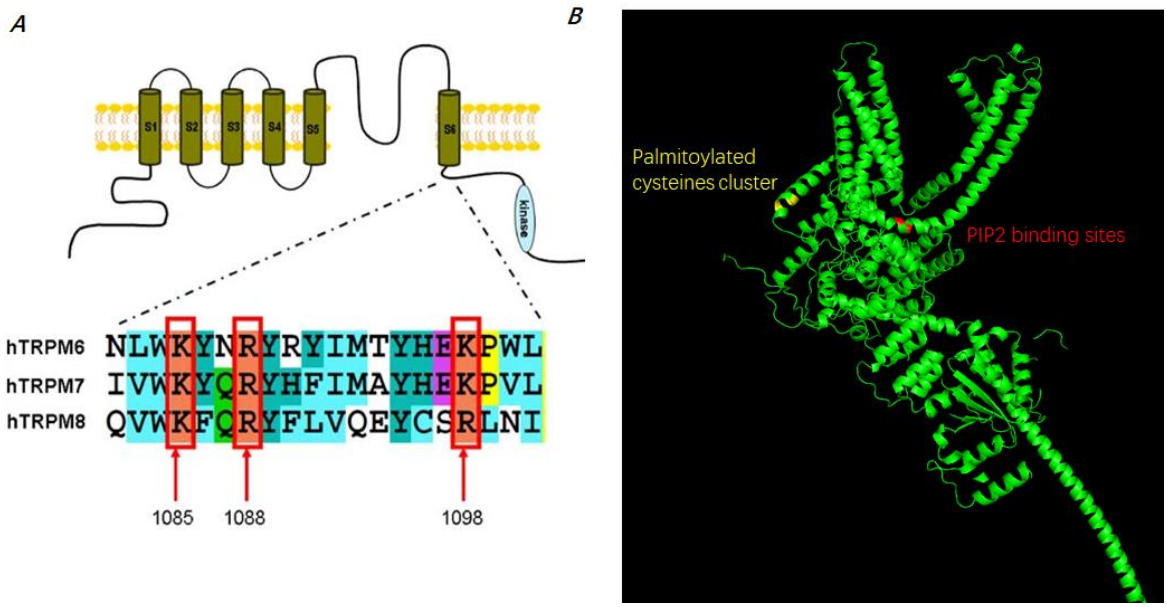

Figure 6.3 Mapping PIP2 binding sites (Xie et al., 2011) and palmitoylation sites in hTRPM7. A) PIP2 binding to the positively charged amino acids in the TRP domain. Alignment of the TRP domain of TRPM6, TRPM7 and TRPM8 illustrates the PIP2 binding sites are highly conserved. The highlighted residues in TRPM8 are the PIP2 binding sites. B) mapping palmitoylated cysteines cluster (Cys1143, 1144 and 1146) and PIP2 binding sites (K1112, R1115, and K1125).

6.5 Influence of palmitoylation on TRPM7 kinase domain

Despite considerable efforts to understand it, the functional relationship between the kinase domain and ion channel of TRPM7 is still unclear. On one hand, site-directed mutational analysis has revealed that kinase-inactivated mutation of ATP-binding motif and zinc finger homology domain results in decrease of TRPM7-mediated currents (Runnels et al., 2001). On the other hand, mutations of auto-phosphorylation sites and key catalytic sites have not altered the whole-cell recording and the inhibition capacity of internal Mg (Matsushita et

al., 2005). It is commonly accepted that TRPM7 kinase domain activity affects the sensitivity of ion channel. TRPM7 ion channel current is inhibited by intracellular Mg as well as other divalent cations (Kozak et al., 2005). However, the kinase activity is enhanced by Mg, decreased by Zn and unaffected by Ca (Matsushita et al., 2005).

In our study, palmitoylation and phosphorylation are two independent modifications since the phosphorylated TRPM7 is equally enriched in the acyl-RAC compared to total TRPM7 (section 5.4.10). Palmitoylation occurs at the cysteines in proximity to the C-terminal end of the TRP domain. The considerable distance from the kinase domain makes it unlikely that there are steric effects of palmitoylation on the kinase domain. However, palmitoylation regulates TRPM7 trafficking which might subsequently affect its association with other proteins. So, palmitoylation might be involved into regulation of many TRPM7-dependent cellular signalling pathways. Meanwhile, TRPM7 is less phosphorylated in cells expressing non-palmitoylated TRPM7-M5 and TRPM7-M2 mutants, which is likely to be a consequence of reduced TRPM7 abundance at the cell surface. In addition, the intracellular Ca influx is inhibited by suppression of TRPM7 palmitoylation. Notably, the Gene ontology cellular compartments (GOCC) analysis of co-purified protein enriched in WT-TRPM7 is largely from the nuclear lumen, whereas those enriched with the non-palmitoylated TRPM7-M5 are mainly from vesicles. This result suggests the cleavage and nuclear localisation of the TRPM7 kinase may be reduced in non-palmitoylated TRPM7-M5 mutant. TRPM7 controls gene expression via histone phosphorylation which relies on its kinase domain cleavage (Desai et al., 2012). Therefore, our GOCC result suggests that palmitoylation might influence the cleavage of TRPM7 and consequently influence cellular gene expression, or the intracellular vesicle resident TRPM7 may not be efficiently cleaved, and therefore may not translocate into the nucleus.

6.6 Enzymes responsible for TRPM7 palmitoylation

As previously mentioned, TRPM7 is palmitoylated throughout the whole secretory pathway by zDHHC-PATs confined to individual cellular compartments (Ohno et al., 2006). Endogenous TRPM7 must be palmitoylated by ER-resident zDHHC-PATs to exit the ER. We were unable to alter endogenous TRPM7 palmitoylation by

over-expressing ER resident zDHHC enzymes, probably because the intrinsic enzymes are sufficient to palmitoylate TRPM7. Therefore, applying specific siRNAs to silence DHHC-PATs would be a better tool. Meanwhile, experiments using the RUSH system to retain TRPM7 in the Golgi suggest that TRPM7 is de-palmitoylated after biotin released form Golgi but the de-palmitoylating enzymes remain unknown.

We found Golgi-resident DHHC17 is one determinant of TRPM7 palmitoylation and trafficking. There are two prolines filtered within consensus zDABMs whose presence was necessary to TRPM7 palmitoylation (Lemonidis et al., 2017). The requirement for both zDABMs suggests zDHHC17 substrate recruitment may be co-operative. DHHC5 is another palmitoyl-transferase of TRPM7 residing in plasma membrane. TRPM7-mediated Calcium uptake has been associated with many pathologies, from the anoxia-induced Ca cascade in brain injury (Turlova et al., 2021) to leptin-induced hypertension in carotid body (Shin et al., 2019). Many TRPM7 channel inhibitors have been developed such as NS8593 (Chubanov and Gudermann, 2020). In contrast, our research addresses a hitherto unexplored route for therapeutic gain via manipulating palmitoylation status of TRPM7 to regulate its cellular/surface distribution. For example, targeting zDHHC17 in the Golgi would prevent delivery of TRPM7 to the surface membrane and block TRPM7-mediated calcium uptake.

6.7 Further directions

Recently, native TRPM7 channel were described as high-molecular-weight multi-protein complexes that contain the putative metal transposer proteins CNNM1-4 and small G-protein ADP-ribosylation factor-like protein 15 (ARL15) (Kollewe et al., 2021b). CNNM3 appears to act as a negative regulator of the TRPM7 kinase domain whereas the ARL15 seems serves as a potent and specific negative modulator of TRPM7 channel (Kollewe et al., 2021b). Meanwhile, PRL (phosphatases of regenerating liver) protein tyrosine phosphatases, the key contributors to metastasis in several cancers, has been identified interaction with CBS1 and CBS2 region of CNNM3 (Kostantin et al., 2016). PRL-2 plays an important role in regulating magnesium homeostasis which collectively controls tumour growth with CNNM3 (Kostantin et al., 2016, Hardy et al., 2015). The potential interaction between PRL-CNNM3 and TRPM7 requires further

investigation. Besides, the influence of palmitoylation on TRPM7-CNNM3 complex formation should be further characterised. Apart from ARL-15 and CNNM3, our proteomics data presents a large number of proteins that differentially interact with WT-TRPM7 and non-palmitoylated TRPM7-M5. Further filtration of those proteins to identify candidates which associated with TRPM7 activity or physiological reactions is a vital high priority.

In addition, importantly, we need explore other methods to measure intracellular [Zn]i and [Mg]i concentration or apply patch-clamp technique to measure TRPM7-current with our inducible stable cell lines, WT-TRPM7 and TRPM7-M5. Previous research illustrated that majority of TRPM7 localized in intracellular vesicles where it serving as Zn storage and releasing Zn to cytosol under oxidative activation (Abiria et al., 2017a). Therefore, measuring effects of TRPM7 palmitoylation on intracellular vesicular Zn concentration might be useful to further investigation its response to oxidative stress. Besides, identification of ER-resident DHHC-PATs responsible for TRPM7 and impacts of palmitoylation on substrate recruitment of its kinase domain are both worthwhile future research avenues. Moreover, a transgenic animal model animal model with non-palmitoylated TRPM7 might be useful to investigate the importance of TRPM7 palmitoylation on disease pathogenesis. And crucial experiments need to be repeated in its closest homology, TRPM6.

In conclusion, our research has established a novel regulatory mechanism of TRPM7. Palmitoylation regulates TRPM7 movement through the secretory pathway and sorting its distribution between intracellular vesicles and plasma membrane. Palmitoylation is required to stabilize the TRPM7 structure by anchoring the C-terminal end of TRP domain to the membrane, as well as it might be the common feature to majority of TRP channels. Meanwhile, palmitoylation might regulate channel gating cooperated with PIP2 due to the later one normally binding to positively charged amino acids in TRP domain. And inhibiting palmitoylation induces significant decrease in TRPM7-mediated Calcium-influx, which also suggests palmitoylation alters the ion channel activity. In contrast, the influence of palmitoylation on TRPM7 kinase domain activity needs further investigation.

List of References

AARTS, M., IIHARA, K., WEI, W.-L., XIONG, Z.-G., ARUNDINE, M., CERWINSKI, W., MACDONALD, J. F. & TYMIANSKI, M. 2003. A key role for TRPM7 channels in anoxic neuronal death. *Cell*, 115, 863-877.

ABIRIA, S. A., KRAPIVINSKY, G., SAH, R., SANTA-CRUZ, A. G., CHAUDHURI, D., ZHANG, J., ADSTAMONGKONKUL, P., DECAEN, P. G. & CLAPHAM, D. E. 2017a. TRPM7 senses oxidative stress to release Zn from unique intracellular vesicles. *Proceedings of the National Academy of Sciences,* 114, E6079-E6088.

ABIRIA, S. A., KRAPIVINSKY, G., SAH, R., SANTA-CRUZ, A. G., CHAUDHURI, D., ZHANG, J., ADSTAMONGKONKUL, P., DECAEN, P. G. & CLAPHAM, D. E. J. P. O. T. N. A. O. S. 2017b. TRPM7 senses oxidative stress to release Zn from unique intracellular vesicles. 114, E6079-E6088.

ADIBEKIAN, A., MARTIN, B. R., CHANG, J. W., HSU, K.-L., TSUBOI, K., BACHOVCHIN, D. A., SPEERS, A. E., BROWN, S. J., SPICER, T. & FERNANDEZ-VEGA, V. 2012. Confirming target engagement for reversible inhibitors in vivo by kinetically tuned activity-based probes. *Journal of the American Chemical Society,* 134, 10345-10348.

ALONSO, A. M., CÓCERES, V. M., DE NAPOLI, M. G., GUIL, A. N., ÁNGEL, S. O. & CORVI, M. M. 2012. Protein palmitoylation inhibition by 2-bromopalmitate alters gliding, host cell invasion and parasite morphology in Toxoplasma gondii. *Molecular and Biochemical Parasitology,* 184, 39-43.

ANDRASI, E., IGAZ, S., MOLNÁR, Z. & MAKO, S. 2000. Disturbances of magnesium concentrations in various brain areas in Alzheimer's disease. *Magnesium research,* 13, 189-196.

ANDRIULĖ, I., PANGONYTĖ, D., ALMANAITYTĖ, M., PATAMSYTĖ, V., KUPRYTĖ, M., KARČIAUSKAS, D., MUBAGWA, K. & MAČIANSKIENĖ, R. 2021. Evidence for the expression of TRPM6 and TRPM7 in cardiomyocytes from all four chamber walls of the human heart. *Scientific reports,* 11, 1-14.

ANTUNES, T. T., CALLERA, G. E., HE, Y., YOGI, A., RYAZANOV, A. G., RYAZANOVA, L. V., ZHAI, A., STEWART, D. J., SHRIER, A. & TOUYZ, R. M. 2016. Transient Receptor Potential Melastatin 7 Cation Channel Kinase: New Player in Angiotensin II–Induced Hypertension. *Hypertension,* 67, 763-773.

ARJONA, F. J., LATTA, F., MOHAMMED, S. G., THOMASSEN, M., VAN WIJK, E., BINDELS, R. J., HOENDEROP, J. G. & DE BAAIJ, J. H. 2019. SLC41A1 is essential for magnesium homeostasis in vivo. *Pflügers Archiv-European Journal of Physiology,* 471, 845-860.

ARNHEITER, H., DUBOIS-DALCQ, M. & LAZZARINI, R. A. 1984. Direct visualization of protein transport and processing in the living cell by microinjection of specific antibodies. *Cell,* 39, 99-109.

ASGHAR, M. Y. & TÖRNQUIST, K. 2020. Transient receptor potential canonical (TRPC) channels as modulators of migration and invasion. *International Journal of Molecular Sciences,* 21, 1739.

AWAD, M. M., DALAL, D., TICHNELL, C., JAMES, C., TUCKER, A., ABRAHAM, T., SPEVAK, P. J., CALKINS, H. & JUDGE, D. P. 2006. Recessive arrhythmogenic right ventricular dysplasia due to novel cryptic splice mutation in PKP2. *Human mutation,* 27, 1157-1157.

AZIZI, S.-A., LAN, T., DELALANDE, C., KATHAYAT, R. S., BANALES MEJIA, F., QIN, A., BROOKES, N., SANDOVAL, P. J. & DICKINSON, B. C. 2021. Development

of an acrylamide-based inhibitor of protein S-acylation. *ACS Chemical Biology,* 16**,** 1546-1556.

BACHOVCHIN, D. A., JI, T., LI, W., SIMON, G. M., BLANKMAN, J. L., ADIBEKIAN, A., HOOVER, H., NIESSEN, S. & CRAVATT, B. F. 2010. Superfamily-wide portrait of serine hydrolase inhibition achieved by library-versus-library screening. *Proceedings of the National Academy of Sciences,* 107**,** 20941-20946.

BAI, Z., FENG, J., FRANKEN, G. A., AL'SAADI, N., CAI, N., YU, A. S., LOU, L., KOMIYA, Y., HOENDEROP, J. G. & DE BAAIJ, J. H. 2021. CNNM proteins selectively bind to the TRPM7 channel to stimulate divalent cation entry into cells. *PLoS biology,* 19**,** e3001496.

BAKER, T. L., ZHENG, H., WALKER, J., COLOFF, J. L. & BUSS, J. E. 2003. Distinct rates of palmitate turnover on membrane-bound cellular and oncogenic H-ras. *Journal of Biological Chemistry,* 278**,** 19292-19300.

BALDOLI, E., CASTIGLIONI, S. & MAIER, J. A. 2013. Regulation and function of TRPM7 in human endothelial cells: TRPM7 as a potential novel regulator of endothelial function. *PloS one,* 8**,** e59891.

BALDOLI, E. & MAIER, J. A. 2012. Silencing TRPM7 mimics the effects of magnesium deficiency in human microvascular endothelial cells. *Angiogenesis,* 15**,** 47-57.

BANCERZ, B., DUŚ-ŻUCHOWSKA, M., CICHY, W. & MATUSIEWICZ, H. 2012. Effect of magnesium on human health. *Gastroenterology Review/Przegląd Gastroenterologiczny,* 7**,** 359-366.

BARBAGALLO, M. & DOMINGUEZ, L. J. 2015. Magnesium and type 2 diabetes. *World journal of diabetes,* 6**,** 1152.

BAYLIE, R. & BRAYDEN, J. 2011. TRPV channels and vascular function. *Acta Physiologica,* 203**,** 99-116.

BECKER, D., MÜLLER, M., LEUNER, K. & JENDRACH, M. 2008. The C-terminal domain of TRPV4 is essential for plasma membrane localization. *Molecular membrane biology,* 25**,** 139-151.

BÉLANGER, C., ANSANAY, H., QANBAR, R. & BOUVIER, M. 2001. Primary sequence requirements for S-acylation of ß2-adrenergic receptor peptides. *FEBS letters,* 499**,** 59-64.

BERRIDGE, M., LIPP, P. & BOOTMAN, M. 1999. Calcium signalling. *Current biology,* 9**,** R157-R159.

BIBAWY, J. N., PARIKH, V., WAHBA, J., BARSOUM, E. A., LAFFERTY, J., KOWALSKI, M. & BEKHEIT, S. 2013. Pantoprazole (proton pump inhibitor) contributing to torsades de pointes storm. *Circulation: Arrhythmia and Electrophysiology,* 6**,** e17-e19.

BLAINE, J., CHONCHOL, M. & LEVI, M. 2015. Renal control of calcium, phosphate, and magnesium homeostasis. *Clinical Journal of the American Society of Nephrology,* 10**,** 1257-1272.

BLANC, M., DAVID, F., ABRAMI, L., MIGLIOZZI, D., ARMAND, F., BÜRGI, J. & VAN DER GOOT, F. G. 2015. SwissPalm: protein palmitoylation database. *F1000Research,* 4.

BO, S. & PISU, E. 2008. Role of dietary magnesium in cardiovascular disease prevention, insulin sensitivity and diabetes. *Current opinion in lipidology,* 19**,** 50-56.

BONCOMPAIN, G., DIVOUX, S., GAREIL, N., DE FORGES, H., LESCURE, A., LATRECHE, L., MERCANTI, V., JOLLIVET, F., RAPOSO, G. & PEREZ, F. 2012. Synchronization of secretory protein traffic in populations of cells. *Nature methods,* 9**,** 493-498.

BOOZ, G. W. & BAKER, K. M. 1995. Molecular signalling mechanisms controlling growth and function of cardiac fibroblasts. *Cardiovascular research,* 30**,** 537-543.

BOUSOVA, K., ZOUHAROVA, M., HERMAN, P., VETYSKOVA, V., JIRASKOVA, K. & VONDRASEK, J. 2021. TRPM7 N-terminal region forms complexes with calcium binding proteins CaM and S100A1. *Heliyon,* 7**,** e08490.

BRAUCHI, S., KRAPIVINSKY, G., KRAPIVINSKY, L. & CLAPHAM, D. E. 2008. TRPM7 facilitates cholinergic vesicle fusion with the plasma membrane. *Proceedings of the National Academy of Sciences,* 105**,** 8304-8308.

BRAUCHI, S., ORTA, G., MASCAYANO, C., SALAZAR, M., RADDATZ, N., URBINA, H., ROSENMANN, E., GONZALEZ-NILO, F. & LATORRE, R. 2007. Dissection of the components for PIP2 activation and thermosensation in TRP channels. *Proceedings of the National Academy of Sciences,* 104**,** 10246-10251.

BREA, R. J., RUDD, A. K. & DEVARAJ, N. K. 2016. Nonenzymatic biomimetic remodeling of phospholipids in synthetic liposomes. *Proceedings of the National Academy of Sciences,* 113**,** 8589-8594.

BRIGIDI, G. S., SANTYR, B., SHIMELL, J., JOVELLAR, B. & BAMJI, S. X. 2015. Activity-regulated trafficking of the palmitoyl-acyl transferase DHHC5. *Nature communications,* 6**,** 1-17.

BRIGIDI, G. S., SUN, Y., BECCANO-KELLY, D., PITMAN, K., MOBASSER, M., BORGLAND, S. L., MILNERWOOD, A. J. & BAMJI, S. X. 2014. Palmitoylation of δ-catenin by DHHC5 mediates activity-induced synapse plasticity. *Nature neuroscience,* 17**,** 522-532.

BROWN, R. W., SHARMA, A. I. & ENGMAN, D. M. 2017. Dynamic protein S-palmitoylation mediates parasite life cycle progression and diverse mechanisms of virulence. *Critical reviews in biochemistry and molecular biology,* 52**,** 145-162.

BUI, D. M., GREGAN, J., JAROSCH, E., RAGNINI, A. & SCHWEYEN, R. J. 1999. The bacterial magnesium transporter CorA can functionally substitute for its putative homologue Mrs2p in the yeast inner mitochondrial membrane. *Journal of Biological Chemistry,* 274**,** 20438-20443.

CAI, N., BAI, Z., NANDA, V. & RUNNELS, L. W. 2017. Mass spectrometric analysis of TRPM6 and TRPM7 phosphorylation reveals regulatory mechanisms of the channel-kinases. *Scientific reports,* 7**,** 1-14.

CALLERA, G. E., HE, Y., YOGI, A., MONTEZANO, A. C., PARAVICINI, T., YAO, G. & TOUYZ, R. M. 2009. Regulation of the novel Mg transporter transient receptor potential melastatin 7 (TRPM7) cation channel by bradykinin in vascular smooth muscle cells. *Journal of hypertension,* 27**,** 155-166.

CALLERA, G. E., MONTEZANO, A. C., YOGI, A., TOSTES, R. C., HE, Y., SCHIFFRIN, E. L. & TOUYZ, R. M. 2005. c-Src–dependent nongenomic signaling responses to aldosterone are increased in vascular myocytes from spontaneously hypertensive rats. *Hypertension,* 46**,** 1032-1038.

CALSOU, P. & SALLES, B. 1994. Properties of damage-dependent DNA incision by nucleotide excision repair in human cell-free extracts. *Nucleic acids research,* 22**,** 4937-4942.

CAO, Y., QIU, T., KATHAYAT, R. S., AZIZI, S.-A., THORNE, A. K., AHN, D., FUKATA, Y., FUKATA, M., RICE, P. A. & DICKINSON, B. C. 2019. ABHD10 is an S-depalmitoylase affecting redox homeostasis through peroxiredoxin-5. *Nature chemical biology,* 15**,** 1232-1240.

CASTILHO, R. F., WARD, M. W. & NICHOLLS, D. G. 1999. Oxidative stress, mitochondrial function, and acute glutamate excitotoxicity in cultured cerebellar granule cells. *Journal of neurochemistry,* 72**,** 1394-1401.

CAT, A. N. D. & JAISSER, F. 2012. Extrarenal effects of aldosterone. *Current opinion in nephrology and hypertension,* 21, 147-156.
CATERINA, M. J., LEFFLER, A., MALMBERG, A. B., MARTIN, W., TRAFTON, J., PETERSEN-ZEITZ, K., KOLTZENBURG, M., BASBAUM, A. & JULIUS, D. 2000. Impaired nociception and pain sensation in mice lacking the capsaicin receptor. *science,* 288, 306-313.
CATERINA, M. J., ROSEN, T. A., TOMINAGA, M., BRAKE, A. J. & JULIUS, D. 1999. A capsaicin-receptor homologue with a high threshold for noxious heat. *Nature,* 398, 436-441.
CEFARATTI, C. & RUSE, C. 2007. Protein kinase A dependent phosphorylation activates Mg efflux in the basolateral region of the liver. *Molecular and cellular biochemistry,* 297, 209-214.
CERRONE, M., MONTNACH, J., LIN, X., ZHAO, Y.-T., ZHANG, M., AGULLO-PASCUAL, E., LEO-MACIAS, A., ALVARADO, F. J., DOLGALEV, I. & KARATHANOS, T. V. 2017. Plakophilin-2 is required for transcription of genes that control calcium cycling and cardiac rhythm. *Nature communications,* 8, 1-16.
CHAKRABORTI, S., CHAKRABORTI, T., MANDAL, M., MANDAL, A., DAS, S. & GHOSH, S. 2002. Protective role of magnesium in cardiovascular diseases: a review. *Molecular and cellular biochemistry,* 238, 163-179.
CHANPUT, W., MES, J. J. & WICHERS, H. J. 2014. THP-1 cell line: an in vitro cell model for immune modulation approach. *International immunopharmacology,* 23, 37-45.
CHAROLLAIS, J. & VAN DER GOOT, F. G. 2009. Palmitoylation of membrane proteins. *Molecular membrane biology,* 26, 55-66.
CHEN, Q., SHE, J., ZENG, W., GUO, J., XU, H., BAI, X.-C. & JIANG, Y. 2017. Structure of mammalian endolysosomal TRPML1 channel in nanodiscs. *Nature,* 550, 415-418.
CHEN, W.-L., BARSZCZYK, A., TURLOVA, E., DEURLOO, M., LIU, B., YANG, B. B., RUTKA, J. T., FENG, Z.-P. & SUN, H.-S. 2015. Inhibition of TRPM7 by carvacrol suppresses glioblastoma cell proliferation, migration and invasion. *Oncotarget,* 6, 16321.
CHENG, W., YANG, F., TAKANISHI, C. L. & ZHENG, J. 2007. Thermosensitive TRPV channel subunits coassemble into heteromeric channels with intermediate conductance and gating properties. *The Journal of general physiology,* 129, 191-207.
CHOKSHI, R., MATSUSHITA, M. & KOZAK, J. A. 2012a. Detailed examination of Mg and pH sensitivity of human TRPM7 channels. *American Journal of Physiology-Cell Physiology,* 302, C1004-C1011.
CHOKSHI, R., MATSUSHITA, M. & KOZAK, J. A. 2012b. Sensitivity of TRPM7 channels to Mg characterized in cell-free patches of Jurkat T lymphocytes. *American Journal of Physiology-Cell Physiology,* 302, C1642-C1651.
CHUBANOV, V., FERIOLI, S., WISNOWSKY, A., SIMMONS, D. G., LEITZINGER, C., EINER, C., JONAS, W., SHYMKIV, Y., BARTSCH, H. & BRAUN, A. 2016. Epithelial magnesium transport by TRPM6 is essential for prenatal development and adult survival. *Elife,* 5, e20914.
CHUBANOV, V. & GUDERMANN, T. 2020. Mapping TRPM7 function by NS8593. *International Journal of Molecular Sciences,* 21, 7017.
CHUBANOV, V., MEDEROS Y SCHNITZLER, M., MEIßNER, M., SCHÄFER, S., ABSTIENS, K., HOFMANN, T. & GUDERMANN, T. 2012. Natural and synthetic modulators of SK (Kca2) potassium channels inhibit

magnesium – dependent activity of the kinase – coupled cation channel TRPM7. *British journal of pharmacology,* 166**,** 1357-1376.
CHUBANOV, V., MEDEROS Y SCHNITZLER, M., WÄRING, J., PLANK, A. & GUDERMANN, T. 2005. Emerging roles of TRPM6/TRPM7 channel kinase signal transduction complexes. *Naunyn-Schmiedeberg's archives of pharmacology,* 371**,** 334-341.
CHUBANOV, V., MITTERMEIER, L. & GUDERMANN, T. 2018. TRPM7 reflected in Cryo-EMirror. *Cell Calcium,* 76**,** 129-131.
CHUBANOV, V., WALDEGGER, S., SCHNITZLER, M. M. Y., VITZTHUM, H., SASSEN, M. C., SEYBERTH, H. W., KONRAD, M. & GUDERMANN, T. 2004. Disruption of TRPM6/TRPM7 complex formation by a mutation in the TRPM6 gene causes hypomagnesemia with secondary hypocalcemia. *Proceedings of the National Academy of Sciences,* 101**,** 2894-2899.
CLAPHAM, D. E. 2003. TRP channels as cellular sensors. *Nature,* 426**,** 517-524.
CLAPHAM, D. E., RUNNELS, L. W. & STRÜBING, C. 2001. The TRP ion channel family. *Nature Reviews Neuroscience,* 2**,** 387-396.
CLARK, K., LANGESLAG, M., VAN LEEUWEN, B., RAN, L., RYAZANOV, A. G., FIGDOR, C. G., MOOLENAAR, W. H., JALINK, K. & VAN LEEUWEN, F. N. 2006. TRPM7, a novel regulator of actomyosin contractility and cell adhesion. *The EMBO journal*, 25**,** 290-301.
CLARK, K., MIDDELBEEK, J., LASONDER, E., DULYANINOVA, N. G., MORRICE, N. A., RYAZANOV, A. G., BRESNICK, A. R., FIGDOR, C. G. & VAN LEEUWEN, F. N. 2008a. TRPM7 regulates myosin IIA filament stability and protein localization by heavy chain phosphorylation. *Journal of molecular biology,* 378**,** 790-803.
CLARK, K., MIDDELBEEK, J., MORRICE, N. A., FIGDOR, C. G., LASONDER, E. & VAN LEEUWEN, F. N. 2008b. Massive autophosphorylation of the Ser/Thr-rich domain controls protein kinase activity of TRPM6 and TRPM7. *PloS one,* 3**,** e1876.
COHEN, L. & KITZES, R. 1985. Early radiation-induced proctosigmoiditis responds to magnesium therapy. *Magnesium,* 4**,** 16-19.
COLLINS, M. O., WOODLEY, K. T. & CHOUDHARY, J. S. 2017. Global, site-specific analysis of neuronal protein S-acylation. *Scientific reports,* 7**,** 1-14.
CORDIER, C., PREVARSKAYA, N. & LEHEN'KYI, V. Y. 2021. TRPM7 ion channel: oncogenic roles and therapeutic potential in breast cancer. *Cancers,* 13**,** 6322.
COREY, D. P., GARCIA-ANOVEROS, J., HOLT, J. R., KWAN, K. Y., LIN, S.-Y., VOLLRATH, M. A., AMALFITANO, A., CHEUNG, E. L.-M., DERFLER, B. H. & DUGGAN, A. 2004. TRPA1 is a candidate for the mechanosensitive transduction channel of vertebrate hair cells. *Nature,* 432**,** 723-730.
CRANE, J. M. & VERKMAN, A. 2009. Reversible, temperature-dependent supramolecular assembly of aquaporin-4 orthogonal arrays in live cell membranes. *Biophysical journal,* 97**,** 3010-3018.
CUAJUNGCO, M. P., SILVA, J., HABIBI, A. & VALADEZ, J. A. 2016. The mucolipin-2 (TRPML2) ion channel: a tissue-specific protein crucial to normal cell function. *Pflügers Archiv-European Journal of Physiology,* 468**,** 177-192.
CUNHA, A. R., D'EL-REI, J., MEDEIROS, F., UMBELINO, B., OIGMAN, W., TOUYZ, R. M. & NEVES, M. F. 2017. Oral magnesium supplementation improves endothelial function and attenuates subclinical atherosclerosis in thiazide-treated hypertensive women. *Journal of hypertension,* 35**,** 89-97.
CURRY, J. N. & ALAN, S. 2018. Magnesium handling in the kidney. *Advances in chronic kidney disease,* 25**,** 236-243.

D'ANGELO, G., PRENCIPE, L., IODICE, L., BEZNOUSSENKO, G., SAVARESE, M., MARRA, P., DI TULLIO, G., MARTIRE, G., DE MATTEIS, M. A. & BONATTI, S. 2009. GRASP65 and GRASP55 sequentially promote the transport of C-terminal valine-bearing cargos to and through the Golgi complex. *Journal of Biological Chemistry,* 284**,** 34849-34860.

DANESHMANDPOUR, Y., DARVISH, H., PASHAZADEH, F. & EMAMALIZADEH, B. 2019. Features, genetics and their correlation in Jalili syndrome: a systematic review. *Journal of Medical Genetics,* 56**,** 358-369.

DAWSON, P. E., MUIR, T. W., CLARK-LEWIS, I. & KENT, S. B. 1994. Synthesis of proteins by native chemical ligation. *Science,* 266**,** 776-779.

DE BAAIJ, J. H. 2015. The art of magnesium transport. *Magnesium Research,* 28**,** 85-91.

DE BAAIJ, J. H., HOENDEROP, J. G. & BINDELS, R. J. 2012. Regulation of magnesium balance: lessons learned from human genetic disease. *Clinical kidney journal,* 5**,** i15-i24.

DE BAAIJ, J. H., HOENDEROP, J. G. & BINDELS, R. J. 2015. Magnesium in man: implications for health and disease. *Physiological reviews*.

DEASON-TOWNE, F., PERRAUD, A.-L. & SCHMITZ, C. 2011. The Mg transporter MagT1 partially rescues cell growth and Mg uptake in cells lacking the channel-kinase TRPM7. *FEBS letters,* 585**,** 2275-2278.

DEASON-TOWNE, F., PERRAUD, A.-L. & SCHMITZ, C. 2012. Identification of Ser/Thr phosphorylation sites in the C2-domain of phospholipase C γ2 (PLCγ2) using TRPM7-kinase. *Cellular signalling,* 24**,** 2070-2075.

DEKKER, F. J., ROCKS, O., VARTAK, N., MENNINGER, S., HEDBERG, C., BALAMURUGAN, R., WETZEL, S., RENNER, S., GERAUER, M. & SCHÖLERMANN, B. 2010. Small-molecule inhibition of APT1 affects Ras localization and signaling. *Nature chemical biology,* 6**,** 449-456.

DEMEUSE, P., PENNER, R. & FLEIG, A. 2006. TRPM7 channel is regulated by magnesium nucleotides via its kinase domain. *The Journal of general physiology,* 127**,** 421-434.

DESAI, B. N., KRAPIVINSKY, G., NAVARRO, B., KRAPIVINSKY, L., CARTER, B. C., FEBVAY, S., DELLING, M., PENUMAKA, A., RAMSEY, I. S. & MANASIAN, Y. 2012. Cleavage of TRPM7 releases the kinase domain from the ion channel and regulates its participation in Fas-induced apoptosis. *Developmental cell,* 22**,** 1149-1162.

DI PALMA, F., BELYANTSEVA, I. A., KIM, H. J., VOGT, T. F., KACHAR, B. & NOBEN-TRAUTH, K. 2002. Mutations in Mcoln3 associated with deafness and pigmentation defects in varitint-waddler (Va) mice. *Proceedings of the National Academy of Sciences,* 99**,** 14994-14999.

DIETRICH, A., MEDEROS Y SCHNITZLER, M., GOLLASCH, M., GROSS, V., STORCH, U., DUBROVSKA, G., OBST, M., YILDIRIM, E., SALANOVA, B. & KALWA, H. 2005. Increased vascular smooth muscle contractility in TRPC6−/− mice. *Molecular and cellular biology,* 25**,** 6980-6989.

DIGGLE, T. A., SEEHRA, C. K., HASE, S. & REDPATH, N. T. 1999. Analysis of the domain structure of elongation factor – 2 kinase by mutagenesis. *FEBS letters,* 457**,** 189-192.

DOROVKOV, M., BEZNOSOV, S., SHAH, S., KOTLYANSKAYA, L. & KOSTYUKOVA, A. 2008. Effect of mutations imitating the phosphorylation by TRPM7 kinase on the function of the N-terminal domain of tropomodulin. *Biophysics,* 53**,** 500-504.

DOROVKOV, M. V., KOSTYUKOVA, A. S. & RYAZANOV, A. G. 2011. Phosphorylation of annexin A1 by TRPM7 kinase: a switch regulating the induction of an α-helix. *Biochemistry,* 50**,** 2187-2193.

DOROVKOV, M. V. & RYAZANOV, A. G. 2004. Phosphorylation of annexin I by TRPM7 channel-kinase. *Journal of Biological Chemistry,* 279**,** 50643-50646.

DOS SANTOS, L. R., MELO, S. R. D. S., SEVERO, J. S., MORAIS, J. B. S., DA SILVA, L. D., DE PAIVA SOUSA, M., DE SOUSA, T. G. V., HENRIQUES, G. S. & DO NASCIMENTO MARREIRO, D. 2021. Cardiovascular diseases in obesity: what is the role of magnesium? *Biological Trace Element Research,* 199**,** 4020-4027.

DROZDETSKIY, A., COLE, C., PROCTER, J. & BARTON, G. J. 2015. JPred4: a protein secondary structure prediction server. *Nucleic acids research,* 43**,** W389-W394.

DU, J., XIE, J., ZHANG, Z., TSUJIKAWA, H., FUSCO, D., SILVERMAN, D., LIANG, B. & YUE, L. 2010. TRPM7-mediated Ca signals confer fibrogenesis in human atrial fibrillation. *Circulation research,* 106**,** 992-1003.

DUAN, J., LI, Z., LI, J., HULSE, R. E., SANTA-CRUZ, A., VALINSKY, W. C., ABIRIA, S. A., KRAPIVINSKY, G., ZHANG, J. & CLAPHAM, D. E. 2018. Structure of the mammalian TRPM7, a magnesium channel required during embryonic development. *Proceedings of the National Academy of Sciences,* 115**,** E8201-E8210.

DUNCAN, J. A. & GILMAN, A. G. 1996. Autoacylation of G protein α subunits. *Journal of Biological Chemistry,* 271**,** 23594-23600.

DUNCAN, L. M., DEEDS, J., HUNTER, J., SHAO, J., HOLMGREN, L. M., WOOLF, E. A., TEPPER, R. I. & SHYJAN, A. W. 1998. Down-regulation of the novel gene melastatin correlates with potential for melanoma metastasis. *Cancer research,* 58**,** 1515-1520.

EBEL, H., HOLLSTEIN, M. & GÜNTHER, T. 2004. Differential effect of imipramine and related compounds on Mg efflux from rat erythrocytes. *Biochimica et Biophysica Acta (BBA)-Biomembranes,* 1667**,** 132-140.

ELIN, R. 1988. Magnesium metabolism in health and disease/Elin RJ. *Disease-a-Month.(Ed. Bone RC). Year Book Medical Publishers, Inc*.

ERLER, I., HIRNET, D., WISSENBACH, U., FLOCKERZI, V. & NIEMEYER, B. A. 2004. Ca-selective transient receptor potential V channel architecture and function require a specific ankyrin repeat. *Journal of Biological Chemistry,* 279**,** 34456-34463.

ERNST, A. M., SYED, S. A., ZAKI, O., BOTTANELLI, F., ZHENG, H., HACKE, M., XI, Z., RIVERA-MOLINA, F., GRAHAM, M. & REBANE, A. A. 2018. S-palmitoylation sorts membrane cargo for anterograde transport in the Golgi. *Developmental cell,* 47**,** 479-493. e7.

ESSANDOH, K., PHILIPPE, J. M., JENKINS, P. M. & BRODY, M. J. 2020. Palmitoylation: a fatty regulator of myocardial electrophysiology. *Frontiers in physiology***,** 108.

FAOUZI, M., KILCH, T., HORGEN, F. D., FLEIG, A. & PENNER, R. 2017a. The TRPM7 channel kinase regulates store-operated calcium entry. *J Physiol,* 595**,** 3165-3180.

FAOUZI, M., KILCH, T., HORGEN, F. D., FLEIG, A. & PENNER, R. 2017b. The TRPM7 channel kinase regulates store – operated calcium entry. *The Journal of physiology,* 595**,** 3165-3180.

FEARNLEY, C. J., RODERICK, H. L. & BOOTMAN, M. D. 2011. Calcium signaling in cardiac myocytes. *Cold Spring Harb Perspect Biol,* 3**,** a004242.

FERIOLI, S., ZIERLER, S., ZAIßERER, J., SCHREDELSEKER, J., GUDERMANN, T. & CHUBANOV, V. 2017. TRPM6 and TRPM7 differentially contribute to the relief of heteromeric TRPM6/7 channels from inhibition by cytosolic Mg and Mg· ATP. *Scientific reports,* 7**,** 1-19.

FIORENTINI, D., CAPPADONE, C., FARRUGGIA, G. & PRATA, C. 2021. Magnesium: biochemistry, nutrition, detection, and social impact of diseases linked to its deficiency. *Nutrients,* 13**,** 1136.

FLEIG, A. & CHUBANOV, V. 2014. TRPM7. *Mammalian transient receptor potential (TRP) cation channels***,** 521-546.

FLEIG, A. & PENNER, R. 2004. The TRPM ion channel subfamily: molecular, biophysical and functional features. *Trends in pharmacological sciences,* 25**,** 633-639.

FLEIG, A., SCHWEIGEL – RÖNTGEN, M. & KOLISEK, M. 2013. Solute carrier family SLC41: what do we really know about it? *Wiley Interdisciplinary Reviews: Membrane Transport and Signaling,* 2**,** 227-239.

FONFRIA, E., MURDOCK, P. R., CUSDIN, F. S., BENHAM, C. D., KELSELL, R. E. & MCNULTY, S. 2006. Tissue distribution profiles of the human TRPM cation channel family. *Journal of Receptors and Signal Transduction,* 26**,** 159-178.

FORMOSO, K., SUSPERREGUY, S., FREICHEL, M. & BIRNBAUMER, L. 2020. RNA-seq analysis reveals TRPC genes to impact an unexpected number of metabolic and regulatory pathways. *Scientific reports,* 10**,** 1-20.

FRASER, N. J., HOWIE, J., WYPIJEWSKI, K. J. & FULLER, W. 2020. Therapeutic targeting of protein S-acylation for the treatment of disease. *Biochemical Society Transactions,* 48**,** 281-290.

FUJIWARA, Y. & MINOR JR, D. L. 2008. X-ray crystal structure of a TRPM assembly domain reveals an antiparallel four-stranded coiled-coil. *Journal of molecular biology,* 383**,** 854-870.

FUNATO, Y., FURUTANI, K., KURACHI, Y. & MIKI, H. 2018. CrossTalk proposal: CNNM proteins are Na/Mg exchangers playing a central role in transepithelial Mg (re) absorption. *The Journal of physiology,* 596**,** 743.

GAO, H., CHEN, X., DU, X., GUAN, B., LIU, Y. & ZHANG, H. 2011. EGF enhances the migration of cancer cells by up-regulation of TRPM7. *Cell calcium,* 50**,** 559-568.

GARCÍA-SANZ, N., FERNÁNDEZ-CARVAJAL, A., MORENILLA-PALAO, C., PLANELLS-CASES, R., FAJARDO-SÁNCHEZ, E., FERNÁNDEZ-BALLESTER, G. & FERRER-MONTIEL, A. 2004. Identification of a tetramerization domain in the C terminus of the vanilloid receptor. *Journal of Neuroscience,* 24**,** 5307-5314.

GAUTHIER-KEMPER, A., IGAEV, M., SÜNDERMANN, F., JANNING, D., BRÜHMANN, J., MOSCHNER, K., REYHER, H.-J., JUNGE, W., GLEBOV, K. & WALTER, J. 2014. Interplay between phosphorylation and palmitoylation mediates plasma membrane targeting and sorting of GAP43. *Molecular biology of the cell,* 25**,** 3284-3299.

GEES, M., COLSOUL, B. & NILIUS, B. 2010. The role of transient receptor potential cation channels in Ca signaling. *Cold Spring Harbor perspectives in biology,* 2**,** a003962.

GILLINGHAM, A. K. & MUNRO, S. 2016. Finding the Golgi: Golgin coiled-coil proteins show the way. *Trends in cell biology,* 26**,** 399-408.

GÖK, C., MAIN, A., GAO, X., KEREKES, Z., PLAIN, F., KUO, C.-W., ROBERTSON, A. D., FRASER, N. J. & FULLER, W. 2021. Insights into the molecular basis of

the palmitoylation and depalmitoylation of NCX1. *Cell calcium,* 97, 102408.
GÖK, C., PLAIN, F., ROBERTSON, A. D., HOWIE, J., BAILLIE, G. S., FRASER, N. J. & FULLER, W. 2020. Dynamic palmitoylation of the sodium-calcium exchanger modulates its structure, affinity for lipid-ordered domains, and inhibition by XIP. *Cell reports,* 31, 107697.
GOLDBERG, M. P. & CHOI, D. W. 1993. Combined oxygen and glucose deprivation in cortical cell culture: calcium-dependent and calcium-independent mechanisms of neuronal injury. *Journal of neuroscience,* 13, 3510-3524.
GORLEKU, O. A., BARNS, A.-M., PRESCOTT, G. R., GREAVES, J. & CHAMBERLAIN, L. H. 2011. Endoplasmic reticulum localization of DHHC palmitoyltransferases mediated by lysine-based sorting signals. *Journal of Biological Chemistry,* 286, 39573-39584.
GOYTAIN, A. & QUAMME, G. A. 2005a. Functional characterization of human SLC41A1, a Mg transporter with similarity to prokaryotic MgtE Mg transporters. *Physiological genomics,* 21, 337-342.
GOYTAIN, A. & QUAMME, G. A. 2005b. Identification and characterization of a novel mammalian Mg transporter with channel-like properties. *BMC genomics,* 6, 1-18.
GRAHAM, L., CAESAR, J. & BUEGEN, A. 1960. Gastrointestinal absorption and excretion of Mg28 in man. *Metabolism,* 9, 646-659.
GRANDL, J., HU, H., BANDELL, M., BURSULAYA, B., SCHMIDT, M., PETRUS, M. & PATAPOUTIAN, A. 2008. Pore region of TRPV3 ion channel is specifically required for heat activation. *Nature neuroscience,* 11, 1007-1013.
GREAVES, J., CARMICHAEL, J. A. & CHAMBERLAIN, L. H. 2011. The palmitoyl transferase DHHC2 targets a dynamic membrane cycling pathway: regulation by a C-terminal domain. *Molecular biology of the cell,* 22, 1887-1895.
GREAVES, J., PRESCOTT, G. R., GORLEKU, O. A. & CHAMBERLAIN, L. H. 2009. The fat controller: roles of palmitoylation in intracellular protein trafficking and targeting to membrane microdomains. *Molecular membrane biology,* 26, 67-79.
GREENMAN, C., STEPHENS, P., SMITH, R., DALGLIESH, G. L., HUNTER, C., BIGNELL, G., DAVIES, H., TEAGUE, J., BUTLER, A. & STEVENS, C. 2007. Patterns of somatic mutation in human cancer genomes. *Nature,* 446, 153-158.
GREKA, A., NAVARRO, B., OANCEA, E., DUGGAN, A. & CLAPHAM, D. E. 2003. TRPC5 is a regulator of hippocampal neurite length and growth cone morphology. *Nature neuroscience,* 6, 837-845.
GRIMM, C., KRAFT, R., SAUERBRUCH, S., SCHULTZ, G. N. & HARTENECK, C. 2003. Molecular and functional characterization of the melastatin-related cation channel TRPM3. *Journal of Biological Chemistry,* 278, 21493-21501.
GRÖBER, U., SCHMIDT, J. & KISTERS, K. 2015. Magnesium in prevention and therapy. *Nutrients,* 7, 8199-8226.
GROENESTEGE, W. M. T., HOENDEROP, J. G., VAN DEN HEUVEL, L., KNOERS, N. & BINDELS, R. J. 2006. The epithelial Mg channel transient receptor potential melastatin 6 is regulated by dietary Mg content and estrogens. *Journal of the American Society of Nephrology,* 17, 1035-1043.
GROSSMANN, C. & GEKLE, M. 2007. Non-classical actions of the mineralocorticoid receptor: misuse of EGF receptors? *Molecular and cellular endocrinology,* 277, 6-12.
GRUBBS, R. D. & MAGUIRE, M. E. 1987. Magnesium as a regulatory cation: criteria and evaluation. *Magnesium,* 6, 113-127.

GUAN, X. & FIERKE, C. A. 2011. Understanding protein palmitoylation: Biological significance and enzymology. *Science China Chemistry,* 54, 1888-1897.
GUILBERT, A., GAUTIER, M., DHENNIN-DUTHILLE, I., HAREN, N., SEVESTRE, H. & OUADID-AHIDOUCH, H. 2009. Evidence that TRPM7 is required for breast cancer cell proliferation. *American Journal of Physiology-Cell Physiology,* 297, C493-C502.
GÜNTHER, T. & VORMANN, J. 1985. Mg efflux is accomplished by an amiloride-sensitive Na Mg antiport. *Biochemical and biophysical research communications,* 130, 540-545.
GÜNTHER, T. & VORMANN, J. 1990. Na (+)-dependent Mg efflux from Mg (2+)-loaded rat thymocytes and HL 60 cells. *Magnesium and trace elements,* 9, 279-282.
GYORKE, S. 2009. Molecular basis of catecholaminergic polymorphic ventricular tachycardia. *Heart Rhythm,* 6, 123-9.
HALLER, H. 1977. Epidermiology and associated risk factors of hyperlipoproteinemia. *Zeitschrift fur die gesamte innere Medizin und ihre Grenzgebiete,* 32, 124-128.
HANAOKA, K., QIAN, F., BOLETTA, A., BHUNIA, A. K., PIONTEK, K., TSIOKAS, L., SUKHATME, V. P., GUGGINO, W. B. & GERMINO, G. G. 2000. Co-assembly of polycystin-1 and-2 produces unique cation-permeable currents. *Nature,* 408, 990-994.
HANTUTE-GHESQUIER, A., HAUSTRATE, A., PREVARSKAYA, N. & LEHEN'KYI, V. Y. 2018. TRPM family channels in cancer. *Pharmaceuticals,* 11, 58.
HANUS, C. & EHLERS, M. D. 2008. Secretory outposts for the local processing of membrane cargo in neuronal dendrites. *Traffic,* 9, 1437-1445.
HARDIE, R. & MINKE, B. 1993. Novel Ca channels underlying transduction in Drosophila photoreceptors: implications for phosphoinositide-mediated Ca mobilization. *Trends in neurosciences,* 16, 371-376.
HARDY, S., UETANI, N., WONG, N., KOSTANTIN, E., LABBÉ, D., BÉGIN, L., MES-MASSON, A., MIRANDA-SAAVEDRA, D. & TREMBLAY, M. 2015. The protein tyrosine phosphatase PRL-2 interacts with the magnesium transporter CNNM3 to promote oncogenesis. *Oncogene,* 34, 986-995.
HARTWIG, A. 2001. Role of magnesium in genomic stability. *Mutation Research/Fundamental and Molecular Mechanisms of Mutagenesis,* 475, 113-121.
HAYASHI, T., RUMBAUGH, G. & HUGANIR, R. L. 2005. Differential regulation of AMPA receptor subunit trafficking by palmitoylation of two distinct sites. *Neuron,* 47, 709-723.
HE, Y., YAO, G., SAVOIA, C. & TOUYZ, R. M. 2005. Transient receptor potential melastatin 7 ion channels regulate magnesium homeostasis in vascular smooth muscle cells: role of angiotensin II. *Circulation research,* 96, 207-215.
HENION, J. D. 1978. Drug analysis by continuously monitored liquid chromatography/mass spectrometry with a quadrupole mass spectrometer. *Analytical Chemistry,* 50, 1687-1693.
HILGEMANN, D. W., FINE, M., LINDER, M. E., JENNINGS, B. C. & LIN, M.-J. 2013. Massive endocytosis triggered by surface membrane palmitoylation under mitochondrial control in BHK fibroblasts. *Elife,* 2, e01293.
HIMMEL, N. J., GRAY, T. R. & COX, D. N. 2020. Phylogenetics identifies two eumetazoan TRPM clades and an eighth TRP family, TRP soromelastatin (TRPS). *Molecular biology and evolution,* 37, 2034-2044.
HIMMEL, N. J., LETCHER, J. M., SAKURAI, A., GRAY, T. R., BENSON, M. N. & COX, D. N. 2019. Drosophila menthol sensitivity and the Precambrian origins of

transient receptor potential-dependent chemosensation. *Philosophical Transactions of the Royal Society B,* 374, 20190369.
HOFFMANN, J. & CHARLES, A. 2018. Glutamate and its receptors as therapeutic targets for migraine. *Neurotherapeutics,* 15, 361-370.
HOFHERR, A. & KÖTTGEN, M. 2011. TRPP channels and polycystins. *Transient Receptor Potential Channels*, 287-313.
HOFMANN, T., CHUBANOV, V., GUDERMANN, T. & MONTELL, C. 2003. TRPM5 is a voltage-modulated and Ca-activated monovalent selective cation channel. *Current biology,* 13, 1153-1158.
HOFMANN, T., SCHÄFER, S., LINSEISEN, M., SYTIK, L., GUDERMANN, T. & CHUBANOV, V. 2014. Activation of TRPM7 channels by small molecules under physiological conditions. *Pflügers Archiv-European Journal of Physiology,* 466, 2177-2189.
HOU, J. & GOODENOUGH, D. A. 2010. Claudin-16 and claudin-19 function in the thick ascending limb. *Current opinion in nephrology and hypertension,* 19, 483.
HOU, J., RENIGUNTA, A., GOMES, A. S., HOU, M., PAUL, D. L., WALDEGGER, S. & GOODENOUGH, D. A. 2009. Claudin-16 and claudin-19 interaction is required for their assembly into tight junctions and for renal reabsorption of magnesium. *Proceedings of the National Academy of Sciences,* 106, 15350-15355.
HOU, J., RENIGUNTA, A., KONRAD, M., GOMES, A. S., SCHNEEBERGER, E. E., PAUL, D. L., WALDEGGER, S. & GOODENOUGH, D. A. 2008. Claudin-16 and claudin-19 interact and form a cation-selective tight junction complex. *The Journal of clinical investigation,* 118, 619-628.
HOU, J., SHAN, Q., WANG, T., GOMES, A. S., YAN, Q., PAUL, D. L., BLEICH, M. & GOODENOUGH, D. A. 2007. Transgenic RNAi depletion of claudin-16 and the renal handling of magnesium. *Journal of Biological Chemistry,* 282, 17114-17122.
HOWIE, J., REILLY, L., FRASER, N. J., WALKER, J. M. V., WYPIJEWSKI, K. J., ASHFORD, M. L., CALAGHAN, S. C., MCCLAFFERTY, H., TIAN, L. & SHIPSTON, M. J. 2014. Substrate recognition by the cell surface palmitoyl transferase DHHC5. *Proceedings of the National Academy of Sciences,* 111, 17534-17539.
HU, F., LI, M., HAN, F., ZHANG, Q., ZENG, Y., ZHANG, W. & CHENG, X. 2021. Role of TRPM7 in cardiac fibrosis: A potential therapeutic target. *Experimental and therapeutic medicine,* 21, 1-1.
HU, Q., AHMAD, A. A., SEIDEL, T., HUNTER, C., STREIFF, M., NIKOLOVA, L., SPITZER, K. W. & SACHSE, F. B. 2020. Location and function of transient receptor potential canonical channel 1 in ventricular myocytes. *Journal of molecular and cellular cardiology,* 139, 113-123.
HUANG, K., SANDERS, S. S., KANG, R., CARROLL, J. B., SUTTON, L., WAN, J., SINGARAJA, R., YOUNG, F. B., LIU, L. & EL-HUSSEINI, A. 2011. Wild-type HTT modulates the enzymatic activity of the neuronal palmitoyl transferase HIP14. *Human Molecular Genetics,* 20, 3356-3365.
HUANG, Y., FLIEGERT, R., GUSE, A. H., LÜ, W. & DU, J. 2020. A structural overview of the ion channels of the TRPM family. *Cell Calcium,* 85, 102111.
HUFFER, K. E., ALEKSANDROVA, A. A., JARA-OSEGUERA, A., FORREST, L. R. & SWARTZ, K. J. 2020. Global alignment and assessment of TRP channel transmembrane domain structures to explore functional mechanisms. *Elife,* 9, e58660.

HURD, T. W., OTTO, E. A., MISHIMA, E., GEE, H. Y., INOUE, H., INAZU, M., YAMADA, H., HALBRITTER, J., SEKI, G. & KONISHI, M. 2013. Mutation of the Mg transporter SLC41A1 results in a nephronophthisis-like phenotype. *Journal of the American Society of Nephrology,* 24**,** 967-977.

IKARI, A., OKUDE, C., SAWADA, H., YAMAZAKI, Y., SUGATANI, J. & MIWA, M. 2008. TRPM6 expression and cell proliferation are up-regulated by phosphorylation of ERK1/2 in renal epithelial cells. *Biochemical and biophysical research communications,* 369**,** 1129-1133.

INOUE, K., BRANIGAN, D. & XIONG, Z.-G. 2010. Zinc-induced neurotoxicity mediated by transient receptor potential melastatin 7 channels. *Journal of Biological Chemistry,* 285**,** 7430-7439.

INOUE, K. & XIONG, Z.-G. 2009. Silencing TRPM7 promotes growth/proliferation and nitric oxide production of vascular endothelial cells via the ERK pathway. *Cardiovascular research,* 83**,** 547-557.

JAHNEN-DECHENT, W. & KETTELER, M. 2012. Magnesium basics. *Clinical kidney journal,* 5**,** i3-i14.

JAHNEN-DECHENT, W., KETTELER, M. J. T. A. P. C. D. R. M. U., BIODYNAMICS, & TESTING, R. O. S. Magnesium basics. Clin Kidney J. 2012; 5 (suppl. 1): i3-i14.

JEE, S. H., MILLER, E. R., GUALLAR, E., SINGH, V. K., APPEL, L. J. & KLAG, M. J. 2002. The effect of magnesium supplementation on blood pressure: a meta-analysis of randomized clinical trials. *American journal of hypertension,* 15**,** 691-696.

JIA, L., CHISARI, M., MAKTABI, M. H., SOBIESKI, C., ZHOU, H., KONOPKO, A. M., MARTIN, B. R., MENNERICK, S. J. & BLUMER, K. J. 2014. A Mechanism Regulating G Protein-coupled Receptor Signaling That Requires Cycles of Protein Palmitoylation and Depalmitoylation*♦. *Journal of Biological Chemistry,* 289**,** 6249-6257.

JIANG, H., ZHANG, X., CHEN, X., ARAMSANGTIENCHAI, P., TONG, Z. & LIN, H. 2018. Protein lipidation: occurrence, mechanisms, biological functions, and enabling technologies. *Chemical reviews,* 118**,** 919-988.

JIANG, J., LI, M. & YUE, L. 2005. Potentiation of TRPM7 inward currents by protons. *The Journal of general physiology,* 126**,** 137-150.

JIANG, Z.-J., LI, W., YAO, L.-H., SAED, B., RAO, Y., GREWE, B. S., MCGINLEY, A., VARGA, K., ALFORD, S. & HU, Y. S. 2021. TRPM7 is critical for short-term synaptic depression by regulating synaptic vesicle endocytosis. *Elife,* 10**,** e66709.

JIN, J., DESAI, B. N., NAVARRO, B., DONOVAN, A., ANDREWS, N. C. & CLAPHAM, D. E. 2008. Deletion of TRPM7 disrupts embryonic development and thymopoiesis without altering Mg homeostasis. *Science,* 322**,** 756-760.

JIN, J., WU, L.-J., JUN, J., CHENG, X., XU, H., ANDREWS, N. C. & CLAPHAM, D. E. 2012. The channel kinase, TRPM7, is required for early embryonic development. *Proceedings of the National Academy of Sciences,* 109**,** E225-E233.

JIN, M., BERROUT, J. & O'NEIL, R. G. 2011. 16 Regulation of TRP Channels by Osmomechanical Stress. *TRP channels*, 353.

JIN, X., TOUHEY, J. & GAUDET, R. 2006. Structure of the N-terminal ankyrin repeat domain of the TRPV2 ion channel. *Journal of Biological Chemistry,* 281**,** 25006-25010.

JORIS, P. J., PLAT, J., BAKKER, S. J. & MENSINK, R. P. 2016. Long-term magnesium supplementation improves arterial stiffness in overweight and obese adults: results of a randomized, double-blind, placebo-controlled

intervention trial. *The American journal of clinical nutrition,* 103, 1260-1266.
JUNG, D. W., APEL, L. & BRIERLEY, G. P. 1990. Matrix free magnesium changes with metabolic state in isolated heart mitochondria. *Biochemistry,* 29, 4121-4128.
KARIN, M., CAO, Y., GRETEN, F. R. & LI, Z.-W. 2002. NF-κB in cancer: from innocent bystander to major culprit. *Nature reviews cancer,* 2, 301-310.
KEENAN, D., ROMANI, A. & SCARPA, A. 1996. Regulation of Mg homeostasis by insulin in perfused rat livers and isolated hepatocytes. *FEBS letters,* 395, 241-244.
KESTELOOT, H. & JOOSSENS, J. V. 1988. Relationship of dietary sodium, potassium, calcium, and magnesium with blood pressure. Belgian Interuniversity Research on Nutrition and Health. *Hypertension,* 12, 594-599.
KIM, J., KO, J., MYEONG, J., KWAK, M., HONG, C. & SO, I. 2019. TRPC1 as a negative regulator for TRPC4 and TRPC5 channels. *Pflügers Archiv-European Journal of Physiology,* 471, 1045-1053.
KIM, S. E., PATAPOUTIAN, A. & GRANDL, J. 2013. Single residues in the outer pore of TRPV1 and TRPV3 have temperature-dependent conformations. *PloS one,* 8, e59593.
KIM, T. Y., SHIN, S. K., SONG, M.-Y., LEE, J. E. & PARK, K.-S. 2012. Identification of the phosphorylation sites on intact TRPM7 channels from mammalian cells. *Biochemical and biophysical research communications,* 417, 1030-1034.
KIRKLAND, A. E., SARLO, G. L. & HOLTON, K. F. 2018. The role of magnesium in neurological disorders. *Nutrients,* 10, 730.
KISTERS, K., KREFTING, E.-R., KOSEL, M., RAHN, K. H. & HAUSBERG, M. 2000. Intracellular Mg++ concentrations in smooth and striated muscle cells in spontaneously hypertensive rats. *American journal of hypertension,* 13, 427-430.
KOLISEK, M., GALAVIZ-HERNÁNDEZ, C., VÁZQUEZ-ALANIZ, F., SPONDER, G., JAVAID, S., KURTH, K., NESTLER, A., RODRÍGUEZ-MORAN, M., VERLOHREN, S. & GUERRERO-ROMERO, F. 2013. SLC41A1 is the only magnesium responsive gene significantly overexpressed in placentas of preeclamptic women. *Hypertension in pregnancy,* 32, 378-389.
KOLISEK, M., LAUNAY, P., BECK, A., SPONDER, G., SERAFINI, N., BRENKUS, M., FROSCHAUER, E. M., MARTENS, H., FLEIG, A. & SCHWEIGEL, M. 2008. SLC41A1 is a novel mammalian Mg carrier. *Journal of Biological Chemistry,* 283, 16235-16247.
KOLISEK, M., NESTLER, A., VORMANN, J. & SCHWEIGEL-RÖNTGEN, M. 2012. Human gene SLC41A1 encodes for the Na/Mg exchanger. *American Journal of Physiology-Cell Physiology,* 302, C318-C326.
KOLISEK, M., ZSURKA, G., SAMAJ, J., WEGHUBER, J., SCHWEYEN, R. J. & SCHWEIGEL, M. 2003. Mrs2p is an essential component of the major electrophoretic Mg influx system in mitochondria. *The EMBO journal,* 22, 1235-1244.
KOLLEWE, A., CHUBANOV, V., TSEUNG, F. T., CORREIA, L., SCHMIDT, E., RÖSSIG, A., ZIERLER, S., HAUPT, A., MÜLLER, C. S. & BILDL, W. 2021a. The molecular appearance of native TRPM7 channel complexes identified by high-resolution proteomics. *Elife,* 10, e68544.
KOLLEWE, A., CHUBANOV, V., TSEUNG, F. T., CORREIA, L., SCHMIDT, E., RÖSSIG, A., ZIERLER, S., HAUPT, A., MÜLLER, C. S. & BILDL, W. 2021b. The

molecular appearance of native TRPM7 channel complexes identified by high-resolution proteomics. *Elife,* 10.

KONG, E., PENG, S., CHANDRA, G., SARKAR, C., ZHANG, Z., BAGH, M. B. & MUKHERJEE, A. B. 2013. Dynamic palmitoylation links cytosol-membrane shuttling of acyl-protein thioesterase-1 and acyl-protein thioesterase-2 with that of proto-oncogene H-ras product and growth-associated protein-43. *Journal of Biological Chemistry,* 288**,** 9112-9125.

KORYCKA, J., ŁACH, A., HEGER, E., BOGUSŁAWSKA, D. M., WOLNY, M., TOPORKIEWICZ, M., AUGOFF, K., KORZENIEWSKI, J. & SIKORSKI, A. F. 2012. Human DHHC proteins: a spotlight on the hidden player of palmitoylation. *European journal of cell biology,* 91**,** 107-117.

KOSTANTIN, E., HARDY, S., VALINSKY, W. C., KOMPATSCHER, A., DE BAAIJ, J. H., ZOLOTAROV, Y., LANDRY, M., UETANI, N., MARTÍNEZ-CRUZ, L. A. & HOENDEROP, J. G. 2016. Inhibition of PRL-2· CNNM3 protein complex formation decreases breast cancer proliferation and tumor growth. *Journal of biological chemistry,* 291**,** 10716-10725.

KOSTER, K. P. & YOSHII, A. 2019. Depalmitoylation by palmitoyl-protein thioesterase 1 in neuronal health and degeneration. *Frontiers in synaptic neuroscience,* 11**,** 25.

KOSTOV, K. & HALACHEVA, L. 2018. Role of magnesium deficiency in promoting atherosclerosis, endothelial dysfunction, and arterial stiffening as risk factors for hypertension. *International journal of molecular sciences,* 19**,** 1724.

KOUSA, A., HAVULINNA, A. S., MOLTCHANOVA, E., TASKINEN, O., NIKKARINEN, M., ERIKSSON, J. & KARVONEN, M. 2006. Calcium: magnesium ratio in local groundwater and incidence of acute myocardial infarction among males in rural Finland. *Environmental health perspectives,* 114**,** 730-734.

KOZAK, J. A., MATSUSHITA, M., NAIRN, A. C. & CAHALAN, M. D. 2005. Charge screening by internal pH and polyvalent cations as a mechanism for activation, inhibition, and rundown of TRPM7/MIC channels. *The Journal of general physiology,* 126**,** 499-514.

KRAFT, R., GRIMM, C., GROSSE, K., HOFFMANN, A., SAUERBRUCH, S., KETTENMANN, H., SCHULTZ, G. & HARTENECK, C. 2004. Hydrogen peroxide and ADP-ribose induce TRPM2-mediated calcium influx and cation currents in microglia. *American Journal of Physiology-Cell Physiology,* 286**,** C129-C137.

KRAPIVINSKY, G., KRAPIVINSKY, L., MANASIAN, Y. & CLAPHAM, D. E. 2014. The TRPM7 chanzyme is cleaved to release a chromatin-modifying kinase. *Cell,* 157**,** 1061-1072.

KRAPIVINSKY, G., MOCHIDA, S., KRAPIVINSKY, L., CIBULSKY, S. M. & CLAPHAM, D. E. 2006. The TRPM7 ion channel functions in cholinergic synaptic vesicles and affects transmitter release. *Neuron,* 52**,** 485-496.

KÜMMEL, D., HEINEMANN, U. & VEIT, M. 2006. Unique self-palmitoylation activity of the transport protein particle component Bet3: a mechanism required for protein stability. *Proceedings of the National Academy of Sciences,* 103**,** 12701-12706.

KUNERT-KEIL, C., BISPING, F., KRÜGER, J. & BRINKMEIER, H. 2006. Tissue-specific expression of TRP channel genes in the mouse and its variation in three different mouse strains. *BMC genomics,* 7**,** 1-14.

LAFAVERS, K. A., MACEDO, E., GARIMELLA, P. S., LIMA, C., KHAN, S., MYSLINSKI, J., MCCLINTICK, J., WITZMANN, F. A., WINFREE, S. & PHILLIPS, C. L. 2019. Circulating uromodulin inhibits systemic oxidative stress by inactivating the TRPM2 channel. *Science translational medicine,* 11**,** eaaw3639.

LAINEZ, S., SCHLINGMANN, K. P., VAN DER WIJST, J., DWORNICZAK, B., VAN ZEELAND, F., KONRAD, M., BINDELS, R. J. & HOENDEROP, J. G. 2014. New TRPM6 missense mutations linked to hypomagnesemia with secondary hypocalcemia. *European Journal of Human Genetics,* 22**,** 497-504.

LAL-NAG, M. & MORIN, P. J. 2009. The claudins. *Genome biology,* 10**,** 1-7.

LANDMAN, N., JEONG, S. Y., SHIN, S. Y., VORONOV, S. V., SERBAN, G., KANG, M. S., PARK, M. K., DI PAOLO, G., CHUNG, S. & KIM, T.-W. 2006. Presenilin mutations linked to familial Alzheimer's disease cause an imbalance in phosphatidylinositol 4, 5-bisphosphate metabolism. *Proceedings of the National Academy of Sciences,* 103**,** 19524-19529.

LANGE, I., YAMAMOTO, S., PARTIDA-SANCHEZ, S., MORI, Y., FLEIG, A. & PENNER, R. 2009. TRPM2 functions as a lysosomal Ca-release channel in ß cells. *Science signaling,* 2**,** ra23-ra23.

LANGESLAG, M., CLARK, K., MOOLENAAR, W. H., VAN LEEUWEN, F. N. & JALINK, K. 2007. Activation of TRPM7 channels by phospholipase C-coupled receptor agonists. *Journal of Biological Chemistry,* 282**,** 232-239.

LARSEN, J. B., JENSEN, M. B., BHATIA, V. K., PEDERSEN, S. L., BJØRNHOLM, T., IVERSEN, L., ULINE, M., SZLEIFER, I., JENSEN, K. J. & HATZAKIS, N. S. 2015. Membrane curvature enables N-Ras lipid anchor sorting to liquid-ordered membrane phases. *Nature chemical biology,* 11**,** 192-194.

LARSSON, S. C., BERGKVIST, L. & WOLK, A. 2005. Magnesium intake in relation to risk of colorectal cancer in women. *Jama,* 293**,** 86-89.

LARSSON, S. C., BURGESS, S. & MICHAËLSSON, K. 2018. Serum magnesium levels and risk of coronary artery disease: Mendelian randomisation study. *BMC medicine,* 16**,** 1-7.

LAUNAY, P., FLEIG, A., PERRAUD, A.-L., SCHARENBERG, A. M., PENNER, R. & KINET, J.-P. 2002. TRPM4 is a Ca-activated nonselective cation channel mediating cell membrane depolarization. *Cell,* 109**,** 397-407.

LE GRIMELLEC, C., GIOCONDI, M. & PHILIPPE, P. 1975. Micropuncture study along the proximal convoluted tubule electrolyte reabsorption in first convolutions. *Pflügers Archiv,* 354**,** 133-150.

LEGRAND, C., MERLINI, J. M., DE SENARCLENS-BEZENÇON, C. & MICHLIG, S. 2020. New natural agonists of the transient receptor potential Ankyrin 1 (TRPA1) channel. *Scientific reports,* 10**,** 1-10.

LEMONIDIS, K., GORLEKU, O. A., SANCHEZ-PEREZ, M. C., GREFEN, C. & CHAMBERLAIN, L. H. 2014. The Golgi S-acylation machinery comprises zDHHC enzymes with major differences in substrate affinity and S-acylation activity. *Molecular biology of the cell,* 25**,** 3870-3883.

LEMONIDIS, K., MACLEOD, R., BAILLIE, G. S. & CHAMBERLAIN, L. H. 2017. Peptide array-based screening reveals a large number of proteins interacting with the ankyrin-repeat domain of the zDHHC17 S-acyltransferase. *Journal of Biological Chemistry,* 292**,** 17190-17202.

LEMONIDIS, K., SANCHEZ-PEREZ, M. C. & CHAMBERLAIN, L. H. 2015. Identification of a novel sequence motif recognized by the ankyrin repeat domain of zDHHC17/13 S-acyltransferases. *Journal of Biological Chemistry,* 290**,** 21939-21950.

LI, B., LV, J., WANG, W. & ZHANG, D. 2017. Dietary magnesium and calcium intake and risk of depression in the general population: a meta-analysis. *Australian & New Zealand Journal of Psychiatry,* 51**,** 219-229.

LI, Q., CHEN, Q., ZHANG, H., XU, Z., WANG, X., PANG, J., MA, J., LING, W. & LI, D. 2020. Associations of serum magnesium levels and calcium–magnesium ratios with mortality in patients with coronary artery disease. *Diabetes & Metabolism,* 46**,** 384-391.

LI, Y., HU, J., HÖFER, K., WONG, A. M., COOPER, J. D., BIRNBAUM, S. G., HAMMER, R. E. & HOFMANN, S. L. 2010. DHHC5 interacts with PDZ domain 3 of post-synaptic density-95 (PSD-95) protein and plays a role in learning and memory. *Journal of Biological Chemistry,* 285**,** 13022-13031.

LIEDTKE, W. B. 2006. *TRP ion channel function in sensory transduction and cellular signaling cascades*, CRC Press.

LIMAN, E. R. 2006. 15 The Ca-Activated TRP Channels: TRPM4 and TRPM5. *TRP ion channel function in sensory transduction and cellular signaling cascades***,** 203.

LIN, D. T. S. & CONIBEAR, E. 2015. ABHD17 proteins are novel protein depalmitoylases that regulate N-Ras palmitate turnover and subcellular localization. *elife,* 4**,** e11306.

LIN, L., YAN, M., WU, B., LIN, R. & ZHENG, Z. 2018. Expression of magnesium transporter SLC41A1 in the striatum of 6-hydroxydopamine-induced parkinsonian rats. *Brain Research Bulletin,* 142**,** 338-343.

LINDER, M. E. & DESCHENES, R. J. 2007. Palmitoylation: policing protein stability and traffic. *Nature reviews Molecular cell biology,* 8**,** 74-84.

LIPTON, P. 1999. Ischemic cell death in brain neurons. *Physiological reviews,* 79**,** 1431-1568.

LIU, M., INOUE, K., LENG, T., GUO, S. & XIONG, Z.-G. 2014. TRPM7 channels regulate glioma stem cell through STAT3 and Notch signaling pathways. *Cellular signalling,* 26**,** 2773-2781.

LOBO, S., GREENTREE, W. K., LINDER, M. E. & DESCHENES, R. J. 2002. Identification of a Ras Palmitoyltransferase inSaccharomyces cerevisiae. *Journal of Biological Chemistry,* 277**,** 41268-41273.

LONDON, R. E. 1991. Methods for measurement of intracellular magnesium: NMR and fluorescence. *Annual review of physiology,* 53**,** 241-258.

LUO, Y., WU, J.-Y., LU, M.-H., SHI, Z., NA, N. & DI, J.-M. 2016. Carvacrol alleviates prostate cancer cell proliferation, migration, and invasion through regulation of PI3K/Akt and MAPK signaling pathways. *Oxidative medicine and cellular longevity,* 2016.

LÜTHI, D., GÜNZEL, D. & MCGUIGAN, J. A. 1999. Mg-ATP binding: its modification by spermine, the relevance to cytosolic Mg buffering, changes in the intracellular ionized Mg concentration and the estimation of Mg by 31P-NMR. *Experimental physiology,* 84**,** 231-252.

MACIANSKIENE, R., MARTISIENE, I., ZABLOCKAITE, D. & GENDVILIENE, V. 2012. Characterization of Mg-regulated TRPM7-like current in human atrial myocytes. *Journal of Biomedical Science,* 19**,** 1-11.

MAIER, J. A. 2012. Endothelial cells and magnesium: implications in atherosclerosis. *Clinical science,* 122**,** 397-407.

MAIER, J. A., NASULEWICZ-GOLDEMAN, A., SIMONACCI, M., BONINSEGNA, A., MAZUR, A. & WOLF, F. I. 2007. Insights into the mechanisms involved in magnesium-dependent inhibition of primary tumor growth. *Nutrition and cancer,* 59**,** 192-198.

MAIN, A. & FULLER, W. 2022. Protein S – Palmitoylation: advances and challenges in studying a therapeutically important lipid modification. *The FEBS Journal,* 289**,** 861-882.

MAISCH, B. 1995. Extracellular matrix and cardiac interstitium: restriction is not a restricted phenomenon. *Herz,* 20**,** 75-80.

MAKKI, N., THIEL, K. W. & MILLER, F. J. 2013. The epidermal growth factor receptor and its ligands in cardiovascular disease. *International journal of molecular sciences,* 14**,** 20597-20613.

MALGAPO, M. I. P. & LINDER, M. E. 2021. Substrate recruitment by zDHHC protein acyltransferases. *Open Biology,* 11**,** 210026.
MARTIN, B. R., WANG, C., ADIBEKIAN, A., TULLY, S. E. & CRAVATT, B. F. 2012. Global profiling of dynamic protein palmitoylation. *Nature methods,* 9**,** 84-89.
MARTIN, H., RICHERT, L. & BERTHELOT, A. 2003. Magnesium deficiency induces apoptosis in primary cultures of rat hepatocytes. *The Journal of nutrition,* 133**,** 2505-2511.
MATSUDA-LENNIKOV, M., BIANCALANA, M., ZOU, J., RAVELL, J. C., ZHENG, L., KANELLOPOULOU, C., JIANG, P., NOTARANGELO, G., JING, H. & MASUTANI, E. 2019. Magnesium transporter 1 (MAGT1) deficiency causes selective defects in N-linked glycosylation and expression of immune-response genes. *Journal of Biological Chemistry,* 294**,** 13638-13656.
MATSUSHITA, M., KOZAK, J. A., SHIMIZU, Y., MCLACHLIN, D. T., YAMAGUCHI, H., WEI, F.-Y., TOMIZAWA, K., MATSUI, H., CHAIT, B. T. & CAHALAN, M. D. 2005. Channel function is dissociated from the intrinsic kinase activity and autophosphorylation of TRPM7/ChaK1. *Journal of Biological Chemistry,* 280**,** 20793-20803.
MAZUR, A., MAIER, J. A., ROCK, E., GUEUX, E., NOWACKI, W. & RAYSSIGUIER, Y. 2007. Magnesium and the inflammatory response: potential physiopathological implications. *Archives of biochemistry and biophysics,* 458**,** 48-56.
MCCALL, K. A., HUANG, C.-C. & FIERKE, C. A. 2000. Function and mechanism of zinc metalloenzymes. *The Journal of nutrition,* 130**,** 1437S-1446S.
MCCORMICK, P. J., DUMARESQ – DOIRON, K., PLUVIOSE, A. S., PICHETTE, V., TOSATO, G. & LEFRANCOIS, S. 2008. Palmitoylation controls recycling in lysosomal sorting and trafficking. *Traffic,* 9**,** 1984-1997.
MCKINNON, K. M. 2018. Flow cytometry: an overview. *Current protocols in immunology,* 120**,** 5.1. 1-5.1. 11.
MCLAFFERTY, F. W. 1981. Tandem mass spectrometry. *Science,* 214**,** 280-287.
MEKAHLI, D., BULTYNCK, G., PARYS, J. B., DE SMEDT, H. & MISSIAEN, L. 2011. Endoplasmic-reticulum calcium depletion and disease. *Cold Spring Harb Perspect Biol,* 3.
MELKONIAN, K. A., OSTERMEYER, A. G., CHEN, J. Z., ROTH, M. G. & BROWN, D. A. 1999. Role of lipid modifications in targeting proteins to detergent-resistant membrane rafts: many raft proteins are acylated, while few are prenylated. *Journal of Biological Chemistry,* 274**,** 3910-3917.
MENG, X., CAI, C., WU, J., CAI, S., YE, C., CHEN, H., YANG, Z., ZENG, H., SHEN, Q. & ZOU, F. 2013. TRPM7 mediates breast cancer cell migration and invasion through the MAPK pathway. *Cancer letters,* 333**,** 96-102.
MIDDELBEEK, J., KUIPERS, A. J., HENNEMAN, L., VISSER, D., EIDHOF, I., VAN HORSSEN, R., WIERINGA, B., CANISIUS, S. V., ZWART, W. & WESSELS, L. F. 2012. TRPM7 is required for breast tumor cell metastasis. *Cancer research,* 72**,** 4250-4261.
MILLER, B. 2006. The role of TRP channels in oxidative stress-induced cell death. *The Journal of membrane biology,* 209**,** 31-41.
MILNERWOOD, A. J., PARSONS, M. P., YOUNG, F. B., SINGARAJA, R. R., FRANCIOSI, S., VOLTA, M., BERGERON, S., HAYDEN, M. R. & RAYMOND, L. A. 2013. Memory and synaptic deficits in Hip14/DHHC17 knockout mice. *Proceedings of the National Academy of Sciences,* 110**,** 20296-20301.
MITCHELL, D. A., VASUDEVAN, A., LINDER, M. E. & DESCHENES, R. J. 2006. Thematic review series: lipid posttranslational modifications. Protein

palmitoylation by a family of DHHC protein S-acyltransferases. *Journal of lipid research,* 47**,** 1118-1127.
MONTEILH-ZOLLER, M. K., HERMOSURA, M. C., NADLER, M. J., SCHARENBERG, A. M., PENNER, R. & FLEIG, A. 2003. TRPM7 provides an ion channel mechanism for cellular entry of trace metal ions. *The Journal of general physiology,* 121**,** 49-60.
MONTELL, C. 2005. The TRP superfamily of cation channels. *Science's STKE,* 2005**,** re3-re3.
MONTELL, C., BIRNBAUMER, L., FLOCKERZI, V., BINDELS, R. J., BRUFORD, E. A., CATERINA, M. J., CLAPHAM, D. E., HARTENECK, C., HELLER, S. & JULIUS, D. 2002. A unified nomenclature for the superfamily of TRP cation channels. *Molecular cell,* 9**,** 229-231.
MONTEZANO, A., CALLERA, G., YOGI, A., HE, Y., TOSTES, R., HE, G., SCHIFFRIN, E. & TOUYZ, R. 2008. Aldosterone and angiotensin II synergistically stimulate migration in vascular smooth muscle cells through c-Src-regulated redox-sensitive RhoA pathways. *Arteriosclerosis, thrombosis, and vascular biology,* 28**,** 1511-1518.
MONTNACH, J., AGULLO-PASCUAL, E., TADROS, R., BEZZINA, C. R. & DELMAR, M. 2018. Bioinformatic analysis of a plakophilin-2-dependent transcription network: implications for the mechanisms of arrhythmogenic right ventricular cardiomyopathy in humans and in boxer dogs. *EP Europace,* 20**,** iii125-iii132.
MORGAN, A. J., PLATT, F. M., LLOYD-EVANS, E. & GALIONE, A. 2011. Molecular mechanisms of endolysosomal Ca signalling in health and disease. *Biochemical Journal,* 439**,** 349-378.
MORISAKI, H., YAMAMOTO, S., MORITA, Y., KOTAKE, Y., OCHIAI, R. & TAKEDA, J. 2000. Hypermagnesemia-induced cardiopulmonary arrest before induction of anesthesia for emergency cesarean section. *Journal of clinical anesthesia,* 12**,** 224-226.
MORRIS, M. 1992. Brain and CSF magnesium concentrations during magnesium deficit in animals and humans: neurological symptoms. *Magnesium Research,* 5**,** 303-313.
NADLER, M. J., HERMOSURA, M. C., INABE, K., PERRAUD, A.-L., ZHU, Q., STOKES, A. J., KUROSAKI, T., KINET, J.-P., PENNER, R. & SCHARENBERG, A. M. 2001. LTRPC7 is a Mg· ATP-regulated divalent cation channel required for cell viability. *Nature,* 411**,** 590-595.
NADOLNI, W. & ZIERLER, S. 2018. The channel-kinase TRPM7 as novel regulator of immune system homeostasis. *Cells,* 7**,** 109.
NASULEWICZ, A., WIETRZYK, J., WOLF, F. I., DZIMIRA, S., MADEJ, J., MAIER, J. A., RAYSSIGUIER, Y., MAZUR, A. & OPOLSKI, A. 2004. Magnesium deficiency inhibits primary tumor growth but favors metastasis in mice. *Biochimica et Biophysica Acta (BBA)-Molecular Basis of Disease,* 1739**,** 26-32.
NGUYEN DINH CAT, A., BRIONES, A. M., CALLERA, G. E., YOGI, A., HE, Y., MONTEZANO, A. C. & TOUYZ, R. M. 2011. Adipocyte-derived factors regulate vascular smooth muscle cells through mineralocorticoid and glucocorticoid receptors. *Hypertension,* 58**,** 479-488.
NILIUS, B., APPENDINO, G. & OWSIANIK, G. 2012. The transient receptor potential channel TRPA1: from gene to pathophysiology. *Pflügers Archiv-European Journal of Physiology,* 464**,** 425-458.
NILIUS, B. & OWSIANIK, G. 2011. The transient receptor potential family of ion channels. *Genome biology,* 12**,** 1-11.

NUMATA, T., SHIMIZU, T. & OKADA, Y. 2007a. Direct mechano-stress sensitivity of TRPM7 channel. *Cellular Physiology and Biochemistry,* 19**,** 1-8.

NUMATA, T., SHIMIZU, T. & OKADA, Y. 2007b. TRPM7 is a stretch-and swelling-activated cation channel involved in volume regulation in human epithelial cells. *American Journal of Physiology-Cell Physiology,* 292**,** C460-C467.

NUNOMURA, A., MOREIRA, P., LEE, H., ZHU, X., CASTELLANI, R., SMITH, M. & PERRY, G. 2007. Neuronal death and survival under oxidative stress in Alzheimer and Parkinson diseases. *CNS & Neurological Disorders-Drug Targets (Formerly Current Drug Targets-CNS & Neurological Disorders),* 6**,** 411-423.

O'FARRELL, P. H. 1975. High resolution two-dimensional electrophoresis of proteins. *Journal of biological chemistry,* 250**,** 4007-4021.

OHNO, Y., KIHARA, A., SANO, T. & IGARASHI, Y. 2006. Intracellular localization and tissue-specific distribution of human and yeast DHHC cysteine-rich domain-containing proteins. *Biochimica et Biophysica Acta (BBA)-Molecular and Cell Biology of Lipids,* 1761**,** 474-483.

OYANAGI, K., KAWAKAMI, E., KIKUCHI‐HORIE, K., OHARA, K., OGATA, K., TAKAHAMA, S., WADA, M., KIHIRA, T. & YASUI, M. 2006. Magnesium deficiency over generations in rats with special references to the pathogenesis of the parkinsonism–dementia complex and amyotrophic lateral sclerosis of Guam. *Neuropathology,* 26**,** 115-128.

PAN, Z., YANG, H. & REINACH, P. S. 2011. Transient receptor potential (TRP) gene superfamily encoding cation channels. *Human genomics,* 5**,** 1-9.

PATAPOUTIAN, A., PEIER, A. M., STORY, G. M. & VISWANATH, V. 2003. ThermoTRP channels and beyond: mechanisms of temperature sensation. *Nature Reviews Neuroscience,* 4**,** 529-539.

PEDRO, M. P., VILCAES, A. A., TOMATIS, V. M., OLIVEIRA, R. G., GOMEZ, G. A. & DANIOTTI, J. L. 2013. 2-Bromopalmitate reduces protein deacylation by inhibition of acyl-protein thioesterase enzymatic activities. *PloS one,* 8**,** e75232.

PEIER, A. M., MOQRICH, A., HERGARDEN, A. C., REEVE, A. J., ANDERSSON, D. A., STORY, G. M., EARLEY, T. J., DRAGONI, I., MCINTYRE, P. & BEVAN, S. 2002. A TRP channel that senses cold stimuli and menthol. *Cell,* 108**,** 705-715.

PENG, G., SHI, X. & KADOWAKI, T. 2015. Evolution of TRP channels inferred by their classification in diverse animal species. *Molecular phylogenetics and evolution,* 84**,** 145-157.

PERRAUD, A.-L., FLEIG, A., DUNN, C. A., BAGLEY, L. A., LAUNAY, P., SCHMITZ, C., STOKES, A. J., ZHU, Q., BESSMAN, M. J. & PENNER, R. 2001. ADP-ribose gating of the calcium-permeable LTRPC2 channel revealed by Nudix motif homology. *Nature,* 411**,** 595-599.

PERRAUD, A.-L., SCHMITZ, C. & SCHARENBERG, A. M. 2003. TRPM2 Ca permeable cation channels: from gene to biological function. *Cell calcium,* 33**,** 519-531.

PERRAUD, A.-L., ZHAO, X., RYAZANOV, A. G. & SCHMITZ, C. 2011. The channel-kinase TRPM7 regulates phosphorylation of the translational factor eEF2 via eEF2-k. *Cellular signalling,* 23**,** 586-593.

PHILIPP SCHUCHARDT, J. & HAHN, A. 2017. Intestinal absorption and factors influencing bioavailability of magnesium-an update. *Current Nutrition & Food Science,* 13**,** 260-278.

PISKACEK, M., ZOTOVA, L., ZSURKA, G. & SCHWEYEN, R. J. 2009. Conditional knockdown of hMRS2 results in loss of mitochondrial Mg+ uptake and cell death. *Journal of cellular and molecular medicine,* 13**,** 693-700.

PLAIN, F., CONGREVE, S. D., YEE, R. S. Z., KENNEDY, J., HOWIE, J., KUO, C.-W., FRASER, N. J. & FULLER, W. 2017. An amphipathic α-helix directs palmitoylation of the large intracellular loop of the sodium/calcium exchanger. *Journal of Biological Chemistry,* 292**,** 10745-10752.

PLAIN, F., HOWIE, J., KENNEDY, J., BROWN, E., SHATTOCK, M. J., FRASER, N. J. & FULLER, W. 2020. Control of protein palmitoylation by regulating substrate recruitment to a zDHHC-protein acyltransferase. *Communications biology,* 3**,** 1-10.

POTTER, J. D., ROBERTSON, S. P. & JOHNSON, J. D. Magnesium and the regulation of muscle contraction. Federation proceedings, 1981. 2653-2656.

POWELL, D., MIFFLIN, R., VALENTICH, J., CROWE, S., SAADA, J. & WEST, A. 1999. Myofibroblasts. I. Paracrine cells important in health and disease. *American Journal of Physiology-Cell Physiology,* 277**,** C1-C19.

PRAWITT, D., MONTEILH-ZOLLER, M. K., BRIXEL, L., SPANGENBERG, C., ZABEL, B., FLEIG, A. & PENNER, R. 2003. TRPM5 is a transient Ca-activated cation channel responding to rapid changes in [Ca] i. *Proceedings of the national academy of sciences,* 100**,** 15166-15171.

PUMROY, R. A., FLUCK III, E. C., AHMED, T. & MOISEENKOVA-BELL, V. Y. 2020. Structural insights into the gating mechanisms of TRPV channels. *Cell Calcium,* 87**,** 102168.

QAZI, M., QAZI, H., NAKHOUL, G. & PROVENZANO, L. F. 2021. Causes of Hypermagnesaemia: A Literature Review. *NEPHROLOGY*.

QIAN, F. & NOBEN-TRAUTH, K. 2005. Cellular and molecular function of mucolipins (TRPML) and polycystin 2 (TRPP2). *Pflügers Archiv,* 451**,** 277-285.

QIN, F. 2007. Regulation of TRP ion channels by phosphatidylinositol-4, 5-bisphosphate. *Transient Receptor Potential (TRP) Channels***,** 509-525.

QIN, N., PLATANO, D., OLCESE, R., COSTANTIN, J. L., STEFANI, E. & BIRNBAUMER, L. 1998. Unique regulatory properties of the type 2a Ca channel ß subunit caused by palmitoylation. *Proceedings of the National Academy of Sciences,* 95**,** 4690-4695.

QUAMME, G. A. 1997. Renal magnesium handling: new insights in understanding old problems. *Kidney international,* 52**,** 1180-1195.

QUAMME, G. A. 2008. Recent developments in intestinal magnesium absorption. *Current opinion in gastroenterology,* 24**,** 230-235.

RAJU, B., MURPHY, E., LEVY, L. A., HALL, R. D. & LONDON, R. E. 1989. A fluorescent indicator for measuring cytosolic free magnesium. *American Journal of Physiology-Cell Physiology,* 256**,** C540-C548.

RAMIREZ, I. B.-R. & LOWE, M. Golgins and GRASPs: holding the Golgi together. Seminars in cell & developmental biology, 2009. Elsevier, 770-779.

RAMSEY, I. S., DELLING, M. & CLAPHAM, D. E. 2006. An introduction to TRP channels. *Annual review of physiology,* 68**,** 619-647.

RANA, M. S., KUMAR, P., LEE, C.-J., VERARDI, R., RAJASHANKAR, K. R. & BANERJEE, A. 2018. Fatty acyl recognition and transfer by an integral membrane S-acyltransferase. *Science,* 359**,** eaao6326.

RANA, M. S., LEE, C.-J. & BANERJEE, A. 2019. The molecular mechanism of DHHC protein acyltransferases. *Biochemical Society Transactions,* 47**,** 157-167.

RANJAN, P., KUMARI, R. & VERMA, S. K. 2019. Cardiac fibroblasts and cardiac fibrosis: precise role of exosomes. *Frontiers in cell and developmental biology*, 318.
RAVELL, J., CHAIGNE-DELALANDE, B. & LENARDO, M. 2014. Xmen disease: A combined immune deficiency with magnesium defect. *Current opinion in pediatrics,* 26, 713.
RAZZAQUE, M. S. 2018. Magnesium: are we consuming enough? *Nutrients,* 10, 1863.
RECHENBERG, K. 2016. Nutritional interventions in clinical depression. *Clinical Psychological Science,* 4, 144-162.
REDDY, S. T., SOMAN, S. S. & YEE, J. 2018. Magnesium balance and measurement. *Advances in chronic kidney disease,* 25, 224-229.
REILLY, L., HOWIE, J., WYPIJEWSKI, K., ASHFORD, M. L., HILGEMANN, D. W. & FULLER, W. 2015. Palmitoylation of the Na/Ca exchanger cytoplasmic loop controls its inactivation and internalization during stress signaling. *The FASEB Journal,* 29, 4532-4543.
RESH, M. D. 2006. Trafficking and signaling by fatty-acylated and prenylated proteins. *Nature chemical biology,* 2, 584-590.
RICCIO, A., MEDHURST, A. D., MATTEI, C., KELSELL, R. E., CALVER, A. R., RANDALL, A. D., BENHAM, C. D. & PANGALOS, M. N. 2002. mRNA distribution analysis of human TRPC family in CNS and peripheral tissues. *Molecular brain research,* 109, 95-104.
RIOS, F. J., ZOU, Z.-G., HARVEY, A. P., HARVEY, K. Y., NOSALSKI, R., ANYFANTI, P., CAMARGO, L. L., LACCHINI, S., RYAZANOV, A. G. & RYAZANOVA, L. 2020. Chanzyme TRPM7 protects against cardiovascular inflammation and fibrosis. *Cardiovascular research,* 116, 721-735.
RODRIGUEZ-BOULAN, E., KREITZER, G. & MÜSCH, A. 2005. Organization of vesicular trafficking in epithelia. *Nature reviews Molecular cell biology,* 6, 233-247.
ROHACS, T. 2009. Phosphoinositide regulation of non-canonical transient receptor potential channels. *Cell calcium,* 45, 554-565.
ROHÁCS, T., LOPES, C., MICHAILIDIS, I. & LOGOTHETIS, D. E. 2005. PI (4, 5) P2 regulates the activation and desensitization of TRPM8 channels through the TRP domain. *Nature neuroscience,* 8, 626-634.
ROMANI, A. 2007a. Magnesium homeostasis in mammalian cells. *Front Biosci,* 12, 308-331.
ROMANI, A. 2007b. Regulation of magnesium homeostasis and transport in mammalian cells. *Archives of biochemistry and biophysics,* 458, 90-102.
ROMANI, A. & SCARPA, A. 1992. Regulation of cell magnesium. *Archives of biochemistry and biophysics,* 298, 1-12.
ROMANI, A. M. 2011. Cellular magnesium homeostasis. *Archives of biochemistry and biophysics,* 512, 1-23.
ROMANI, A. M. 2018. Beneficial role of Mg in prevention and treatment of hypertension. *International Journal of Hypertension,* 2018.
ROSADO, J. A., BROWNLOW, S. L. & SAGE, S. O. 2002. Endogenously expressed Trp1 is involved in store-mediated Ca entry by conformational coupling in human platelets. *Journal of Biological Chemistry,* 277, 42157-42163.
ROSADO, J. A. & SAGE, S. O. 2000. Coupling between inositol 1, 4, 5-trisphosphate receptors and human transient receptor potential channel 1 when intracellular Ca stores are depleted. *Biochemical Journal,* 350, 631-635.
ROTH, A. F., WAN, J., GREEN, W. N., YATES, J. R. & DAVIS, N. G. 2006. Proteomic identification of palmitoylated proteins. *Methods,* 40, 135-142.

ROYUELA, M., RODRÍGUEZ-BERRIGUETE, G., FRAILE, B. & PANIAGUA, R. 2008. TNF-alpha/IL-1/NF-kappaB transduction pathway in human cancer prostate. *Histology and histopathology,* 23**,** 1279-1290.
RUDD, A. K., BREA, R. J. & DEVARAJ, N. K. 2018. Amphiphile-Mediated Depalmitoylation of Proteins in Living Cells. *Journal of the American Chemical Society,* 140**,** 17374-17378.
RUNNELS, L. W., YUE, L. & CLAPHAM, D. E. 2001. TRP-PLIK, a bifunctional protein with kinase and ion channel activities. *Science,* 291**,** 1043-1047.
RUNNELS, L. W., YUE, L. & CLAPHAM, D. E. 2002. The TRPM7 channel is inactivated by PIP2 hydrolysis. *Nature cell biology,* 4**,** 329-336.
RUTTER, G. A., OSBALDESTON, N., MCCORMACK, J. & DENTON, R. 1990. Measurement of matrix free Mg concentration in rat heart mitochondria by using entrapped fluorescent probes. *Biochemical journal,* 271**,** 627-634.
RYAZANOVA, L. V., HU, Z., SUZUKI, S., CHUBANOV, V., FLEIG, A. & RYAZANOV, A. G. 2014. Elucidating the role of the TRPM7 alpha-kinase: TRPM7 kinase inactivation leads to magnesium deprivation resistance phenotype in mice. *Scientific reports,* 4**,** 1-11.
RYAZANOVA, L. V., RONDON, L. J., ZIERLER, S., HU, Z., GALLI, J., YAMAGUCHI, T. P., MAZUR, A., FLEIG, A. & RYAZANOV, A. G. 2010. TRPM7 is essential for Mg homeostasis in mammals. *Nature communications,* 1**,** 1-9.
SAH, R., MESIRCA, P., MASON, X., GIBSON, W., BATES-WITHERS, C., VAN DEN BOOGERT, M., CHAUDHURI, D., PU, W. T., MANGONI, M. E. & CLAPHAM, D. E. 2013. Timing of myocardial TRPM7 deletion during cardiogenesis variably disrupts adult ventricular function, conduction, and repolarization. *Circulation,* 128**,** 101-114.
SAHNI, J., NELSON, B. & SCHARENBERG, A. M. 2007. SLC41A2 encodes a plasma-membrane Mg transporter. *Biochemical Journal,* 401**,** 505-513.
SALAUN, C., GREAVES, J. & CHAMBERLAIN, L. H. 2010. The intracellular dynamic of protein palmitoylation. *Journal of Cell Biology,* 191**,** 1229-1238.
SAMANTA, A., HUGHES, T. E. & MOISEENKOVA-BELL, V. Y. 2018. Transient receptor potential (TRP) channels. *Membrane protein complexes: Structure and function***,** 141-165.
SANTALUCIA JR, J. & HICKS, D. 2004. The thermodynamics of DNA structural motifs. *Annu. Rev. Biophys. Biomol. Struct.,* 33**,** 415-440.
SANTONI, G., SANTONI, M., MAGGI, F., MARINELLI, O. & MORELLI, M. B. 2020. Emerging role of mucolipins TRPML channels in cancer. *Frontiers in Oncology,* 10**,** 659.
SARIS, N.-E. L., MERVAALA, E., KARPPANEN, H., KHAWAJA, J. A. & LEWENSTAM, A. 2000. Magnesium: an update on physiological, clinical and analytical aspects. *Clinica chimica acta,* 294**,** 1-26.
SATOH, A., WANG, Y., MALSAM, J., BEARD, M. B. & WARREN, G. 2003. Golgin – 84 is a rab1 binding partner involved in Golgi structure. *Traffic,* 4**,** 153-161.
SCHLINGMANN, K. P., WALDEGGER, S., KONRAD, M., CHUBANOV, V. & GUDERMANN, T. 2007. TRPM6 and TRPM7—Gatekeepers of human magnesium metabolism. *Biochimica et Biophysica Acta (BBA)-Molecular Basis of Disease,* 1772**,** 813-821.
SCHLINGMANN, K. P., WEBER, S., PETERS, M., NIEMANN NEJSUM, L., VITZTHUM, H., KLINGEL, K., KRATZ, M., HADDAD, E., RISTOFF, E. & DINOUR, D. 2002. Hypomagnesemia with secondary hypocalcemia is caused by mutations in

TRPM6, a new member of the TRPM gene family. *Nature genetics,* 31**,** 166-170.
SCHMIDT, E., NARANGODA, C., NÖRENBERG, W., EGAWA, M., RÖSSIG, A., LEONHARDT, M., SCHAEFER, M., ZIERLER, S., KURNIKOVA, M. G. & GUDERMANN, T. 2022. Structural mechanism of TRPM7 channel regulation by intracellular magnesium. *Cellular and Molecular Life Sciences,* 79**,** 1-18.
SCHMITZ, C., DOROVKOV, M. V., ZHAO, X., DAVENPORT, B. J., RYAZANOV, A. G. & PERRAUD, A.-L. 2005. The channel kinases TRPM6 and TRPM7 are functionally nonredundant. *Journal of Biological Chemistry,* 280**,** 37763-37771.
SCHMITZ, C., PERRAUD, A.-L., JOHNSON, C. O., INABE, K., SMITH, M. K., PENNER, R., KUROSAKI, T., FLEIG, A. & SCHARENBERG, A. M. 2003. Regulation of vertebrate cellular Mg homeostasis by TRPM7. *Cell,* 114**,** 191-200.
SCHNITZLER, M. M. Y., WÄRING, J., GUDERMANN, T. & CHUBANOV, V. 2008. Evolutionary determinants of divergent calcium selectivity of TRPM channels. *The FASEB Journal,* 22**,** 1540-1551.
SENGUPTA, P. 2013. Potential health impacts of hard water. *International journal of preventive medicine,* 4**,** 866.
SEO, J. W. & PARK, T. J. 2008. Magnesium metabolism. *Electrolyte & blood pressure,* 6**,** 86-95.
SGAMBATO, A., WOLF, F. I., FARAGLIA, B. & CITTADINI, A. 1999. Magnesium depletion causes growth inhibition, reduced expression of cyclin D1, and increased expression of P27Kip1 in normal but not in transformed mammary epithelial cells. *Journal of cellular physiology,* 180**,** 245-254.
SHAHINIAN, S. & SILVIUS, J. R. 1995. Doubly-lipid-modified protein sequence motifs exhibit long-lived anchorage to lipid bilayer membranes. *Biochemistry,* 34**,** 3813-3822.
SHIN, M.-K., ERASO, C. C., MU, Y.-P., GU, C., YEUNG, B. H., KIM, L. J., LIU, X.-R., WU, Z.-J., PAUDEL, O. & PICHARD, L. E. 2019. Leptin induces hypertension acting on transient receptor potential melastatin 7 channel in the carotid body. *Circulation research,* 125**,** 989-1002.
SHIPSTON, M. J. 2011. Ion channel regulation by protein palmitoylation. *Journal of Biological Chemistry,* 286**,** 8709-8716.
SIMENTAL-MENDIA, L. E., SAHEBKAR, A., RODRIGUEZ-MORAN, M. & GUERRERO-ROMERO, F. 2016. A systematic review and meta-analysis of randomized controlled trials on the effects of magnesium supplementation on insulin sensitivity and glucose control. *Pharmacological research,* 111**,** 272-282.
SIMON, D. B., LU, Y., CHOATE, K. A., VELAZQUEZ, H., AL-SABBAN, E., PRAGA, M., CASARI, G., BETTINELLI, A., COLUSSI, G. & RODRIGUEZ-SORIANO, J. 1999. Paracellin-1, a renal tight junction protein required for paracellular Mg resorption. *Science,* 285**,** 103-106.
SINGARAJA, R. R., HADANO, S., METZLER, M., GIVAN, S., WELLINGTON, C. L., WARBY, S., YANAI, A., GUTEKUNST, C.-A., LEAVITT, B. R. & YI, H. 2002. HIP14, a novel ankyrin domain-containing protein, links huntingtin to intracellular trafficking and endocytosis. *Human molecular genetics,* 11**,** 2815-2828.
SMOTRYS, J. E. & LINDER, M. E. 2004a. Palmitoylation of intracellular signaling proteins: regulation and function. *Annual review of biochemistry,* 73**,** 559-587.

SMOTRYS, J. E. & LINDER, M. E. 2004b. Palmitoylation of intracellular signaling proteins: regulation and function. *Annual review of biochemistry,* 73, 559.
SOBHANI, A. R., FARSHIDI, H., AZARKISH, F., ESLAMI, M., EFTEKHAR, E., KESHAVARZ, M. & SOLTANI, N. 2020. Magnesium sulfate improves some risk factors for atherosclerosis in patients suffering from one or two coronary artery diseases: a double-blind clinical trial study. *Clinical Pharmacology: Advances and Applications,* 12, 159.
SOBOCIŃSKA, J., ROSZCZENKO-JASIŃSKA, P., CIESIELSKA, A. & KWIATKOWSKA, K. 2018. Protein palmitoylation and its role in bacterial and viral infections. *Frontiers in immunology,* 8, 2003.
SONTIA, B. & TOUYZ, R. M. 2007. Magnesium transport in hypertension. *Pathophysiology,* 14, 205-211.
STAAF, S., FRANCK, M. C., MARMIGÈRE, F., MATTSSON, J. P. & ERNFORS, P. 2010. Dynamic expression of the TRPM subgroup of ion channels in developing mouse sensory neurons. *Gene Expression Patterns,* 10, 65-74.
STANDLEY, P. R. & STANDLEY, C. A. 2002. Identification of a functional Na/Mg exchanger in human trophoblast cells. *American journal of hypertension,* 15, 565-570.
STIX, R., SONG, J., BANERJEE, A. & FARALDO-GÓMEZ, J. D. 2020. DHHC20 palmitoyl-transferase reshapes the membrane to foster catalysis. *Biophysical journal,* 118, 980-988.
STOCKAND, J. D. & MESZAROS, J. G. 2003. Aldosterone stimulates proliferation of cardiac fibroblasts by activating Ki-RasA and MAPK1/2 signaling. *American Journal of Physiology-Heart and Circulatory Physiology,* 284, H176-H184.
STORY, G. M., PEIER, A. M., REEVE, A. J., EID, S. R., MOSBACHER, J., HRICIK, T. R., EARLEY, T. J., HERGARDEN, A. C., ANDERSSON, D. A. & HWANG, S. W. 2003. ANKTM1, a TRP-like channel expressed in nociceptive neurons, is activated by cold temperatures. *Cell,* 112, 819-829.
STOWERS, R. S. & ISACOFF, E. Y. 2007. Drosophila huntingtin-interacting protein 14 is a presynaptic protein required for photoreceptor synaptic transmission and expression of the palmitoylated proteins synaptosome-associated protein 25 and cysteine string protein. *Journal of Neuroscience,* 27, 12874-12883.
STUIVER, M., LAINEZ, S., WILL, C., TERRYN, S., GÜNZEL, D., DEBAIX, H., SOMMER, K., KOPPLIN, K., THUMFART, J. & KAMPIK, N. B. 2011. CNNM2, encoding a basolateral protein required for renal Mg handling, is mutated in dominant hypomagnesemia. *The american journal of human Genetics,* 88, 333-343.
STURGEON, M. & PERRY WU, R. C. 2016. SLC41A1 and TRPM7 in magnesium homeostasis and genetic risk for Parkinson's disease. *Journal of neurology & neuromedicine,* 1, 23.
SU, L.-T., AGAPITO, M. A., LI, M., SIMONSON, W. T., HUTTENLOCHER, A., HABAS, R., YUE, L. & RUNNELS, L. W. 2006. TRPM7 regulates cell adhesion by controlling the calcium-dependent protease calpain. *Journal of Biological Chemistry,* 281, 11260-11270.
SUN, Y., SUKUMARAN, P., SCHAAR, A. & SINGH, B. B. 2015a. TRPM7 and its role in neurodegenerative diseases. *Channels (Austin),* 9, 253-61.
SUN, Y., SUKUMARAN, P., SCHAAR, A. & SINGH, B. B. 2015b. TRPM7 and its role in neurodegenerative diseases. *Channels,* 9, 253-261.
SUNDIVAKKAM, P. C., KWIATEK, A. M., SHARMA, T. T., MINSHALL, R. D., MALIK, A. B. & TIRUPPATHI, C. 2009. Caveolin-1 scaffold domain interacts with

TRPC1 and IP3R3 to regulate Ca store release-induced Ca entry in endothelial cells. *American Journal of Physiology-Cell Physiology,* 296**,** C403-C413.
SWAMINATHAN, R. 2003. Magnesium metabolism and its disorders. *The Clinical Biochemist Reviews,* 24**,** 47.
SWARTHOUT, J. T., LOBO, S., FARH, L., CROKE, M. R., GREENTREE, W. K., DESCHENES, R. J. & LINDER, M. E. 2005. DHHC9 and GCP16 constitute a human protein fatty acyltransferase with specificity for H-and N-Ras. *Journal of Biological Chemistry,* 280**,** 31141-31148.
TABACZAR, S., CZOGALLA, A., PODKALICKA, J., BIERNATOWSKA, A. & SIKORSKI, A. F. 2017. Protein palmitoylation: Palmitoyltransferases and their specificity. *Experimental Biology and Medicine,* 242**,** 1150-1157.
TAKEZAWA, R., SCHMITZ, C., DEMEUSE, P., SCHARENBERG, A. M., PENNER, R. & FLEIG, A. 2004. Receptor-mediated regulation of the TRPM7 channel through its endogenous protein kinase domain. *Proceedings of the National Academy of Sciences,* 101**,** 6009-6014.
TAKIMOTO, K., YANG, E.-K. & CONFORTI, L. 2002. Palmitoylation of KChIP splicing variants is required for efficient cell surface expression of Kv4. 3 channels. *Journal of Biological Chemistry,* 277**,** 26904-26911.
TALAVERA, K., STARTEK, J. B., ALVAREZ-COLLAZO, J., BOONEN, B., ALPIZAR, Y. A., SANCHEZ, A., NAERT, R. & NILIUS, B. 2020. Mammalian transient receptor potential TRPA1 channels: from structure to disease. *Physiological Reviews*.
TALAVERA, K., YASUMATSU, K., VOETS, T., DROOGMANS, G., SHIGEMURA, N., NINOMIYA, Y., MARGOLSKEE, R. F. & NILIUS, B. 2005. Heat activation of TRPM5 underlies thermal sensitivity of sweet taste. *Nature,* 438**,** 1022-1025.
TANG, D., YUAN, H. & WANG, Y. 2010. The role of GRASP65 in Golgi cisternal stacking and cell cycle progression. *Traffic,* 11**,** 827-842.
TANGVORAPHONKCHAI, K. & DAVENPORT, A. 2018. Magnesium and cardiovascular disease. *Advances in chronic kidney disease,* 25**,** 251-260.
TANIYAMA, Y. & GRIENDLING, K. K. 2003. Reactive oxygen species in the vasculature: molecular and cellular mechanisms. *Hypertension,* 42**,** 1075-1081.
THEBAULT, S., ALEXANDER, R. T., GROENESTEGE, W. M. T., HOENDEROP, J. G. & BINDELS, R. J. 2009. EGF increases TRPM6 activity and surface expression. *Journal of the American Society of Nephrology,* 20**,** 78-85.
TOMAS, A., FUTTER, C. E. & EDEN, E. R. 2014. EGF receptor trafficking: consequences for signaling and cancer. *Trends in cell biology,* 24**,** 26-34.
TOMATIS, V. M., TRENCHI, A., GOMEZ, G. A. & DANIOTTI, J. L. 2010. Acyl-protein thioesterase 2 catalizes the deacylation of peripheral membrane-associated GAP-43. *PloS one,* 5**,** e15045.
TORII, S., KOBAYASHI, K., TAKAHASHI, M., KATAHIRA, K., GORYO, K., MATSUSHITA, N., YASUMOTO, K.-I., FUJII-KURIYAMA, Y. & SOGAWA, K. 2009. Magnesium deficiency causes loss of response to intermittent hypoxia in paraganglion cells. *Journal of Biological Chemistry,* 284**,** 19077-19089.
TORTOSA, E., ADOLFS, Y., FUKATA, M., PASTERKAMP, R. J., KAPITEIN, L. C. & HOOGENRAAD, C. C. 2017. Dynamic palmitoylation targets MAP6 to the axon to promote microtubule stabilization during neuronal polarization. *Neuron,* 94**,** 809-825. e7.
TOUYZ, R. M. 2004. Magnesium in clinical medicine. *Front Biosci,* 9**,** 1278-1293.

TOUYZ, R. M., HE, Y., MONTEZANO, A. C., YAO, G., CHUBANOV, V., GUDERMANN, T. & CALLERA, G. E. 2006. Differential regulation of transient receptor potential melastatin 6 and 7 cation channels by ANG II in vascular smooth muscle cells from spontaneously hypertensive rats. *American Journal of Physiology-Regulatory, Integrative and Comparative Physiology,* 290**,** R73-R78.

TREBAK, M., VAZQUEZ, G., BIRD, G. S. J. & PUTNEY JR, J. W. 2003. The TRPC3/6/7 subfamily of cation channels. *Cell calcium,* 33**,** 451-461.

TULLOCH, L. B., HOWIE, J., WYPIJEWSKI, K. J., WILSON, C. R., BERNARD, W. G., SHATTOCK, M. J. & FULLER, W. 2011. The inhibitory effect of phospholemman on the sodium pump requires its palmitoylation. *Journal of Biological Chemistry,* 286**,** 36020-36031.

TURLOVA, E., BAE, C. Y., DEURLOO, M., CHEN, W., BARSZCZYK, A., HORGEN, F. D., FLEIG, A., FENG, Z.-P. & SUN, H.-S. 2016a. TRPM7 regulates axonal outgrowth and maturation of primary hippocampal neurons. *Molecular neurobiology,* 53**,** 595-610.

TURLOVA, E., BAE, C. Y. J., DEURLOO, M., CHEN, W., BARSZCZYK, A., HORGEN, F. D., FLEIG, A., FENG, Z. P. & SUN, H. S. 2016b. TRPM7 Regulates Axonal Outgrowth and Maturation of Primary Hippocampal Neurons. *Mol Neurobiol,* 53**,** 595-610.

TURLOVA, E., WONG, R., XU, B., LI, F., DU, L., HABBOUS, S., HORGEN, F. D., FLEIG, A., FENG, Z.-P. & SUN, H.-S. 2021. TRPM7 mediates neuronal cell death upstream of calcium/calmodulin-dependent protein kinase II and calcineurin mechanism in neonatal hypoxic-ischemic brain injury. *Translational Stroke Research,* 12**,** 164-184.

URESHINO, R. P., ROCHA, K. K., LOPES, G. S., BINCOLETTO, C. & SMAILI, S. S. 2014. Calcium signaling alterations, oxidative stress, and autophagy in aging. *Antioxidants & Redox Signaling,* 21**,** 123-137.

VALINSKY, W. C., JOLLY, A., MIQUEL, P., TOUYZ, R. M. & SHRIER, A. 2016. Aldosterone upregulates transient receptor potential melastatin 7 (TRPM7). *Journal of Biological Chemistry,* 291**,** 20163-20172.

VAN DER WIJST, J., BLANCHARD, M. G., WOODROOF, H. I., MACARTNEY, T. J., GOURLAY, R., HOENDEROP, J. G., BINDELS, R. J. & ALESSI, D. R. 2014. Kinase and channel activity of TRPM6 are co-ordinated by a dimerization motif and pocket interaction. *Biochemical Journal,* 460**,** 165-175.

VARTAK, N., PAPKE, B., GRECCO, H. E., ROSSMANNEK, L., WALDMANN, H., HEDBERG, C. & BASTIAENS, P. I. 2014. The autodepalmitoylating activity of APT maintains the spatial organization of palmitoylated membrane proteins. *Biophysical journal,* 106**,** 93-105.

VENKATACHALAM, K., VAN ROSSUM, D. B., PATTERSON, R. L., MA, H.-T. & GILL, D. L. 2002. The cellular and molecular basis of store-operated calcium entry. *Nature cell biology,* 4**,** E263-E272.

VERARDI, R., KIM, J.-S., GHIRLANDO, R. & BANERJEE, A. 2017. Structural basis for substrate recognition by the ankyrin repeat domain of human DHHC17 palmitoyltransferase. *Structure,* 25**,** 1337-1347. e6.

VERKRUYSE, L. A. & HOFMANN, S. L. 1996. Lysosomal targeting of palmitoyl-protein thioesterase. *Journal of Biological Chemistry,* 271**,** 15831-15836.

VERONESE, N., ZURLO, A., SOLMI, M., LUCHINI, C., TREVISAN, C., BANO, G., MANZATO, E., SERGI, G. & RYLANDER, R. 2016. Magnesium status in Alzheimer's disease: a systematic review. *American Journal of Alzheimer's Disease & Other Dementias®,* 31**,** 208-213.

VESA, J., HELLSTEN, E., VERKRUYSE, L. A., CAMP, L. A., RAPOLA, J., SANTAVUORI, P., HOFMANN, S. L. & PELTONEN, L. 1995. Mutations in the

palmitoyl protein thioesterase gene causing infantile neuronal ceroid lipofuscinosis. *Nature,* 376**,** 584-587.
VINCENZI, B., SANTINI, D., GALLUZZO, S., RUSSO, A., FULFARO, F., SILLETTA, M., BATTISTONI, F., ROCCI, L., ZOBEL, B. B. & ADAMO, V. 2008. Early magnesium reduction in advanced colorectal cancer patients treated with cetuximab plus irinotecan as predictive factor of efficacy and outcome. *Clinical cancer research,* 14**,** 4219-4224.
VINK, R., COOK, N. L. & VAN DEN HEUVEL, C. 2009. Magnesium in acute and chronic brain injury: an update.
VISSER, D., MIDDELBEEK, J., VAN LEEUWEN, F. N. & JALINK, K. 2014. Function and regulation of the channel-kinase TRPM7 in health and disease. *European journal of cell biology,* 93**,** 455-465.
VOETS, T., DROOGMANS, G., WISSENBACH, U., JANSSENS, A., FLOCKERZI, V. & NILIUS, B. 2004. The principle of temperature-dependent gating in cold- and heat-sensitive TRP channels. *Nature,* 430**,** 748-754.
VOLPE, S. L. 2008. Magnesium, the metabolic syndrome, insulin resistance, and type 2 diabetes mellitus. *Critical reviews in food science and nutrition,* 48**,** 293-300.
VORMANN, J. 2003. Magnesium: nutrition and metabolism. *Molecular aspects of medicine,* 24**,** 27-37.
VRIENS, J., OWSIANIK, G., HOFMANN, T., PHILIPP, S. E., STAB, J., CHEN, X., BENOIT, M., XUE, F., JANSSENS, A. & KERSELAERS, S. 2011. TRPM3 is a nociceptor channel involved in the detection of noxious heat. *Neuron,* 70**,** 482-494.
WABAKKEN, T., RIAN, E., KVEINE, M. & AASHEIM, H.-C. 2003. The human solute carrier SLC41A1 belongs to a novel eukaryotic subfamily with homology to prokaryotic MgtE Mg transporters. *Biochemical and biophysical research communications,* 306**,** 718-724.
WALDER, R. Y., YANG, B., STOKES, J. B., KIRBY, P. A., CAO, X., SHI, P., SEARBY, C. C., HUSTED, R. F. & SHEFFIELD, V. C. 2009. Mice defective in TRPM6 show embryonic mortality and neural tube defects. *Human molecular genetics,* 18**,** 4367-4375.
WANG, H., CHENG, X., TIAN, J., XIAO, Y., TIAN, T., XU, F., HONG, X. & ZHU, M. X. 2020. TRPC channels: structure, function, regulation and recent advances in small molecular probes. *Pharmacology & therapeutics,* 209**,** 107497.
WEGLICKI, W. B., PHILLIPS, T. M., FREEDMAN, A. M., CASSIDY, M. M. & DICKENS, B. F. 1992. Magnesium-deficiency elevates circulating levels of inflammatory cytokines and endothelin. *Molecular and cellular biochemistry,* 110**,** 169-173.
WES, P. D., CHEVESICH, J., JEROMIN, A., ROSENBERG, C., STETTEN, G. & MONTELL, C. 1995. TRPC1, a human homolog of a Drosophila store-operated channel. *Proceedings of the National Academy of Sciences,* 92**,** 9652-9656.
WHELTON, P. K. & KLAG, M. J. 1989. Magnesium and blood pressure: review of the epidemiologic and clinical trial experience. *The American journal of cardiology,* 63**,** G26-G30.
WINKLER, P. A., HUANG, Y., SUN, W., DU, J. & LÜ, W. 2017. Electron cryo-microscopy structure of a human TRPM4 channel. *Nature,* 552**,** 200-204.
WOLF, F., COVACCI, V., BRUZZESE, N., DI FRANCESCO, A., SACCHETTI, A., CORDA, D. & CITTADINI, A. 1998. Differentiation of HL – 60 promyelocytic

leukemia cells is accompanied by a modification of magnesium homeostasis. *Journal of cellular biochemistry,* 71, 441-448.
WOLF, F., MAIER, J., NASULEWICZ, A., FEILLET-COUDRAY, C., SIMONACCI, M., MAZUR, A. & CITTADINI, A. 2007. Magnesium and neoplasia: from carcinogenesis to tumor growth and progression or treatment. *Archives of biochemistry and biophysics,* 458, 24-32.
WOLF, F. I., DI FRANCESCO, A., COVACCI, V., CORDA, D. & CITTADINI, A. 1996. Regulation of intracellular magnesium in ascites cells: Involvement of different regulatory pathways. *Archives of biochemistry and biophysics,* 331, 194-200.
WOLF, F. I. & TRAPANI, V. 2008. Cell (patho) physiology of magnesium. *Clinical science,* 114, 27-35.
WOLF, F. I. & TRAPANI, V. 2011. MagT1: a highly specific magnesium channel with important roles beyond cellular magnesium homeostasis. *Magnesium Research,* 24, 86-91.
WON, S. J., CHEUNG SEE KIT, M. & MARTIN, B. R. 2018. Protein depalmitoylases. *Critical reviews in biochemistry and molecular biology,* 53, 83-98.
WON, S. J., DAVDA, D., LABBY, K. J., HWANG, S. Y., PRICER, R., MAJMUDAR, J. D., ARMACOST, K. A., RODRIGUEZ, L. A., RODRIGUEZ, C. L. & CHONG, F. S. 2016. Molecular mechanism for isoform-selective inhibition of acyl protein thioesterases 1 and 2 (APT1 and APT2). *ACS chemical biology,* 11, 3374-3382.
WRIGHT, M. H., HEAL, W. P., MANN, D. J. & TATE, E. W. 2010. Protein myristoylation in health and disease. *Journal of chemical biology,* 3, 19-35.
XIAO, Y., LV, X., CAO, G., BIAN, G., DUAN, J., AI, J., SUN, H., LI, Q., YANG, Q. & CHEN, T. 2010. Overexpression of Trpp5 contributes to cell proliferation and apoptosis probably through involving calcium homeostasis. *Molecular and cellular biochemistry,* 339, 155-161.
XIE, J., SUN, B., DU, J., YANG, W., CHEN, H.-C., OVERTON, J. D., RUNNELS, L. W. & YUE, L. 2011. Phosphatidylinositol 4, 5-bisphosphate (PIP2) controls magnesium gatekeeper TRPM6 activity. *Scientific reports,* 1, 1-12.
XIONG, W., LIANG, Y., LI, X., LIU, G. & WANG, Z. 2016. Erythrocyte intracellular Mg concentration as an index of recognition and memory. *Scientific reports,* 6, 1-12.
YAMAGUCHI, H., MATSUSHITA, M., NAIRN, A. C. & KURIYAN, J. 2001. Crystal structure of the atypical protein kinase domain of a TRP channel with phosphotransferase activity. *Molecular cell,* 7, 1047-1057.
YAMAZAKI, D., MIYATA, H., FUNATO, Y., FUJIHARA, Y., IKAWA, M. & MIKI, H. 2016. The Mg transporter CNNM4 regulates sperm Ca homeostasis and is essential for reproduction. *Journal of cell science,* 129, 1940-1949.
YAN, Z., ZHANG, W., HE, Y., GORCZYCA, D., XIANG, Y., CHENG, L. E., MELTZER, S., JAN, L. Y. & JAN, Y. N. 2013. Drosophila NOMPC is a mechanotransduction channel subunit for gentle-touch sensation. *Nature,* 493, 221-225.
YANG, F., CUI, Y., WANG, K. & ZHENG, J. 2010. Thermosensitive TRP channel pore turret is part of the temperature activation pathway. *Proceedings of the National Academy of Sciences,* 107, 7083-7088.
YANG, G. & CYNADER, M. S. 2011. Palmitoyl acyltransferase zD17 mediates neuronal responses in acute ischemic brain injury by regulating JNK activation in a signaling module. *Journal of Neuroscience,* 31, 11980-11991.

YANG, H.-Q., MARTINEZ-ORTIZ, W., HWANG, J., FAN, X., CARDOZO, T. J. & COETZEE, W. A. 2020. Palmitoylation of the KATP channel Kir6. 2 subunit promotes channel opening by regulating PIP2 sensitivity. *Proceedings of the National Academy of Sciences,* 117, 10593-10602.

YEE, N. S. 2017. Role of TRPM7 in cancer: potential as molecular biomarker and therapeutic target. *Pharmaceuticals,* 10, 39.

YEE, N. S., KAZI, A. A., LI, Q., YANG, Z., BERG, A. & YEE, R. K. 2015. Aberrant over-expression of TRPM7 ion channels in pancreatic cancer: required for cancer cell invasion and implicated in tumor growth and metastasis. *Biology open,* 4, 507-514.

YEE, N. S., KAZI, A. A. & YEE, R. K. 2014. Cellular and developmental biology of TRPM7 channel-kinase: implicated roles in cancer. *Cells,* 3, 751-777.

YESTE-VELASCO, M., LINDER, M. E. & LU, Y.-J. 2015. Protein S-palmitoylation and cancer. *Biochimica et Biophysica Acta (BBA)-Reviews on Cancer,* 1856, 107-120.

YEUNG, E. W., CHEUNG, K.-K. & SUN, K.-T. 2017. Biological Role of TRPC1 in Myogenesis, Regeneration, and Disease. *The Plasticity of Skeletal Muscle*. Springer.

YILDIRIM, E. & BIRNBAUMER, L. 2007. TRPC2: molecular biology and functional importance. *Transient Receptor Potential (TRP) Channels*, 53-75.

YOGI, A., CALLERA, G. E., O'CONNOR, S., ANTUNES, T. T., VALINSKY, W., MIQUEL, P., MONTEZANO, A. C., PERRAUD, A.-L., SCHMITZ, C. & SHRIER, A. 2013. Aldosterone signaling through transient receptor potential melastatin 7 cation channel (TRPM7) and its α-kinase domain. *Cellular signalling,* 25, 2163-2175.

YU, L.-R., STEWART, N. A. & VEENSTRA, T. D. 2010. Proteomics: the deciphering of the functional genome. *Essentials of genomic and personalized medicine*. Elsevier.

YU, X., GUAN, P.-P., ZHU, D., LIANG, Y.-Y., WANG, T., WANG, Z.-Y. & WANG, P. 2018. Magnesium ions inhibit the expression of tumor necrosis factor α and the activity of γ-secretase in a ß-amyloid protein-dependent mechanism in APP/PS1 transgenic mice. *Frontiers in Molecular Neuroscience,* 11, 172.

YU, Y., CHEN, S., XIAO, C., JIA, Y., GUO, J., JIANG, J. & LIU, P. 2014. TRPM7 is involved in angiotensin II induced cardiac fibrosis development by mediating calcium and magnesium influx. *Cell Calcium,* 55, 252-260.

YURTSEVER, D. & LORENT, J. H. 2020. Structural modifications controlling membrane raft partitioning and curvature in human and viral proteins. *The Journal of Physical Chemistry B,* 124, 7574-7585.

ZÁDORI, D., VERES, G., SZALÁRDY, L., KLIVÉNYI, P. & VÉCSEI, L. 2018. Alzheimer's disease: recent concepts on the relation of mitochondrial disturbances, excitotoxicity, neuroinflammation, and kynurenines. *Journal of Alzheimer's Disease,* 62, 523-547.

ZEIDMAN, R., BUCKLAND, G., CEBECAUER, M., EISSMANN, P., DAVIS, D. M. & MAGEE, A. I. 2011. DHHC2 is a protein S-acyltransferase for Lck. *Molecular membrane biology,* 28, 473-486.

ZENG, Z., LENG, T., FENG, X., SUN, H., INOUE, K., ZHU, L. & XIONG, Z.-G. 2015. Silencing TRPM7 in mouse cortical astrocytes impairs cell proliferation and migration via ERK and JNK signaling pathways. *PloS one,* 10, e0119912.

ZHANG, F. L. & CASEY, P. J. 1996. Protein prenylation: molecular mechanisms and functional consequences. *Annual review of biochemistry,* 65, 241-269.

ZHANG, M. M., TSOU, L. K., CHARRON, G., RAGHAVAN, A. S. & HANG, H. C. 2010. Tandem fluorescence imaging of dynamic S-acylation and protein turnover. *Proceedings of the National Academy of Sciences,* 107, 8627-8632.

ZHANG, X., LI, Y., DEL GOBBO, L. C., ROSANOFF, A., WANG, J., ZHANG, W. & SONG, Y. 2016. Effects of magnesium supplementation on blood pressure: a meta-analysis of randomized double-blind placebo-controlled trials. *Hypertension,* 68, 324-333.

ZHANG, Y.-H., SUN, H.-Y., CHEN, K.-H., DU, X.-L., LIU, B., CHENG, L.-C., LI, X., JIN, M.-W. & LI, G.-R. 2012a. Evidence for functional expression of TRPM7 channels in human atrial myocytes. *Basic research in cardiology,* 107, 1-12.

ZHANG, Y. & SEEMANN, J. 2021. Rapid degradation of GRASP55 and GRASP65 reveals their immediate impact on the Golgi structure. *Journal of Cell Biology,* 220.

ZHANG, Y. H., SUN, H. Y., CHEN, K. H., DU, X. L., LIU, B., CHENG, L. C., LI, X., JIN, M. W. & LI, G. R. 2012b. Evidence for functional expression of TRPM7 channels in human atrial myocytes. *Basic Res Cardiol,* 107, 282.

ZHANG, Z., TÓTH, B., SZOLLOSI, A., CHEN, J. & CSANÁDY, L. 2018. Structure of a TRPM2 channel in complex with Ca explains unique gating regulation. *Elife,* 7.

ZHANG, Z., WANG, M., FAN, X.-H., CHEN, J.-H., GUAN, Y.-Y. & TANG, Y.-B. 2012c. Upregulation of TRPM7 channels by angiotensin II triggers phenotypic switching of vascular smooth muscle cells of ascending aorta. *Circulation research,* 111, 1137-1146.

ZHANG, Z., YU, H., HUANG, J., FAOUZI, M., SCHMITZ, C., PENNER, R. & FLEIG, A. 2014. The TRPM6 kinase domain determines the Mg· ATP sensitivity of TRPM7/M6 heteromeric ion channels. *Journal of Biological Chemistry,* 289, 5217-5227.

ZHAO, Z., PEI, Y., HUANG, X., LIU, Y., YANG, W., SUN, J., SI, N., XING, X., LI, M. & WANG, O. 2013. Novel TRPM6 mutations in familial hypomagnesemia with secondary hypocalcemia. *American Journal of Nephrology,* 37, 541-548.

ZHELTOVA, A. A., KHARITONOVA, M. V., IEZHITSA, I. N. & SPASOV, A. A. 2016. Magnesium deficiency and oxidative stress: an update. *BioMedicine,* 6, 1-7.

ZHENG, J. 2013. Molecular mechanism of TRP channels. *Comprehensive Physiology,* 3, 221.

ZHENG, J. & RAMIREZ, V. D. 2000. Inhibition of mitochondrial proton F0F1 – ATPase/ATP synthase by polyphenolic phytochemicals. *British journal of pharmacology,* 130, 1115-1123.

ZHENG, W., YANG, J., BEAUCHAMP, E., CAI, R., HUSSEIN, S., HOFMANN, L., LI, Q., FLOCKERZI, V., BERTHIAUME, L. G. & TANG, J. 2016. Regulation of TRPP3 channel function by N-terminal domain palmitoylation and phosphorylation. *Journal of Biological Chemistry,* 291, 25678-25691.

ZHIVOTOVSKY, B. & ORRENIUS, S. 2011. Calcium and cell death mechanisms: a perspective from the cell death community. *Cell Calcium,* 50, 211-21.

ZHOU, H. & CLAPHAM, D. E. 2009. Mammalian MagT1 and TUSC3 are required for cellular magnesium uptake and vertebrate embryonic development. *Proceedings of the National Academy of Sciences,* 106, 15750-15755.

ZHU, M. X. & TANG, J. TRPC channel interactions with calmodulin and IP~ 3 receptors. Novartis Foundation Symposium, 2004. Chichester; New York; John Wiley; 1999, 44-62.
ZHU, X., CHU, P. B., PEYTON, M. & BIRNBAUMER, L. 1995. Molecular cloning of a widely expressed human homologue for the Drosophila trp gene. *FEBS letters,* 373, 193-198.
ZOU, Z.-G., RIOS, F. J., MONTEZANO, A. C. & TOUYZ, R. M. 2019. TRPM7, magnesium, and signaling. *International journal of molecular sciences,* 20, 1877.
ZOU, Z.-G., RIOS, F. J., NEVES, K. B., ALVES-LOPES, R., LING, J., BAILLIE, G. S., GAO, X., FULLER, W., CAMARGO, L. L. & GUDERMANN, T. 2020. Epidermal growth factor signaling through transient receptor potential melastatin 7 cation channel regulates vascular smooth muscle cell function. *Clinical Science,* 134, 2019-2035.
ZOUHAROVA, M., HERMAN, P., HOFBAUEROVÁ, K., VONDRASEK, J. & BOUSOVA, K. 2019. TRPM6 N-terminal CaM-and S100A1-binding domains. *International journal of molecular sciences,* 20, 4430.
ZSURKA, G., GREGÁŇ, J. & SCHWEYEN, R. J. 2001. The human mitochondrial Mrs2 protein functionally substitutes for its yeast homologue, a candidate magnesium transporter. *Genomics,* 72, 158-168.

Appendices

Table S1. Overlapped genes of Clapham and Our proteomics data.

There are 76 potential proteins in unique vesicles which are associated with TRPM7.

76 common genes in "Clapham" and "Xing"	Protein name
AGRN	Agrin;Agrin N-terminal 110 kDa subunit;Agrin C-terminal 110 kDa subunit;Agrin C-terminal 90 kDa fragment;Agrin C-terminal 22 kDa fragment
HERC2	E3 ubiquitin-protein ligase HERC2
SGPL1	Sphingosine-1-phosphate lyase 1
GLG1	Golgi apparatus protein 1
FLOT2	Flotillin-2
TBL2	Transducin beta-like protein 2
AP2M1	AP-2 complex subunit mu
CAT	Catalase
MYO1D	Unconventional myosin-Id
PKP2	Plakophilin-2
IPO4	Importin-4
GOT2	Aspartate aminotransferase, mitochondrial
SLC25A10	Mitochondrial dicarboxylate carrier
CTSD	Cathepsin D;Cathepsin D light chain;Cathepsin D heavy chain
ELAC2	Zinc phosphodiesterase ELAC protein 2
MRPS23	28S ribosomal protein S23, mitochondrial
MRPS27	28S ribosomal protein S27, mitochondrial
OSBPL8	Oxysterol-binding protein-related protein 8; Oxysterol-binding protein
NCKAP1	Nck-associated protein 1
SPTBN2	Spectrin beta chain, non-erythrocytic 2
LGALS3BP	Galectin-3-binding protein
DNM2	Dynamin-2
GRSF1	G-rich sequence factor 1
IPO9	Importin-9
RAI14	Ankycorbin
HADHB	Trifunctional enzyme subunit beta, mitochondrial;3-ketoacyl-CoA thiolase
PCM1	Pericentriolar material 1 protein
TNPO1	Transportin-1
DNAJC10	DnaJ homolog subfamily C member 10
FXR2	Fragile X mental retardation syndrome-related protein 2
HSD17B4	Peroxisomal multifunctional enzyme type 2;(3R)-hydroxyacyl-CoA dehydrogenase;Enoyl-CoA hydratase 2

GNB1	Guanine nucleotide-binding protein G(I)/G(S)/G(T) subunit beta-1
DDOST	Dolichyl-diphosphooligosaccharide--protein glycosyltransferase 48 kDa subunit
ABCD3	ATP-binding cassette sub-family D member 3
MYO1C	Unconventional myosin-Ic
ACSL3	Long-chain-fatty-acid--CoA ligase 3
HADHA	Trifunctional enzyme subunit alpha, mitochondrial;Long-chain enoyl-CoA hydratase;Long chain 3-hydroxyacyl-CoA dehydrogenase
MYO1B	Unconventional myosin-Ib
COPB2	Coatomer subunit beta
GNAI3	Guanine nucleotide-binding protein G(k) subunit alpha
ESYT1	Extended synaptotagmin-1
LRRC59	Leucine-rich repeat-containing protein 59
HACD3	Very-long-chain (3R)-3-hydroxyacyl-CoA dehydratase 3
TOP2A	DNA topoisomerase 2-alpha
RPN2	Dolichyl-diphosphooligosaccharide--protein glycosyltransferase subunit 2
DHX30	Putative ATP-dependent RNA helicase DHX30
IPO7	Importin-7
CKAP5	Cytoskeleton-associated protein 5
IQGAP1	Ras GTPase-activating-like protein IQGAP1
COPA	Coatomer subunit alpha;Xenin;Proxenin
VDAC1	Voltage-dependent anion-selective channel protein 1
TLN1	Talin-1
PPIB	Peptidyl-prolyl cis-trans isomerase B
PLEC	Plectin
ATP5C1	ATP synthase subunit gamma, mitochondrial
LBR	Lamin-B receptor
DNAJA1	DnaJ homolog subfamily A member 1
RPN1	Dolichyl-diphosphooligosaccharide--protein glycosyltransferase subunit 1
MKI67	Antigen KI-67
IPO5	Importin-5
EMD	Emerin
CAND1	Cullin-associated NEDD8-dissociated protein 1
COPB1	Coatomer subunit beta
CORO1C	Coronin-1C;Coronin
RPL18A	60S ribosomal protein L18a
EPPK1	Epiplakin
ATP2A2	Sarcoplasmic/endoplasmic reticulum calcium ATPase 2
CSE1L	Exportin-2
RPL7	60S ribosomal protein L7

PPP1CC	Serine/threonine-protein phosphatase PP1-gamma catalytic subunit;Serine/threonine-protein phosphatase
DYNC1H1	Cytoplasmic dynein 1 heavy chain 1
RPL15	60S ribosomal protein L15;Ribosomal protein L15
EPRS	Bifunctional glutamate/proline--tRNA ligase;Glutamate--tRNA ligase;Proline--tRNA ligase
RPL6	60S ribosomal protein L6
PCBP1	Poly(rC)-binding protein 1
PCBP2	Poly(rC)-binding protein 2